Effects of Near-field and Far-field ground motions on Non-linear response of RC Buildings

A Dissertation Report Submitted in Partial Fulfilment of the requirement

for the Award of the Degree of

Master of Engineering

in

Structural Engineering

Submitted by

YASHSWI BANSAL

(802124025)

Under Supervision of

Dr. Trishna Choudhury
Assistant Professor
Department of Civil Engineering
TIET, Patiala

Er. Divey Mahajan
Director
Fostertechs Pvt. Ltd
Noida

DEPARTMENT OF CIVIL ENGINEERING

THAPAR INSTITUTE OF ENGINEERING &TECHNOLOGY

(DEEMED TO BE UNIVERSITY)

PATIALA-147004 (PUNJAB)

July 2023

DECLARATION

I hereby declare that work which is presented in this seminar report entitled **"Effects of near-field and far-field ground motions on Non-Linear response of RC buildings"** as per the requirements for the award of **Master of Engineering** in **Structural Engineering**, submitted in the Department of Civil Engineering, Thapar Institute of Engineering and Technology (TIET), Patiala. This work is carried out by me under the guidance of **Dr. Trishna Choudhury, Assistant Professor, Department of Civil Engineering, Thapar Institute of Engineering and Technology, Patiala** and **Er. Divey Mahajan, Director, Fostertechs Pvt. Ltd., Noida.** It is declared that this work is original and has not been submitted anywhere else for the award of any other degree or certificate.

Yashswi

Date: 29-07-2023

(YASHSWI BANSAL)

802124025

This is to certify that the above declaration made by the student concerned is correct according to the best of my knowledge and belief.

Dr. Trishna Choudhury

Assistant Professor

Department of Civil Engineering

TIET Patiala

Er. Divey Mahajan

Director

Fostertechs Pvt. Ltd.

Noida

ACKNOWLEDGEMENT

With immense praise, I take this delightful opportunity to express my special thanks of gratitude to the Department of Civil Engineering, T.I.E.T, Patiala for providing the worthwhile opportunity to get involved and understand this innovative project.

I express my profound thanks to **Dr Trishna Choudhury** for her colossal guidance & unending support. I feel highly indebted to her, for her sheer guidance and constant supervision as well as systematically providing all the relevant information and helping me accomplish the target most efficiently.

I would like to express my heartful thanks to **Er. Divey Mahajan** for his sheer guidance. Every single day, he drove me to the right path for utilizing my knowledge and skillsets gained in academic with practical aspects with an appropriate exposure to practical aspects of industry. His consistent motivation and counselling, lead me to be the best version of me.

Yashswi

Yashswi Bansal

(802124025)

Fostertechs Pvt. Ltd.
Engineering and Project Management Solutions
Fostertechs
502, Tower II, A-13, Highway Towers, Sector-62, Noida-201309

REF. No.: FPL/07/23
DATE: 17/07/2023

CERTIFICATE OF INDUSTRIAL TRAINING

This is to certify that Mr. Yashswi Bansal (Roll. No. **802124025),**a student of M.E. (Structural Engineering) at Thapar Institute of Engineering & Technology Patiala, has completed his industrial training with Fostertechs Pvt. Ltd from 23-Aug-2022 to 30-June-2023.

His performance has been satisfactory. We have found him dedicated, sincere and hardworking regarding all the tasks and assignments provided.

We wish him all the best for his future endeavors.

FOSTERTECHS PVT. LTD. NOIDA

(Authorized Signatory)
Mr. Divey Mahajan
CEO
Fostertechs Pvt. Ltd.

: +91 9999268782, +91 9810454656, : www.fostertechs.com, : info@fostertechs.com, fostertechsprojects@gmail.com
REGISTERED OFFICE : 1, Brijpuri Extension, Parwana Road, Delhi-110051, INDIA

ABSTRACT

To perform a design or assessment considering earthquakes, Non-Linear Time History Analysis (NLTHA) is the approach that attempts to fully represent the seismic response of buildings without any of the major simplifying assumptions, such as ignoring nonlinearity and /or dynamic effects. Even though there is a clear need for analysis, there are many uncertainties regarding its application the primary difficulty in using this type of recording is the lacking of a unified criterion in the selection of the ground motion parameters. Therefore, this situation creates a necessity to investigate methods for earthquake selection and their respective reliability verification.

The present study describes the procedure for the selection of ground motion and identifying ground motion parameters to understand their effect on the response of the structure. Characterisation is one of the necessary studies to compare about the behaviour varying the type of earthquake (near field/far field) ground.

Furthermore, the study aims at obtaining the seismic response of building incorporating the effects of near-field and far-field ground motions on building structure and comparison of results for both types of ground motions.

TABLE OF CONTENTS

LIST OF FIGURES

LIST OF TABLES

LIST OF SYMBOLS AND ABBREVIATIONS

f_y	Yield strength of steel
f_d	Dominant Frequency
f_{ck}	Characteristic compressive strength of concrete cube
fu	Minimum Tensile stress of steel
f_{ye}	Expected yield stress of steel
f_{ue}	Expected tensile stress of steel
f_m'	Masonary prism strength
E_c	Modulus of Elasticity of Concrete
E_m	Modulus of Elasticity of Prism
l_p	Hinge length
AI	Arias Intensity
BF	Bare Frame
FI	Fully Infilled
FF	Far-field
NF	Near-field
PE	Potential Energy
PGA	Peak Ground Acceleration
SED	Specific Energy Density
NLTHA	Non-Linear Time History Analysis

CHAPTER - 1

INTRODUCTION

1.1. Overview

Earthquakes have been a major destructive natural hazard causing extensive damage to human lives and property. Therefore, it's always been our interest to analyze and study different aspects of ground motion shakings and simultaneously apply them to building structures to minimize human and property damage.

So far, Nonlinear Time History Analysis is the approach that attempts to fully represent the seismic response of buildings without any of the major simplifying assumptions such as ignoring nonlinearity and /or dynamic effects. Even though there is a clear need for analysis, there are many uncertainties regarding its application the primary difficulty in using this type of recording is the lacking of a unified criterion in the selection of the ground motion parameter.

1.2. Performance of buildings in past earthquakes

Shaking of ground is the principal cause of earthquake-induced damage. As the earth vibrates, all buildings on the ground surface will respond to that vibration in varying degrees. Earthquake-induced velocities, accelerations and displacements can damage or destroy a building unless it has been designed and constructed to be earthquake resistant. Therefore, effect of ground shaking on buildings is a principal area of consideration for designing earthquake-resistant buildings. Seismic design loads are very difficult to determine due to the random nature of earthquake motions. However, experiences from past strong earthquakes have shown that reasonable and prudent practices can keep a building safe during an earthquake.

RCC structures have withstood earthquakes well, without significant damage. When there is horizontal bending, a tough member capable of taking bending is found to perform better during earthquakes. Even more strength can be gained by adding steel bars to the corner portions or holes. Even the dry-packed stone masonry walls having continuous lintel bands over openings and cross walls didn't undergo any damage. Failure factors for RC frame buildings:

Failures are mainly due to lack of good design of beams /columns frame action and foundation.

Poor construction quality, insufficient detailing, or improper placement of reinforcement, notably at joints and in columns and beams for ductility. Inadequate diaphragm action of roof and floors. Inadequate treatment of masonry walls. Common type of damage in RC frame buildings includes the damage is mostly due to failure of infill, or failure of columns or beams. Spalling of concrete in columns. The column may sustain damage from cracking or buckling as a result of excessive bending mixed with dead weight. When columns are thin and stirrup spacing is wide, there is a significant amount of column buckling. Due to shearing action, a major fracture appears close to the rigid joints of the frame, which could cause the structure to completely collapse. Additionally, the differential settlement results in too many moments in the frame, which could cause failure. Because beam failure is less harmful than common failure, the frame should be designed so that the plastic hinge is only used on the beam.

1.3. Major Concerns and Motivation of the Study

There are numerous metrics that can be used to describe the ground motion of an earthquake, each of which indicates a distinct aspect of the shaking, such as the peak amplitudes, the frequency content, or the energy carried in the signal. A complete characterization of the ground motion must include a measure of its duration, or more specifically the duration of that part of the signal that is strong. The most distinguished characteristic of near-field ground motions is the pulses generated by the directivity effect and fling-step effect. The acceleration-time, velocity-time, and displacement-time histories of these pulse-type ground motions usually contain one or more discrete pulses, with the velocity history occurring more frequently. The effects of near-field ground motions were evident and the studies were carried out as early as 1978 but still, in present times it lacks a proper definition.

Somerville et al. (1997) defines near field ground motions as record obtained in the vicinity of a fault with apparent velocity pulse (pulse duration larger than 1.0 s), the distance of the fault of the ground motion record less than 10 km, and the peak ground velocity/peak ground acceleration (PGV/PGA) value which is larger than 0.1 s. Stewart et al. (2001) recommended that 20~60 km should be the appropriate range of the upper limit to the distance from the sites to the fault. Many more definitions have been developed over time, but still, no precise one is being adopted.

1.4. Objectives of the Present Study

The primary objectives of the present work are -

- Selection of ground motions and its characterization.
- Performance assessment of fully-infilled reinforced concrete frame.
- Study on the influence of ground motion parameters on the nonlinear response of fully-infilled reinforced concrete frame.
- Effects of NF and FF ground motion records on response of fully-infilled frame

1.5. Organization and Outline of the Thesis

To carry out the considered objectives, the present thesis is divided into **five chapters** and is structured as follows:

Chapter 1 serves as the Introduction, providing an overview of Near-field (NF) and Far-field (FF) ground motions and addressing the key concerns and motivations behind the study. It includes a brief summary of NF and FF and its effects on RC Buildings, outlines the objectives of the research, and sets the stage for the subsequent chapters. **Chapter 2** presents a comprehensive review of previous research conducted on the characteristics and properties of NF and FF earthquake records. The primary focus is on differentiating characteristics of both types of earthquakes. Through this review, the need for the current research is identified based on the existing gaps and limitations in the literature.

Chapter 3 presents the overall workflow and methodology to be adopted in the study. It briefly explains the input parameters to be taken as raw data and applied to the modelled frame to derive the response of the frame after the application of Non-Linear Time History Analysis. **Chapter 4** describes the input parameters in detail and the characterization of ground motions to evaluate different energy and spectral parameters for NF and FF ground motions and their inter-relationship b/w each other through various comparative graphs.

Chapter 5 evaluates the effects with and without infill on various parameters, such as Displacement, Potential Energy, and Base Shear to characterized parameters such as PGA etc. and on the lateral response of different frame configurations. Several Comparative plots are prepared to derive various conclusions. **Chapter 6** summarizes the major outcomes drawn from the study.

***

CHAPTER - 2

LITERATURE REVIEW

2.1. Overview

There are numerous characteristics that can be used to describe the ground motion of an earthquake, each of which indicates a distinct aspect of the shaking, such as the peak amplitudes, the frequency content, or the energy contained in the signal. The duration of the ground motion, or more specifically the duration of the signal's strong portion, must be measured in order to fully characterize it.

Many studies about of nature of ground motion shaking have been investigated and computed mathematically but still due to a lack of proper application and a unified approach in the design of the structure. To date the seismic damage is related to Peak Ground Acceleration, Peak Ground Velocity and Peak Ground Displacement computed using different codal provisions and methodologies to compute and thereafter provide reinforcement incorporating seismic effects.

2.2. History of NF and FF ground motions

The complexity in study of earthquake ground motion is primarily due to the listed three factors: (i) the seismic waves that are generated at the time of earthquake fault movement are not of a homogeneous character (source effect), (ii) as these waves travel through earth on their way from the fault to project site, they are modified by the soil and rock media (path effect), and (iii) once they reach the project site, these seismic waves undergo further modifications, which are dependent upon the characteristics of the ground and soil at the site (local site effects).

The source effect will be discussed in further contexts.

The effects of near-field ground motions were evident and the studies were carried out as early as 1978. All the methods at that time used standard ground response spectrum shapes and effective acceleration values smaller than the expected peak values, which are not reliable at near-fault sites. Therefore, additional research needed to take place on the different parameters that define the characteristics of severe, long-duration pulses, i.e., the 19

largest incremental velocity and the associated 'effective' acceleration that can be developed according to the faulting mechanism and the mechanical characteristics of the soil present at a site.

(Singh et al. 1985) further detailed the near-field properties and emphasized the importance of studying the different characteristics of near-field characteristics and their co-relation with Peak Ground Acceleration (PGA), Peak Ground Velocity (PGV) and Peak Ground Displacement (PGD) and concluded that PGA did saturated and showed up less dependency upon source distance, while PGV and PGD show a somewhat stronger dependency but due to lack of near-field ground motion datasets, the study was not able to conclude the characteristics appropriately.

(Bolt et al. 2003) defines Near-fault ground motions as motions which often contain large long-period (2–5 s) wave pulses. They can be generated by (i) constructive interference of the radiated waves due to the directivity of the fault rupture, or (ii) movement of the ground associated with the permanent geodetic offset. To distinguish b/w the two effects, separate, the terms "directivity pulse" and "fling-step" are coined for the rupture directivity and elastic rebound effects, respectively. **Krawinkler et al. 1998).**

2.3. Characterization of near and far field ground motions

The rupture directivity effect is essentially a manifestation of Doppler's effect in seismic wave propagation and affects the ground motion in a fault parallel direction. This occurs when velocity of the rupture is close to velocity of the shear waves in rock mass near the source. When compared to seismic waves seen at an equally spaced location in the opposite direction of the direction of the fault rupture, seismic waves at a site in the direction of the fault rupture will have a higher frequency. This phenomenon is illustrated schematically in Figure 2.1. The rupture directivity effect, in particular, causes a large amplitude, short duration pulse at the site in the direction of the rupture and a small amplitude, long duration pulse at the site in the direction opposite to the direction of the fault rupture.

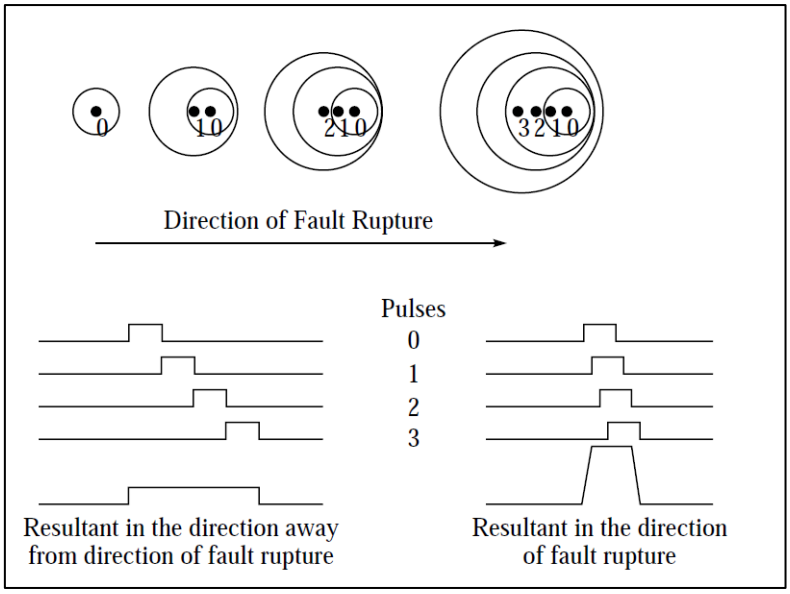

Figure 2.1 Illustration of directivity effect on ground motion at sites toward and away from the direction of fault rupture (Singh et al. 1985)

The 1999 Turkey and Taiwan earthquakes produced some near-field strong motion data that revealed some permanent ground displacement that happens over a ruptured fault. This static displacement termed the fling step, occurs over a finite time interval of several seconds as the fault slip is developed. The fling step involves a large, unidirectional velocity pulse to accommodate this displacement in the slip-parallel direction and is not strongly coupled with the rupture directivity pulse. In strike-slip faulting, the directivity pulse occurs on the strike-normal component while the fling step occurs on the strike-parallel component. In dip-slip faulting, both the fling step and the directivity pulse occur on the strike-normal component. Figure 2.2 shows a schematic illustration of the orientations of fling step and rupture directivity pulse.

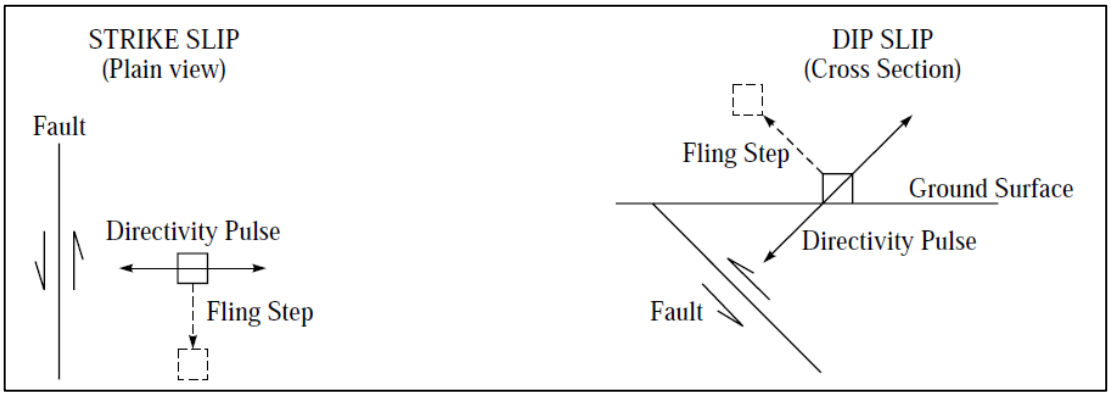

Figure 2.2 Schematic illustration of the orientations of fling step and directivity pulse in strike-slip and dip-slip faults (Singh et al. 1985)

The most destructive aspect of the rupture directivity effect is the large velocity pulse, which might result in one yield reversal with a large ductility demand. On the other hand, the fling step affects the peak velocity and displacement of ground motions. These near-fault source effects, which comprise brief and impulsive ground motions, cannot be adequately described in the frequency domain which characterizes a uniform distribution of energy throughout the duration of motion. Thus, the conventional characterization of design ground motion in the form of response spectra needs to be augmented with a simplified description of the near-source pulses in the time domain. A simple characterization is indeed possible with the use of approximate period of the dominant pulse (Tv), Peak Horizontal Velocity (PHV), and the number of significant half-cycles of motion in the larger, fault-normal direction **(Krawinkler et al. 1998).**

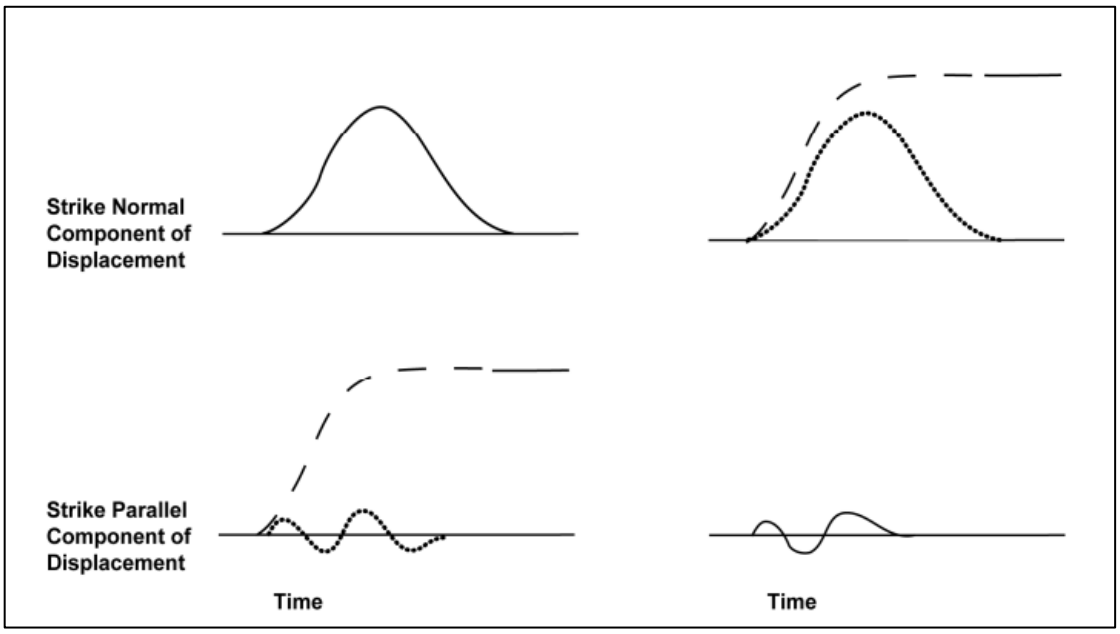

Figure 2.3 Schematic partition of the rupture directivity pulse and fault displacement between the strike normal and strike parallel components of ground displacement. Waveforms containing static ground displacement are shown as dashed lines; versions of these waveforms with the static displacement removed are shown as dotted lines. (Krawinkler et al. 1998)

2.4. Understanding the nature of near and far field ground motions

Burks et al. 2014

The basic aim of this study revolves around computing the structural capacity of nonlinear SDOFs using multiple versions of the same ground motion record, including a baseline corrected version with static offsets preserved, a filtered version from the NGA database with static offsets removed, and artificial versions with an idealized pulse added to the filtered record.

Three idealized pulses referred to as type *A*, type *B*, and type *C*, to analyze the effects, where type *A* and type *C* represent fling and type *B* represents a directivity pulse with no static offset. 40 variations of each type of pulse, each with a different Tp and a constant maximum acceleration, Ap (each set of pulses was additionally high-pass filtered at a cutoff frequency, *fc*, of 0.2 Hz and 0.5 Hz to investigate the effect of record filtering on collapse capacity (Makris et al. 2004).

With the other two fling parameters remaining constant, each fling parameter was changed 40 times, giving each recording a total of 120 pulse C displacements. Also, pulse C displacements to each filtered NGA recording were added in order to represent the artificial fling to filtered near-fault records (Stewart et al. 2001, Abrahamson et al. 2002).

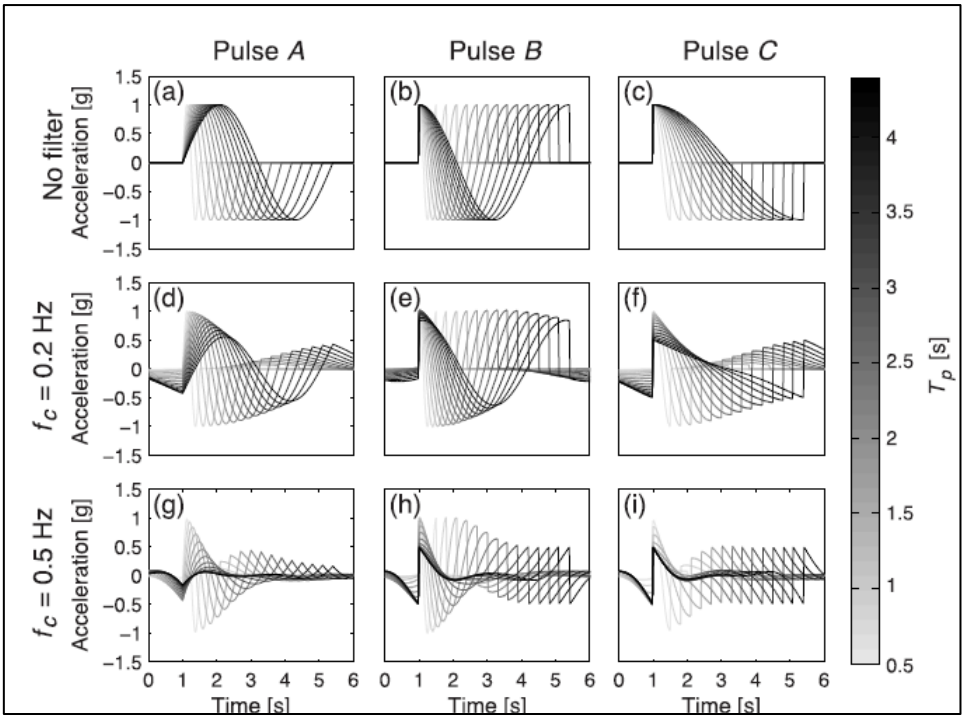

Figure 2.4 Acceleration time histories of selected pulses used to compute collapse capacity (Burks et al. 2014)

Table 2.1 Fling parameters of the baseline corrected versions of the three ground motion records used in this study (Burks et. al. 2014)

EQ Name	Year	Mw	Station Name	Orientation	Dp (cm)	Tp (s)	t_1 (s)
Chi-Chi	1999	7.6	TCU068	N/S	551.0	3.19	33.9
Darfield	2010	7.0	GDLC	E/W	134.2	3.37	17.9
Kocaeli	1999	7.5	YPT	N/S	148.4	2.84	10.2

where Dp is displacement amplitude, Tp is pulse period, and t_1 is the arrival time

Two systems namely SDOF 1 (natural period of 1.32 s) and SDOF 2 (natural period of 3s). SDOF 1 is based on an SDOF approximation of a 4- story experimental structure **(Lignos et al. 2011)** and SDOF 2 with a longer natural period is closer to the observed pulse periods from the recorded ground motions.

Until instability and collapse take place, Incremental Dynamic Analysis (IDA) is accomplished by incrementally scaling up a single ground motion and computing a structural demand parameter, such as inter-story drift or floor acceleration. The IDA is repeated for a set of ground motions to get a probabilistic description of collapse **(Ibarra et al. 2005)**. On SDOF 1, several IDAs were carried out using the idealized pulse ground motions, which were categorized according to the pulse type and filter cutoff frequency.The filter cutoff frequency of 0.2 Hz has a negligible effect on the collapse capacity for all pulse types, while the cutoff frequency of 0.5 Hz causes an

increase in collapse capacity for all pulse types. This rise is likely due to decrease in the energy of pulses from filtering.

For all three records, the version with static offsets preserved via baseline correction and the version with static offsets removed via filtering from the NGA database resulted in a similar collapse capacity. This shows that the dynamic part of the fling is kept even though the static offset is removed from the NGA version. Additionally, the filtered NGA version's collapse capacity was reduced for the majority of records and fling parameters when pulse C was added. The collapse capacity did, however, increase in a few notable cases, such as a few tiny displacement amplitudes for the TCU068 record and extremely brief periods for all records.

2.5. Defining parameters of near and far-field ground motions

Near-field ground motions are characterized by several parameters out of which the distance closest to the rupture fault and the ratio PGV/PGA is the most prominent to be studied. Table 2.2 describes parameters adopted by different literature.

Table 2.2 Literature for defining NF ground motions

Sr. No.	Reference	R_{jb} (km)	PGV/PGA (sec)
1	Kalkan et. al. 2006	-	>0.1
2	Adanur et. al. 2012	<10	>0.1
3	Zhang and Wang 2013	-	>0.1
4	Davoodi et. al. 2015	<30	>0.1
5	Sharma et. al. 2021	<15	>0.1
6	Nabid et. al. 2019	<12	>0.1
7	Bhandari et. al. 2019	<15-20	>0.1
8	Emamikoupaei et. al. 2023	-	>0.1

2.6. Ground motion parameters related to near-field ground motions

(Poreddy et al. 2022)

The study focuses on the relationship between ground motion parameters (GMPs) and seismic damage of different types of structures subjected to a set of near-field ground motions with magnitudes ranging from M_w 6.9 – M_w 8.8. When engineers do seismic studies of structures, it is well recognized that peak ground values of acceleration, velocity, and displacement are more significant. Peak values alone, though, do not

reveal the full extent of powerful ground motions' ability to harm structures. Therefore, a total of 16 parameters are selected to analyze the relationship with strong ground motions which are defined as follows-

Table 2.3 Ground motion parameters used for analysis in this study (Poreddy et al. 2022)

Sr. No.	Parameter	Definition/Mathematical Formulation	Reference
1	Peak Ground Acceleration (PGA)	The maximum absolute value of acceleration time history obtained from the accelerogram	(Gutenberg et al. 1942)
2	Peak Ground Velocity (PGV)	The maximum absolute value of velocity time history	(Rosenblueth et al. 1964)
3	Peak Ground Displacement (PGD)	The maximum absolute value of displacement time history	(Newmark et al. 1973)
4	Significant Duration	$T_{\text{sig}} = T_{5-95\%}([a(t)]^2)$	(Trifunac et al. 1975)
5	PGV/PGA	The ratio between PGV and PGA of the ground motion	
6	Root Mean Square Acceleration (Arms	$a_{rms} = \sqrt{\frac{1}{T_{\text{sig}}}\int_{t_1}^{t_2}[a(t)]^2 dt}$	(Housner et al. 1964)
7	Root Mean Square Velocity (Vrms)	$v_{rms} = \sqrt{\frac{1}{T_{sig}}\int_{t_1}^{t_2}[v(t)]^2 dt}$	
8	Arias Intensity (Ia)	$I_a = \frac{\pi}{2g}\int_0^{T_{sig}}[a(t)]^2 dt$	(Arias,1970)
9	Characteristic Intensity (Ic)	$I_c = (a_{RMS})^{1.5} \cdot (T_{sig})^{0.5}$	(Park et al. 1985)
10	Specific Energy Density (SED)	$= \int_0^{T_{sig}}[v(t)]^2 dt$	
11	Cumulative Absolute Velocity (CAV)	$= \int_0^{T_{sig}}\lvert a(t)\rvert dt$	(EPRI et al. 1988)
12	Acceleration Spectrum Intensity (ASI)	$ASI(\xi) = \int_{0.1}^{0.5} PSA(\xi_{0.05}, T)dT$	(Von Thun et al. 1988)
13	Velocity Spectrum Intensity (VSI)	$\text{VSI}(\xi) = \int_{0.1}^{0.5} \text{VSA}\ (\xi_{0.05}, T)dT$	(Housner et al. 1952)
14	Sustained Maximum Acceleration (SMA)	The third highest absolute value of acceleration in the time history record	(Nuttli et al. 1979)
15	Velocity Pulse Amplitude (A_{Pulse})	The ground motion contains large motions with pulse wave forms that differ from either in the acceleration, velocity, or displacement time series.	
16	Velocity Pulse Period (TPulse)	Time is taken to complete one cycle in the velocity pulse waveform.	

For the analysis, three types of buildings namely, low-rise buildings, mid-rise buildings, and high-rise buildings whose fundamental periods are 0.4 s, 0.82 s, and 1.1 s respectively are chosen.

The correlation coefficients b/w different parameters are described below in table-

Table 2.4 Correlation coefficients of ground motion parameters and damage of

different types of buildings (Poreddy et al. 2022)

	PGA	PGV	PGD	T_D	$(V/A)_{max}$	A_{rms}	V_{rms}	AI	Ic	SED	CAV	ASI	VSI	SMA	A_{Pulse}	T_{Pulse}	D_L	D_M	D_H
PGA	1.00																		
PGV	0.27	1.00																	
PGD	0.14	0.30	1.00																
T_D	0.18	0.34	-0.04	1.00															
$(V/A)_{max}$	-0.51	0.37	-0.06	-0.03	1.00														
A_{rms}	0.80	0.47	0.08	0.54	-0.43	1.00													
V_{rms}	0.09	0.73	0.77	0.26	0.30	0.25	1.00												
AI	0.44	0.49	0.02	0.82	-0.18	0.80	0.32	1.00											
Ic	0.60	0.28	0.08	0.60	-0.37	0.77	0.14	0.58	1.00										
SED	0.04	0.56	0.40	0.33	0.21	0.23	0.63	0.24	0.37	1.00									
CAV	0.38	0.48	0.01	0.92	-0.14	0.76	0.31	0.97	0.68	0.32	1.00								
ASI	0.86	0.38	0.16	0.39	-0.52	0.90	0.17	0.63	0.76	0.14	0.59	1.00							
VSI	0.36	0.74	0.10	0.65	-0.03	0.71	0.50	0.81	0.48	0.54	0.80	0.53	1.00						
SMA	0.80	0.42	0.23	0.40	-0.47	0.86	0.27	0.66	0.76	0.21	0.63	0.92	0.58	1.00					
A_{Pulse}	0.21	0.91	0.13	0.31	0.39	0.43	0.62	0.51	0.19	0.47	0.48	0.31	0.75	0.38	1.00				
T_{Pulse}	-0.27	0.25	-0.06	0.01	0.62	-0.27	0.19	-0.13	-0.14	0.12	-0.09	-0.25	-0.09	-0.26	0.23	1.00			
D_L	-0.11	0.11	0.21	-0.02	0.16	-0.04	0.21	-0.04	-0.08	0.01	-0.02	-0.07	0.03	-0.11	0.08	0.21	1.00		
D_M	-0.22	0.07	0.20	-0.03	0.30	-0.18	0.24	-0.11	-0.19	0.20	-0.10	-0.20	0.01	-0.21	0.09	0.29	0.71	1.00	
D_H	-0.17	0.08	0.21	-0.01	0.26	-0.13	0.25	-0.06	-0.16	0.18	-0.06	-0.15	0.03	-0.17	0.09	0.26	0.77	0.97	1.00

where Yellow has a Very Strong correlation (0.9-1.0), Orange has a Strong correlation (0.7-0.89), and Blue has a Moderate correlation (0.4-0.69).

Therefore, it can be concluded that PGA is strongly correlated with A_{rms} (0.8), ASI (0.86), and SMA (0.8). Given that the pulse velocity is generated from the velocity time history the parameter PGV is very strongly correlated with A_{Pulse} (0.91). However, PGV is strongly correlated with V_{rms} (0.73).

2.7. Performance of RC frames under near and far- field

Moniri et al. 2017

The aim of this study revolves around acquiring the responses of 6, 10 and 15-storey moment RC frames to near-fault ground motions and the extent of differences existing in comparison with those of far-fault ground motions using critical parameters like maximum top displacements, inter-storey drift ratios (IDR) using the incremental dynamic analysis (IDA) method.

14 far-field and 14 near-field ones i.e.,total 28 ground motion records have been used, for this purpose. Far-field ground motions of 6.1–7.5 magnitudes at distances 50–115 km from the site and recorded on soft or firm soils are the first group of records. The second group involves near-field ground motions of 6.6 and 7.6 magnitude recorded at

distances 0.24–11 km from the site and on soft or firm soils.

28 records for each building model i.e., 84 nonlinear time history analyses have been obtained.

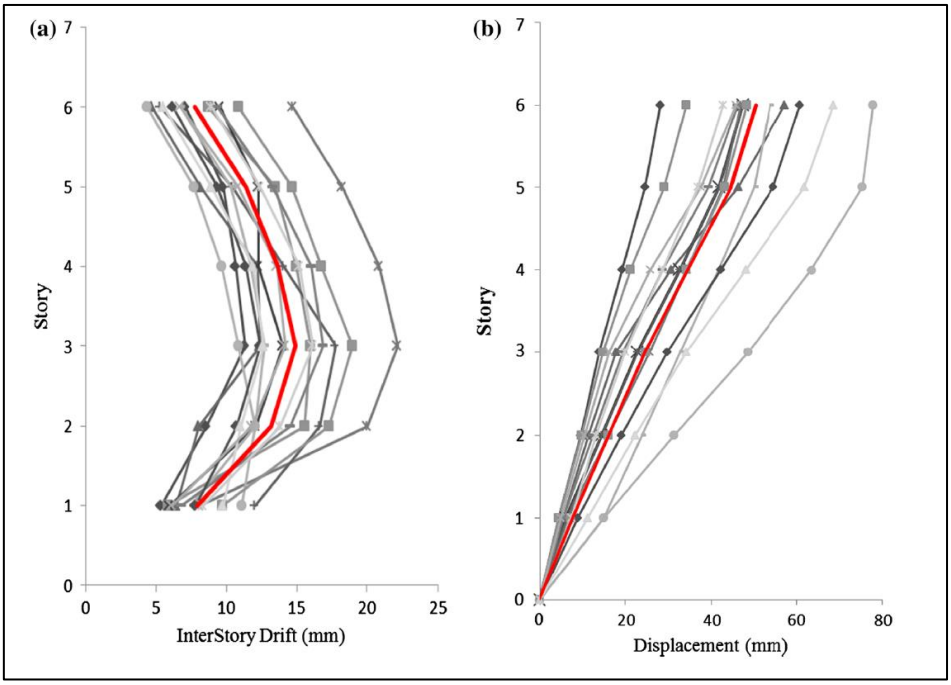

Figure 2.5 Seismic response for 6-storey RC frame under far fault ground motions; (a) inter- Storey Drift's profile, (b) top displacement profile (Moniri et al. 2017)

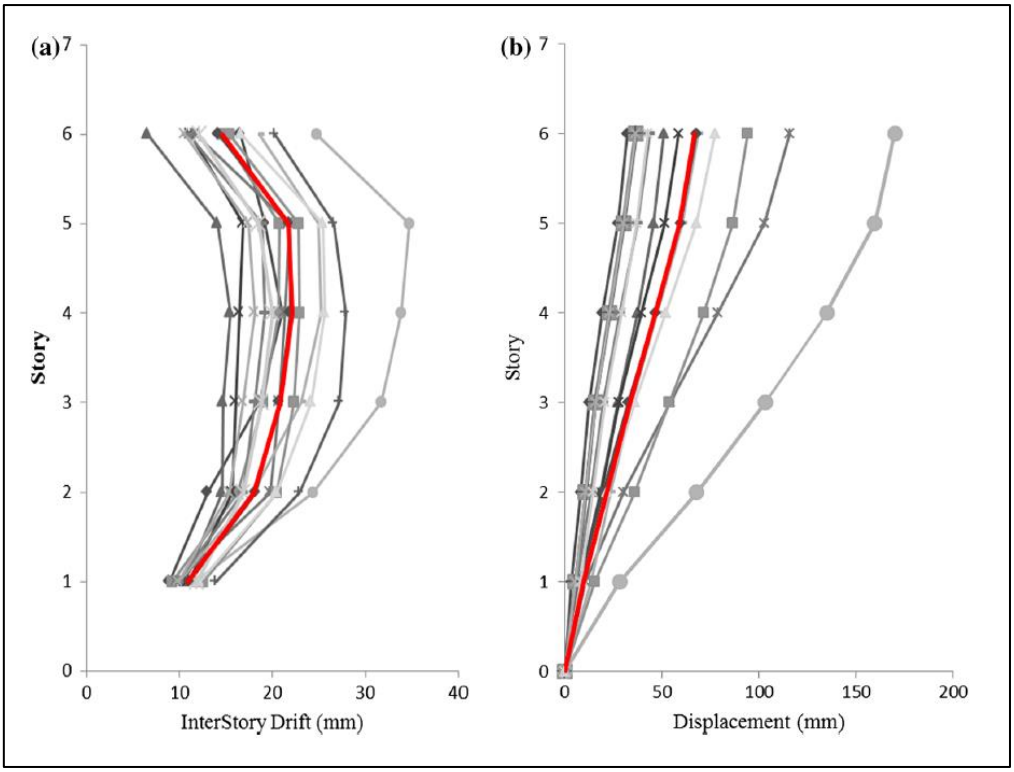

Figure 2.6 Seismic response for 6-storey RC frame under near-fault ground motions; (a) inter- Storey Drift's profile, (b) top displacement profile (Moniri et al. 2017)

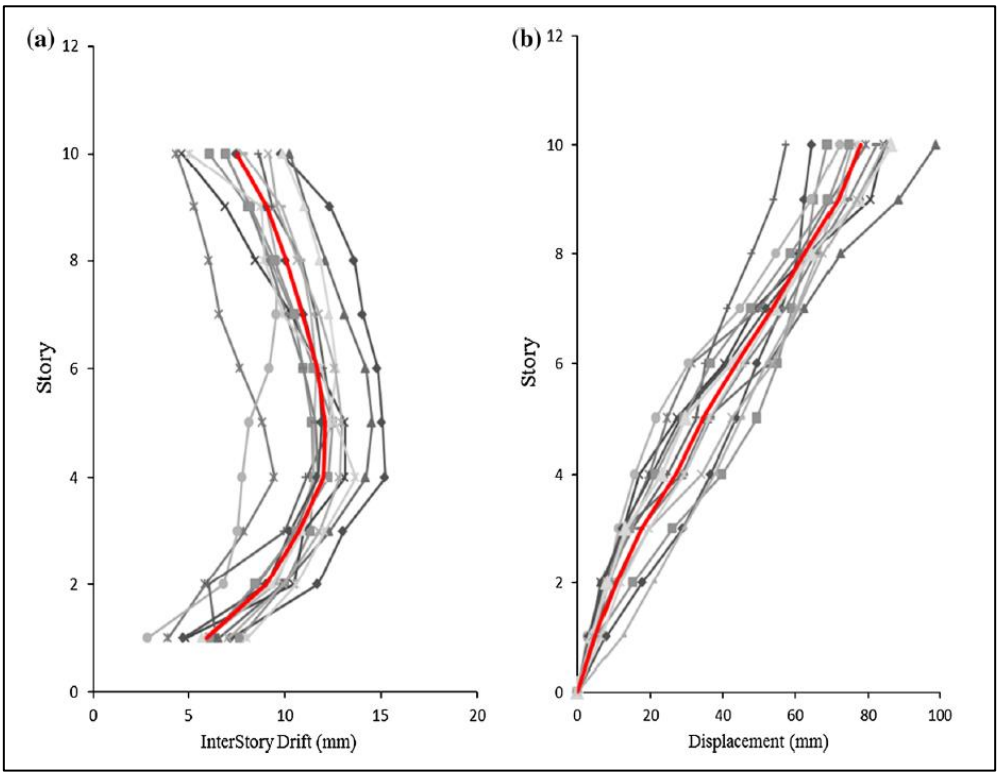

Figure 2.7 Seismic response for 10-storey RC frame under far fault ground motions; (a) inter- Storey Drift's profile, (b) top displacement profile (Moniri et al. 2017)

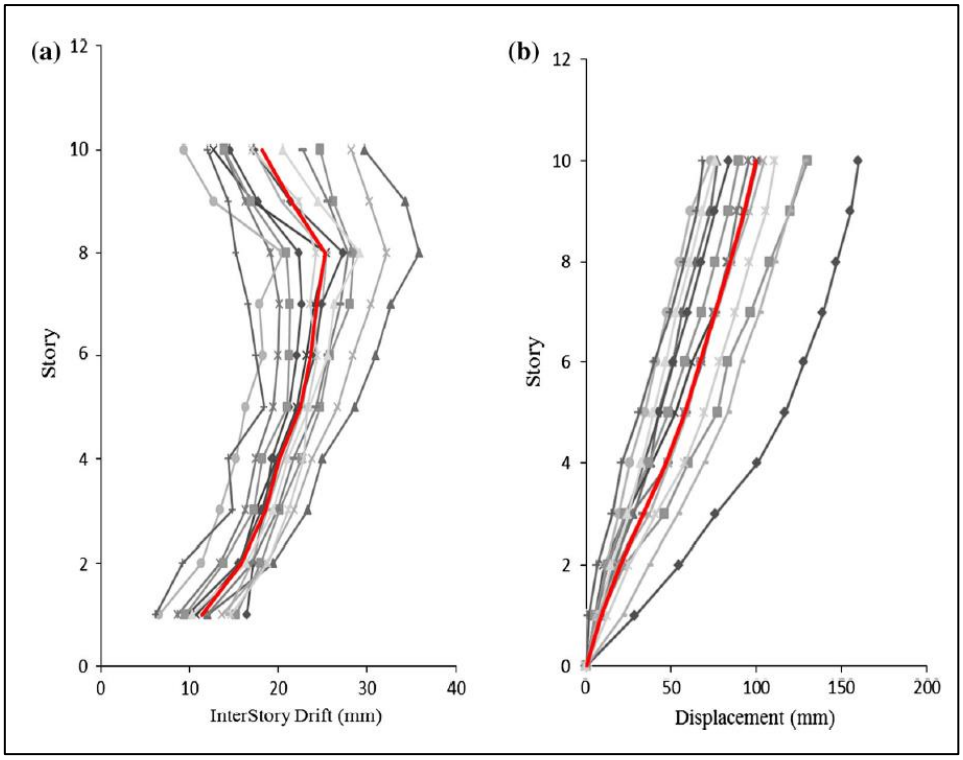

Figure 2.8 Seismic response for 10-storey RC frame under near-fault ground motions; (a) inter- Storey Drift's profile, (b) top displacement profile (Moniri et al. 2017)

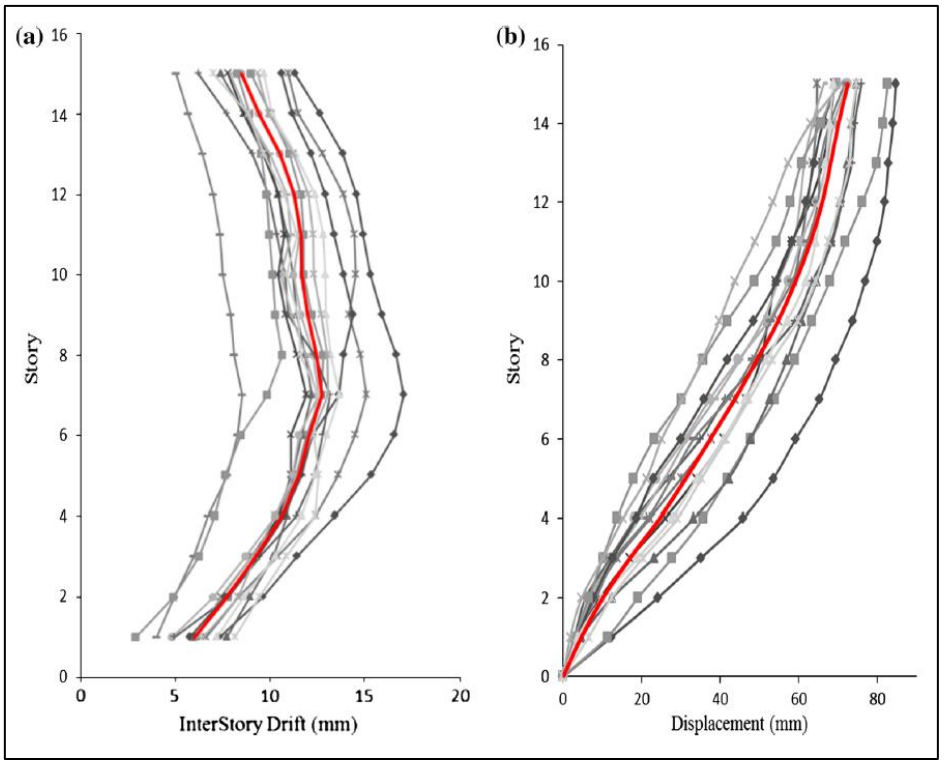

Figure 2.9 Seismic response for 15-storey RC frame under far fault ground motions; (a) inter- Storey Drift's profile, (b) top displacement profile (Moniri et al. 2017)

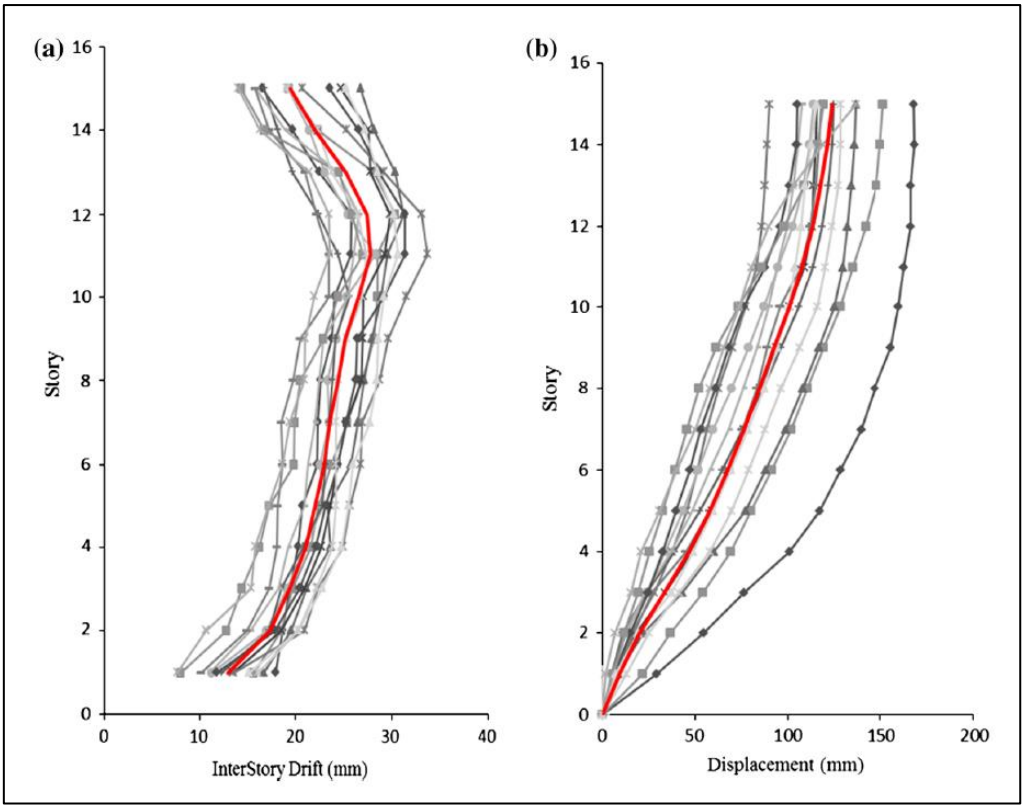

Figure 2.10 Seismic response for 15-storey RC frame under near-fault ground motions; (a) inter- Storey Drift's profile, (b) top displacement profile (Moniri et al. 2017)

The results show that inter-story drift is more significant in near-field records as compared to far-field records. Near-field records also tend to introduce significant demands on the upper floors of the structure.

A similar trend was observed by Displacement graphs, being more in near-field as compared to far-field ones.

Far-fault motions enter input energy into the system gradually. Although, on average, deformation demands are less than those in the near-fault records, structural systems are subjected to more plastic cycles. Therefore, the cumulative effects of far-fault records are minor.

2.8. Fragility Curve under Incremental Dynamic Analysis

(Nazri et al. 2015)

A new approach for seismic design has been discussed namely performance-based seismic design (PBSD), which is a new approach to earthquake-resistant design of structures. The main aim of this study is to derive fragility curves of steel and concrete

frames and calibrate Incremental Dynamic Analysis (IDA) curves based on building materials and frame heights.

In this study, structure frames, which are three and six storeys in height, are to analyse the dynamic loading of the structures. Seven ground motions classified as Near Field (NF) and Far Field (FF) excitations are used for analysis purposes. The following criteria were used to select the ground motion records: (a) for NF the Joyner–Boore distance is less than 20 km, however it is more than 20 km for FF records(Li et al. 2015) and (b) the earthquake magnitude is within the range of 5–6. These ground motions were scaled to correspond to the spectra of the elastic response. The elastic response spectra generated ranged from 0.05 to 0.6 g in increments of 0.05 g.

The five performance levels prescribed by FEMA-273 namely Operational Phase (OP) with 0.5% drift, Immediate Occupancy (IO) with 1% drift, Damage Control (DC) with 1.5% drift, Life Safety LS with less than 2.5% drift, and Collapse Prevention (CP) with more than 2.5% drift are used as structure performance benchmarks in generating the IDA curve.

The fragility curve is defined as a log-normal function that expresses the probability of reaching or exceeding a specific damage state. The fragility curve is a highly useful method for predicting the extent of probable damage.It can indicate the likelihood that a structure will sustain damage beyond a specific state when subjected to different levels of ground shaking **(Silva et al. 2014. Ibrahim et al. 2011)**

The following conclusions from the above-mentioned study performed can be-

(i) The drift profiles of the three- and six-storey structures under the NF records are almost similar. However, they have a different drift percentage. Similar findings are obtained from the structures under the FF records. The drift profiles indicate that the steel frame is stiffer than the concrete frame for the three-storey structures under the NF and FF records. For six-story constructions, the NF and FF records show that the concrete frame is stiffer than the steel frame.

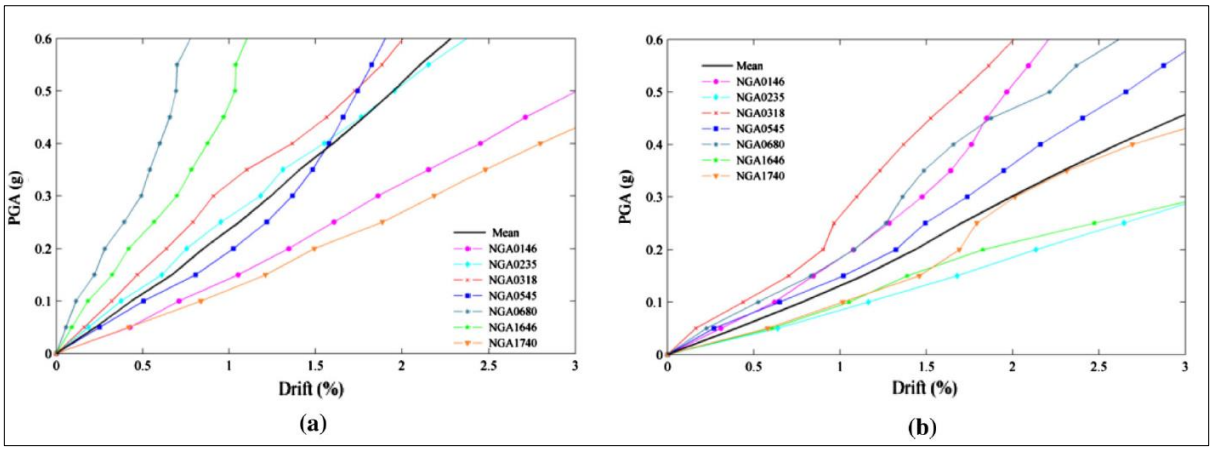

Figure 2.11 IDA curves based on NF records for a (a) three-storied concrete frame structure. (b) Six-storey concrete frame (Nazri et al. 2015)

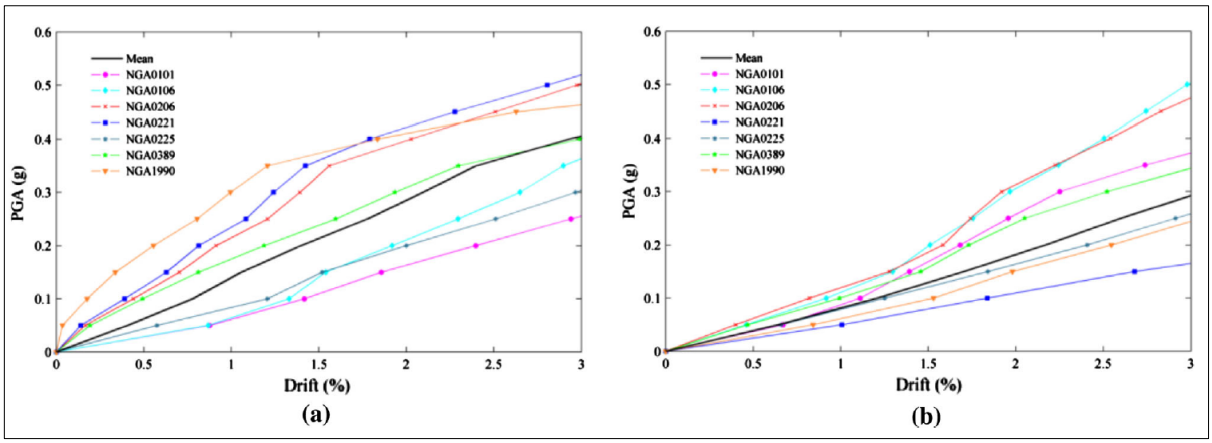

Figure 2.12 IDA curves based on FF records for a (a) three-storied concrete frame structure. (b) Six-storey concrete frame (Nazri et al. 2015)

(ii) Based on the ground motion data for NF, the three-storey steel frame exhibits the highest probability of attaining or exceeding the OP (72%) and CP (7%) values.The concrete frame has the highest probability of reaching or exceeding the OP level at 98% for the six-storey structures. The steel frame has the highest probability of damage at the CP level (50 %). The concrete frame has the highest probability of reaching or exceeding the OP level based on the FF records, which registers 89% for the three-storey structures and 100% for the six-storey structures. Additionally, the concrete frame has the highest probability for both storeys at the CP level, registering 5% for three- and six-story constructions, respectively.

(iii) A comparison of the fragility curves between NF and FF records revealed that the FF records had a higher likelihood of reaching the OP level. Concrete material exhibited a higher probability of OP for both NF and FF records. However, NF records showed

that at the CP level stage, the steel frame construction had the highest likelihood of damage. Meanwhile, a concrete frame has the highest probability of damage for the frame structure exposed to the FF records.

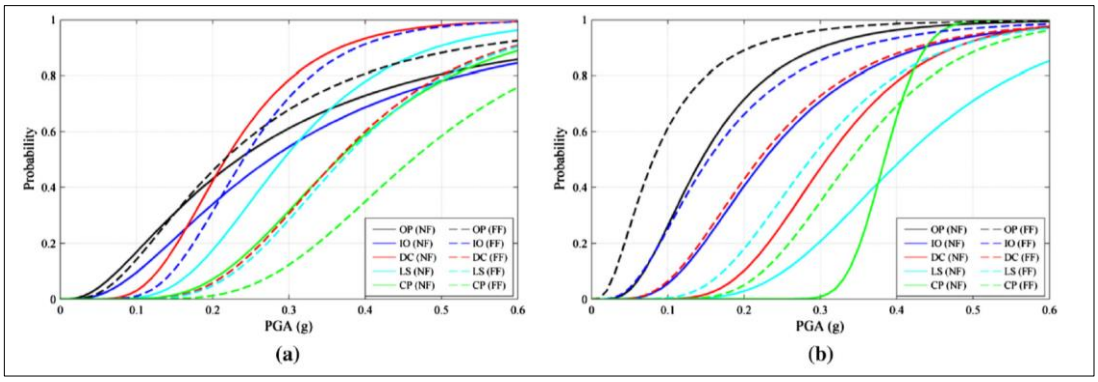

Figure 2.13 Fragility curve for a three-storey frame. (a) Fragility curve for a steel frame. (b) Fragility curve for a concrete frame (Nazri et al. 2015)

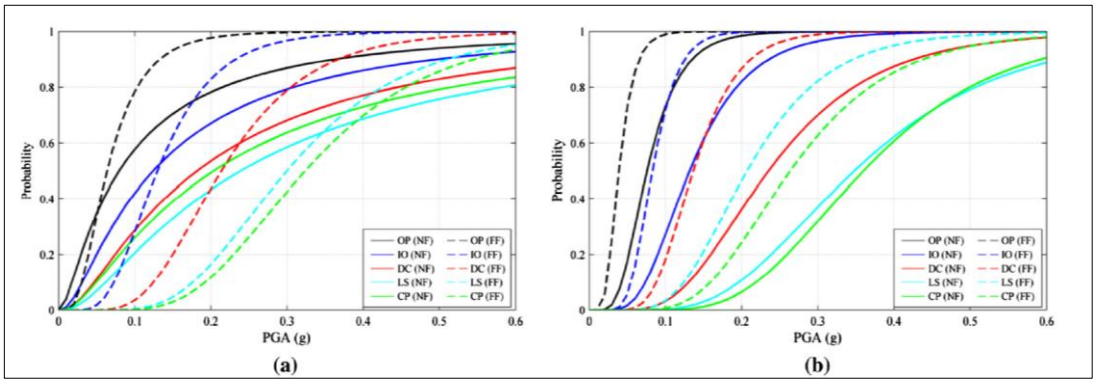

Figure 2.14 Fragility curve for a six-storey frame. (a) Fragility curve for a steel frame. (b) Fragility curve for a concrete frame (Nazri et al. 2015)

2.9. Summary and Research Gap

From the review made regarding the non-linear analysis of a structure using near-field and far-field ground motion, only PGA and PGV are the most efficient parameters for the assessment of seismic damage to date and corresponding factors for design.

The near-field ground motions exhibit pulse-like ground motions which constitute a significant challenge to the performance of buildings, as they are characterized by long intense velocity, displacement, or acceleration pulses.

Since NF ground motions exhibits strong pulse-like waves, which exhibits a completely different nature as compared to FF ones. Therefore, there is a need to characterize the ground motions differently and apply to a portal frame in order to observe the effects

on seismic response by application of both types of ground motions.

Selection of ground motions parameters and their correlation is another crucial study which needs to be carried out in to observe the effects of NF and FF ground motions.

CHAPTER - 3

WORK METHODOLOGY

3.1. Overview

The present study discusses the overall workflow and adopted methodology to see the effects of NF and FF ground motions. The input ground motion characterization has been discussed briefly. Modelling of two different configurations of reinforced concrete (RC) building frames has been done using SAP: 2000. Beams and columns are modelled as flexible members, while the equivalent diagonal strut method has been adopted to model Masonry infill. NF and FF ground motions are applied and the effects of both these are observed via different parameters after successfully performing Non-Linear Time History Analysis (NLTHA).

3.2. Work Methodology

Earthquake records for two types of ground motions namely Near Field (NF) and Far Field (FF) earthquake records were collected in the form of time history (acceleration vs time) from PEER-NGA West 2. The raw data is treated as input data to the modelled frame as discussed in the coming sections. After running the complete analysis, the required output parameters are derived. The workflow of the process in discussed below-

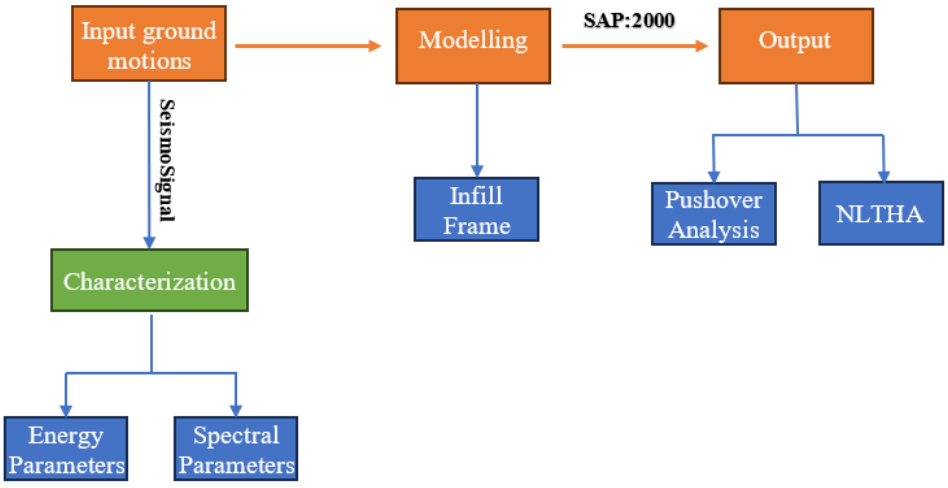

Figure 3.1 Workflow chart of the adopted methodology

3.2.1. Softwares Used

1. SeismoSignal v2023- SeismoSignal is a signal processing software that constitutes an easy and effective way to process strong-motion data, having a user-friendly interface and being capable of deriving several strong-motion parameters at any instant. The software is capable to read accelerograms saved in different text file formats, which may then be filtered and baseline-corrected. Polynomials up to the 3rd order may be employed for the latter, whilst three different digital filters are available, all of which capable of carrying out, causal or acausal, high pass, lowpass, bandpass and band stop filtering.

2. Microsoft Excel- It is a software program by Microsoft that uses spreadsheets to organize numbers and data with formulas and functions. It consists of various features which make it simple to access data in graphical format and make derive further results from the same.

3. SAP-2000 (v19.2.1)- SAP2000 is general-purpose civil-engineering software used for the analysis and design of any type of structural system, including stadiums, towers, industrial plants, offshore structures, piping systems, buildings, dams, soils, machine parts and many others.
4. Plot Digitizer (v2.6.9)- PlotDigitizer is a data extraction tool that allows users to extract data from graphs and scientific visuals. For this purpose, the image is imported into the software. After that, both the axes are calibrated with the image and the required plot is selected in order to further extract data.

3.2.2. Input ground motion parameters

For analysis purposes, PEER-NGA West-2 was used to collect an unscaled data file for a particular earthquake by defining the characteristic and parameters required. The clubbed data is downloaded in the form of zip format having various notepad files containing different acceleration files of that earthquake with an excel file sorted according to the parameters of the earthquakes. The raw acceleration file was used as an input in SeismoSignal to analyze and obtain the different properties and plots for the earthquake. The required plots were made from the data extracted from the

SeismoSignal.

3.2.3. Modelling

Three-bay, four-story (3B-4S) frames were modelled to validate the research carried out by Kaushik *et. al. 2009*. RC frame is assumed to be fixed at the bottom and soil-structure interaction in the present study. 3B-4S frame is modelled for validation purposes as discussed further, while single storied frame derived from 3B-4S was used for further study. The structural details of the frame are shown in Figure 3.2

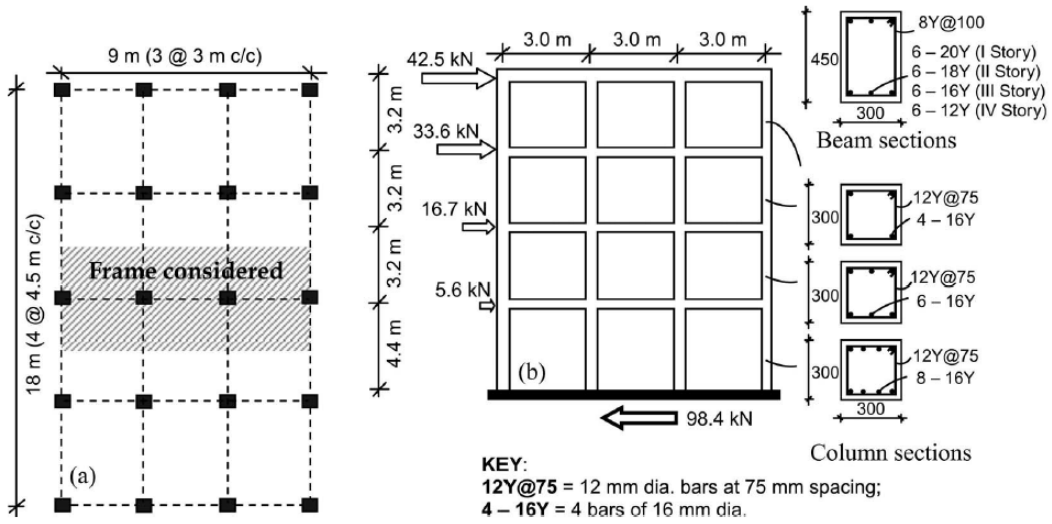

Figure 3.2 Details of the four-story RC building considered in the present study (a) Plan of the building; (b) Elevation of the frame and section (Kaushik et. Bal., 2009)

Two types of configurations have been modelled as listed below-

a. Bare Frame (BF)- No masonry infill provided. The strength and stiffness of the infill are neglected in all stories (Figure 3.3 (a)).
b. Fully-infilled Frame (FI)- Masonry infill is provided at all story levels. The strength and stiffness of the infill are ignored in all stories (Figure 3.3 (b)).

The sections are designed in "Section Designer" of SAP:2000, in order to facilitate fibre hinges and sections as discussed in further sections. The detailed modelling for both frames has been discussed in further contexts.

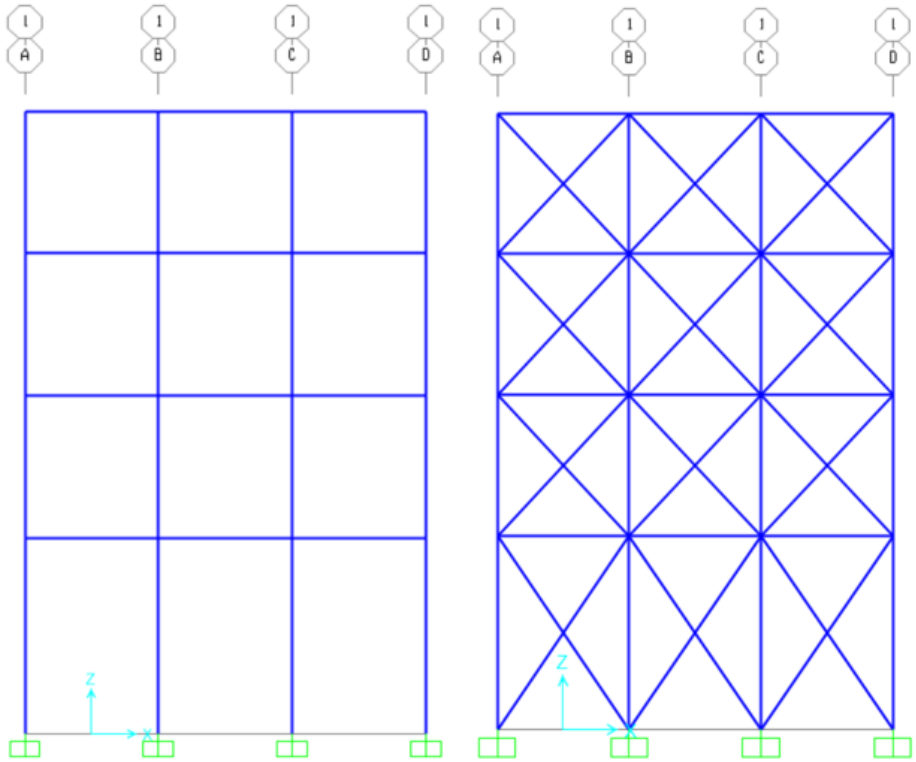

(a) (b)

Figure 3.3 3B-4S frame modelled in SAP:2000 for validation (a) BF (b) FI

Bare frame (BF)

The four-story bare frame was modelled in SAP:2000 as shown in Figure 3.2 (a) with the use of material properties as listed in Table 3.1.

Table 3.1 Material properties of BF (Kaushik et. al. 2009)

Concrete	
M25	Cube strength f_{ck}=25MPa, Modulus of elasticity of concrete E_c=25000MPa
Steel	
Fe415	Yield Strength, f_y=415MPa
Strain at the onset of strain hardening	0.02
Ultimate Strain Capacity	0.13

Fully-Infill Frame (FI)

The four-story fully-infilled frame was modelled in SAP:2000 with the material properties as listed in Table 3.2

Table 3.2 Material Properties of FI as input in software (Kaushik et. al. 2009)

Concrete	
M25	Cube strength f_{ck}=25MPa, Modulus of elasticity of concrete E_c=25000MPa
Steel	
Min. Yield Strength	f_y=415 MPa
Min. Tensile Stress	f_u=518.750 MPa
Excepted Yield Stress	f_{ye}=456.50 MPa
Excepted Tensile Stress	f_{ue}=666.5938 MPa
Strain at the onset of strain hardening	0.02
Ultimate Strain Capacity	0.025
Infill	
E_m=550 f_m' (where f_m' is the masonry prism strength in MPa) =550×4.1=2255 MPa	

Stress-strain values for the infill material for 1:0:6 material are as shown in Table 3.1. The stress-strain curve for the same is shown in Figure 3.4

Table 3.3 Stress-strain relationship for 1:0:6 material (Kaushik et al 2007)

Stress (MPa)	Strain
1.4	0.0009
3.1	0.0021
3.7	0.0029
4.1	0.0036
2.6	0.0059

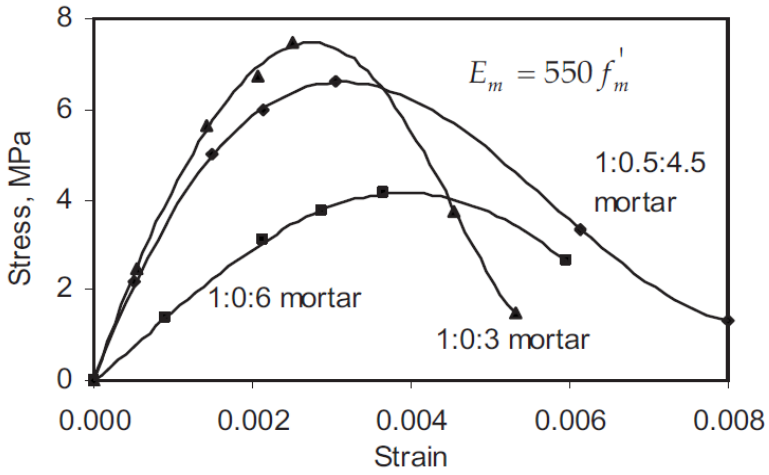

Figure 3.4 Stress-strain curve adopted for masonry (Kaushik et al 2007)

A damping of 5% has been considered and a combination of (DL+0.25*LL) has been analyzed as Gravity load, before Non-Linear Analysis.

Load Calculations

Dead Load

Distributed Load = Unit Weight of Concrete × Thickness × Unit length

Ground Floor = 25kN/m^3 × 0.12 m × 1m = 3kN/m

First Floor = 25kN/m^3× 0.12 m × 1m = 3kN/m

Second Floor = 25kN/m^3 ×0.12 m ×1m = 3kN/m

Third Floor = 25kN/m^3 ×0.12 m ×1m = 3kN/m

Live Load

Ground floor:

Total Load one whole floor = 2kN/m^2 × 4.5m × 9m = 81kN

Distributed Live load on slab = $\frac{81\ kN}{9\ m}$ = 9 kN/m

First floor:

Total Load one whole floor = 2kN/m^2 ×4.5m× 9m = 81kN

Distributed Live load on slab = $\frac{81\ kN}{9\ m}$= 9 kN/m

Second floor:

Total Load one whole floor = 2kN/m^2 ×4.5m ×9m = 81kN

Distributed Live load on slab = $\frac{81\ kN}{9\ m}$ = 9 kN/m

Third floor:

Total Load one whole floor = 0.75kN/m^2 ×4.5m ×9m = 30.375kN

Distributed Live load on slab = $\frac{30.375\ kN}{9\ m}$ = 3.375 kN/m

Infill Load

For the calculation of infill load, the frame is idealised in order to derive load for a general frame as shown in Figure 3.5.

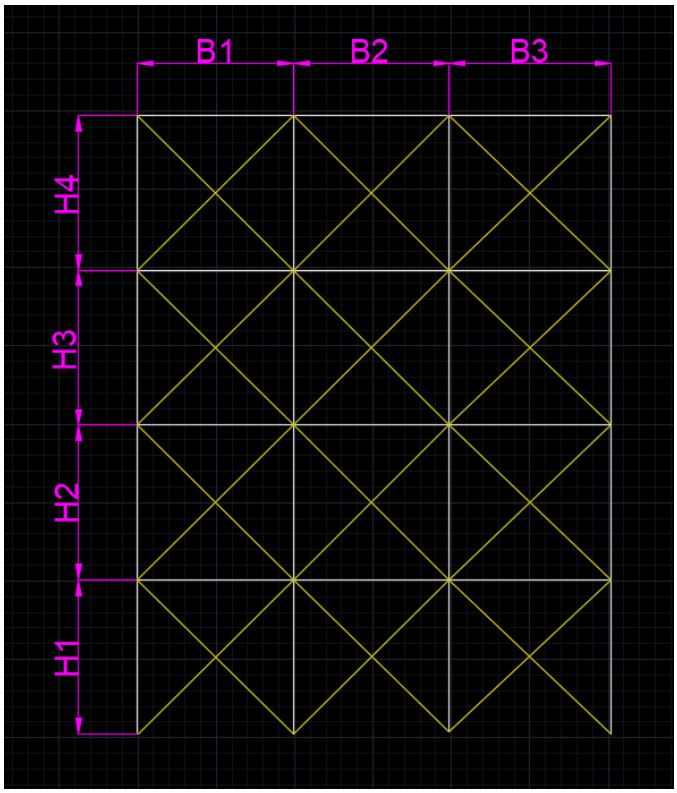

Figure 3.5 Representative model for infill load calculation for 3B-4S frame

Ground floor:

Volume enclosed = $\left(\frac{\{(B1 \times H2) + (B2 \times H2) + (B3 \times H2)\}}{2} + \frac{\{(B1 \times H1) + (B2 \times H1) + (B3 \times H1)\}}{2}\right)$xt

= $\left(\frac{\{(3 \times 3.2) + (3 \times 3.2) + (3 \times 3..2)\}}{2} + \frac{\{(3 \times 4.4) + (3 \times 4.4) + (3 \times 4.4)\}}{2}\right)$ x 0.22

= 7.524 m^3

Total weight = (Volume enclosed × 18) kN = 135.432 kN

Distributed weight = $\frac{Total\ weight}{B1+B2+B3}$ = $\frac{135.432}{9}$ = 15.048 kN/m

First floor:

Volume enclosed = ($\frac{\{(B1 \times H3) + (B2 \times H3) + (B3 \times H3)\}}{2}$ + $\frac{\{(B1 \times H2) + (B2 \times H2) + (B3 \times H2)\}}{2}$)xt

= ($\frac{\{(3 \times 3.2) + (3 \times 3.2) + (3 \times 3..2)\}}{2}$ + $\frac{\{(3 \times 3.2) + (3 \times 3.2) + (3 \times 3..2)\}}{2}$) x 0.22

= 6.336 m^3

Total weight = (Volume enclosed × 18) kN = 114.048 kN

Distributed weight = $\frac{Total\ weight}{B1+B2+B3}$ = $\frac{114.048}{9}$ = 12.672 kN/m

Second floor:

Volume enclosed = ($\frac{\{(B1 \times H4) + (B2 \times H4) + (B3 \times H4)\}}{2}$ + $\frac{\{(B1 \times H3) + (B2 \times H3) + (B3 \times H3)\}}{2}$)xt

= ($\frac{\{(3 \times 3.2) + (3 \times 3.2) + (3 \times 3..2)\}}{2}$ + $\frac{\{(3 \times 3.2) + (3 \times 3.2) + (3 \times 3..2)\}}{2}$) x 0.22

= 6.336 m^3

Total weight = (Volume enclosed × 18) kN = 114.048 kN

Distributed weight = $\frac{Total\ weight}{B1+B2+B3}$ = $\frac{114.048}{9}$ = 12.672 kN/m

Third floor:

Volume enclosed = $\frac{(B1 \times H4) + (B2 \times H4) + (B3 \times H4)}{2}$ x t

= ($\frac{\{(3 \times 3.2) + (3 \times 3.2) + (3 \times 3..2)\}}{2}$) x 0.22

= 3.168 m^3

Total weight = (Volume enclosed × 18) kN = 57.024 kN

Distributed weight = $\frac{Total\ weight}{B1+B2+B3}$ = $\frac{57.024}{9}$ = 6.336 kN/m

Non-Linear Static Analysis

The P-M interaction surface and M-θ curves (flexural plastic hinges) for RC members are specified using auto hinges provided by FEMA 356 (2000). The five points A, B, C, D, and E are used to define the backbone for the hinge rotation behaviour of RC members. Point A corresponds to the unloaded condition. Point B corresponds to the nominal yield strength of steel. Point C indicates resistance equal to the nominal

strength. Line CD represents to initial failure of the member. It may be associated with phenomena such as fracture of the flexural reinforcement, spalling of concrete or shear failure following initial yield. Line DE represents the member's residual strength. Point E corresponds to the deformation limit. Three more points., IO (Immediate Occupancy), LS (Life Safety), and CP (Collapse Prevention) are used to define the acceptance criteria of the hinge as shown in Figure 3.6.

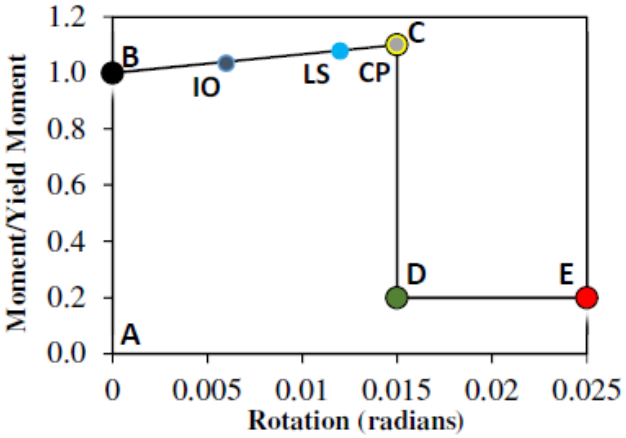

Figure 3.6 Idealized Moment Rotation curve for flexural members (FEMA356-2000)

Non-Linear Hinges

Fibre hinges obtained using section designer integrated with SAP:2000 was used to model a custom cross-section that defines non-linearity in RC members, therefore, enabling to perform nonlinear time-history analysis. Fibre hinges are ideal for dynamic behaviour since they capture nonlinear hysteretic effects efficiently. In fibre hinges, the cross-section is discretized into a series of representative axial fibres, which extend longitudinally along its hinge length. Depending on the material in its tributary area, each fibre has its stress-strain relationship. The stress-strain curve for was defined above in Table 3.3

The Pivot hysteretic model (Cavaleri and Trapani 2014) was used for the equivalent strut to model the hysteretic effects in masonry infill as shown in Figure 3.7. The points S1, S2 and S3 on the compression envelope represent, the yield, the peak and the restoring force, respectively, which corresponds to a reduction of 30% of the peak strength. S1 and S2 are the yield and peak displacements, respectively, and S3 is the final displacement after softening. I, II, and Ill define the yielding, peak and softening branches of the model. The pivot model is primarily based on geometric rules (which

define loading and unloading branches rather than analytical rules. This reduces not only the computational effort but also the number of hysteretic parameters involved. Moreover, the Pivot model has great flexibility in modelling unsymmetrical tension-compression behaviour, as in the case of infill (equivalent diagonal struts).

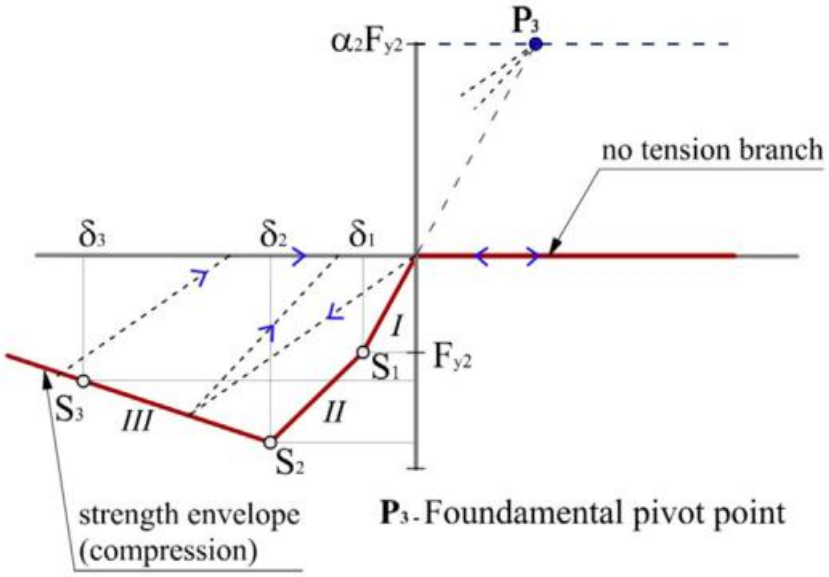

Figure 3.7 Hysteretic Pivot Law for equivalent diagonal strut (Cavaleri and Trapani 2014)

Hinge Length Calculation:

The hinge length for beams and column used in this model were calculated using the formula provided by Paulay and Priestley 1992 as given in Eq. 3.1-

$$lp = 0.08L + 0.022d_b f_y \qquad \text{(Eq. 3.1)}$$

where:

lp = Hinge length (in m)

L = length of member (in m)

db = diameter of longitudinal steel (in m)

fy = yield strength of longitudinal steel (in MPa)

The hinge length for Infill hinges is taken as one-fourth of strut length.

$$lp = \frac{Ls}{4}$$

where Ls = Length of strut

For Columns-

Ground Floor:

$$lp = (0.08\times 4.4)+(0.022\times \frac{16}{1000} \times 415) = 0.4981 \text{ m}$$

First, Second and Third floors:

$$lp = (0.08\times 3.2)+(0.022\times \frac{16}{1000} \times 415) = 0.4021 \text{ m}$$

For Beams-

Ground and First Floor =

$$lp = (0.08\times 3)+(0.022\times \frac{20}{1000} \times 415) = 0.4226 \text{ m}$$

Second Floor =

$$lp = (0.08\times 3)+(0.022\times \frac{16}{1000} \times 415) = 0.38608 \text{ m}$$

Third Floor =

$$lp = (0.08\times 3)+(0.022\times \frac{12}{1000} \times 415) = 0.34956 \text{ m}$$

Location of plastic hinges:

For Beams: (lp+depth of column)/2

For Columns: (lp+depth of beam)/2

For infill strut: At the centre of the strut (i.e., relative distance=0.5)

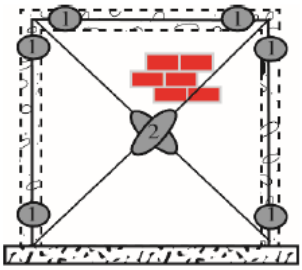

Figure 3.8 Location of flexural hinge in RC members and axial hinge in equivalent strut modelled for masonry infill

3.2.4. Output

The bare frame and fully-infilled frames were replicated as per *Kaushik et al 2009* so as to validate the research by comparing the output Pushover Curve for the modelled frame and as per the research. Both frames were calibrated with the research in order to carry out further study.

Furthermore, structural response to a particular ground motion was obtained using Non-Linear Time History Analysis was performed for a single-story frame. The structural response consists of the complete history of any particular response of the structure when a ground motion is applied at the base of the structure. The equation of motion as shown in Eq. 3.2

$$M\ddot{u}(t) + C\dot{u}(t) + Ku(t) = -M\ddot{u}_g(t) \qquad \text{(Eq. 3.2)}$$

Here, K is the stiffness matrix, C is the damping matrix, M is the diagonal mass matrix, $u, \dot{u}$ and $\ddot{u}$ are the displacement, velocity and acceleration of the structure at any instant t, in case of earthquake loading these are relative values with respect to ground, and $\ddot{u}_g$ is the ground acceleration.

Fast Non-Linear Analysis (FNA) integrated method in SAP:2000 was used to imply he given data inputs and conditions and run the analysis. A set of ground motions are applied at the base of the structure in order to assess the seismic performance of the structure with varying earthquake intensity.

The comparative graphs for response and energy parameters were plotted in order to conclude the properties of near and far-field earthquake records.

CHAPTER - 4

CHARACTERISATION OF GROUND MOTION

4.1. Overview

The principal objective of engineering seismology is to provide quantitative estimates of expected levels of seismic ground-motion as the basic input to earthquake-resistant design, the evaluation of collateral seismic hazards and seismic risk assessment. This invariably entails characterizing the complex nature of strong-motion accelerograms using simple parameters to correlate with the outputs. This chapter, thus discusses the identification and estimation of ground motion characteristics to identify the destructive potential of the ground motion.

4.2. Ground Motion Database Record

The ground motion acceleration is downloaded in raw (unscaled form) from the PEER-NGA database. NGA-West 2 ground motion database was used to search for the unscaled data. The present study intends to compare the effects of near-field (NF) and far-field (FF) records for a particular earthquake. NF ground motions are characterized by its closest distance from the rupture fault and PGV/PGA ratio. The closest distance is known as Joyner Boore distance (R_{jb}). For NF, R_{jb} should be less than 15 km and PGV/PGA ratio to be more than 0.1 sec, whereas the FF ground motions have R_{jb} more than 15 km and PGV/PGA ratio less than 0.1 sec. Therefore, a pulse is selected as an “Only pulse record” to obtain the near-field records and “Non-Pulse Records” to obtain the far-field time series. Data is downloaded as a zip file containing several time histories with an MS excel file governing different parameters and stations.

For each ground motion, two stations are chosen such that one belongs to NF and the other FF category. The selected acceleration files are then used as an input to the software SeismoSignal **SeismoSoft (2023)** to extract and characterize the parameters required for seismic damage analysis. The final selection of ground motion data is done to obtain a good variation in their characterizing parameters. Detailed characterization of selected ground motions and their values for NF and FF are given in Table 4.1 and Table 4.2, respectively and are discussed next.

Table 4.1 Properties of selected NF ground motion records (PEER-NGA West2)

Sr. No.	Year	Earthquake	Station	M	PGA	$(V/A)_{max}$	AI	SED (cm^2/s)	Dominant Freq. f_d
1	1971	San Fernado	Pacoima Dam (upper left abut)	6.61	1.219	0.095	8.947	9636.98	4.773
2	1979	Coyote Lake	Gilroy Array #6	5.74	0.422	0.107	0.775	763.132	0.976
3	1979	Imperial Valley	Agrarias	6.53	0.287	0.124	0.964	981.811	0.806
4	1979	Montenegro	Bar-Skupstina Opstine	6.80	0.373	0.113	1.982	2794.618	1.074
5	1980	Irpinia	Sturno(STN)	6.90	0.227	0.166	1.184	1972.886	2.531
6	1981	San Salvador	NationalGeograficalInst	7.14	0.404	0.142	1.093	2341.360	1.172
7	1981	Westmorland	ParachuteTestSite	6.90	0.232	0.244	0.711	3541.773	1.513
8	1986	Kalamata	Kalamata (bsmt) (2nd trigger)	5.40	0.162	0.081	0.105	44.515	3.458
9	1987	Superstition Hills	Parachute Test Site	6.54	0.432	0.317	3.741	14118.206	0.537
10	1989	Loma Prieta	Gilroy - Historic Bldg	6.93	0.285	0.155	0.721	1102.642	0.659
11	1992	Cape Mendocino	Bunker Hill FAA	7.01	0.177	0.390	0.645	4431.712	0.635
12	1992	Landers	Lucerne	7.28	0.131	0.160	0.207	1013.363	0.256
13	1994	Northridge	Jensen Filter Plant Administrative Building	6.69	0.287	0.124	0.964	981.81	1.025
14	1995	Kobe	Takarazuka	6.90	0.697	0.010	3.070	5021.827	0.586
15	1999	Kocaeli	Yarimca	7.51	0.226	0.313	1.330	14273.258	0.268
16	2000	Tottori	TTR008	6.20	0.314	0.113	1.696	1710.846	0.925
17	2003	Bam	Bam	6.60	0.287	0.124	0.964	981.81	1.025
18	2004	Parkfield	PARKFIELD - EADES	6.00	0.317	0.086	0.636	444.285	1.147
19	2007	Chetsu-oki	Joetsu Kakizakiku Kakizaki	6.80	0.303	0.165	1.318	4182.131	0.696
20	2009	L'Aquilla	L'Aquila - Parking	7.10	0.336	0.098	1.011	1356.477	0.561
21	2011	Christchurch	Pages Road Pumping Station	6.20	0.596	0.139	2.165	7024.832	0.635

Table 4.2 Properties of selected FF ground motion records. (PEER-NGA West2)

Sr. No.	Year	Earthquake	Station	M	PGA	$(V/A)_{max}$	AI	SED (cm^2/s)	Dominant Freq. f_d
1	1971	San Fernado	Cholame - Shandon Array #8	6.61	0.005	0.240	0.001	7.943	0.708
2	1978	Tabas	Kashmar	7.35	0.033	0.283	0.052	247.257	0.635
3	1979	Coyote Lake	Halls Valley	5.74	0.037	0.066	0.018	1003.54	2.685
4	1979	Imperial Valley	DELTA	6.53	0.061	0.033	0.025	2.17	2.783
5	1979	Montengero	Debar - Skupstina Opstine	7.1	0.053	0.054	0.057	17.205	5.359
6	1980	Irpinia	Tricarico	6.9	0.021	0.159	0.009	21.935	1.074
7	1981	Westmorland	Niland Fire Station	5.9	0.101	0.043	0.121	35.015	4.248
8	1987	Superstition Hills	Calipatria Fire Station	6.54	0.189	0.088	0.345	294.678	3.906
9	1989	Loma Prieta	APEEL 2 - Redwood City	6.93	0.274	0.199	1.258	2556.562	0.952
10	1992	Cape Mendocino	Butler Valley Station 2	7.01	0.154	0.100	0.351	286.996	1.367
11	1992	Landers	Anaheim - W Ball Rd	7.28	0.052	0.326	0.103	850.673	0.488
12	1994	Northridge	Anacapa Island	6.69	0.067	0.049	0.073	10.963	4.663
13	1995	Kobe	FUK	6.90	0.034	0.126	0.038	66.098	1.465
14	1999	Duzce	Ambarli	7.14	0.038	0.181	0.039	186.595	0.549
15	1999	Kocaeli	Tokat	7.51	0.001	0.183	0.00006	0.241	1.605
16	2000	Tottori	Tricarico	6.61	0.076	0.056	0.118	26.063	3.712
17	2003	Bam	Andoohjerd	6.60	0.032	0.090	0.019	23.651	2.746
18	2004	Niigata	FKS020	6.63	0.048	0.132	0.081	278.273	0.369
19	2004	Parkfield	Fresno - NSMP USGS Office	6.00	0.005	0.0805	0.00035	0.62	1.501
20	2007	Chetsu-oki	Joetsu Kita	6.80	0.091	0.146	0.348	871.049	0.684
21	2009	L'Aquilla	Badia Tedalda	6.30	0.002	0.145	0.00018	0.519	1.343
22	2010	Darfield	DCZ	7.00	0.001	0.462	0.00003	0.93458	0.140
23	2011	Christchurch	BDCS	6.20	0.002	0.0821	0.00007	0.02191	6.079

4.3. Ground Motion Time History

Time history refers to a record of ground motion over time during an earthquake event. It is a graphical representation or a set of numerical values that describe the acceleration, velocity, or displacement of the ground at a specific location as a function of time. The time history record of ground motion can be used to assess the structural response, including stresses, strains, and deformations, and evaluate the potential for structural damage or failure through time history analysis. It captures the dynamic characteristics of the earthquake, including its duration, frequency content, and amplitude variations over time. This detailed analysis helps in designing structures to withstand the anticipated ground motions and ensures the safety and resilience of infrastructure in earthquake-prone regions. Acceleration time history for NF and FF records of selected ground motions are shown in Figure 4.1 and Figure 4.2, respectively.

As discussed in the literature, the near and far-field exhibit very different types of characteristics, therefore having different types of behaviour and damage to the buildings. Near-field earthquakes have a shorter duration and typically exhibit higher frequency content as compared to far-field. Moreover, NF ground motions carry complexity in their waveform due to directivity and local site effects making it an important parameter to study.

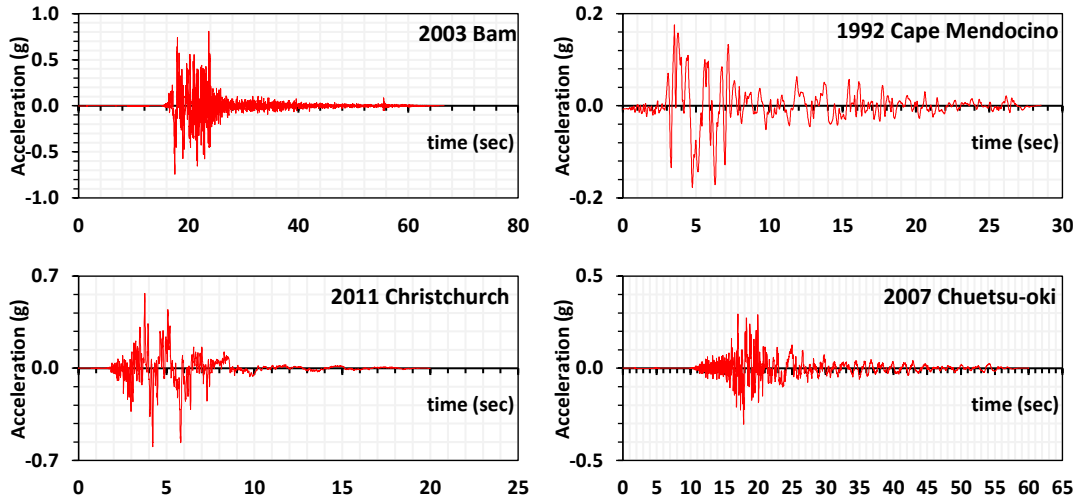

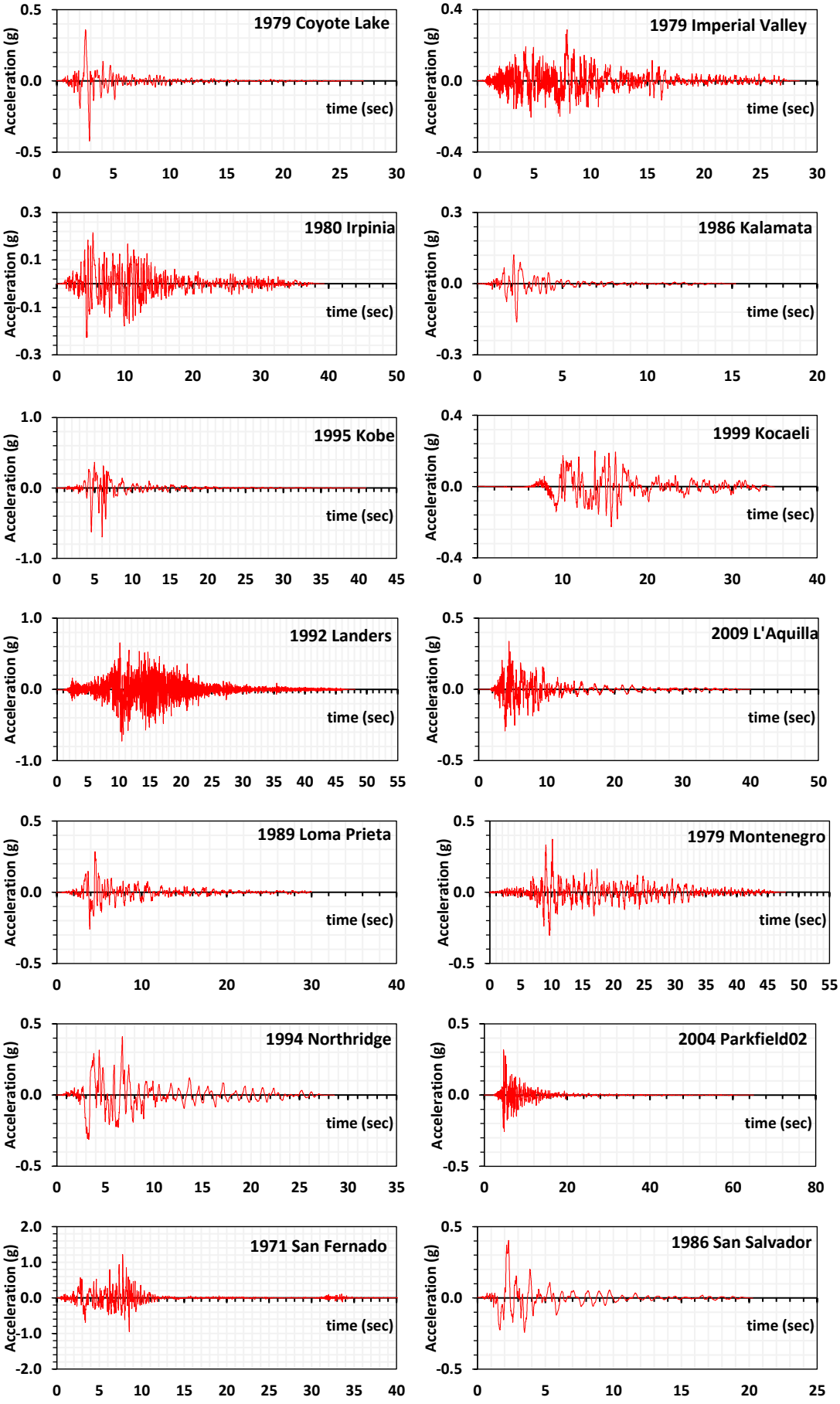
1979 Coyote Lake
1979 Imperial Valley
1980 Irpinia
1986 Kalamata
1995 Kobe
1999 Kocaeli
1992 Landers
2009 L'Aquilla
1989 Loma Prieta
1979 Montenegro
1994 Northridge
2004 Parkfield02
1971 San Fernado
1986 San Salvador
Acceleration (g)
time (sec)

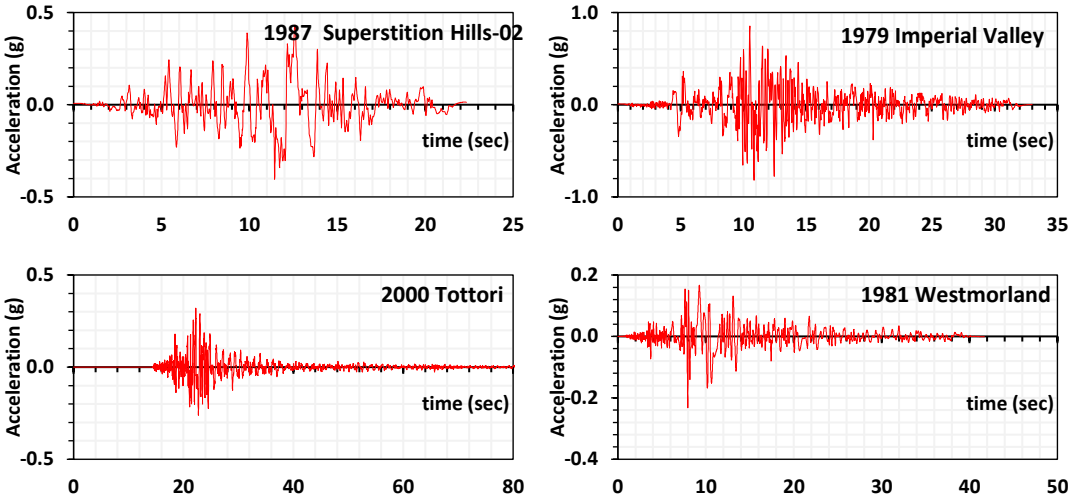

Figure 4.1 Acceleration Time histories for selected Near Field (NF) records

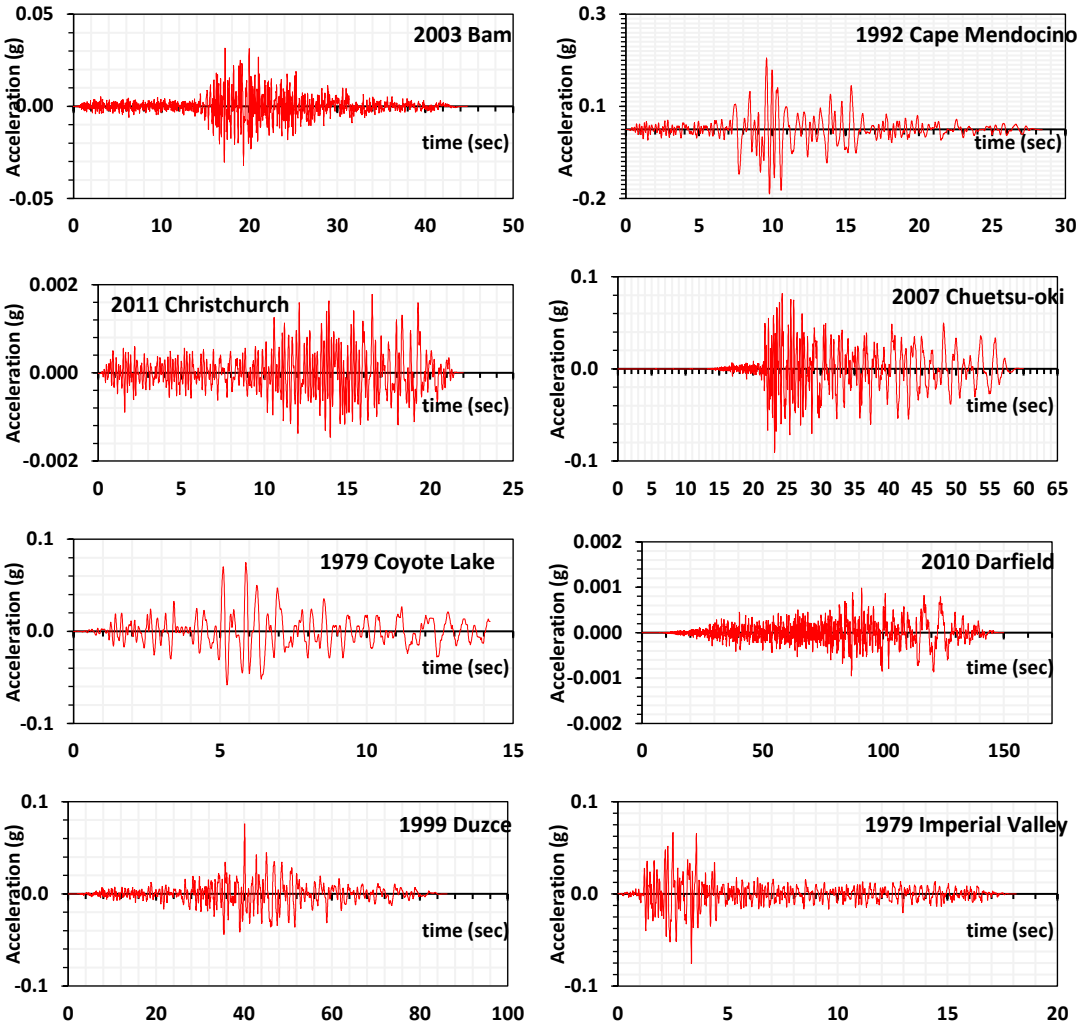

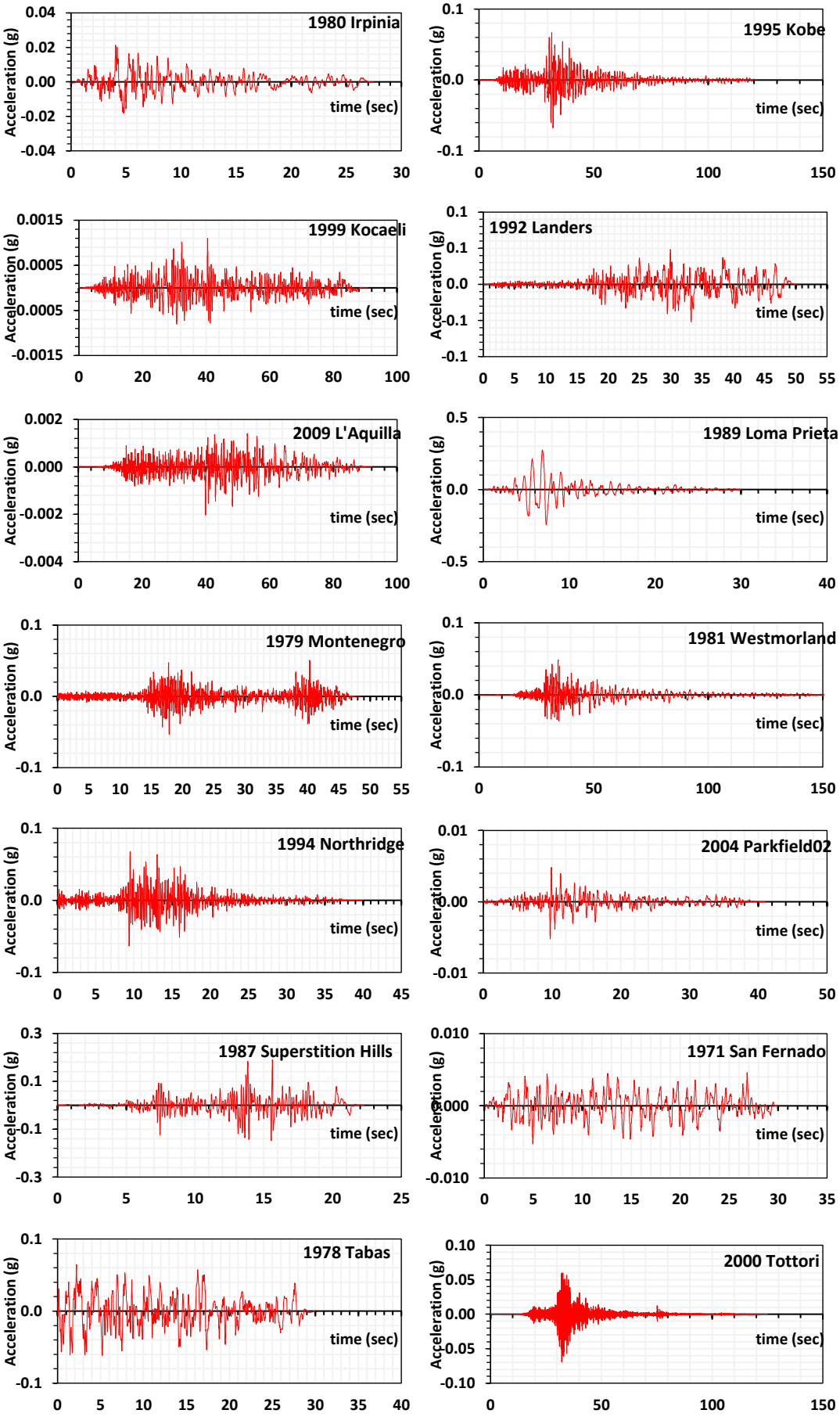
1980 Irpinia
1995 Kobe
1999 Kocaeli
1992 Landers
2009 L'Aquilla
1989 Loma Prieta
1979 Montenegro
1981 Westmorland
1994 Northridge
2004 Parkfield02
1987 Superstition Hills
1971 San Fernado
1978 Tabas
2000 Tottori
Acceleration (g)
time (sec)

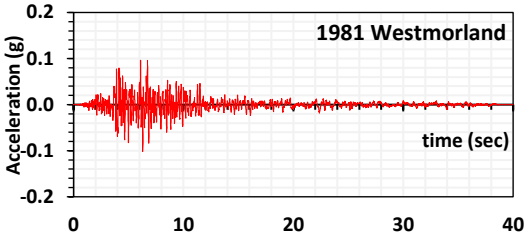

Figure 4.2 Acceleration Time history plots for selected FF ground motion records

4.4. Characterization of Ground Motion

The ground motion characterization has been done based on the following energy parameters – viz. Arias Intensity, Energy Flux, Fourier Amplitude, and Power Amplitude each of which is discussed in detail in the following section. The spectrum characteristics, such as the Fourier spectra, dominant frequency and the power spectra are also discussed.

4.4.1. Energy Parameters

Arias Intensity (AI)

Arias Intensity can be seen as a premise that the damage experienced during an earthquake is proportional to the energy per unit weight dissipated by the structure during the total duration of the earthquake (Villaverde, 2009). It has been observed to be one of the most prominent parameters to access the probabilistic damage to the structure during an earthquake. Arias Intensity has been calculated by using Eq. 4.1,

$$I_a = \frac{\Pi}{2g}\int_0^{\mathrm{T}} [a(t)]^2 dt \qquad \text{(Eq. 4.1)}$$

where g is the acceleration due to gravity, a(t) is the recorded acceleration time history, T is the duration of ground motion.

A typical plot of Arias Intensity (AI) vs Period is shown in Figure 4.3 for both NF and FF records and a comparative plot in Figure 4.4 for all earthquakes considered.

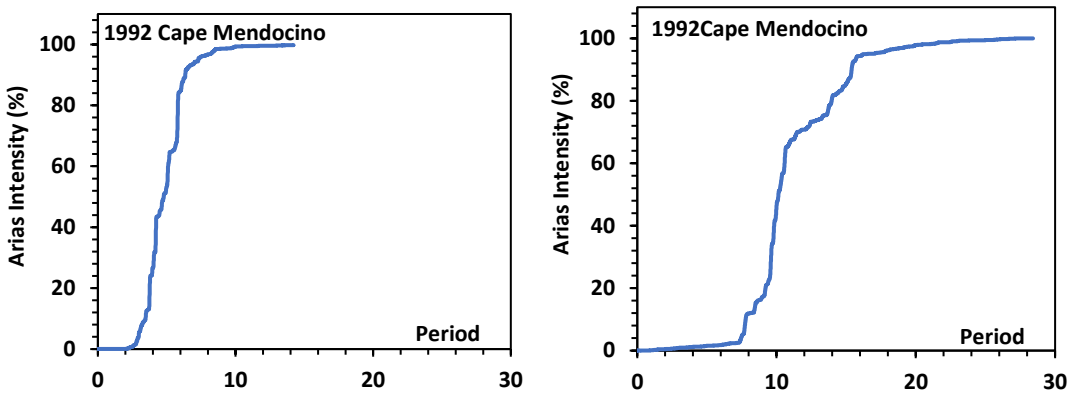

(a) (b)

Figure 4.3 Typical plot of Arias Intensity (%) vs Period for Cape Mendocino ground motion – (a) NF (Left) and (b) FF (Right).

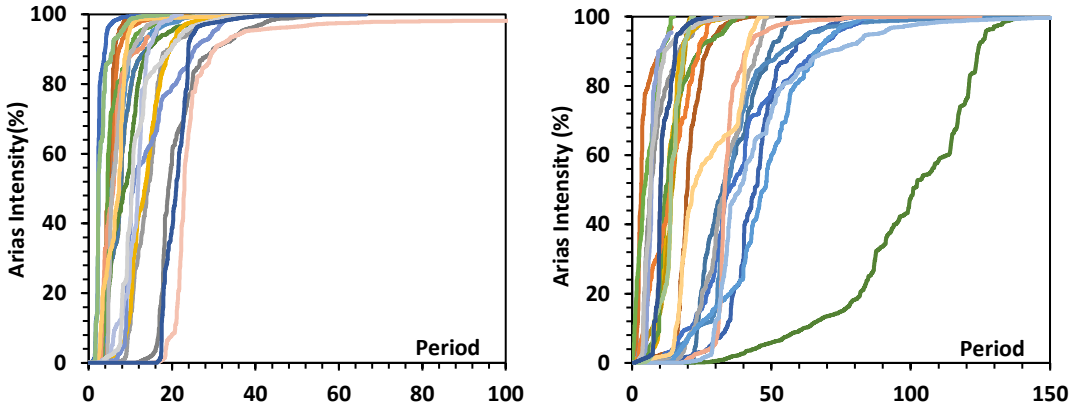

(a) (b)

Figure 4.4 Comparative plots of Arias Intensity (%) vs Period for all the ground motions – (a) NF (Left) and (b) FF (Right)

NF ground motions constitutes for more early peaks of Arias intensity as compared to FF ground motions. On an average, NF ground motion attains its peak of Arias intensity in 0 to 20 secs, while FF ground motions attain its peak in 0 to 40 secs. Also, NF constitutes a higher value of Arias intensity as compared to FF ones.

Energy Flux

Energy flux is defined as the amount of energy transmitted per unit of time through a medium. Measuring and analyzing energy flux in earthquake engineering is important for understanding the potential impact of seismic waves on structures and

infrastructure. It helps engineers assess the dynamic response and structural vulnerability of buildings, bridges, dams, and other critical facilities.

Specific Energy Density is calculated using the formula given below in Eq. 4.2., where v(t) represents velocity at any time (t).

$$SED = \int_0^{t_{total}} \mathrm{v}[(\mathrm{t})]^2 dt \qquad \text{(Eq. 4.2)}$$

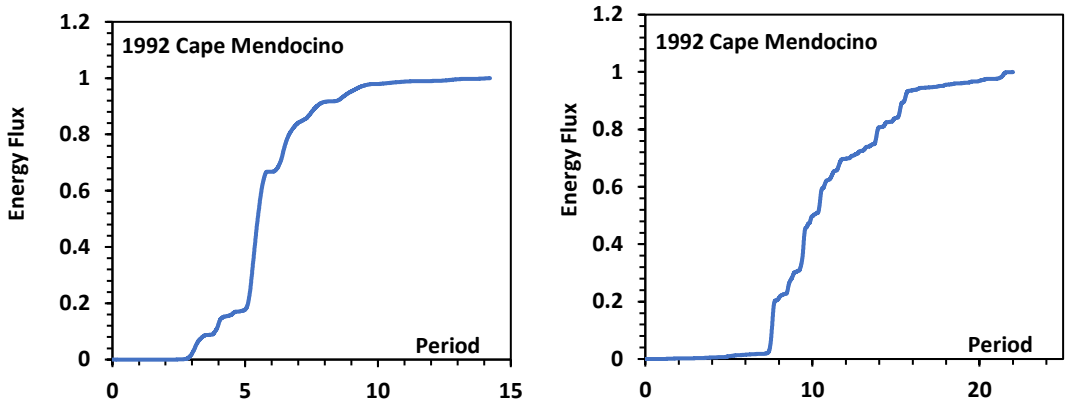

(a) (b)

Figure 4.5 Typical plot of Energy Flux vs Period for Cape Mendocino ground motion – (a) NF (Left) and (b) FF (Right).

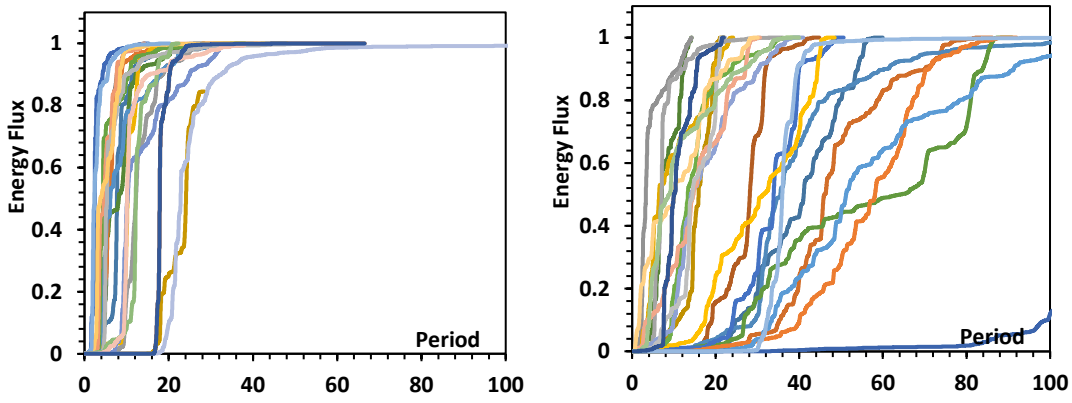

(a) (b)

Figure 4.6 Comparative plots of Energy Flux vs Period for all the ground motions – (a) NF (Left) and (b) FF (Right)

A similar trend of Energy Flux has been observed as that of Arias Intensity. On an individual level, the energy flux of a NF ground motion is considerably large as

compared to FF. On the other hand, the comparative plots depict that, NF ground motions achieve their maximum value of energy flux much earlier than FF ones.

4.4.2. Spectral Parameters

Fourier Amplitude

Fourier amplitude is used to study the frequency content or spectral characteristics of the seismic waves generated by the earthquake. The Fourier amplitude spectrum of seismic waves provides information about the amplitudes or magnitudes of different frequencies present in the waveforms and helps in understanding the distribution of energy across different frequency ranges. Specifically, the Fourier amplitude spectrum can be used to determine the dominant frequencies or resonance frequencies of the earthquake waves. This information is crucial for assessing the potential impact on structures and infrastructure, as different structures have different natural frequencies of vibration, and resonance with the earthquake waves can lead to amplification of ground motion. Overall, Fourier amplitude analysis plays a significant role in earthquake seismology by providing valuable information about the frequency content, energy distribution, and characteristics of seismic waves, which is essential for earthquake monitoring, hazard assessment, and engineering design. Figure 4.7 shows a typical plot of Fourier Amplitude w.r.t Frequency for Westmorland (both NF and FF) ground motion record. The dominant frequency as observed for NF is 1.51367 Hz and that for FF is 4.24805 Hz.

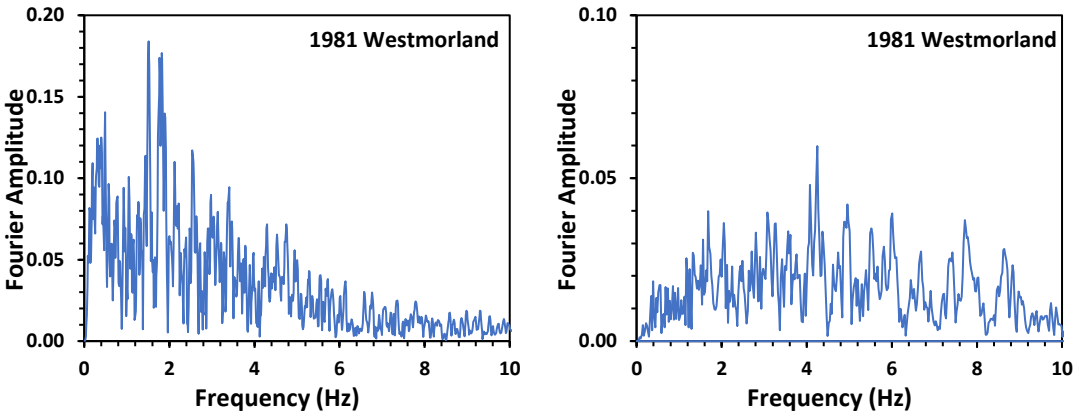

(a) (b)

Figure 4.7 Typical plot of Fourier Amplitude vs Frequency for Cape Mendocino ground motion – (a) NF (Left) and (b) FF (Right).

Differences can be observed very strongly by observing the peaks in NF and FF. NF ground motions have a higher value of amplitude in a shorter time as compared to FF ones, making a structure more prone to damage. While FF ground motions exhibit an overall compressed peak as compared to NF ones and give less damage to the structure. Also, the peak amplitude can be seen more in NF as compared to FF.

Dominant Frequency/ Period

Dominant frequency, mentioned in the above context is defined as frequency corresponding to maximum Fourier amplitude (Telgarsky et. al., 2013) It is one of the significant parameters as the dynamic response of structures strongly depends on their natural frequencies and the frequency content of the ground motion. If the dominant frequency of the ground motion matches or is close to the natural frequency of a structure, it can lead to resonance, causing increased vibrations and potential damage to the structure. Understanding the dominant frequency allows us to design structures to attenuate resonance effects and ensure their stability during earthquakes.

Dominant frequency for selected NF and FF ground motions have been listed in Table 4.3.

Table 4.3 Dominant frequency for selected NF and FF ground motion records

Sr. No.	Year	Earthquake	Dominant Freq. NF	Dominant Freq. FF
1	1971	San Fernando	4.773	0.708
2	1978	Tabas		0.635
3	1979	Coyote Lake	0.976	2.685
4	1979	Imperial Valley	0.806	2.783
5	1979	Montenegro	1.074	5.359
6	1980	Irpinia	2.531	1.074
7	1981	San Salvador		1.172
8	1981	Westmorland	1.513	4.248
9	1986	Kalamata		3.458
10	1987	Superstition Hills	0.537	3.906
11	1989	Loma Prieta	0.659	0.952
12	1992	Cape Mendocino	0.635	1.367

13	1992	Landers	0.256	0.488
14	1994	Northridge	1.025	4.663
15	1995	Kobe	0.586	1.465
16	1999	Duzce		0.549
17	1999	Kocaeli	0.268	1.605
18	2000	Tottori	0.925	3.712
19	2003	Bam	1.025	2.746
20	2004	Niigata		0.369
21	2004	Parkfield	1.147	1.501
22	2007	Chetsu-oki	0.696	0.684
23	2009	L'Aquilla	0.561	1.343
24	2010	Darfield		0.140
25	2011	Christchurch	0.635	6.079

Frequency Ratio is defined as ratio of dominant frequency and frequency of the building. The values for all the ground motions have been listen in Table-4.1.

Power Amplitude

Power Amplitude represents the distribution of power or energy across different frequencies in a signal. It is derived from the Fourier amplitude spectrum by squaring the amplitudes at each frequency. It provides information about the relative contributions of different frequencies to the overall power or energy content of the signal. This is particularly important when assessing the response of structures to earthquake ground motion since the energy content can be more relevant than the amplitude alone.

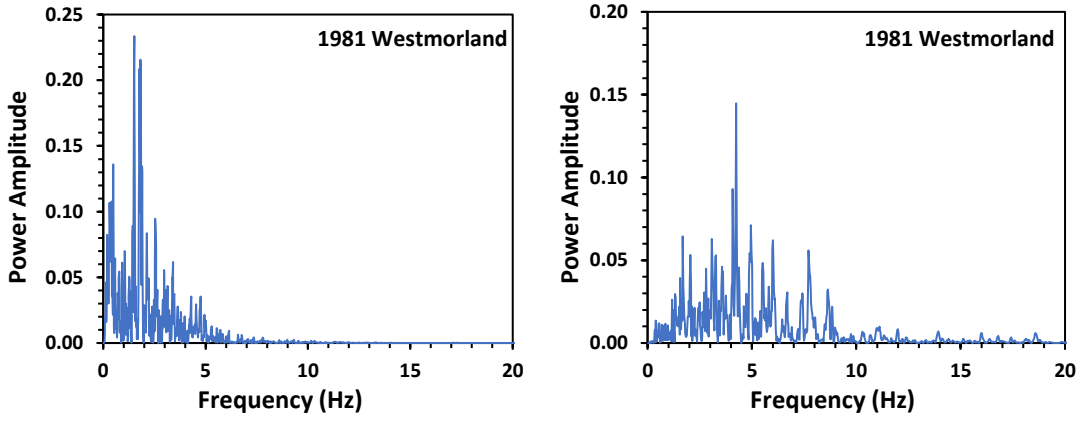

(a) (b)

Figure 4.8 Typical plot of Power Amplitude vs Frequency for Cape Mendocino ground motion – (a) NF (Left) and (b) FF (Right).

Response Spectrum

Response spectrum is a graphical representation of the maximum response of a structure to a range of ground motion intensities at different frequencies. It is commonly used in structural engineering to assess the dynamic behaviour and seismic performance of buildings, bridges, and other structures. The response spectrum shows how the structure would respond to various ground motion inputs, such as earthquake accelerations, by plotting the maximum structural response (displacement, velocity, or acceleration) against the corresponding frequency content of the ground motion. The spectrum is typically represented as a curve or a set of curves.

The shape of the response spectrum curve is determined by the characteristics of the ground motion, including its amplitude and frequency content. It provides valuable information about the structure's vulnerability to different frequency components of ground motion. The higher the peak amplitude of the response spectrum at a particular frequency, the more significant the structural response will be at that frequency. Response spectra are often derived from recorded seismic accelerations or synthesized ground motion records. These spectra can be created for different ground motion intensities, such as design-basis earthquakes, to evaluate the potential structural response under different seismic events.

The acceleration response is observed for all the ground motion records considered. Combined spectra are observed by calculation of the Average and Square Root of the Sum of Squares (SRSS). The spectra have been shown in Figure 4.9 and Figure 4.10 for NF and FF ground motion records respectively.

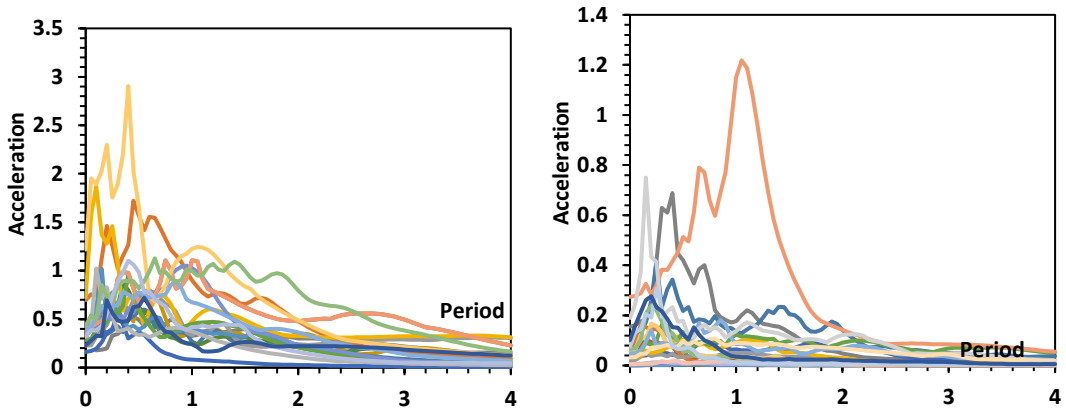

(a) (b)

Figure 4.9 Response spectrum for (a) NF ground motions (b) FF ground motion records

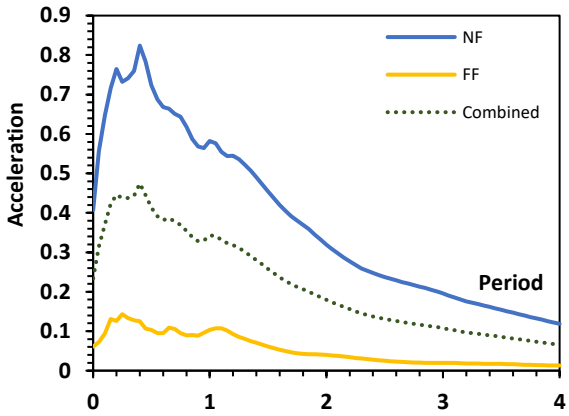

Figure 4.10 Average Response spectrum for NF and FF ground motion records

4.5. Comparative plots

The comparative plots of other parameters w.r.t (V/A) were plotted and represented in Figure 4.11 and Figure 4.12 for NF and FF ground motions respectively. The scattering of plots signifies that ground motions (both NF and FF) are selected so that, the diversification could account for better analysis as each ground motion possess a different range of selected parameter. The following observations were drawn from respective plots-

Arias Intensity: Most of the values of Arias Intensity lie in b/w V/A ratio of 0.1 to 0.2 sec, having a value ranging from 0.2 to 12 m/sec for NF, while this ranges b/w 0.2 to 0.4 m/sec for FF ground motions.

Predominant Period: Most of the values of the Predominant period lie b/w V/A ratio of 0 to 0.2 sec, having a value ranging from 0.1 to 1 sec for NF and 0 to 0.8 sec for FF ground motions.

Specific Energy Density: Most of the values of specific energy density lie b/w 0 to 9 cm^2/sec for NF and 0.1 to 30 cm^2/sec for FF.

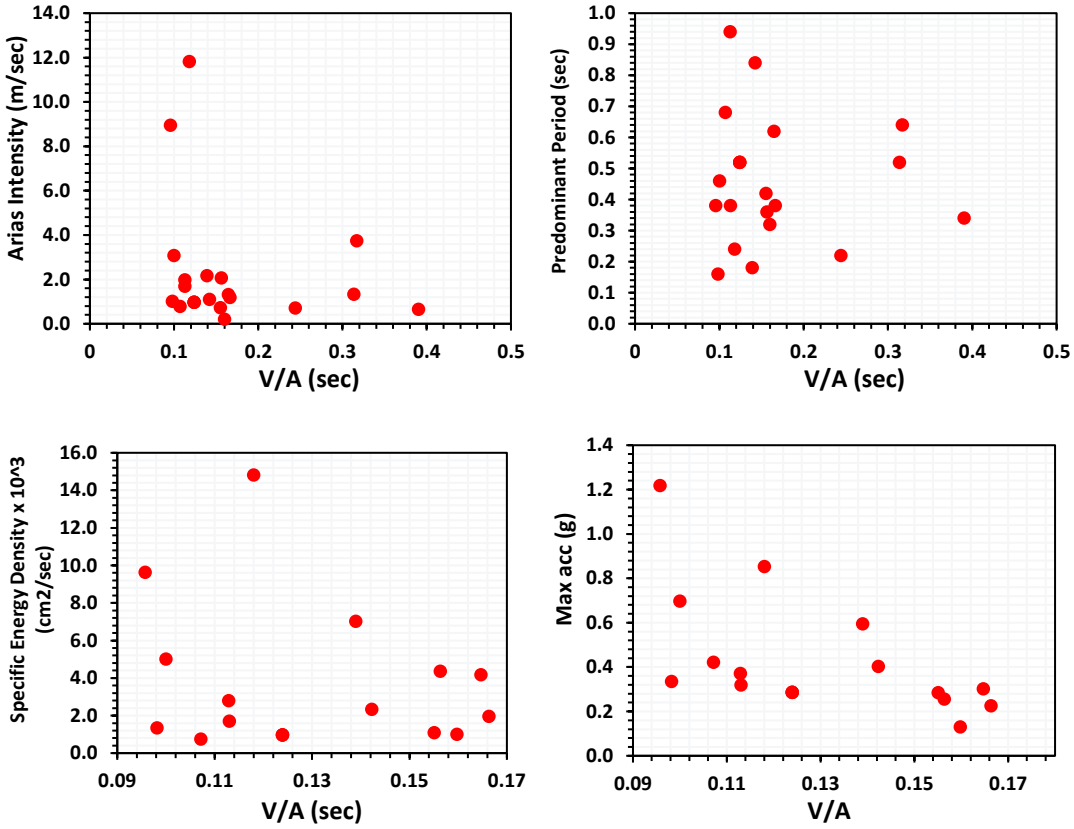

Figure 4.11 Comparative plots of NF ground motion parameters w.r.t V/A ratio

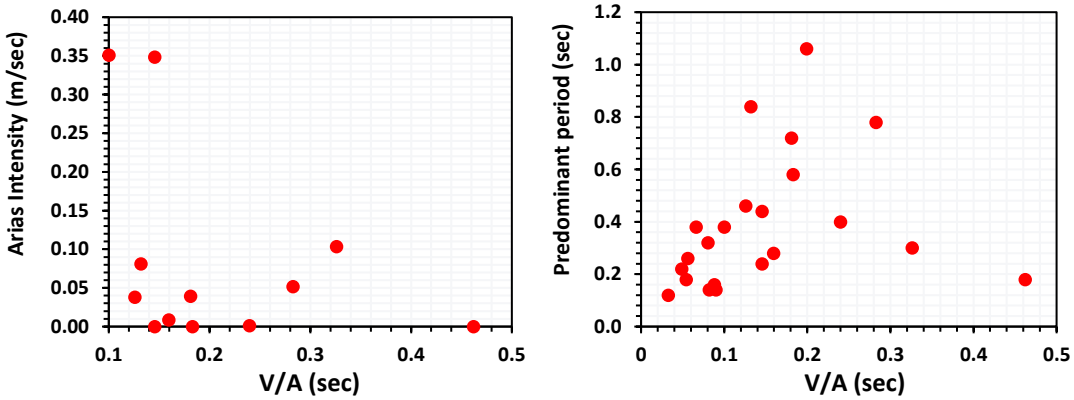

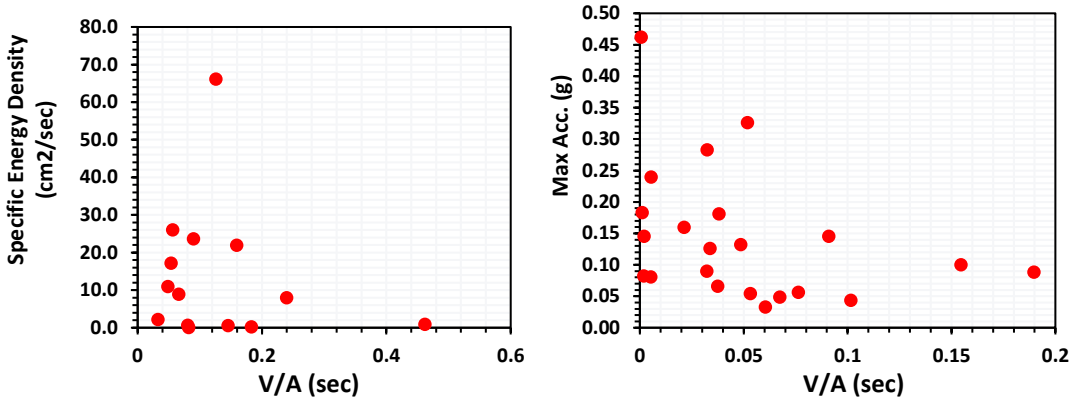

Figure 4.12 Comparative plots of FF ground motion parameters w.r.t V/A ratio

4.6. Chapter Summary

This chapter focuses primarily on input ground motion datasets. This briefly discusses from the extraction of raw ground motion data from PEER-NGA for characterization for further analysis. Two types of characterization have been discussed viz. Energy Parameters and Spectral Parameters. Several Co-relative graphs have been built to understand the characteristics and nature of NF and FF ground motions.

CHAPTER - 5

NON-LINEAR ANALYSIS OF RC FRAME

5.1. Overview

After characterizing the ground motion and modelling of the application frame as per the study, the pushover results of Four-storey, three-bay frames are validated as per Kaushik et. al. 2009. Single storey frame was derived further to perform Non-Linear Time History Analysis and observe the trends of different parameters and their correlation with different lateral responses of the frame.

5.2. Validation of Kaushik et al 2009

As described in previous chapters, the validation frame was replicated as per given in ***Kaushik et al 2009***. The capacity curve obtained by Pushover Analysis of BF and FI is as shown in Figure 5.1 and Figure 5.2.

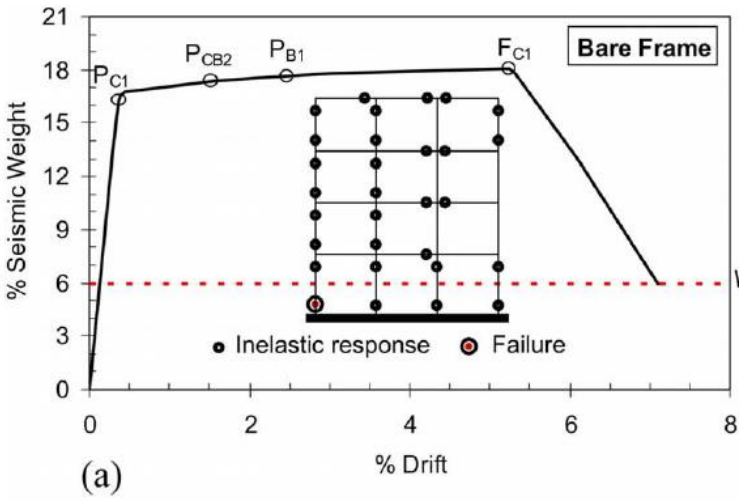

Figure 5.1 Pushover curve for BF (Kaushik et. al. 2009)

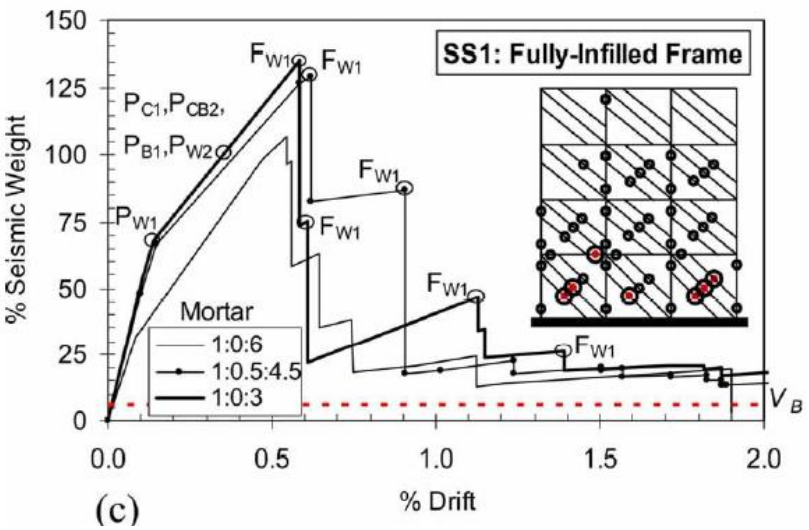

Figure 5.2 Pushover curve for FI (Kaushik et. al. 2009)

For comparison of the present study with the research, Seismic weight was converted into Base shear by derived value from SAP:2000 and drift were converted into displacement by multiplication with storey height. The comparison plots obtained for validation are as shown in Figure 5.3 and Figure 5.4

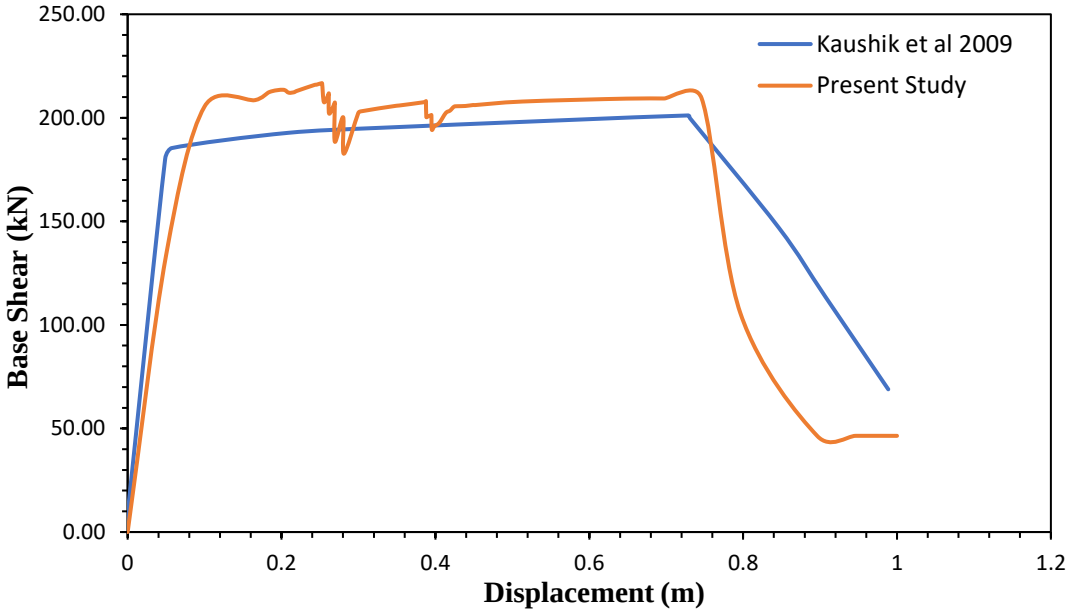

Figure 5.3 Pushover Curve for validating Bare Frame (BF)

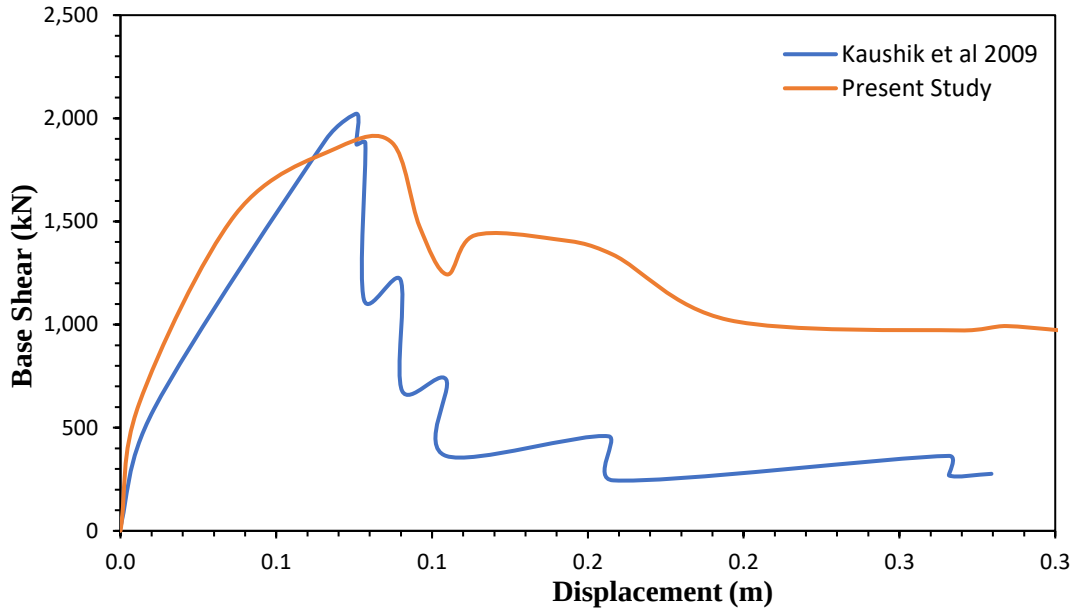

Figure 5.4 Pushover Curve for validating Fully-Infilled Frame (FI)

5.3. Output

Non-Linear Time History Analysis was performed for one bayed, single-storey frame derived frame from a four-storied validation frame. Each acceleration value of an earthquake was divided by its maximum absolute value. This scaling was done for every earthquake before input to SAP:2000. Six load cases were created to analyze the results corresponding to the multipliers of PGA i.e., 0.1g, 0.3g, 0.5g, 0.7g, 0.9g, 1.1g for each earthquake. The corresponding, response was observed for the frame with parameters as listed in further sections.

5.3.1. Displacement Response

Displacement refers to the shifting of ground from its original position. It is one of the most crucial parameters of all as it directly influences the response of a structure. Displacement vs time plot is a basic to analyse the behaviour of a structure, as it gives displacement at any instant of time. A typical displacement vs time graph for specified accelerations is shown in Figure 5.5

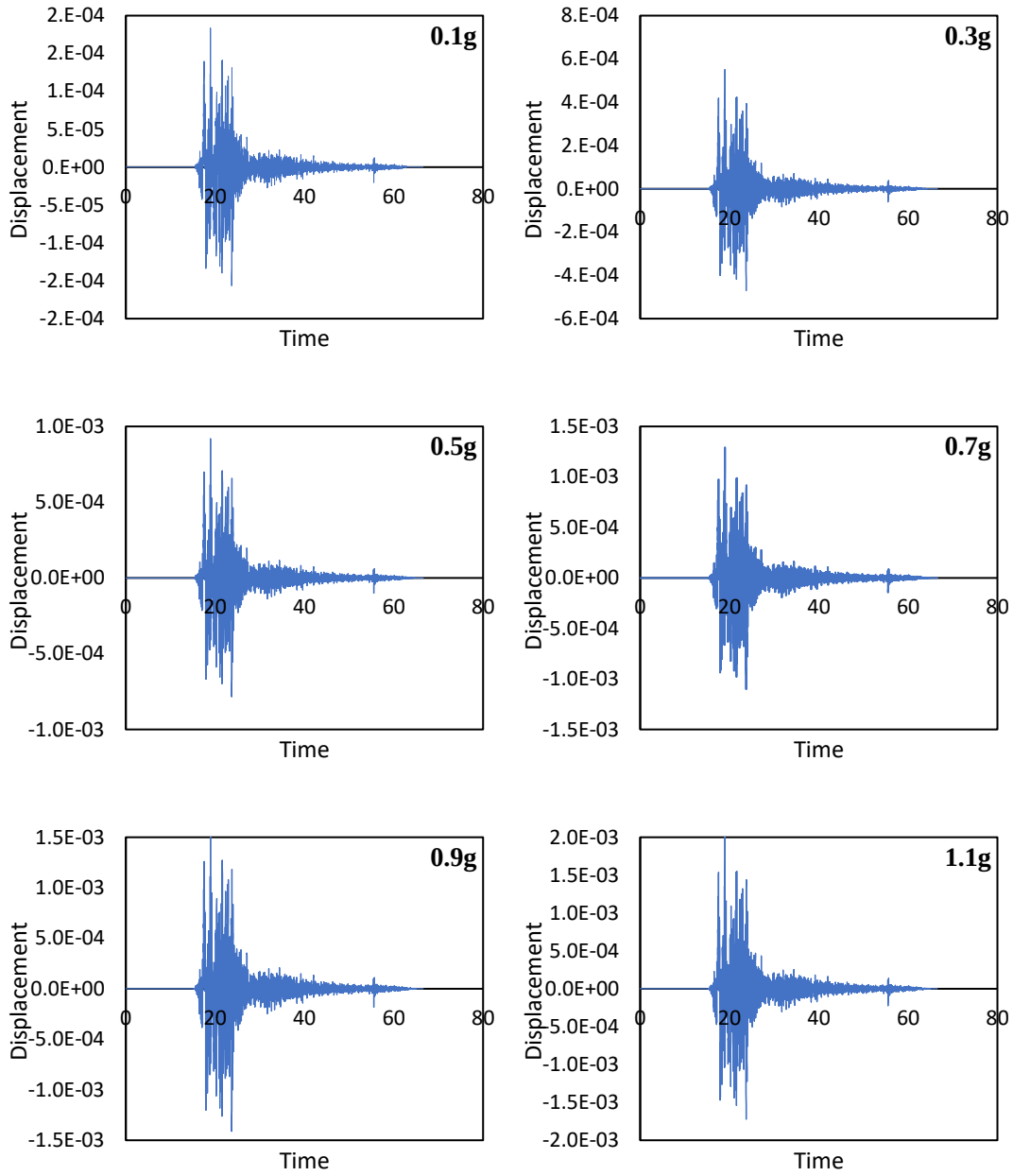

Figure 5.5 Typical Displacement vs Time curve for Bam-NF earthquake record at defined acceleration values

The maximum absolute displacement was extracted from Joint Displacement vs Time plot from SeismoSignal. Correspondingly, the maximum absolute displacement was calculated and plotted against PGA for both NF and FF earthquake records. The comparative plots have been shown in Figure 5.6.

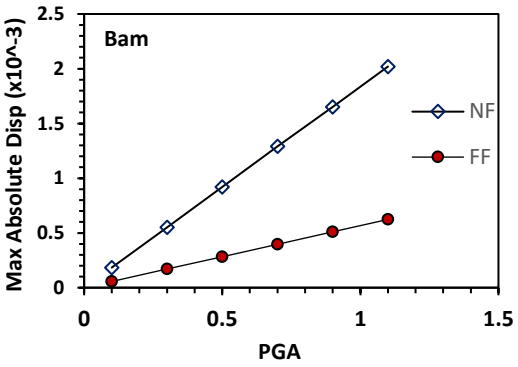
Bam
Max Absolute Disp (x10^-3)
PGA
NF
FF

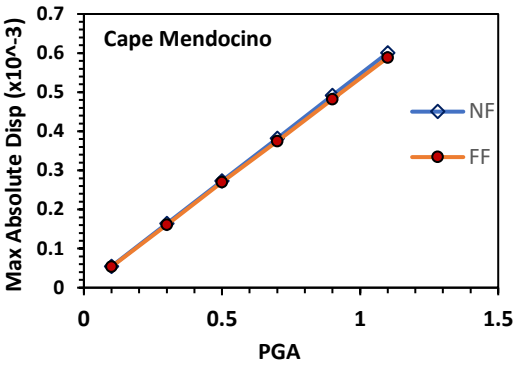
Cape Mendocino
Max Absolute Disp (x10^-3)
PGA
NF
FF

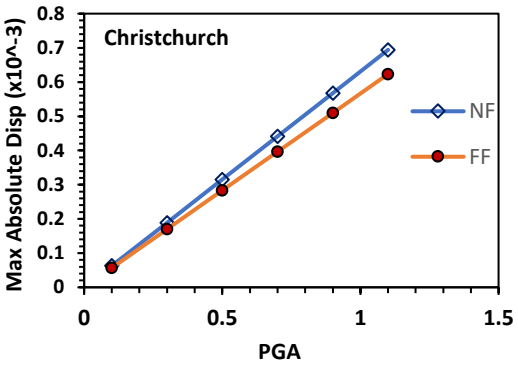
Christchurch
Max Absolute Disp (x10^-3)
PGA
NF
FF

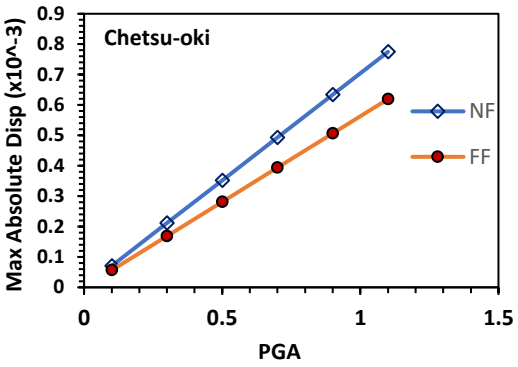
Chetsu-oki
Max Absolute Disp (x10^-3)
PGA
NF
FF

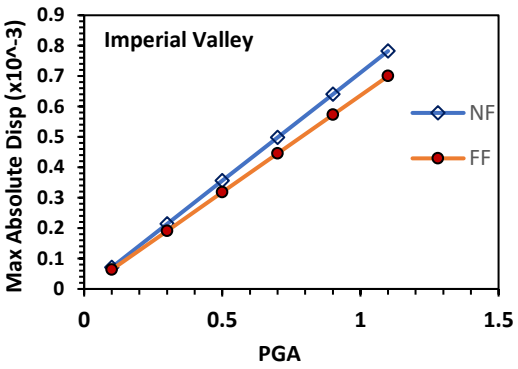
Imperial Valley
Max Absolute Disp (x10^-3)
PGA
NF
FF

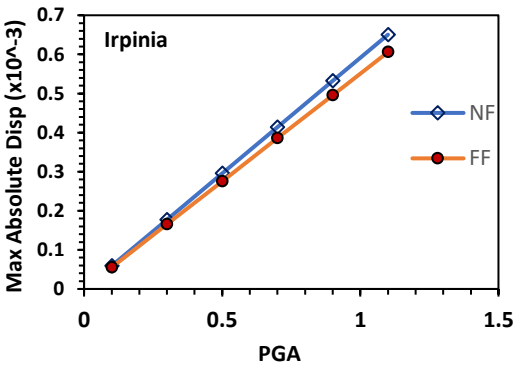
Irpinia
Max Absolute Disp (x10^-3)
PGA
NF
FF

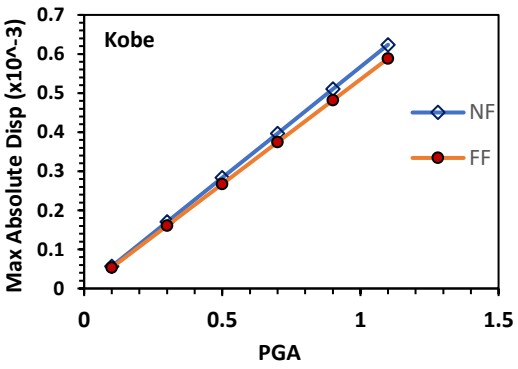
Kobe
Max Absolute Disp (x10^-3)
PGA
NF
FF

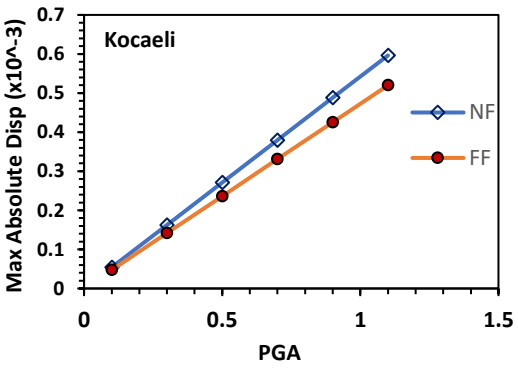
Kocaeli
Max Absolute Disp (x10^-3)
PGA
NF
FF

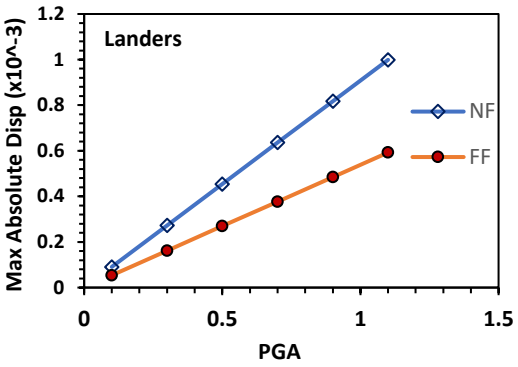
Landers
Max Absolute Disp (x10^-3)
PGA
NF
FF

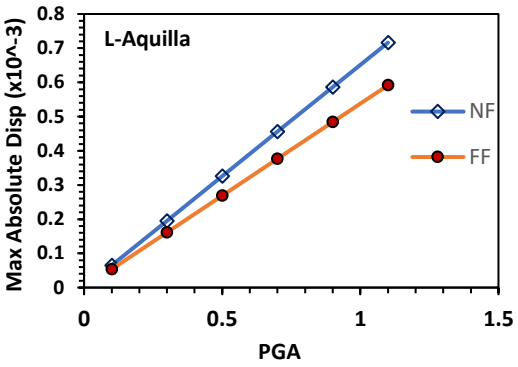
L-Aquilla
Max Absolute Disp (x10^-3)
PGA
NF
FF

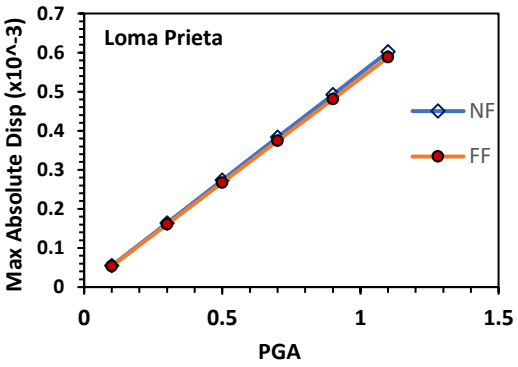
Loma Prieta
Max Absolute Disp (x10^-3)
PGA
NF
FF

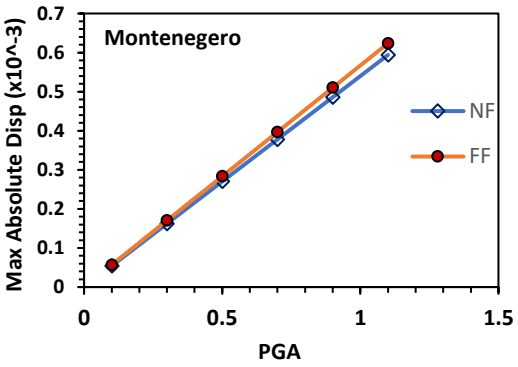
Montenegero
Max Absolute Disp (x10^-3)
PGA
NF
FF

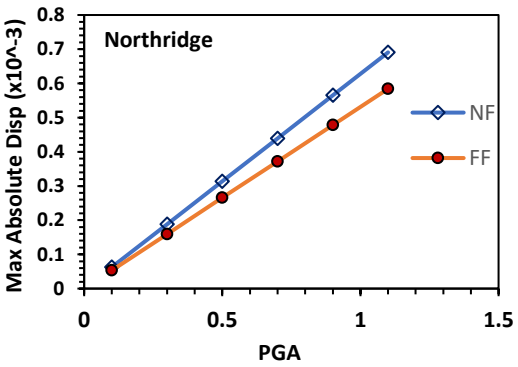
Northridge
Max Absolute Disp (x10^-3)
PGA
NF
FF

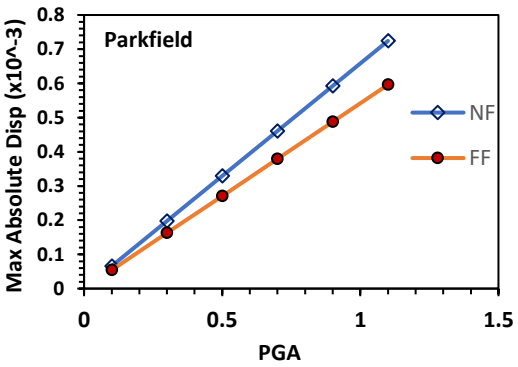
Parkfield
Max Absolute Disp (x10^-3)
PGA
NF
FF

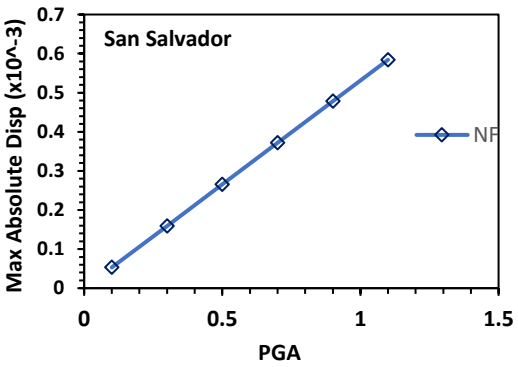
San Salvador
Max Absolute Disp (x10^-3)
PGA
NF

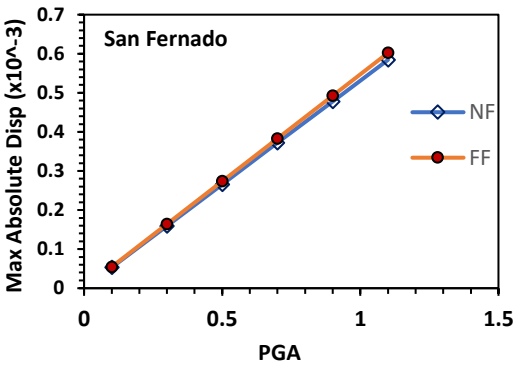
San Fernado
Max Absolute Disp (x10^-3)
PGA
NF
FF

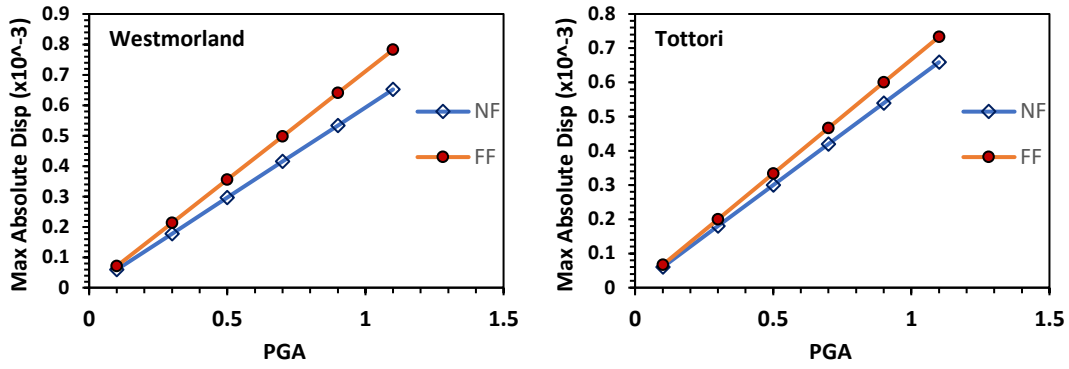

Figure 5.6 Comparative plots of Maximum Absolute displacement vs PGA for NF and FF earthquake records

For a particular ground motion, NF constitutes a higher displacement impact on a structure as compared to FF ones. Figure 5.7 depicts the correlation b/w the two.

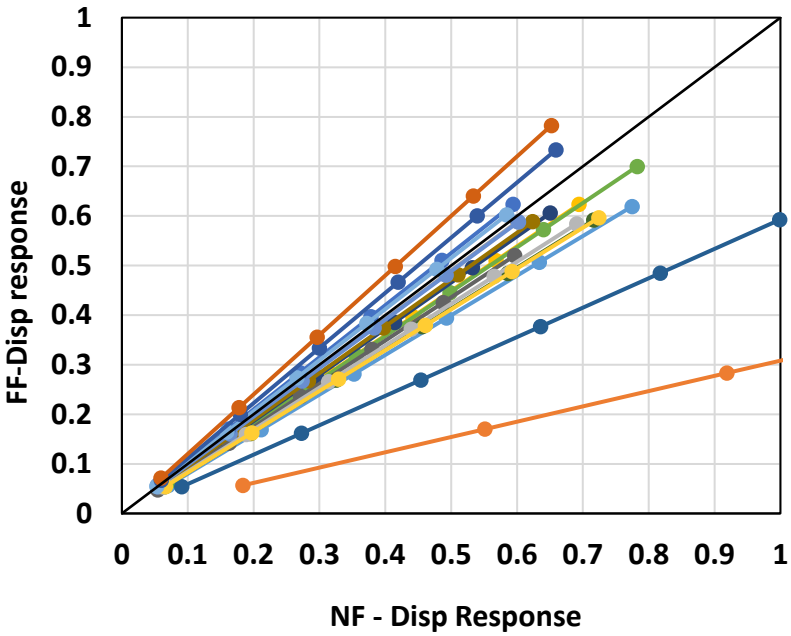

Figure 5.7 FF vs NF displacement response

The mean of absolute displacement for all earthquake records is calculated and plotted in Figure 5.8

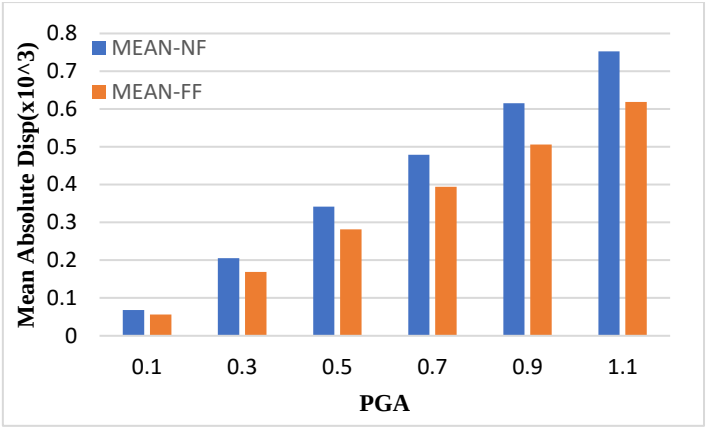

Figure 5.8 Mean of absolute displacement for NF and FF for specified acceleration values

Furthermore, the maximum displacement response has been correlated with PGA and Arias Intensity as shown in Figure

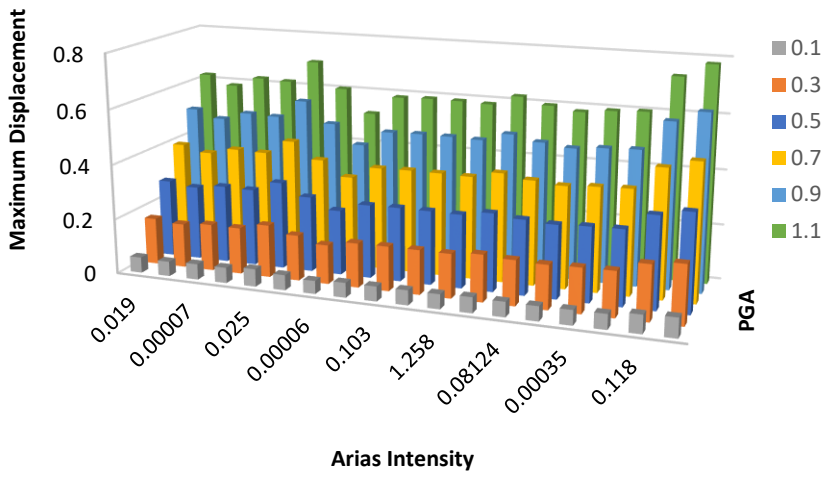

Figure 5.9 Correlation plot of maximum displacement response with PGA and Arias Intensity for NF ground motions

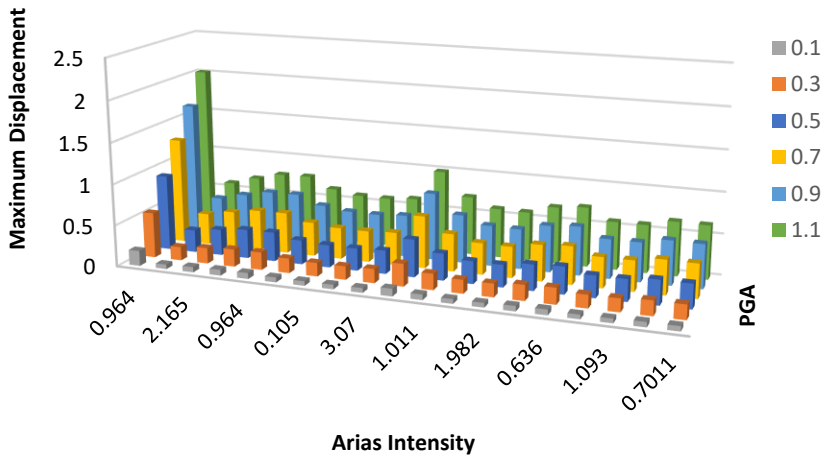

Figure 5.10 Correlation plot of maximum displacement response with PGA and Arias Intensity for FF ground motions

5.3.2. Potential Energy

In earthquake engineering, potential energy refers to the energy stored within a system that can be released during an earthquake. This energy is primarily associated with the elastic deformation of the Earth's crust and the subsequent release of stored stress along fault lines. Therefore, Potential Energy becomes one of the crucial energy parameters to be analyzed. A typical Potential Energy vs time plot is shown in Figure 5.12

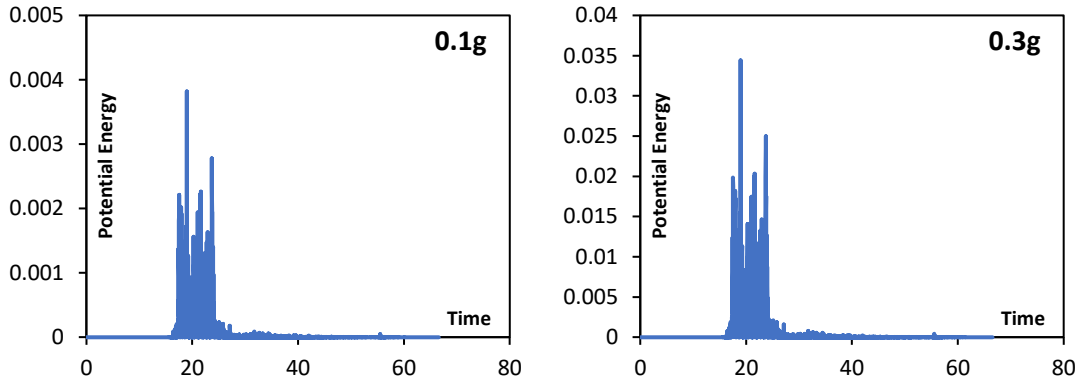

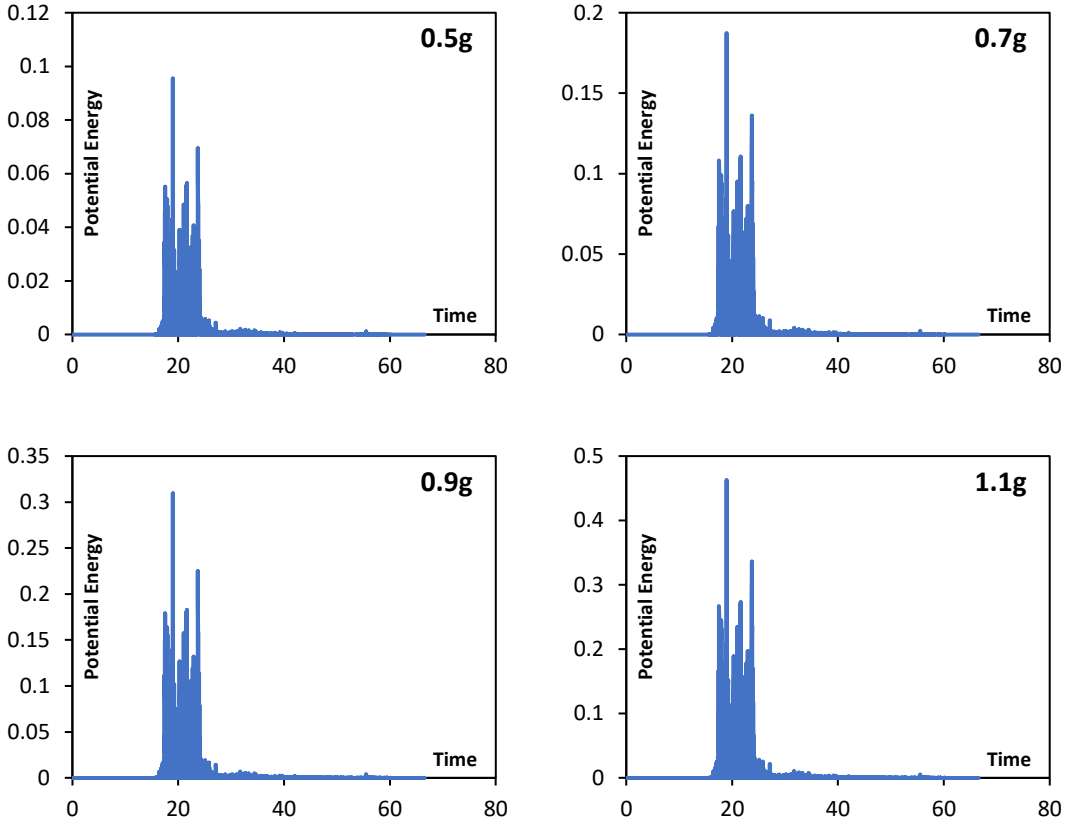

Figure 5.11 Typical Potential Energy vs Time plot for Bam-NF earthquake

The maximum potential energy was calculated and plotted against PGA for both NF and FF earthquake records. The comparative plots have been shown in Figure 5.13

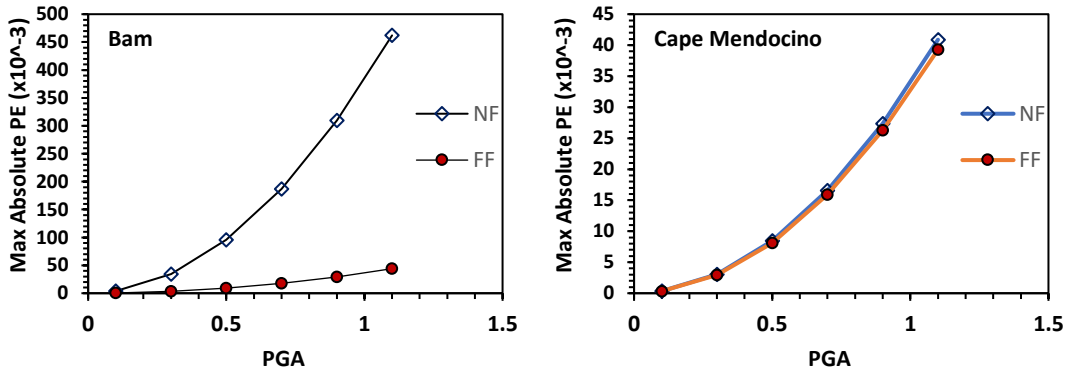

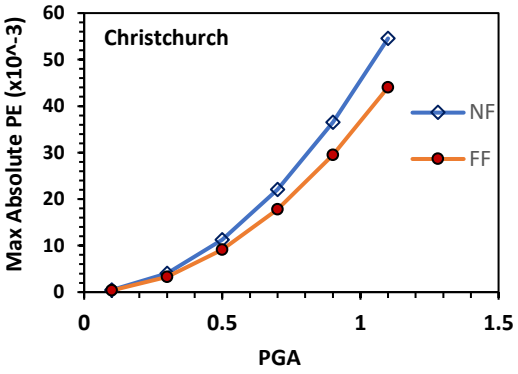
Christchurch
Max Absolute PE (x10^-3)
PGA
NF
FF

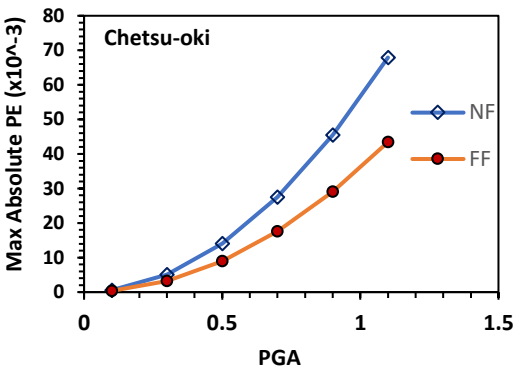
Chetsu-oki
Max Absolute PE (x10^-3)
PGA
NF
FF

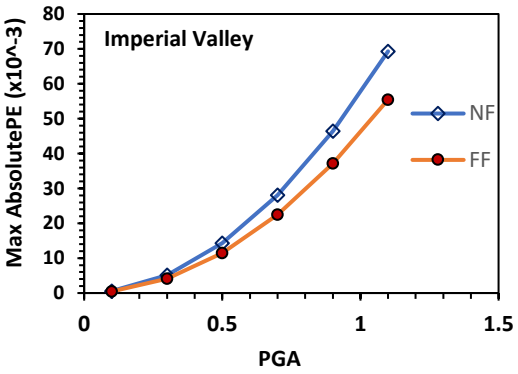
Imperial Valley
Max AbsolutePE (x10^-3)
PGA
NF
FF

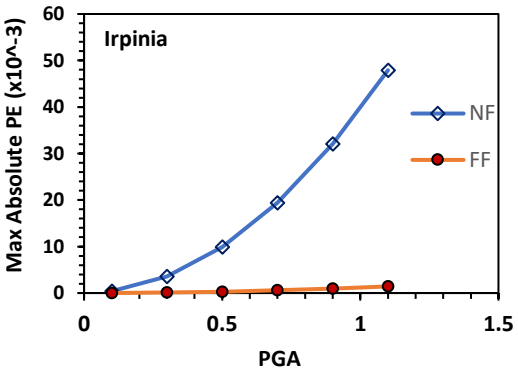
Irpinia
Max Absolute PE (x10^-3)
PGA
NF
FF

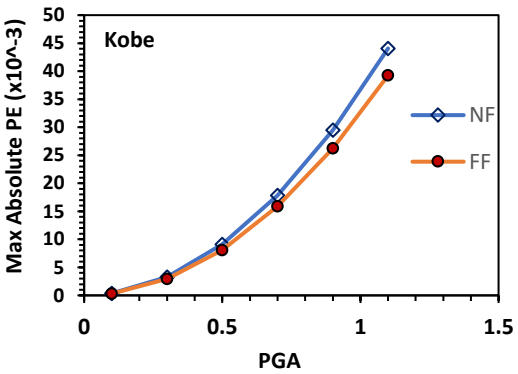
Kobe
Max Absolute PE (x10^-3)
PGA
NF
FF

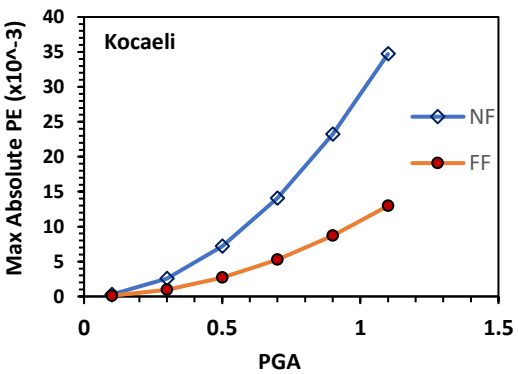
Kocaeli
Max Absolute PE (x10^-3)
PGA
NF
FF

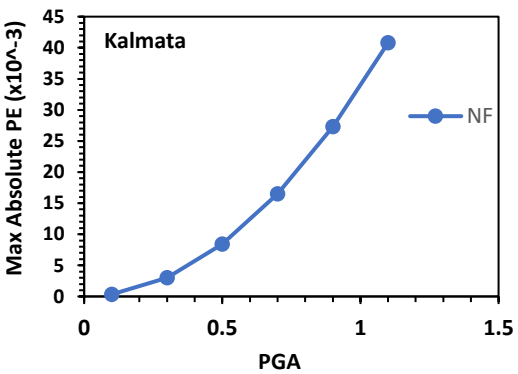
Kalmata
Max Absolute PE (x10^-3)
PGA
NF

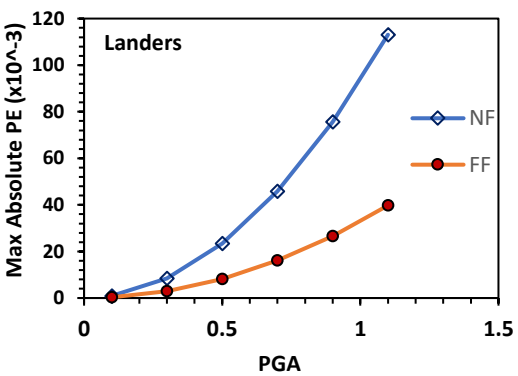
Landers
Max Absolute PE (x10^-3)
PGA
NF
FF

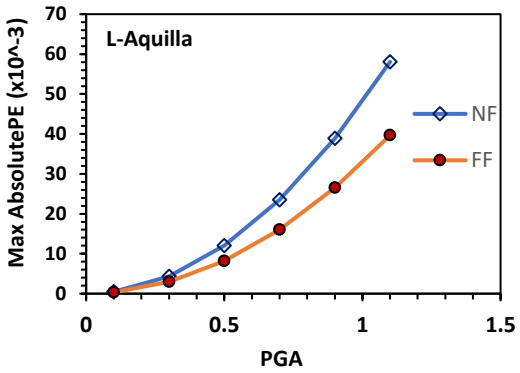
L-Aquilla
Max AbsolutePE (x10^-3)
PGA
NF
FF

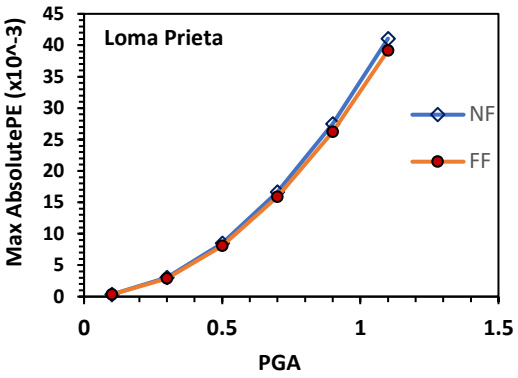
Loma Prieta
Max AbsolutePE (x10^-3)
PGA
NF
FF

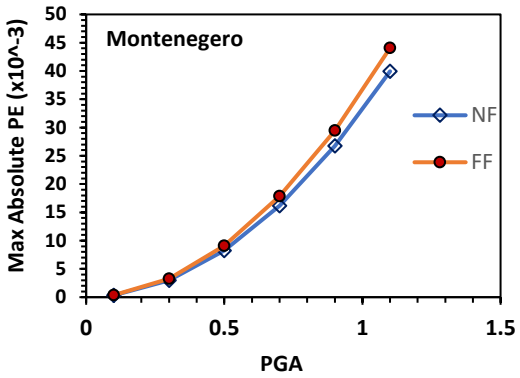
Montenegero
Max Absolute PE (x10^-3)
PGA
NF
FF

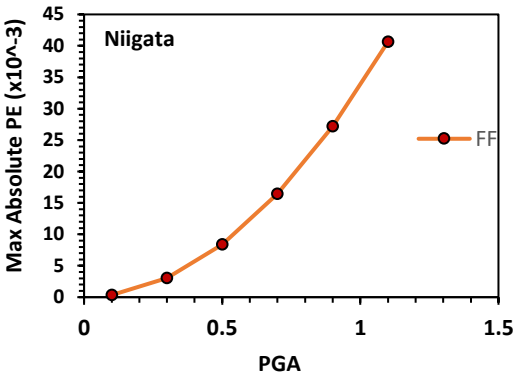
Niigata
Max Absolute PE (x10^-3)
PGA
FF

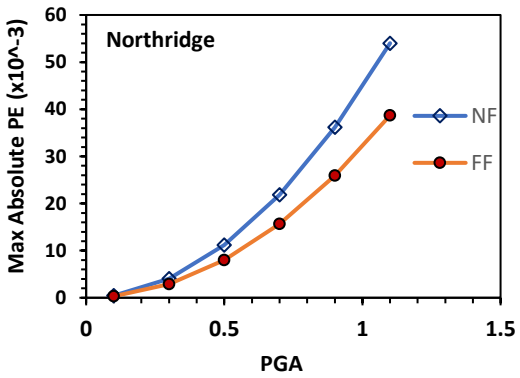
Northridge
Max Absolute PE (x10^-3)
PGA
NF
FF

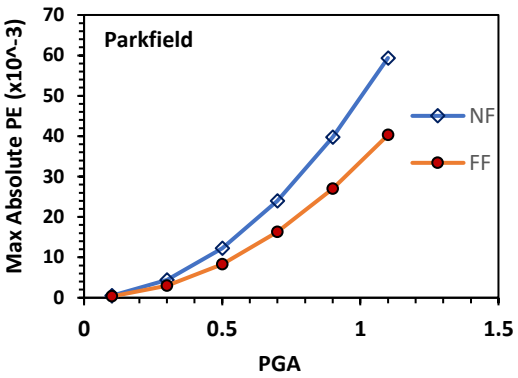
Parkfield
Max Absolute PE (x10^-3)
PGA
NF
FF

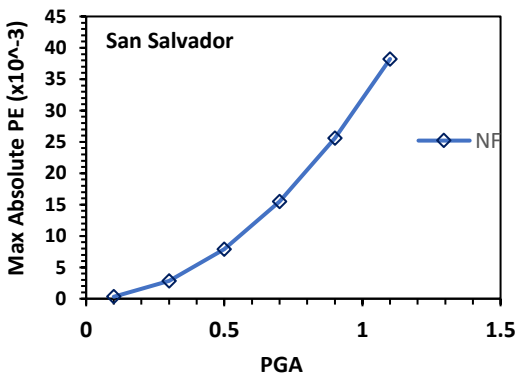
San Salvador
Max Absolute PE (x10^-3)
PGA
NF

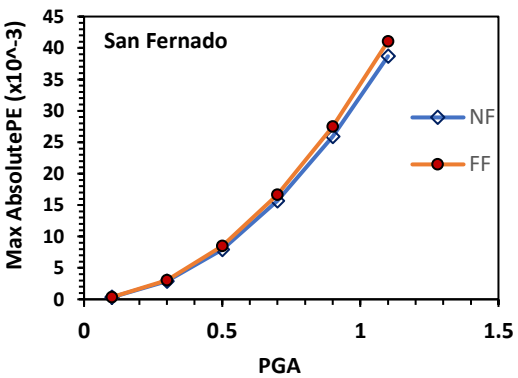
San Fernado
Max AbsolutePE (x10^-3)
PGA
NF
FF

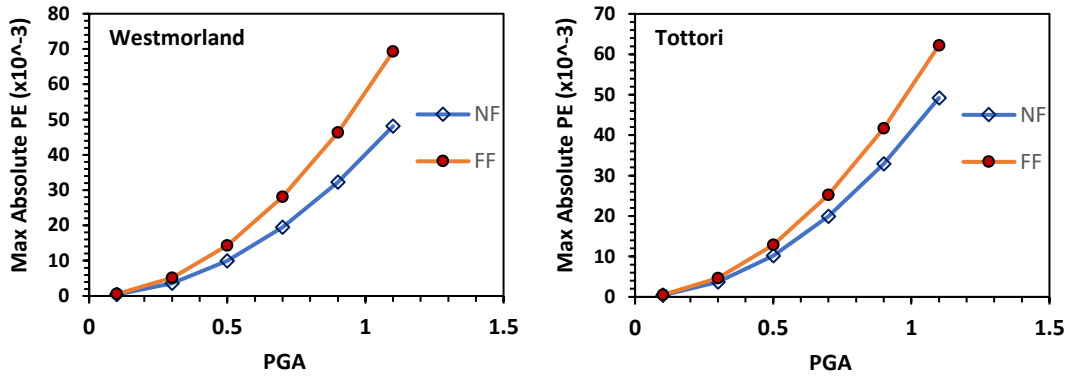

Figure 5.12 Comparative plots of Maximum Absolute Potential vs PGA for NF and FF earthquake records

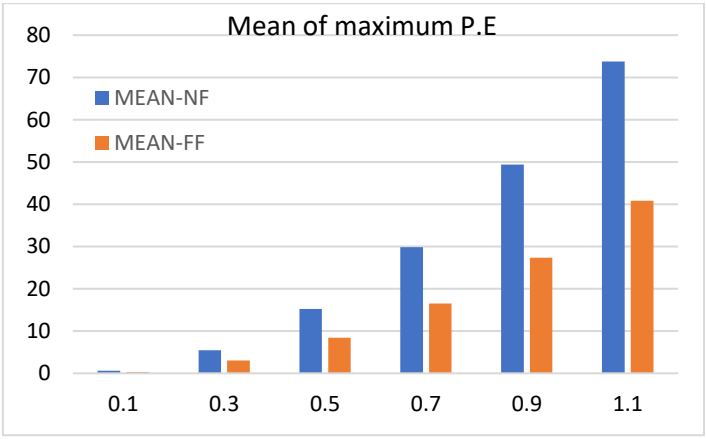

Figure 5.13 Mean of absolute potential energy for NF and FF for specified acceleration values

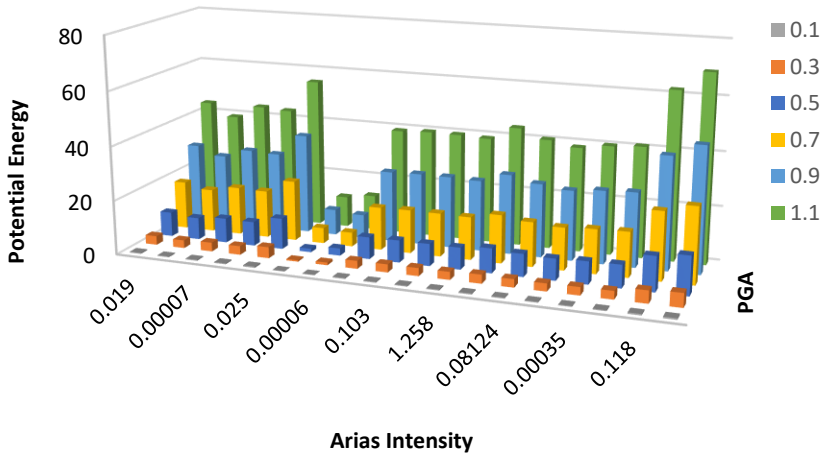

Figure 5.14 Correlation plot of maximum potential energy response with PGA and Arias Intensity for NF ground motions

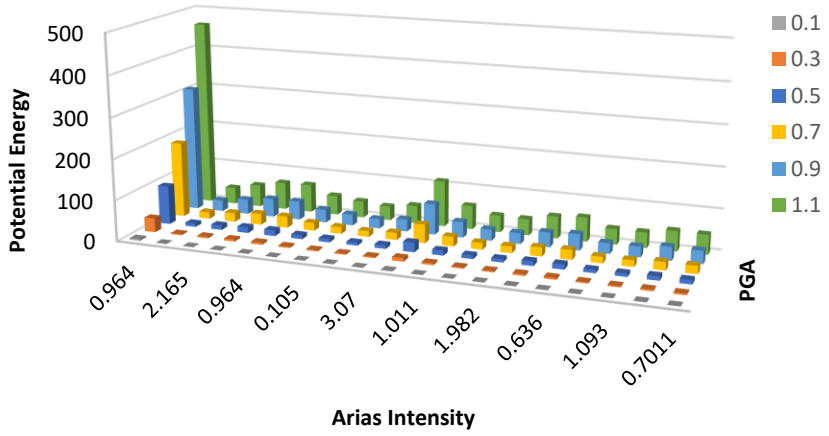

Figure 5.15 Correlation plot of maximum potential energy response with PGA and Arias Intensity for FF ground motions

5.3.3. Base Shear

Base shear refers to the total lateral force that is exerted at the base of a structure during an earthquake. It represents the horizontal force that acts on a building or structure due to ground motion caused by an earthquake.

By designing structures to resist the base shear forces, the aim is to minimize the potential for structural damage, ensure the safety of occupants, and enhance the overall seismic performance of buildings during earthquakes. A typical Base shear vs time plot is shown in Figure 5.18

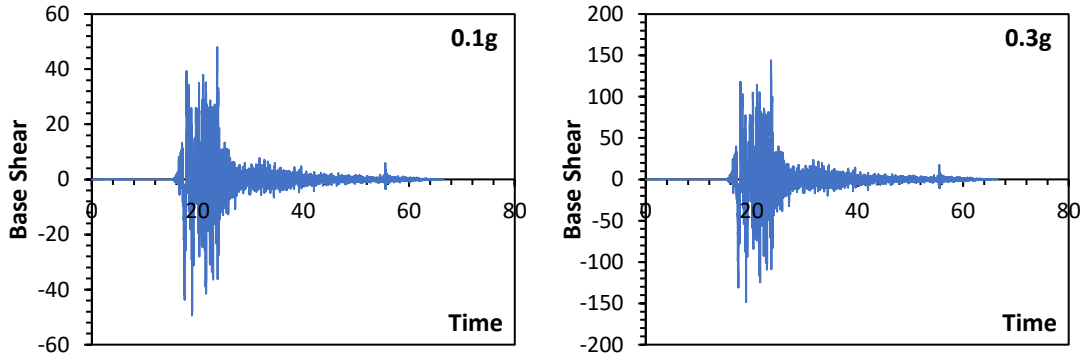

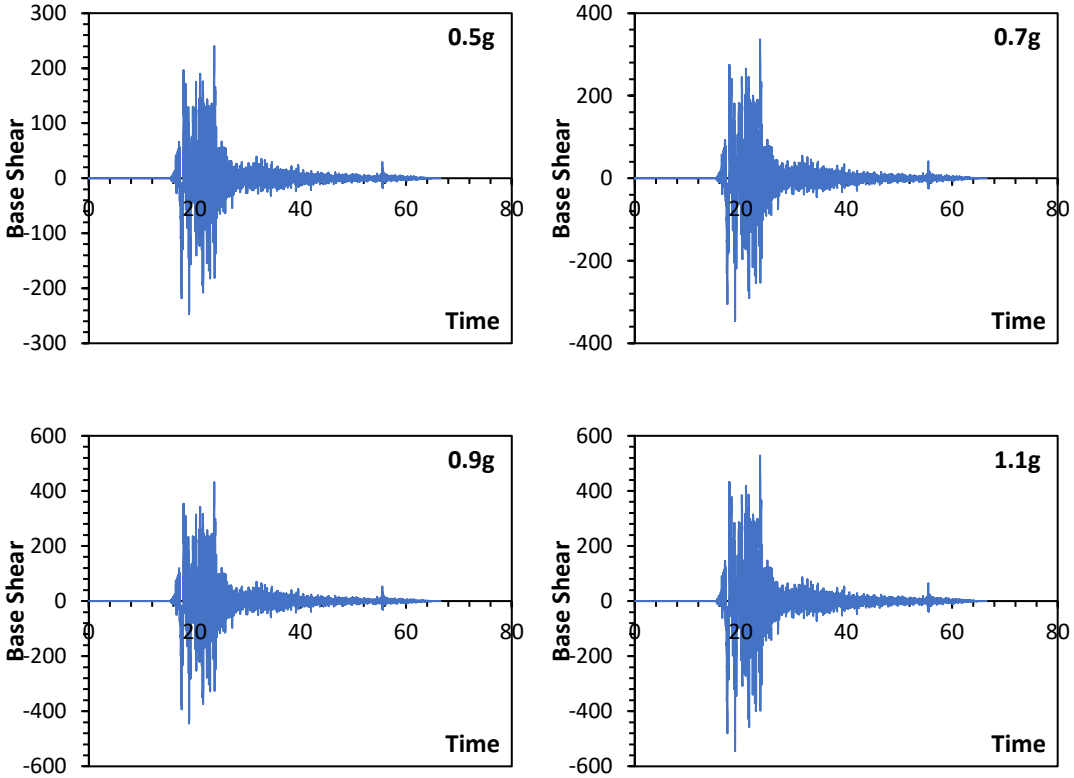

Figure 5.16 Typical Base Shear vs Time Plot for BAM-NF ground motion

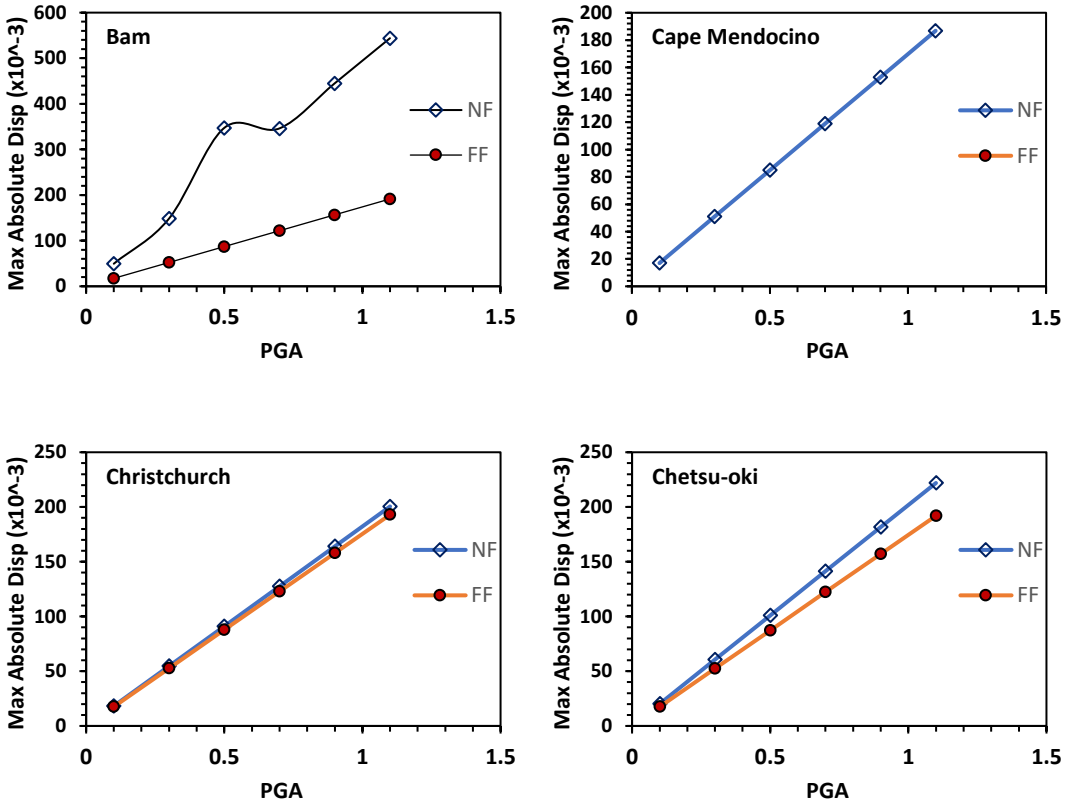

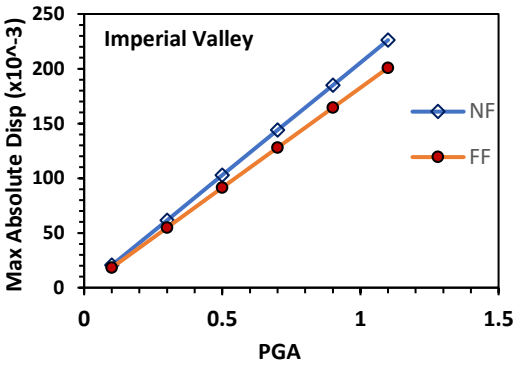
Imperial Valley
Max Absolute Disp (x10^-3)
PGA
NF
FF

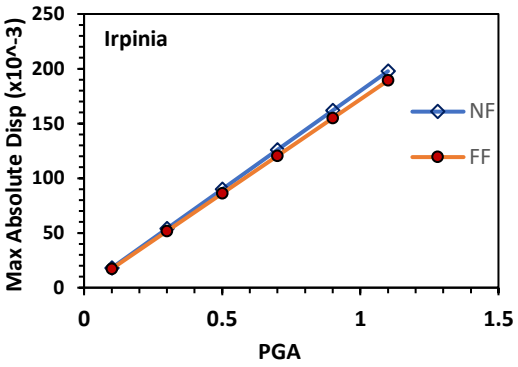
Irpinia
Max Absolute Disp (x10^-3)
PGA
NF
FF

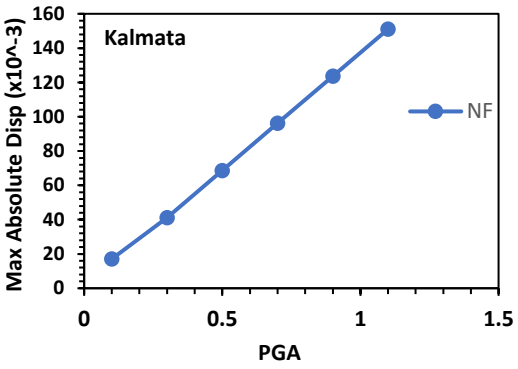
Kalmata
Max Absolute Disp (x10^-3)
PGA
NF

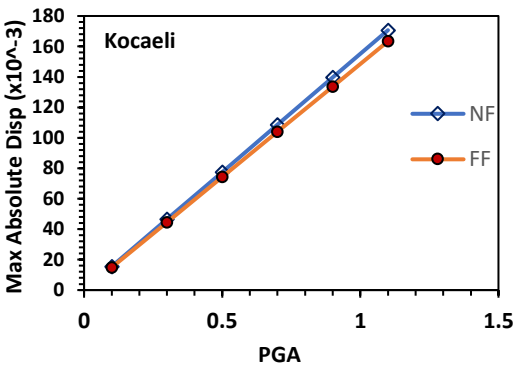
Kocaeli
Max Absolute Disp (x10^-3)
PGA
NF
FF

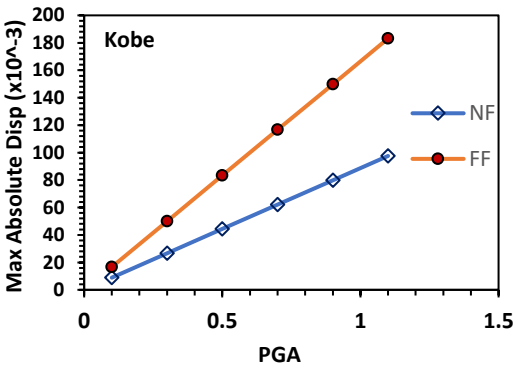
Kobe
Max Absolute Disp (x10^-3)
PGA
NF
FF

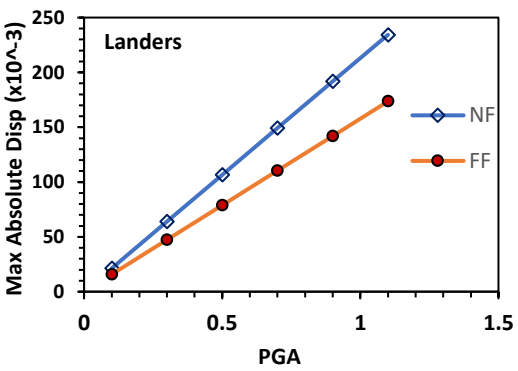
Landers
Max Absolute Disp (x10^-3)
PGA
NF
FF

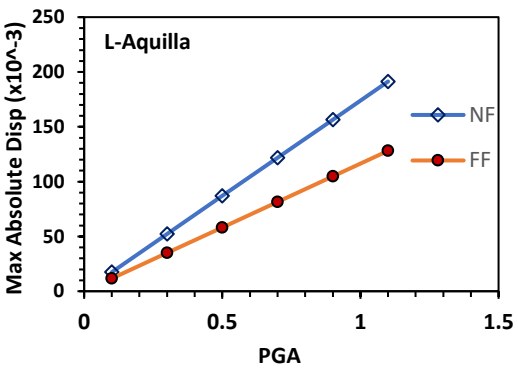
L-Aquilla
Max Absolute Disp (x10^-3)
PGA
NF
FF

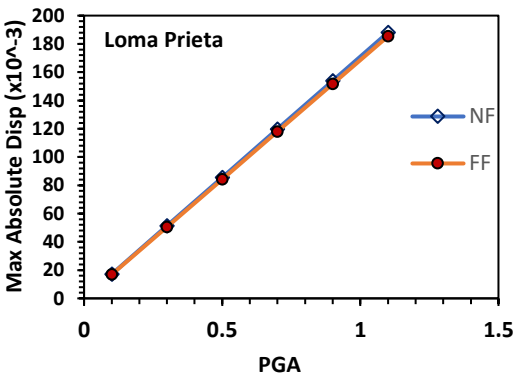
Loma Prieta
Max Absolute Disp (x10^-3)
PGA
NF
FF

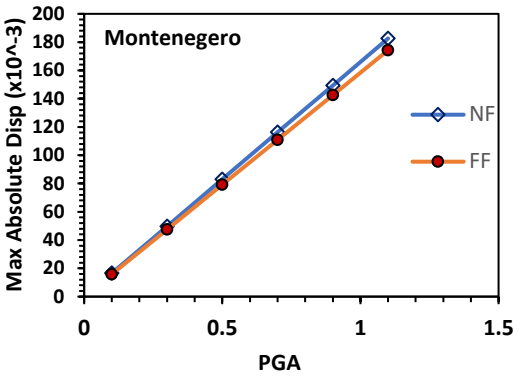
Montenegero
Max Absolute Disp (x10^-3)
PGA
NF
FF

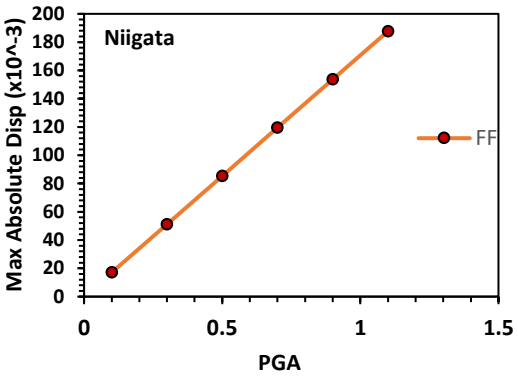
Niigata
Max Absolute Disp (x10^-3)
PGA
FF

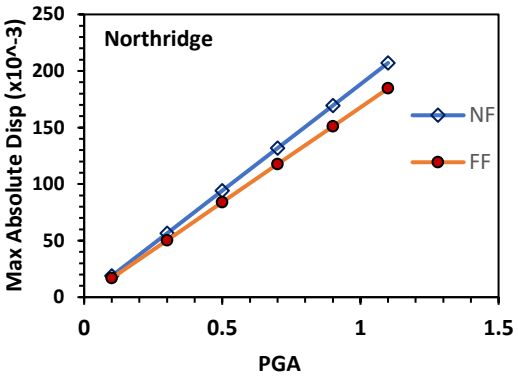
Northridge
Max Absolute Disp (x10^-3)
PGA
NF
FF

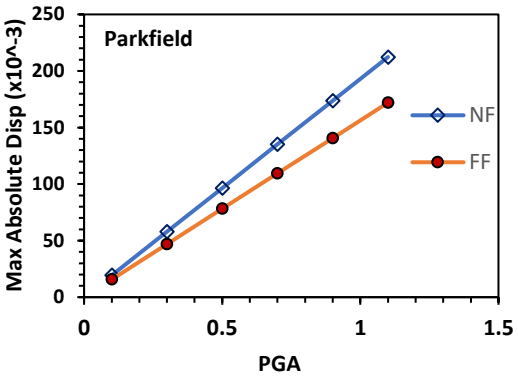
Parkfield
Max Absolute Disp (x10^-3)
PGA
NF
FF

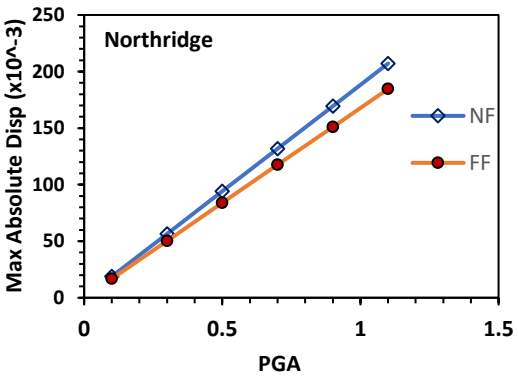
Northridge
Max Absolute Disp (x10^-3)
PGA
NF
FF

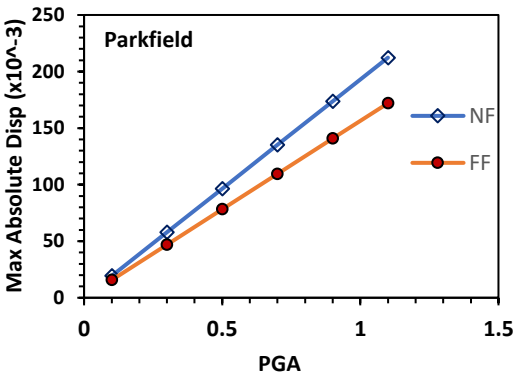
Parkfield
Max Absolute Disp (x10^-3)
PGA
NF
FF

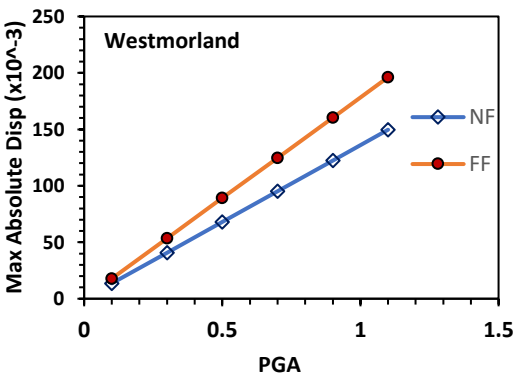
Westmorland
Max Absolute Disp (x10^-3)
PGA
NF
FF

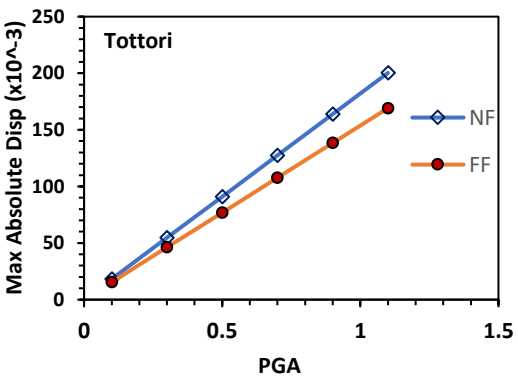
Tottori
Max Absolute Disp (x10^-3)
PGA
NF
FF

Figure 5.17 Comparative plots of Maximum Absolute Base Shear vs PGA for NF and FF earthquake records

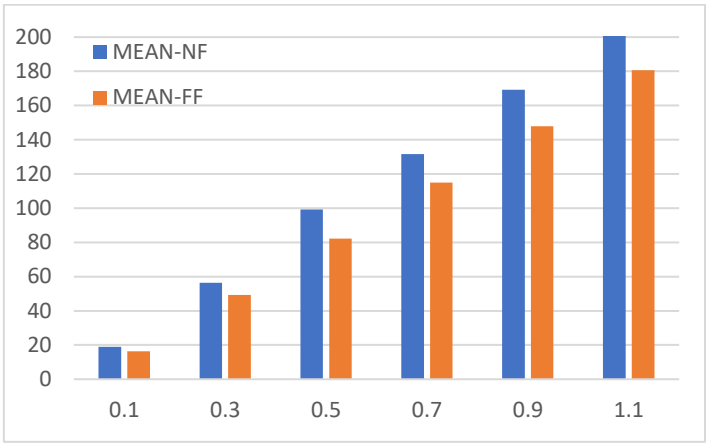

Figure 5.18 Mean of absolute potential energy for NF and FF for specified acceleration values

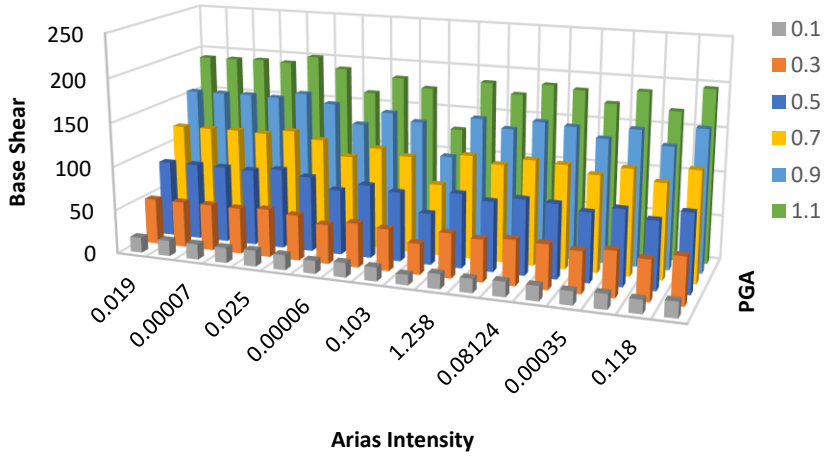

Figure 5.19 Correlation plot of maximum base shear with PGA and Arias Intensity for NF ground motions

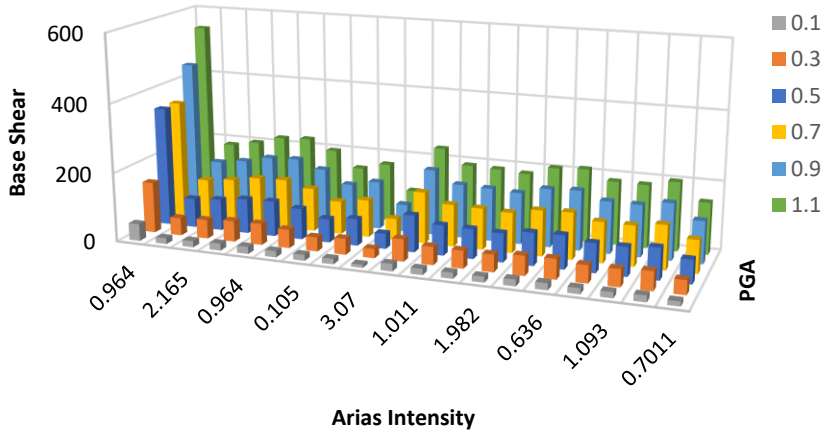

Figure 5.20 Correlation plot of maximum base shear with PGA and Arias Intensity for FF ground motions

5.3.4. Regression Analysis

The regression analysis was performed for both ground motions (NF and FF). The inter-relationships derived from regression has been shown from Equation 5.1 to Equation 5 .6.

Coefficient of Determination, R^2- It is a statistical measure which represents the proportion of variance for a dependent variable that can be explained by independent variables in regression analysis. More the value of R^2, the stronger relation holds between the dependent and the independent variables of regression model. When the variance accounts to be high, the data points tend to fall closer to the fitted regression line as illustrated in Figure 5.21

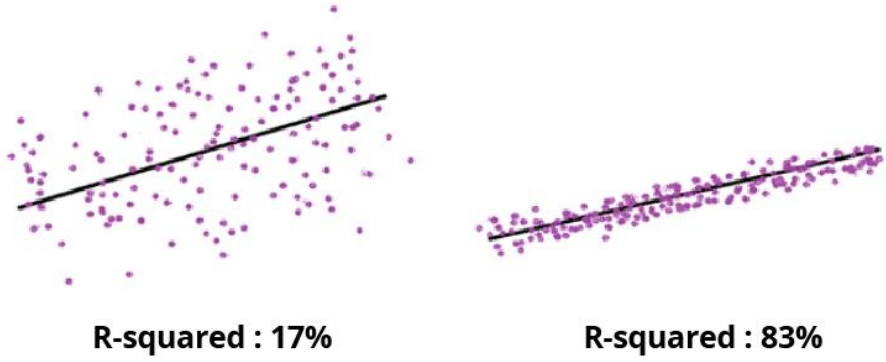

Figure 5.21 Visual representation of R^2

The observed value for R^2 is greater than 0.9(90%) for FF ground motions, while greater than 0.55(55%) for NF ground motions. This clearly indicates that regression model with considered parameters holds a strong relationship in case of FF ground motions as compared to NF

For NF-ground motions (R^2>0.55)

Max Disp. = 0.095-0.0019*AI+0.676*PGA-0.162*(V/A)-0.027* f_d (Eqn. 5.1)

Max. P.E. = 1.412+0.764*AI+73.045*PGA-22.45*(V/A) -4.305* f_d (Eqn. 5.2)

Max. Base Sh. = 15.85+1.219*AI+187.158*PGA+14.273*(V/A) -4.878* f_d (Eqn. 5.3)

For FF-ground motions (R^2>0.90)

Max. Disp. = 0.024-0.046*AI+0.563*PGA-0.246*(V/A) +0.0024*f_d (Eqn. 5.4)

Max. P.E.= -4.604-11.42*AI+41.096*PGA-42.88*(V/A)+0.487*f_d (Eqn. 5.5)

Max. Base Sh/= 3.898 -3.755 *AI+164.834*PGA-40.75*(V/A) +0.984*f_d (Eqn. 5.6)

CHAPTER - 6

SUMMARY AND CONCLUSIONS

6.1. Overall Summary

NF ground motions exhibits strong pulse waves which are very different in nature as compared to FF ground motions. Therefore, difference b/w both type of ground motions has been observed. The input ground motions have been characterized and response spectrum has been plotted to observe the affects. The ground motions have been input to one-story fully infilled portal frame in order to access the difference in response of NF and FF on seismic response.

6.2. Conclusions

The following conclusions are drawn from the nonlinear analysis using the considered NF and FF ground motions in the present study –

1. Characterization of ground motion: Ground motions have been characterized based on Energy parameters (Arias Intensity and Energy Flux) and Spectral Parameters (Fourier Amplitude and Power Amplitude). The scattering of plots signifies that ground motions (both NF and FF) are selected so that, the diversification could account for better analysis as each ground motion possess a different range of selected parameter. Specific Energy Plots shows the most scattering amongst all signifying more variations in NF and FF response. Response spectrum peaks have been comparatively large for NF, making structures more prone to seismic damage as compared to FF ones. NF Response spectrum more seismic demands as compared to FF and even combined response spectrum. Dominant frequency was observed to be greater for FF which signifies that FF ground motions reaches its maximum amplitude after NF and having strong short pulses in case of NF.
2. Non-Lineear Time History Analysis (NLTHA**)**: Regression Analysis have been performed and inter-relationship between response (Output) with ground motion parameters (AI, PGA, f_d, SED, $(V/A)_{max}$) was derived. The regression model for FF holds a strong validation as compared to NF ground motions. FF ground motions hold a strong correlation with PGA, AI and f_d. (V/A) and f_d shows a good correlation amongst output response parameters.

6.3. Future Scope

The present study considered the response of single-story portal frame over varying ground motion parameters to visualize the effects of NF and FF ground motions. A multi-storey frame can be analyzed in similar manner and subsequently response parameters such as Interstory Drift, Displacement etc. can be accessed for NF and FF ground motions separately.

REFERENCES

Abrahamson NR. “Velocity Pulses in Near-Fault Ground Motions (2002)”; In: CUREE Symposium; Berkeley, CA.

Arias, A. (1970). “A measure of earthquake intensity.” In: Hansen, R.J. (Ed.), *Seismic Design for Nuclear Power Plants*. MIT Press, Cambridge, pp. 438–483.

B. A. Bolt and N. A. Abrahamson, "*Estimation of strong ground motion*," in International Handbook of Earthquake Engineering Seismology, IASPEI, (2003), pp. 983-1001.

Bommer, J. J., Magenes, G., Hancock, J., and Penazzo, P. (2004). “The influence of strong-motion duration on the seismic response of masonry structures.” *Bulletin of Earthquake Engineering*, Vol. 2, pp. 1-26.

Campione, G., Cavaleri, L., Macaluso, G., & Amato, G. (2014). “Evaluation of infilled frames: an updated in-plane-stiffness macro-model considering the effects of vertical loads”.

FEMA-273: 73: NEHRP guidelines for the seismic rehabilitation of buildings. Federal Emergency Management Agency (1997)

FEMA 356 (2000), Prestandard and Commentary for the Seismic Rehabilitation of Buildings, Washington, D.C.

Ghaffarzadeh, H., and Nazeri, A. (2015). “The effect of the vertical excitation on horizontal response of structures.” Earthquakes and Structures, Vol. 9(3), pp. 625-637.

Gutenberg, B., Richter, C.F., (1942). “Earthquake magnitude: intensity, energy and acceleration”. Bulletin of Seismological Society of America Vol. 32, 163–191.

Hancock, J., and J. J. Bommer (2006). “A state-of-knowledge review of the influence of strong-motion duration on structural damage,” Earthquake Spectra 22, Vol. 3, 827–845.

Hancock, J., and J. J. Bommer (2007). Using spectral matched records to explore the influence

of strong-motion duration on inelastic structural response, Soil Dynamics and Earthquake Engineering, Vol. 4, 291–299.

Housner, G.W., (1952). “Spectrum intensity of strong motion earthquakes.” In: Proceedings of the Symposium on Earthquakes and Blast Effects on Structures. Earthquake Engineering Research Institute, California, pp. 20–36.

Housner, G.W., Jennings, P.C., (1964). “Generation of artificial earthquakes.” J. Eng. Mech. Div. ASCE 90, 113–152.

H. Moniri, “Evaluation of seismic performance of reinforced concrete (RC) buildings under near-field earthquakes,” pp. 13-25, (2017).

Ibarra LF, Krawinkler H. “Global collapse of frame structures under seismic excitations (2005);” Blume Earthquake Engineering Center Technical Report 152; Stanford, CA.

Ibrahim, Y.E.; El-Shami, M.M. “Seismic fragility curves for midrise reinforced concrete frames in Kingdom of Saudi Arabia.” IES J. Part A Civil Structural Engineering Vol. 4(4), 213–223 (2011)

J. P. Singh and M. EERI, "Earthquake Ground Motions: Implications for Designing Structures and Reconciling Structural Damage," Earthquake Spectra, Vol. 1, no. 2, pp. 239-270, (1985).

Kaushik, H. B., Rai, D. C., & Jain, S. K. (2009). “Effectiveness of Some Strengthening Options for Masonry-Infilled RC Frames with Open First Story.” ASCE, 925-937.

Kim, S.J. and Elnashai, A.S. (2008), “Seismic assessment of RC structures considering vertical ground motion”, MAE Center Report, No. 08-03.

Krawinkler, H. and Alavi, B., “Development of Improved Design Procedures for Near Fault Ground Motions”, In *SMIP98, Seminar on Utilization of Strong Motion Data*, Oakland, California, (1998).

Lignos D, Krawinkler H, Whittaker AS. “Prediction and validation of sidesway collapse of two

scale models of a 4-story steel moment frame." Earthquake Engineering & Structural Dynamics (2011); Vol. 40: 807–825

Li,Y.; Fan, F.;Hong, H. "Influence of number of records and scaling on the statistics of seismic demand for lattice structure." Thin-Walled Struct. Vol. 87, 115–126 (2015)

Louie, J. (2011). "Plate Tectonics, the cause of Earthquakes." Retrieved April 4, 2016
Makris N, Black CJ. Dimensional Analysis of Rigid-Plastic and Elastoplastic Structures under Pulse-Type Excitations. Journal of Engineering Mechanics 2004; Vol. 130 (9): 1006–1018

Park, Y.J., Ang, A.H.S., Wen, Y.K., (1985). "Seismic damage analysis of reinforced concrete buildings." Journal of Structural. Engineering, Vol. 111, 740–757.

Rosenblueth, E., 1964. "Probabilistic design to resist earthquakes". J. Eng. Mech. Div. ASCE 90, 189–219.

Sharma, V., Shrimali, M. K., Bharti, S. D., & Datta, T. K. (2020). "Seismic fragility evaluation of semi-rigid frames subjected to near-field earthquakes." Journal of Constructional Steel Research.

Silva, V. et al.: "Evaluation of analytical methodologies used to derive vulnerability functions." Earthquake Engineering & Structural Dynamics Vol. 43(2), 181– 204 (2014)

S. L. Burks and W. J. Baker, "Fling In Near-Fault Ground Motions and Its Effect on Structural Collapse Capacity," in Tenth U.S. National Conference on Earthquake Engineering, Anchorage, Alaska, (2014).

Stewart JP, Chiou SJ, Bray JD, Graves RW, Somerville PG, Abrahamson NA. Ground Motion "Evaluation Procedures for Performance-Based Design 2001"; Pacific Earthquake Engineering Research Center Technical Report (2001/09); Berkeley, CA.

Trifunac, M.D., Brady, A.G., (1975). "A study on the duration of strong earthquake ground Motion". Bulletin of Seismological Society of America, Vol. 65, 581–626.

UpSeis. (2007). What are seismic waves? Retrieved April 4, 2016, from http://www.geo.mtu.edu/UPSeis/waves.html

Von Thun, J.L., Rochim, L.H., Scott, G.A., Wilson, J.A., (1988). “Earthquake Ground Motions for Design and Analysis of Dams, Earthquake Engineering and Soil Dynamics II- Recent Advance in Ground Motion Evaluation”, Vol. 20. Geotechnical Special Publication, New York, pp. 463–481. ASCE.

V. V. Beretero, S. A. Mahin and R. A. Herrera, "Aseisimic Design Implications of Near-Fault San Fernado Earthquake Records," Earthquake Engineering and Structural Dynamics, Vol. 6, pp. 31-42, (1978).

Zhang, S., & Wang, G. (2013). “Effects of near-fault and far-fault ground motions on nonlinear dynamic response and seismic damage of concrete gravity dams”. Soil Dynamics and Earthquake Engineering, 217-229

APPENDIX-I

CHARACTERIZATION OF GROUND MOTIONS:

Energy parameters:-

Arias Intensity (NF):

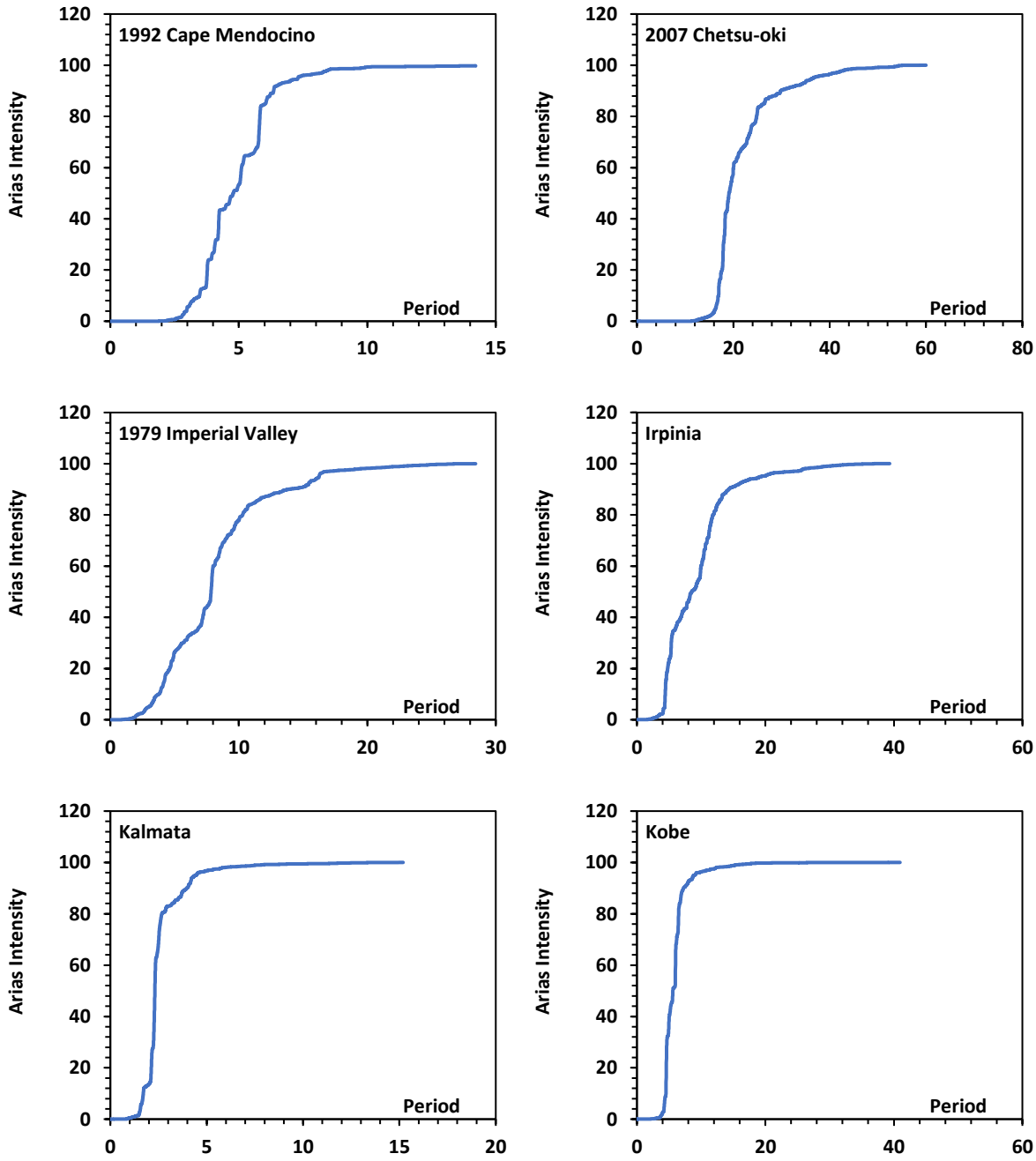

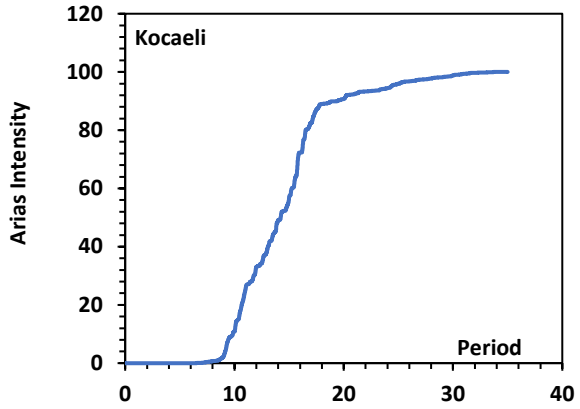
Kocaeli
Arias Intensity
Period
0
20
40
60
80
100
120
0
10
20
30
40

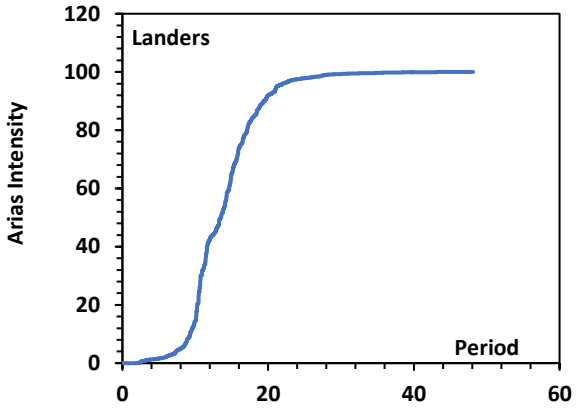
Landers
Arias Intensity
Period
0
20
40
60
80
100
120
0
20
40
60

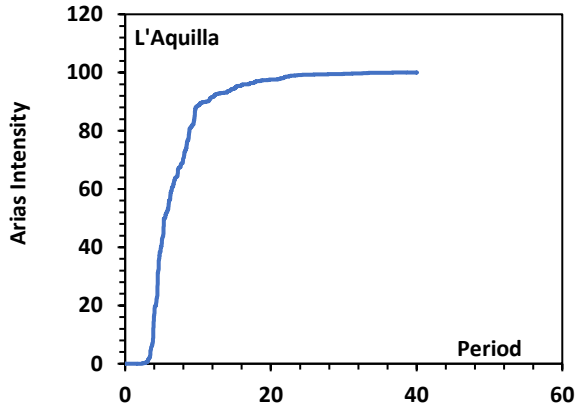
L'Aquilla
Arias Intensity
Period
0
20
40
60
80
100
120
0
20
40
60

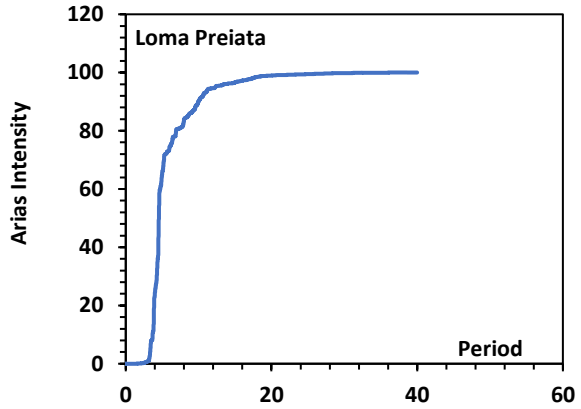
Loma Preiata
Arias Intensity
Period
0
20
40
60
80
100
120
0
20
40
60

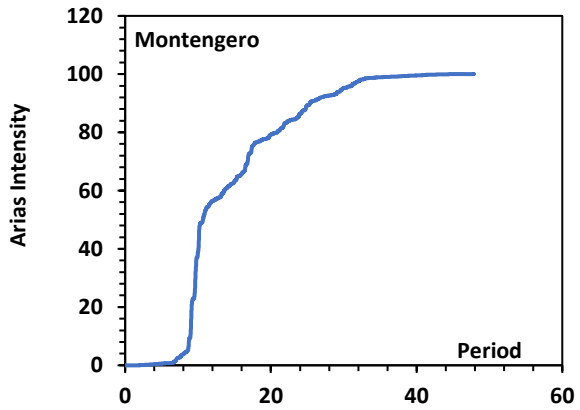
Montengero
Arias Intensity
Period
0
20
40
60
80
100
120
0
20
40
60

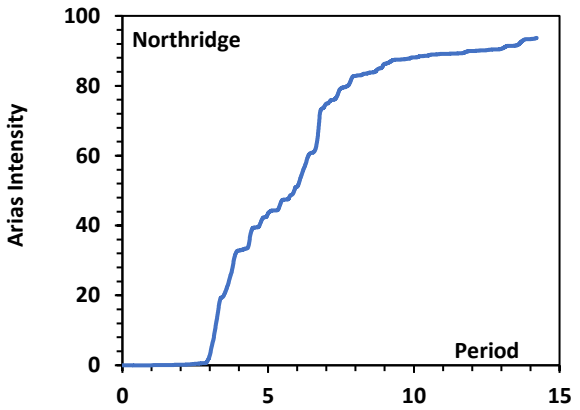
Northridge
Arias Intensity
Period
0
20
40
60
80
100
0
5
10
15

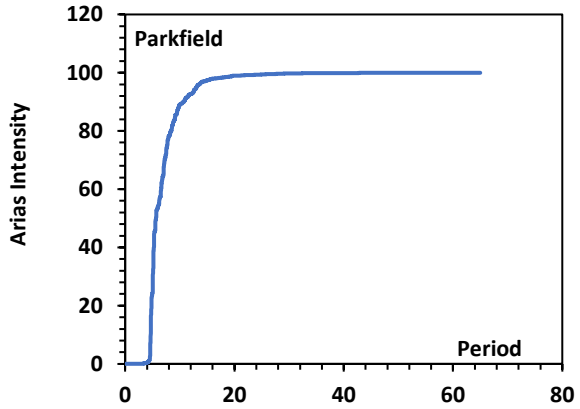
Parkfield
Arias Intensity
Period
0
20
40
60
80
100
120
0
20
40
60
80

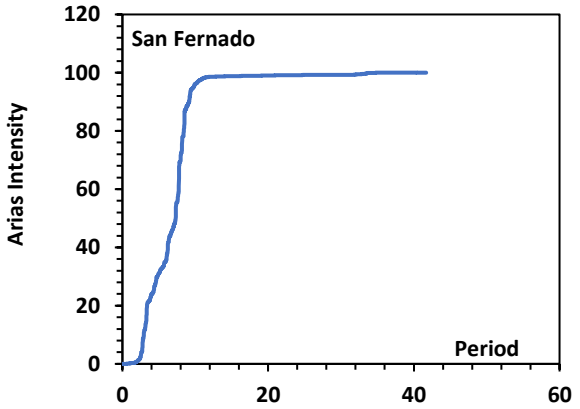
San Fernado
Arias Intensity
Period
0
20
40
60
80
100
120
0
20
40
60

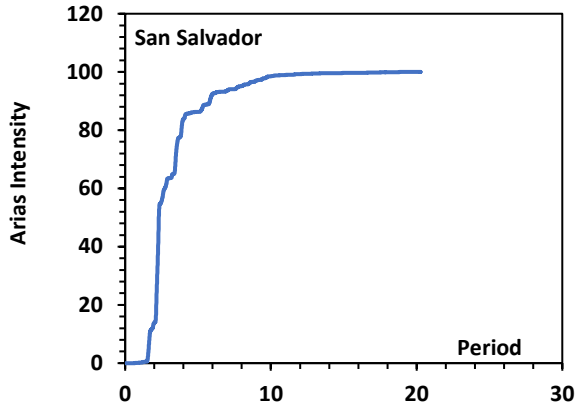

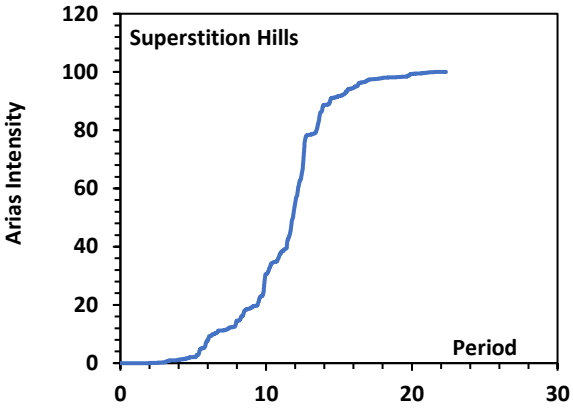

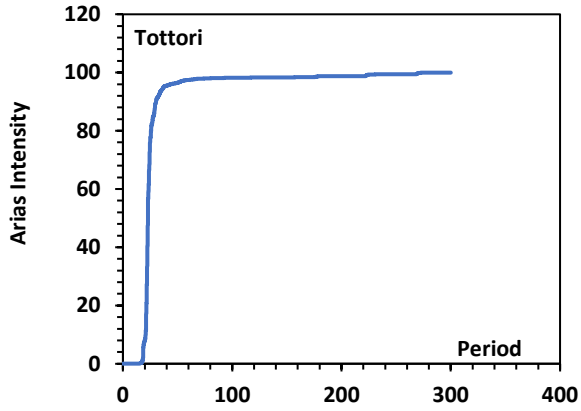

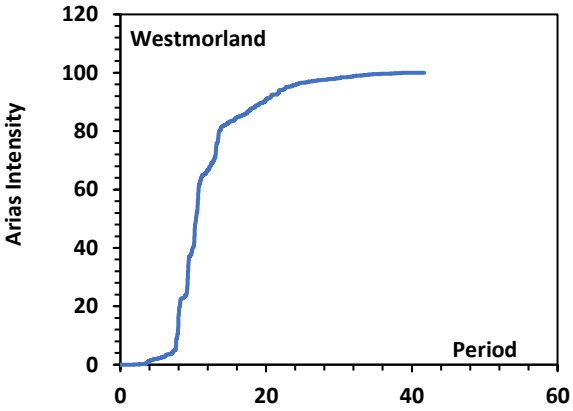

Arias Intensity (FF):

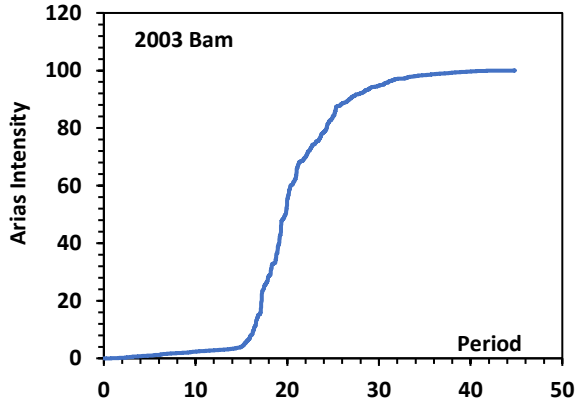

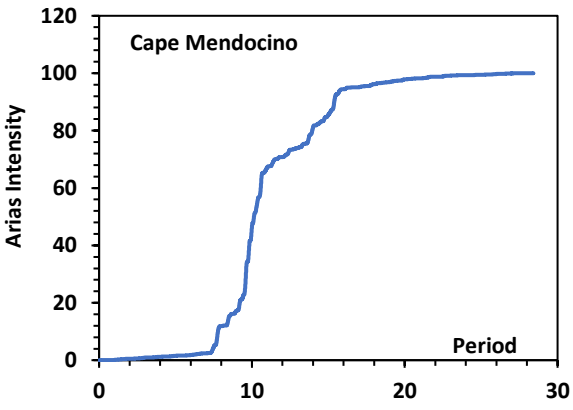

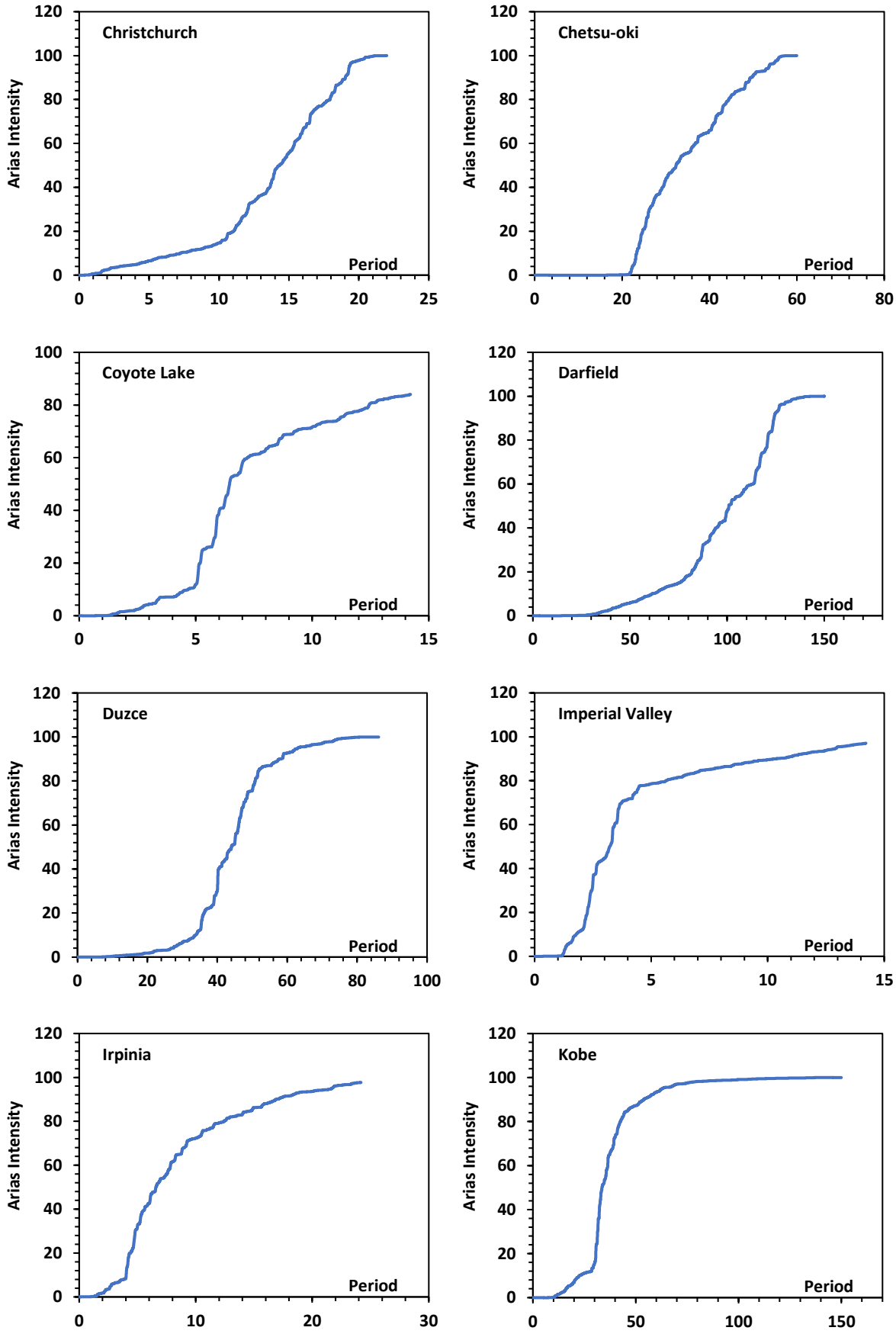
Christchurch
Arias Intensity
Period
Chetsu-oki
Arias Intensity
Period
Coyote Lake
Arias Intensity
Period
Darfield
Arias Intensity
Period
Duzce
Arias Intensity
Period
Imperial Valley
Arias Intensity
Period
Irpinia
Arias Intensity
Period
Kobe
Arias Intensity
Period

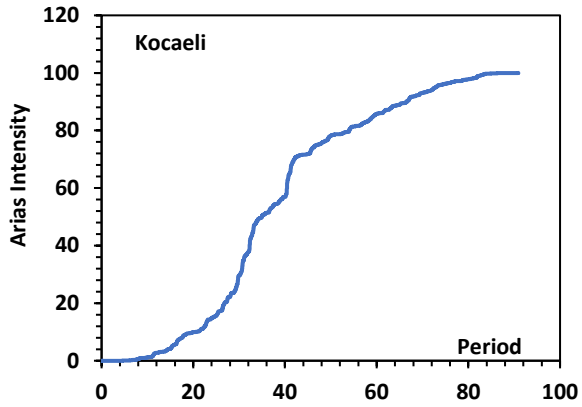
Kocaeli
Arias Intensity
Period
0
20
40
60
80
100
120

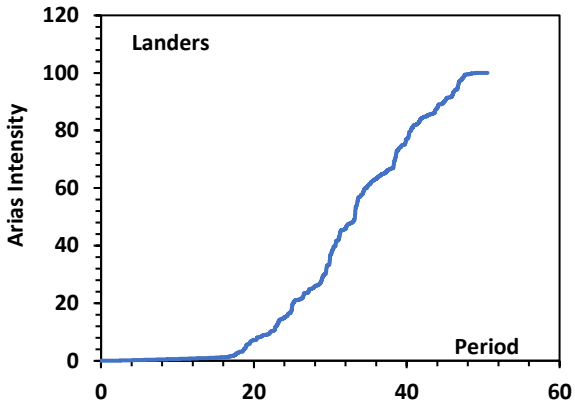
Landers
Arias Intensity
Period
0
20
40
60
80
100
120

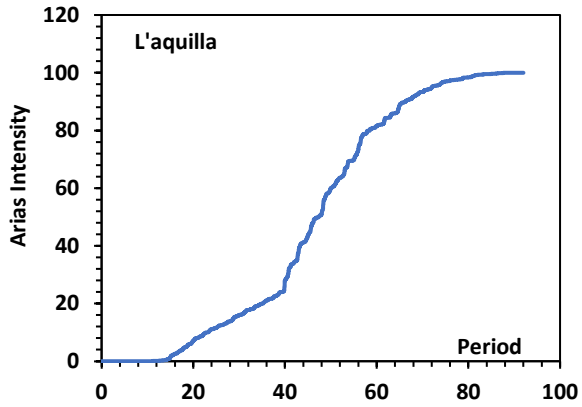
L'aquilla
Arias Intensity
Period
0
20
40
60
80
100
120

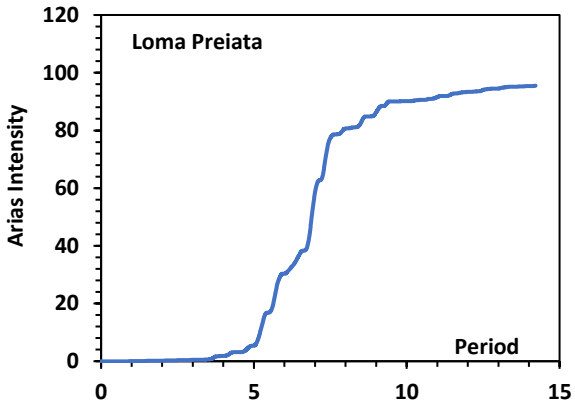
Loma Preiata
Arias Intensity
Period
0
5
10
15
20
40
60
80
100
120

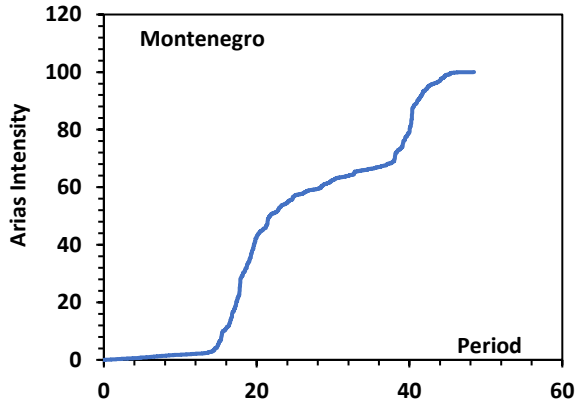
Montenegro
Arias Intensity
Period
0
20
40
60
80
100
120

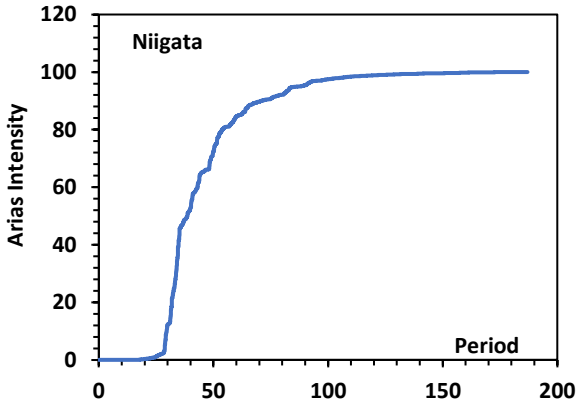
Niigata
Arias Intensity
Period
0
50
100
150
200
20
40
60
80
100
120

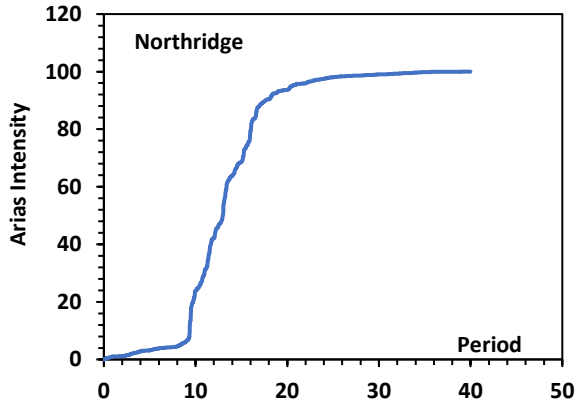
Northridge
Arias Intensity
Period
0
10
20
30
40
50
60
80
100
120

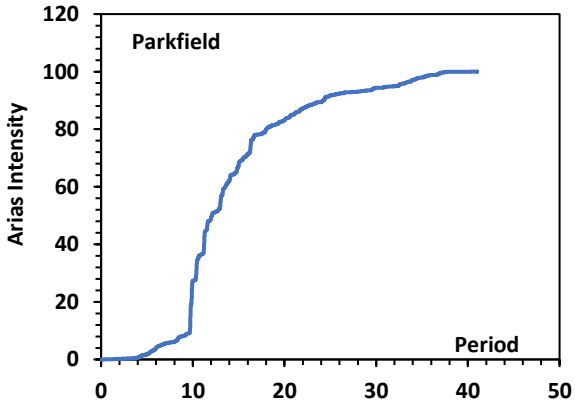
Parkfield
Arias Intensity
Period
0
10
20
30
40
50
60
80
100
120

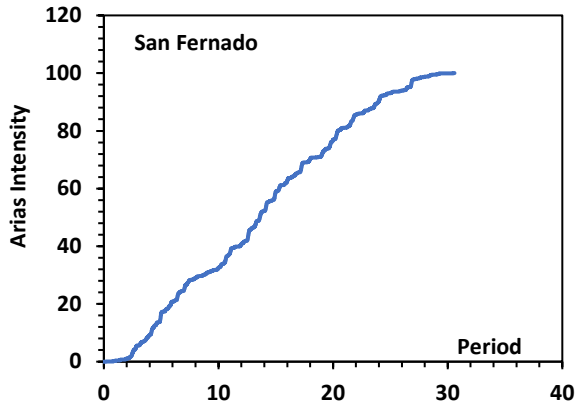

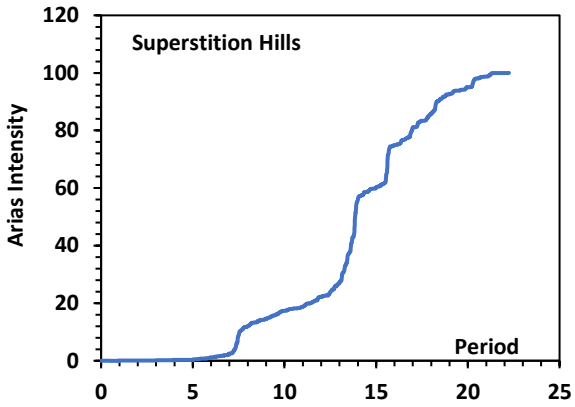

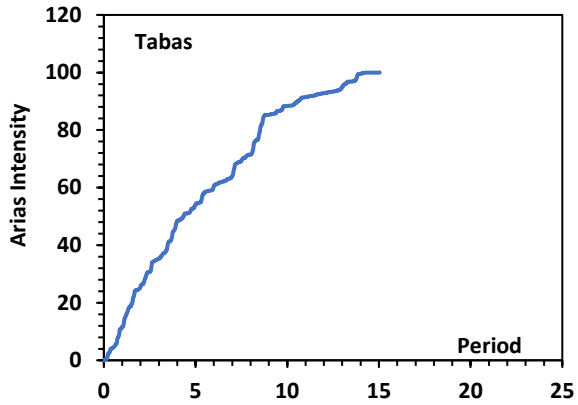

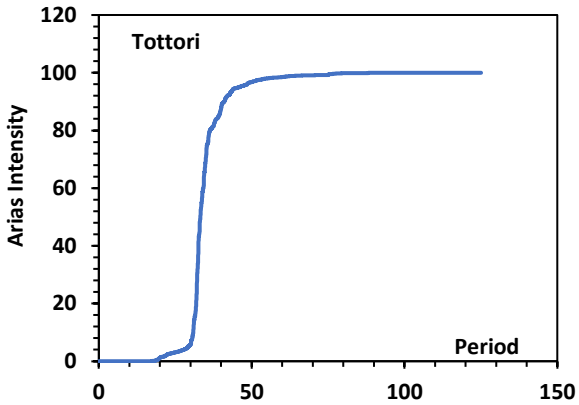

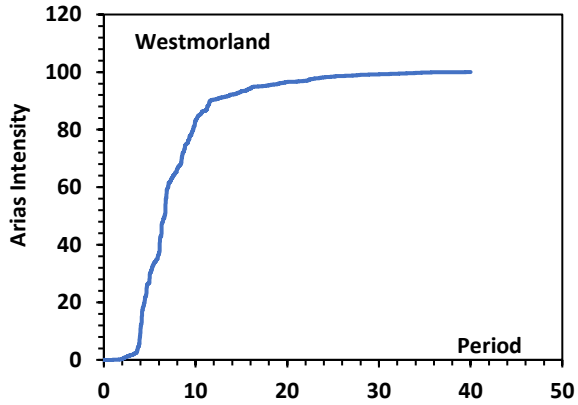

Energy Flux (NF):

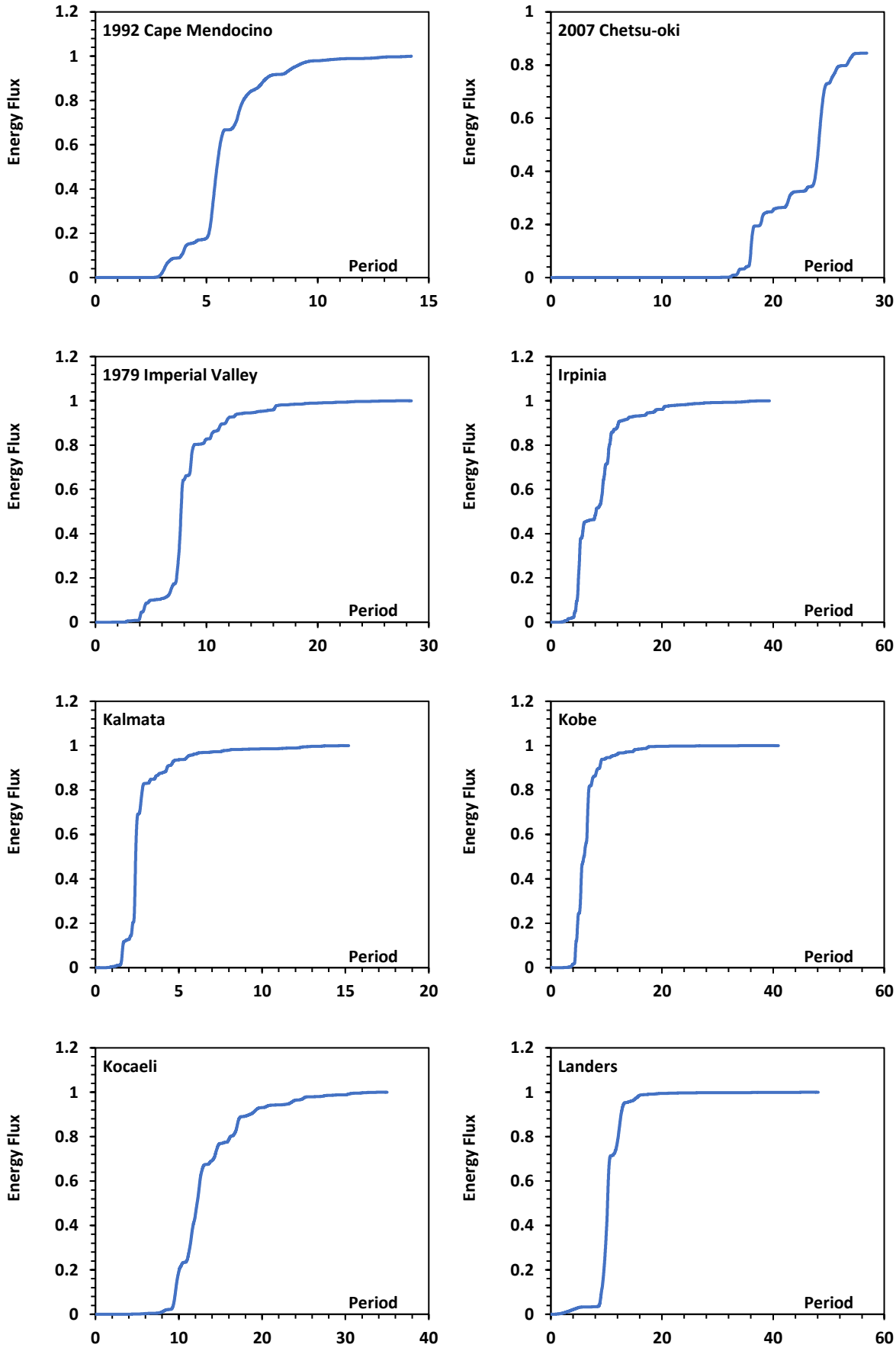
1992 Cape Mendocino
Energy Flux
Period
2007 Chetsu-oki
Energy Flux
Period
1979 Imperial Valley
Energy Flux
Period
Irpinia
Energy Flux
Period
Kalmata
Energy Flux
Period
Kobe
Energy Flux
Period
Kocaeli
Energy Flux
Period
Landers
Energy Flux
Period

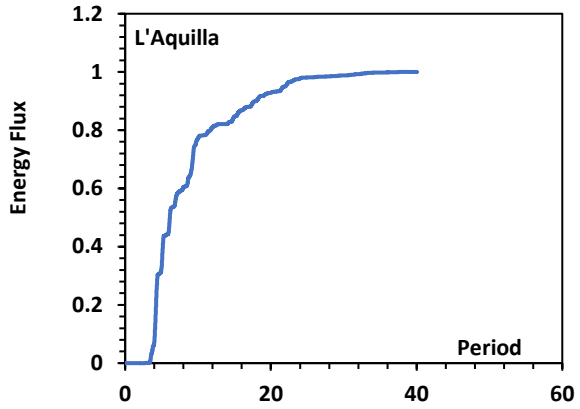
L'Aquilla
Energy Flux
Period
1.2
1
0.8
0.6
0.4
0.2
0
0
20
40
60

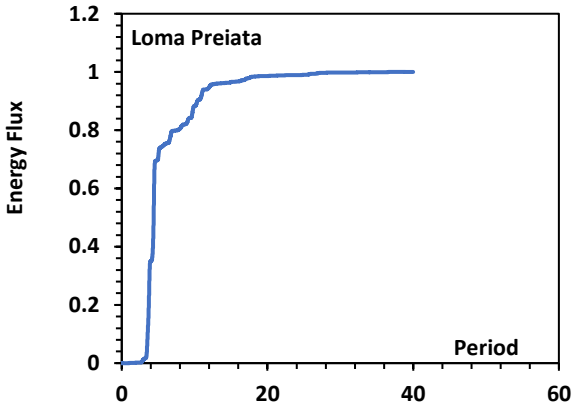
Loma Preiata
Energy Flux
Period
1.2
1
0.8
0.6
0.4
0.2
0
0
20
40
60

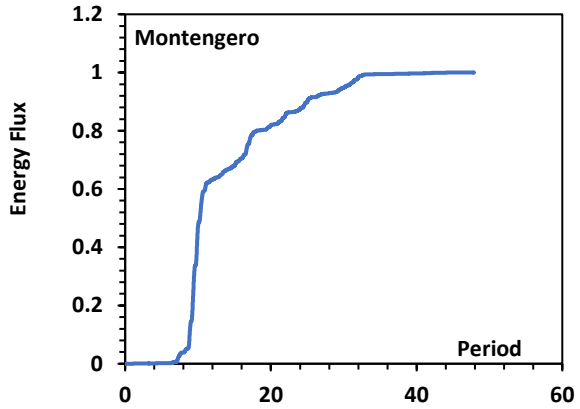
Montengero
Energy Flux
Period
1.2
1
0.8
0.6
0.4
0.2
0
0
20
40
60

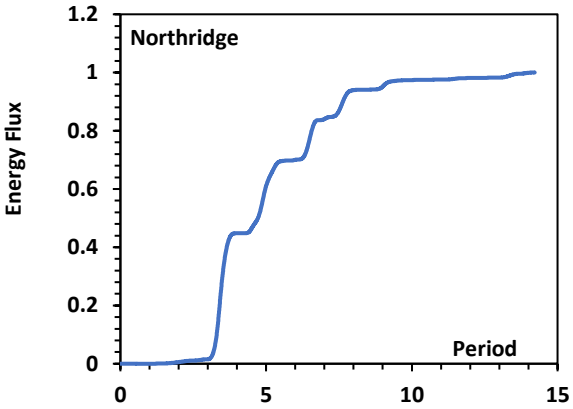
Northridge
Energy Flux
Period
1.2
1
0.8
0.6
0.4
0.2
0
0
5
10
15

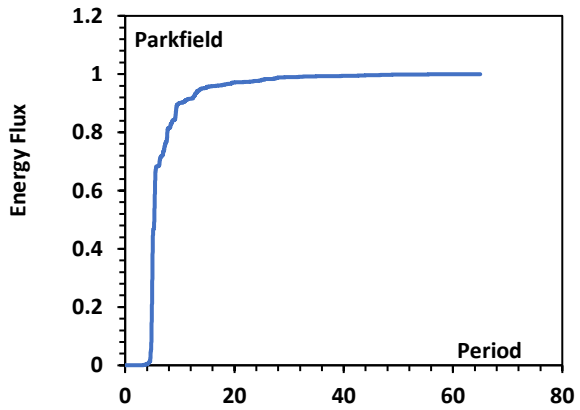
Parkfield
Energy Flux
Period
1.2
1
0.8
0.6
0.4
0.2
0
0
20
40
60
80

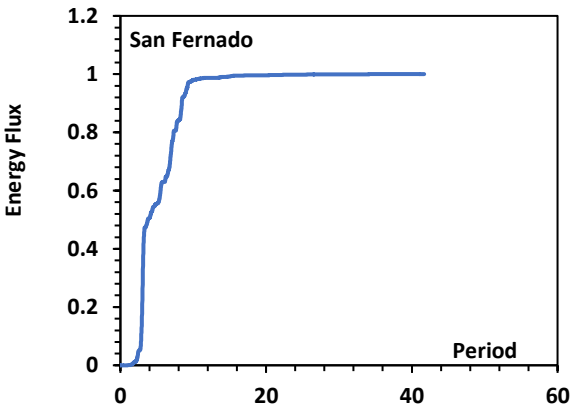
San Fernado
Energy Flux
Period
1.2
1
0.8
0.6
0.4
0.2
0
0
20
40
60

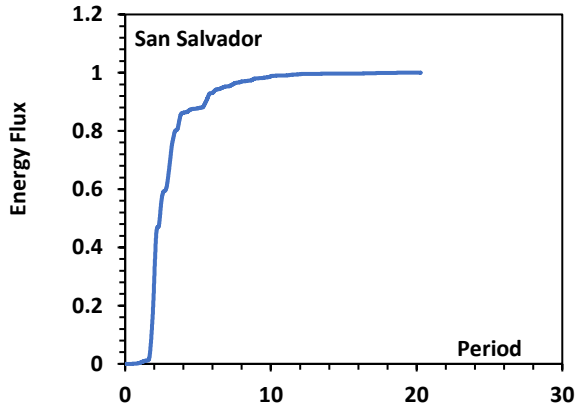
San Salvador
Energy Flux
Period
1.2
1
0.8
0.6
0.4
0.2
0
0
10
20
30

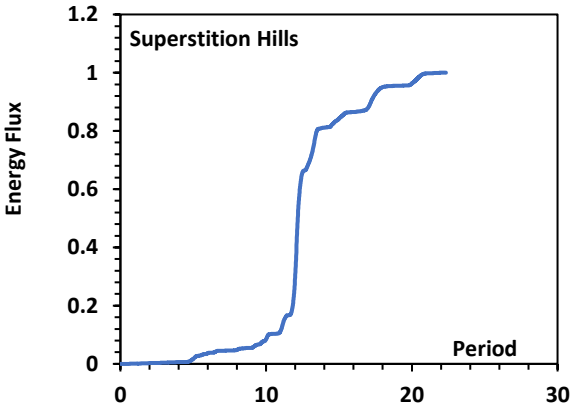
Superstition Hills
Energy Flux
Period
1.2
1
0.8
0.6
0.4
0.2
0
0
10
20
30

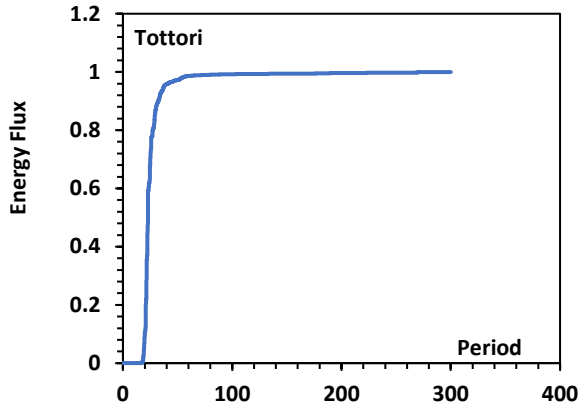

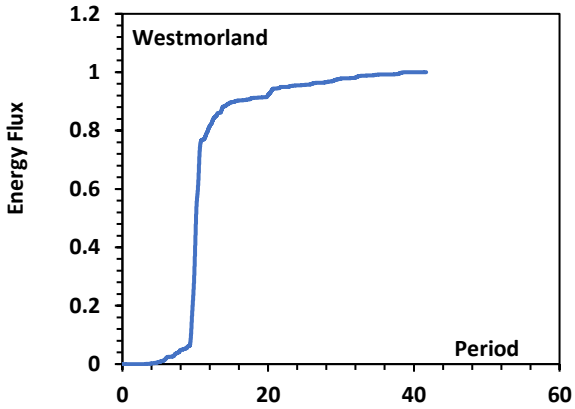

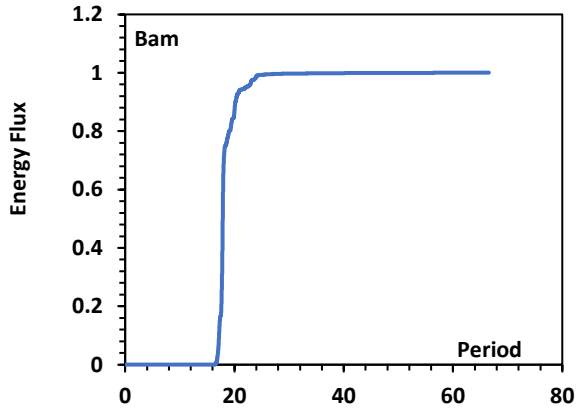

Energy Flux (FF):

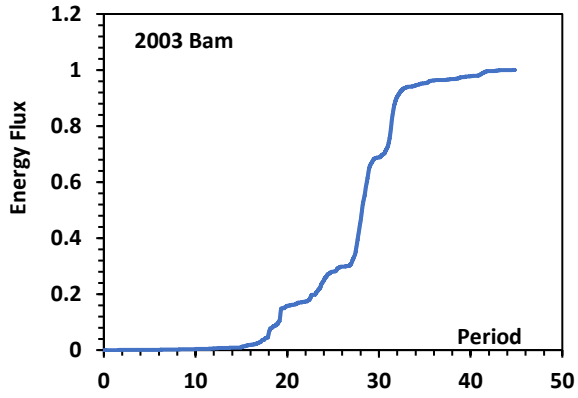

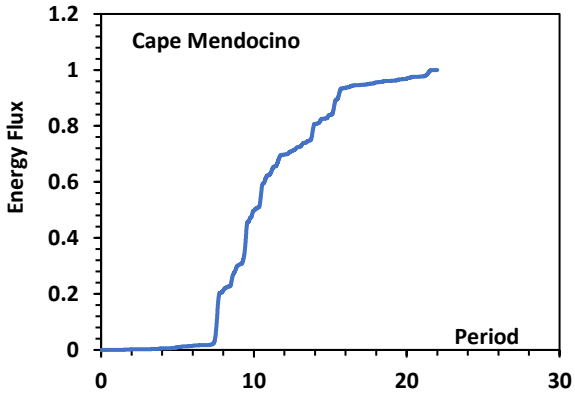

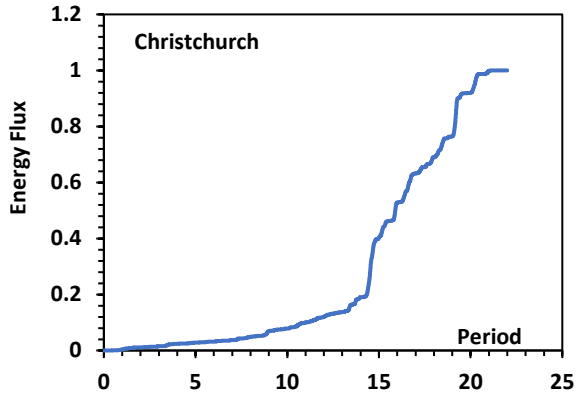
Christchurch
Energy Flux
Period
0
0.2
0.4
0.6
0.8
1
1.2
0
5
10
15
20
25

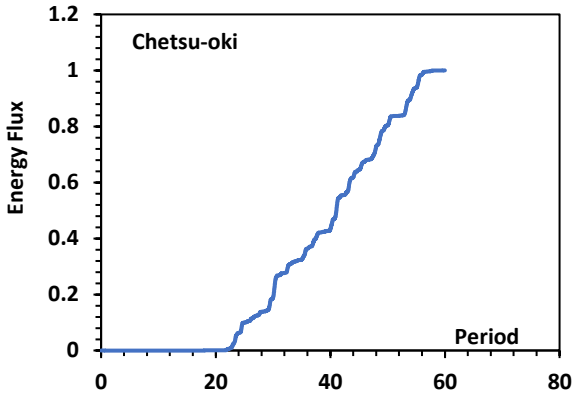
Chetsu-oki
Energy Flux
Period
0
0.2
0.4
0.6
0.8
1
1.2
0
20
40
60
80

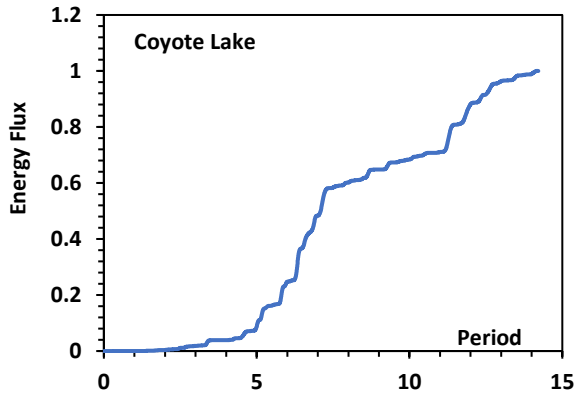
Coyote Lake
Energy Flux
Period
0
0.2
0.4
0.6
0.8
1
1.2
0
5
10
15

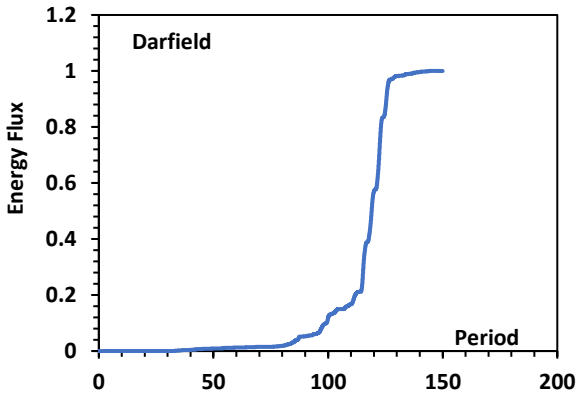
Darfield
Energy Flux
Period
0
0.2
0.4
0.6
0.8
1
1.2
0
50
100
150
200

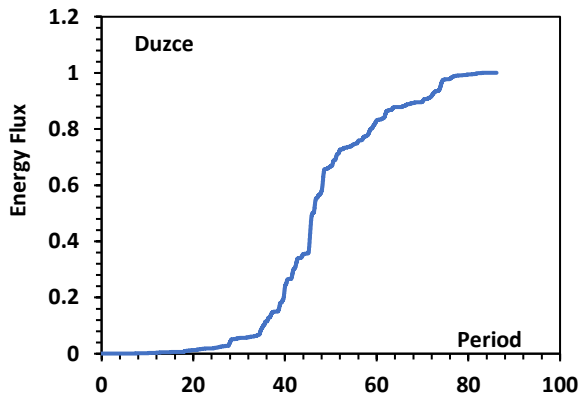
Duzce
Energy Flux
Period
0
0.2
0.4
0.6
0.8
1
1.2
0
20
40
60
80
100

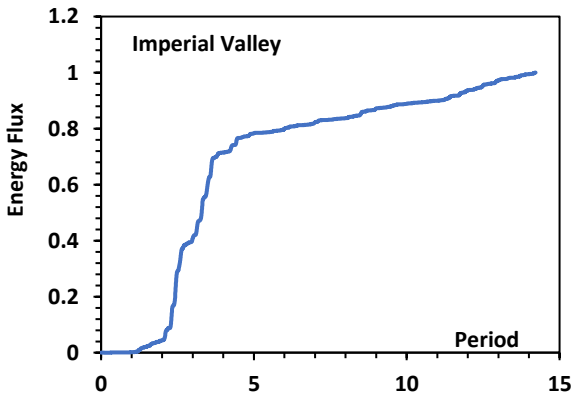
Imperial Valley
Energy Flux
Period
0
0.2
0.4
0.6
0.8
1
1.2
0
5
10
15

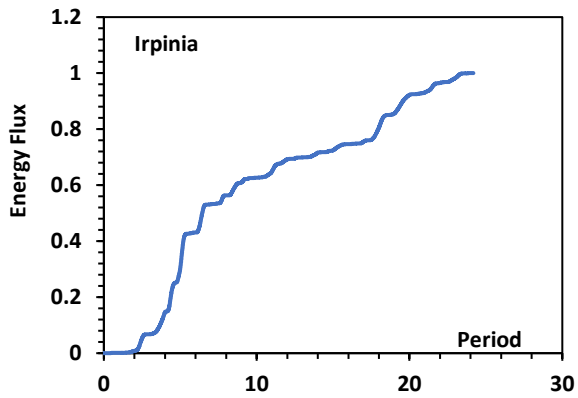
Irpinia
Energy Flux
Period
0
0.2
0.4
0.6
0.8
1
1.2
0
10
20
30

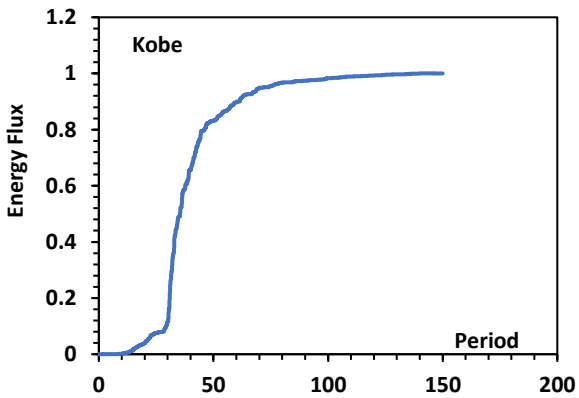
Kobe
Energy Flux
Period
0
0.2
0.4
0.6
0.8
1
1.2
0
50
100
150
200

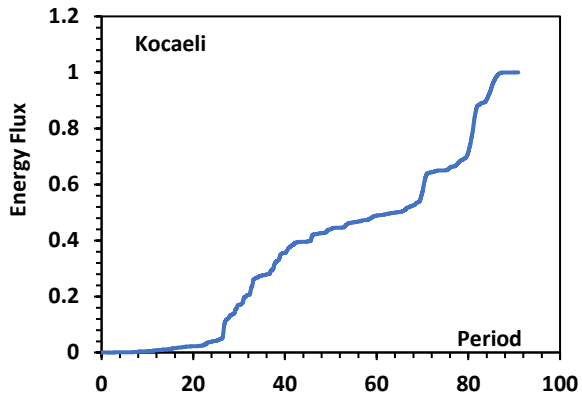
Kocaeli
Energy Flux
Period
0
0.2
0.4
0.6
0.8
1
1.2
0
20
40
60
80
100

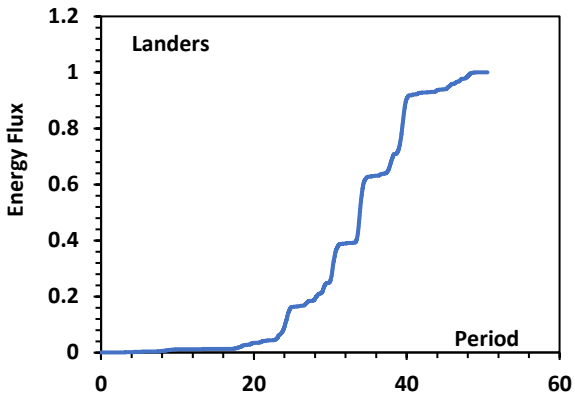
Landers
Energy Flux
Period
0
0.2
0.4
0.6
0.8
1
1.2
0
20
40
60

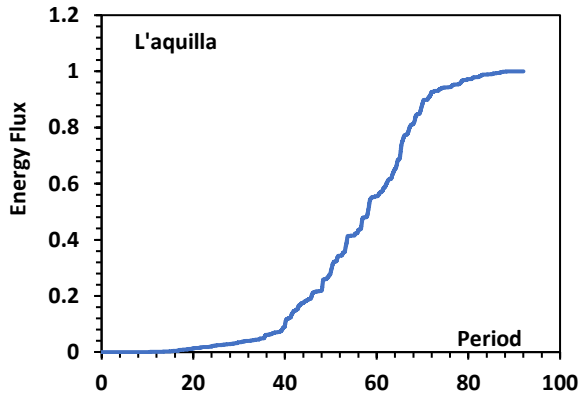
L'aquilla
Energy Flux
Period
0
0.2
0.4
0.6
0.8
1
1.2
0
20
40
60
80
100

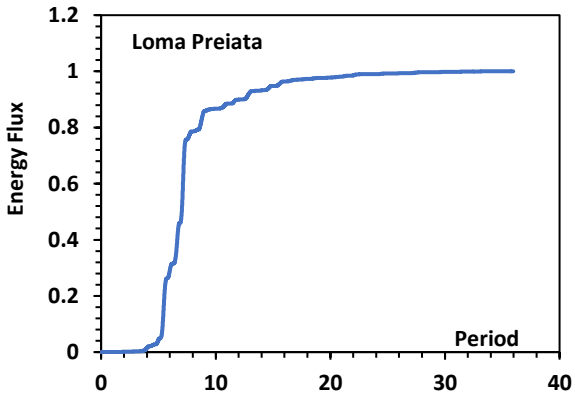
Loma Preiata
Energy Flux
Period
0
0.2
0.4
0.6
0.8
1
1.2
0
10
20
30
40

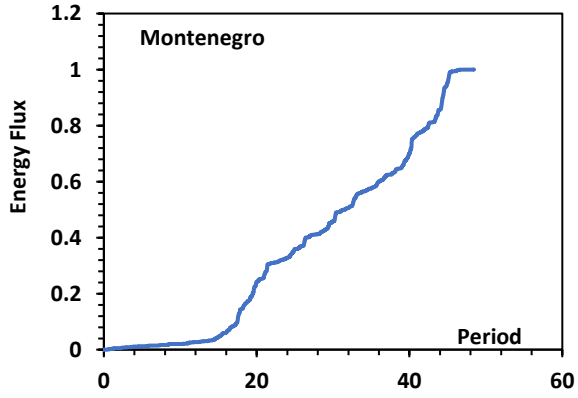
Montenegro
Energy Flux
Period
0
0.2
0.4
0.6
0.8
1
1.2
0
20
40
60

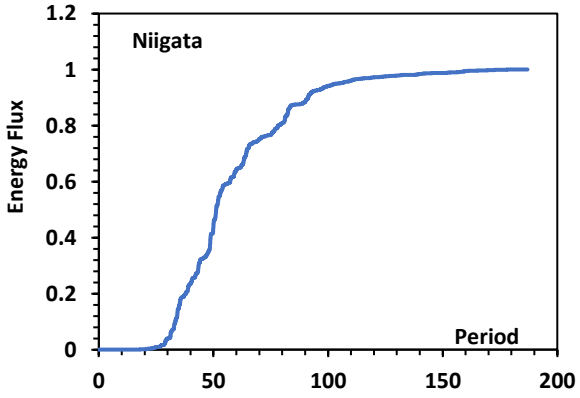
Niigata
Energy Flux
Period
0
0.2
0.4
0.6
0.8
1
1.2
0
50
100
150
200

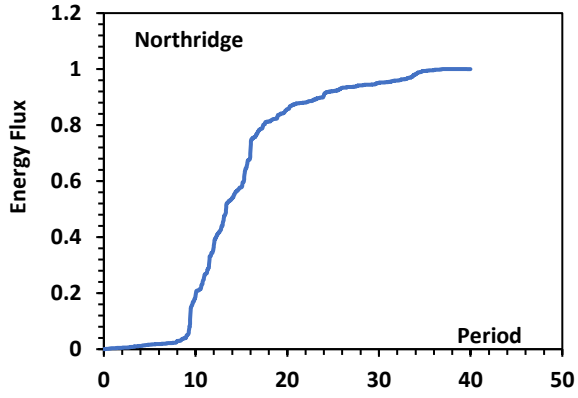
Northridge
Energy Flux
Period
0
0.2
0.4
0.6
0.8
1
1.2
0
10
20
30
40
50

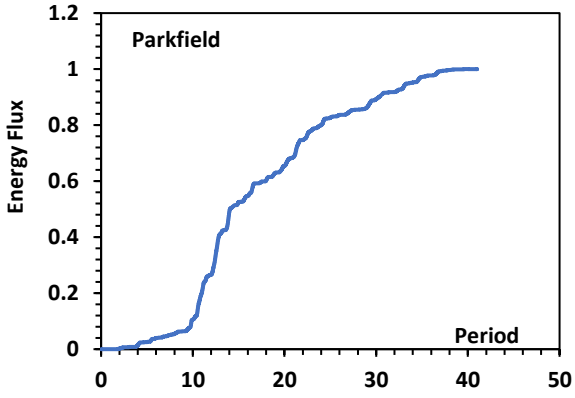
Parkfield
Energy Flux
Period
0
0.2
0.4
0.6
0.8
1
1.2
0
10
20
30
40
50

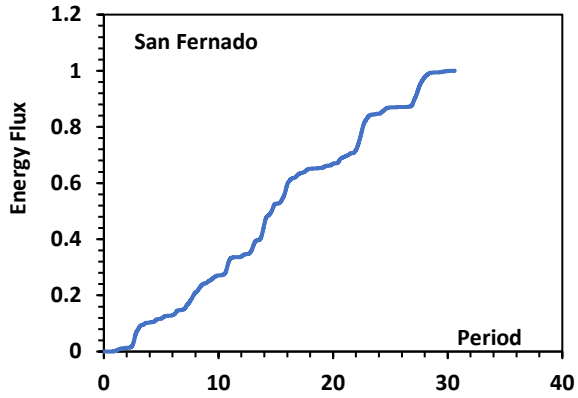
San Fernado
Energy Flux
Period
1.2
1
0.8
0.6
0.4
0.2
0
0
10
20
30
40

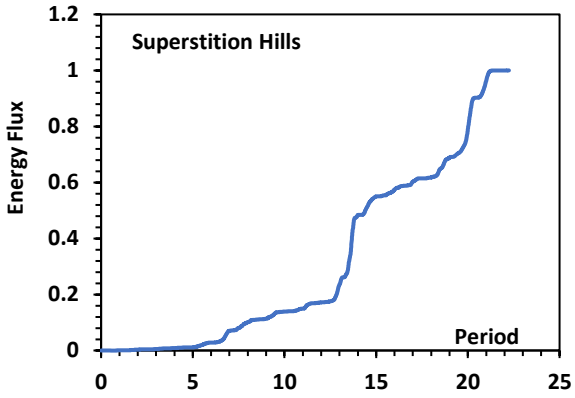
Superstition Hills
Energy Flux
Period
1.2
1
0.8
0.6
0.4
0.2
0
0
5
10
15
20
25

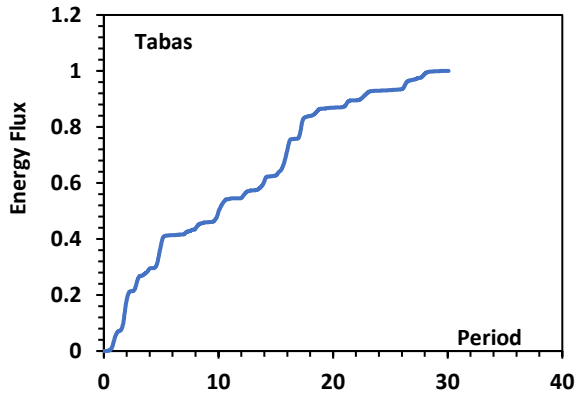
Tabas
Energy Flux
Period
1.2
1
0.8
0.6
0.4
0.2
0
0
10
20
30
40

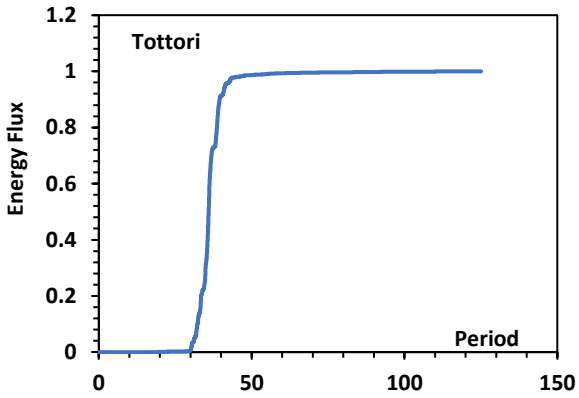
Tottori
Energy Flux
Period
1.2
1
0.8
0.6
0.4
0.2
0
0
50
100
150

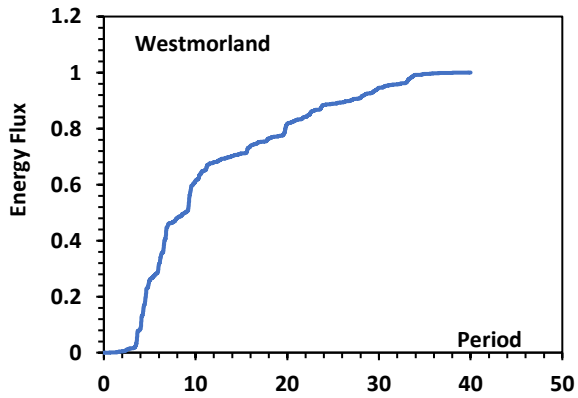
Westmorland
Energy Flux
Period
1.2
1
0.8
0.6
0.4
0.2
0
0
10
20
30
40
50

Spectral parameters:-

Fourier Amplitude (NF):

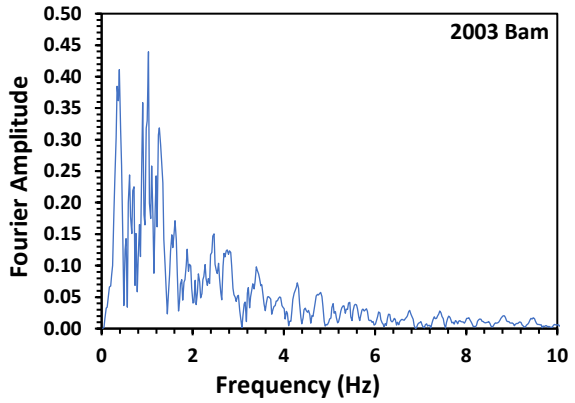

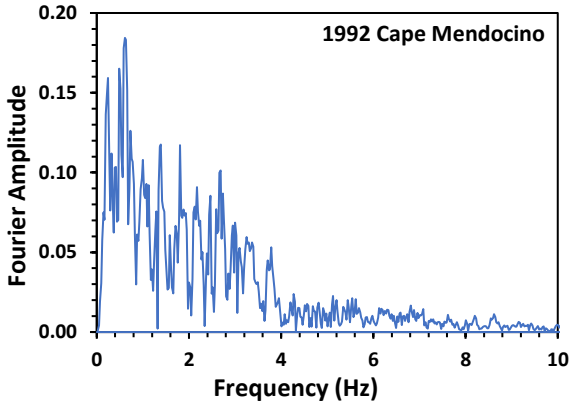

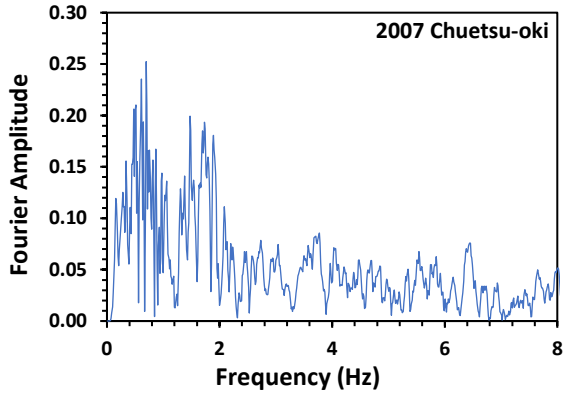

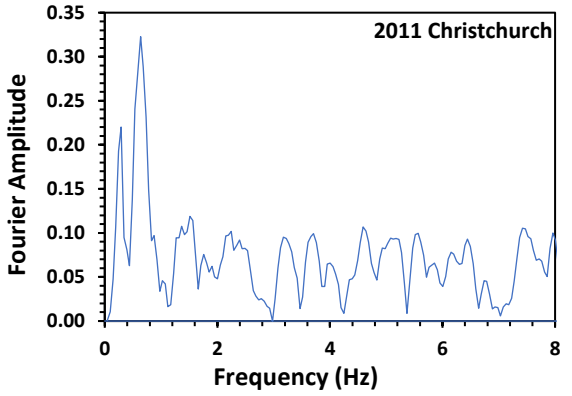

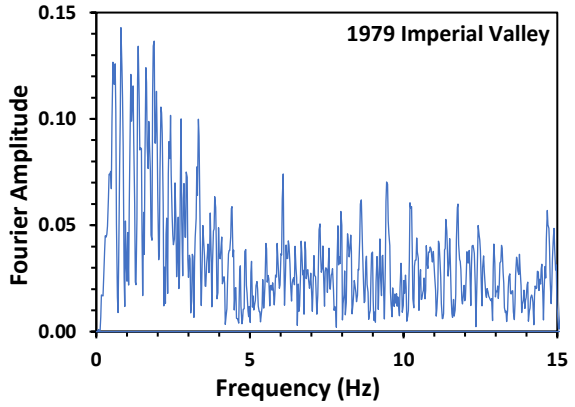

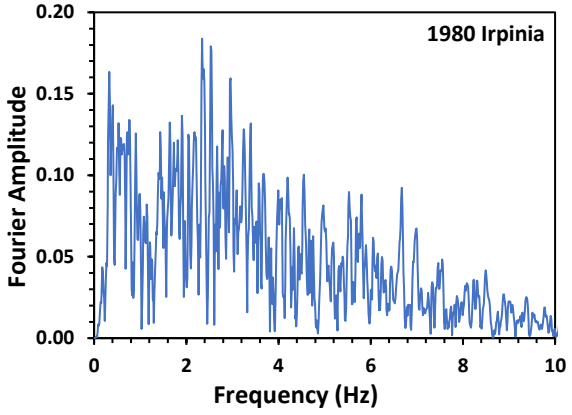

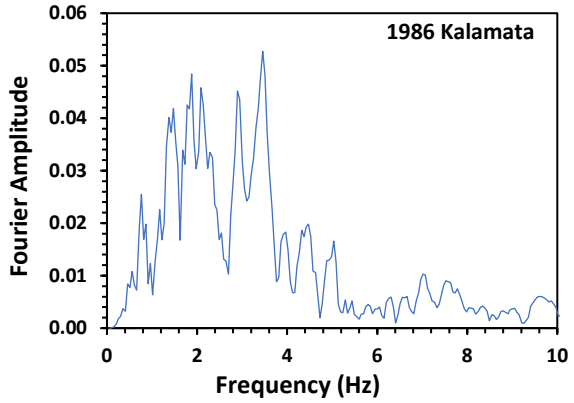
1986 Kalamata
Fourier Amplitude
Frequency (Hz)

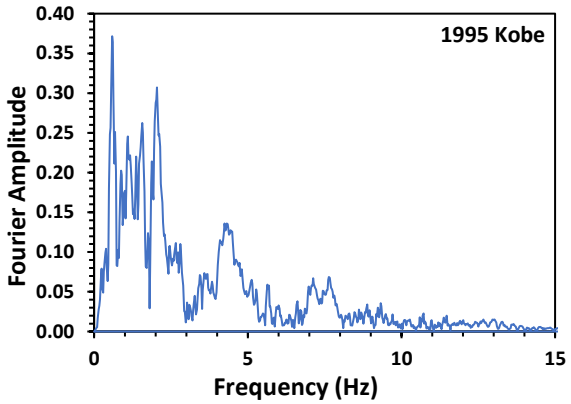
1995 Kobe
Fourier Amplitude
Frequency (Hz)

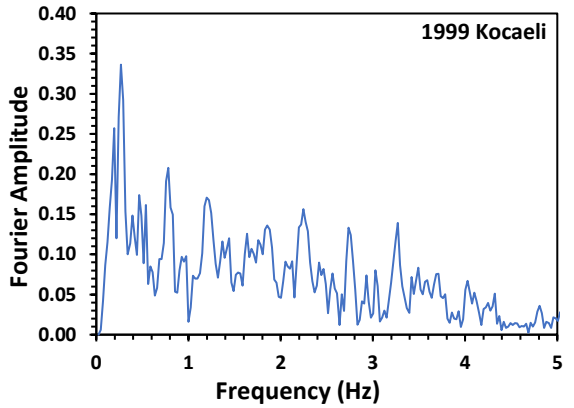
1999 Kocaeli
Fourier Amplitude
Frequency (Hz)

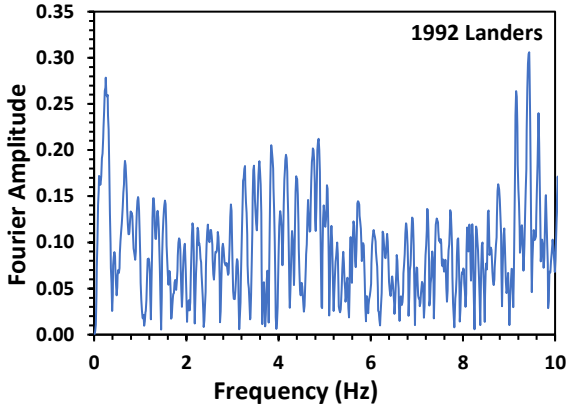
1992 Landers
Fourier Amplitude
Frequency (Hz)

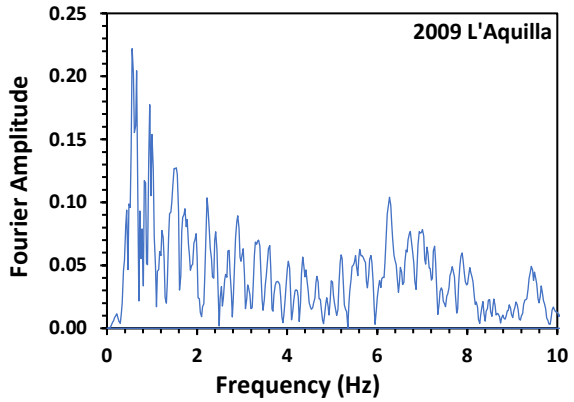
2009 L'Aquilla
Fourier Amplitude
Frequency (Hz)

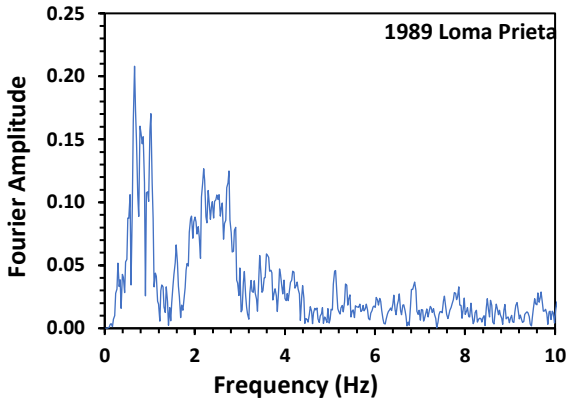
1989 Loma Prieta
Fourier Amplitude
Frequency (Hz)

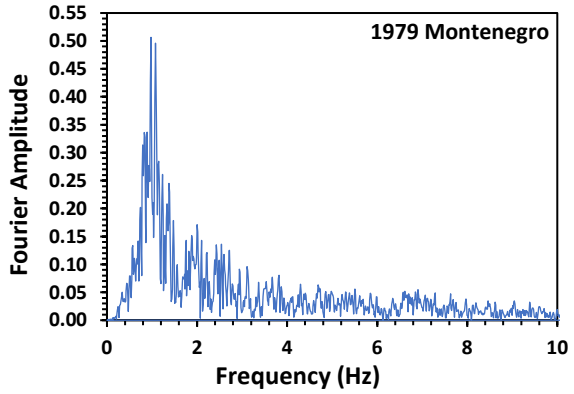
1979 Montenegro
Fourier Amplitude
Frequency (Hz)

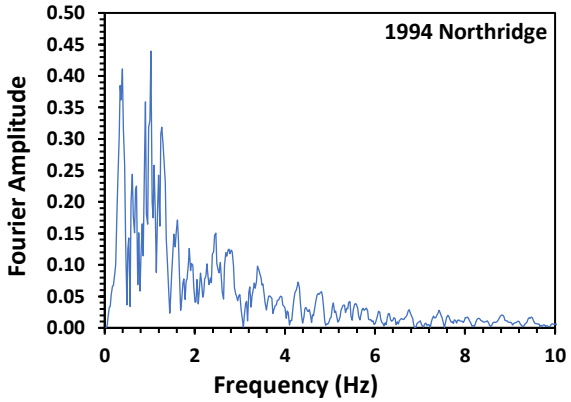
1994 Northridge
Fourier Amplitude
Frequency (Hz)

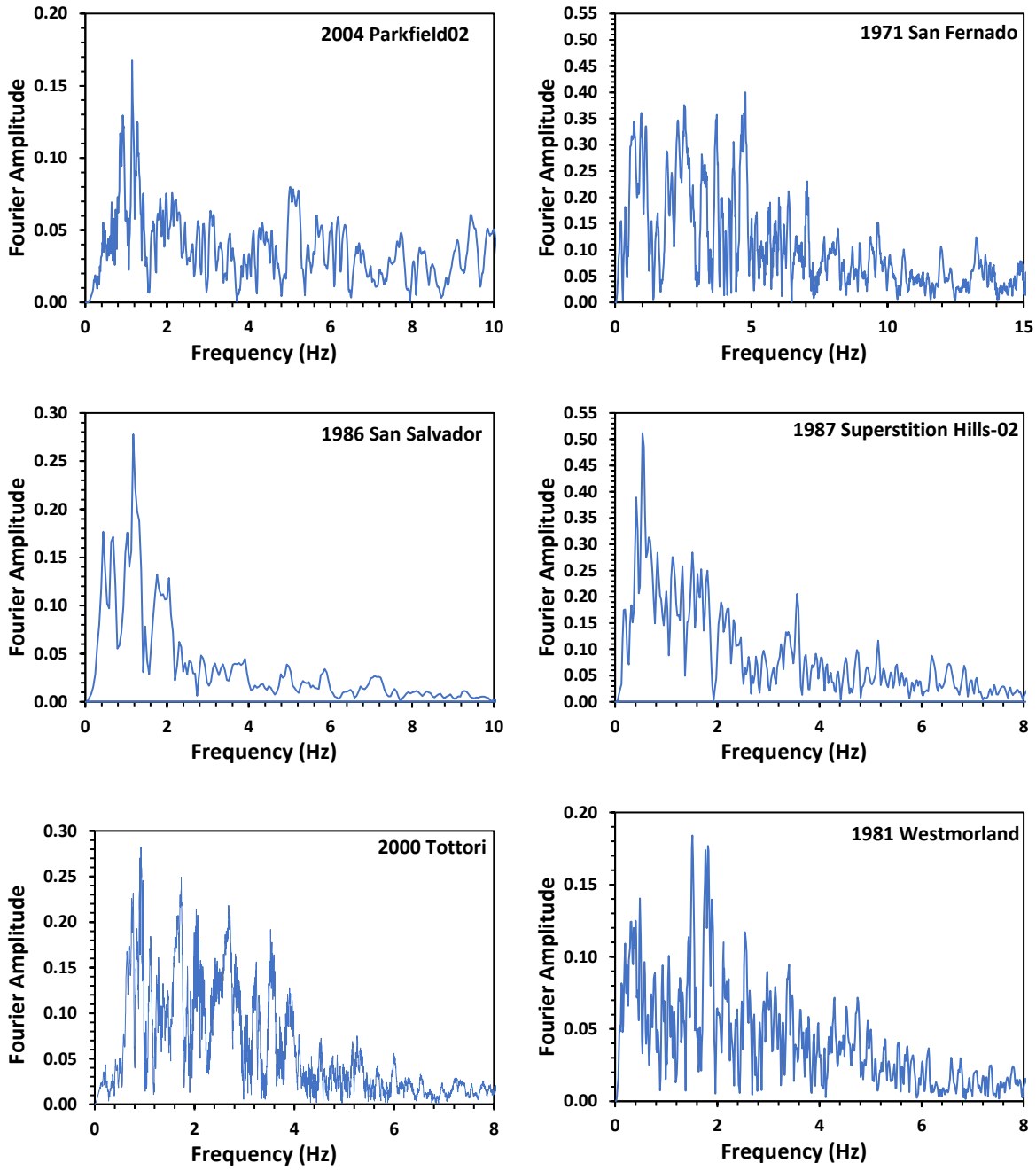

Fourier Amplitude (FF):

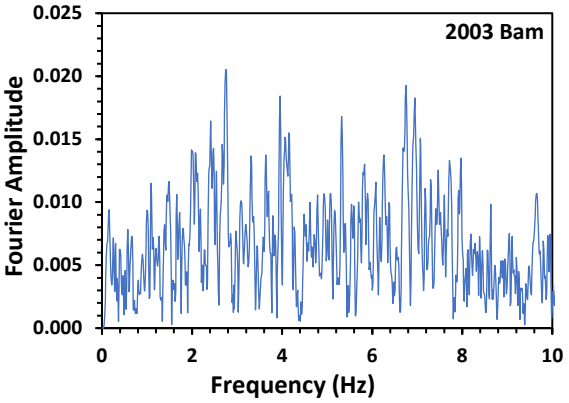
2003 Bam
Fourier Amplitude
0.025
0.020
0.015
0.010
0.005
0.000
0
2
4
6
8
10
Frequency (Hz)

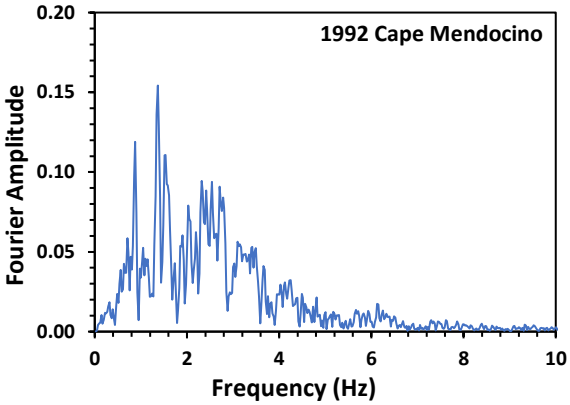
1992 Cape Mendocino
Fourier Amplitude
0.20
0.15
0.10
0.05
0.00
0
2
4
6
8
10
Frequency (Hz)

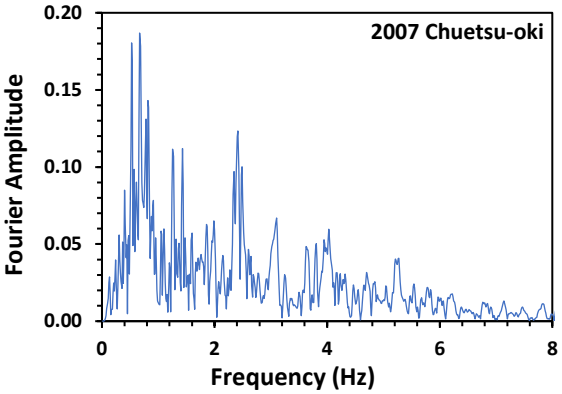
2007 Chuetsu-oki
Fourier Amplitude
0.20
0.15
0.10
0.05
0.00
0
2
4
6
8
Frequency (Hz)

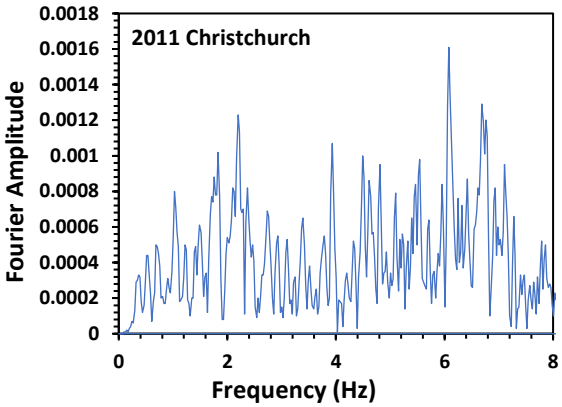
2011 Christchurch
Fourier Amplitude
0.0018
0.0016
0.0014
0.0012
0.001
0.0008
0.0006
0.0004
0.0002
0
0
2
4
6
8
Frequency (Hz)

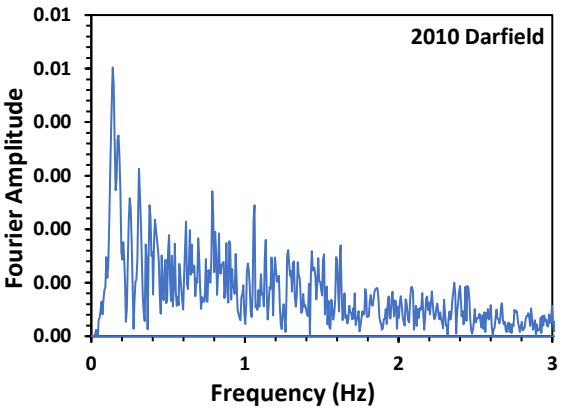
2010 Darfield
Fourier Amplitude
0.01
0.01
0.00
0.00
0.00
0.00
0
1
2
3
Frequency (Hz)

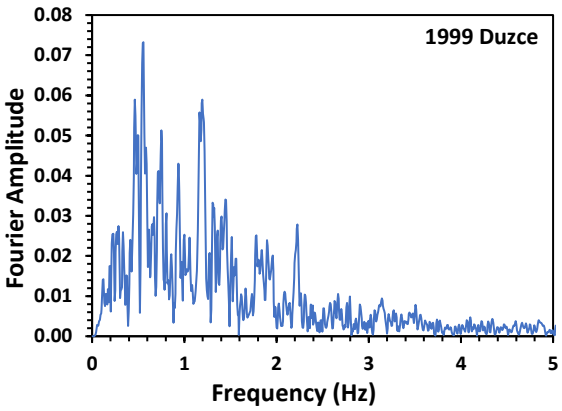
1999 Duzce
Fourier Amplitude
0.08
0.07
0.06
0.05
0.04
0.03
0.02
0.01
0.00
0
1
2
3
4
5
Frequency (Hz)

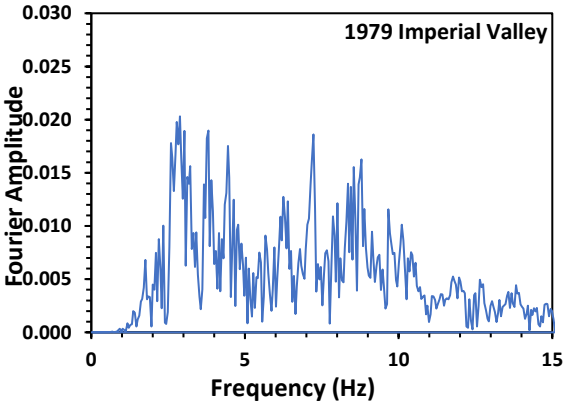
1979 Imperial Valley
Fourier Amplitude
0.030
0.025
0.020
0.015
0.010
0.005
0.000
0
5
10
15
Frequency (Hz)

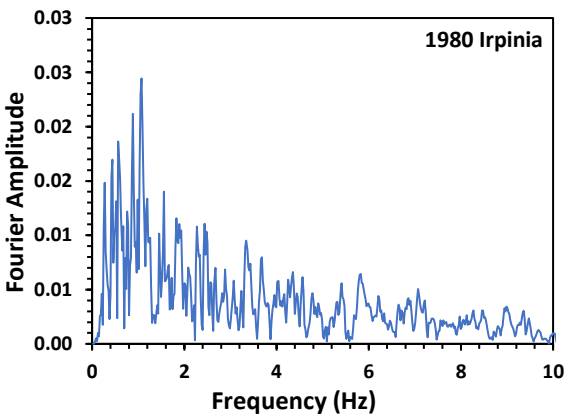
1980 Irpinia
Fourier Amplitude
0.03
0.03
0.02
0.02
0.01
0.01
0.00
0
2
4
6
8
10
Frequency (Hz)

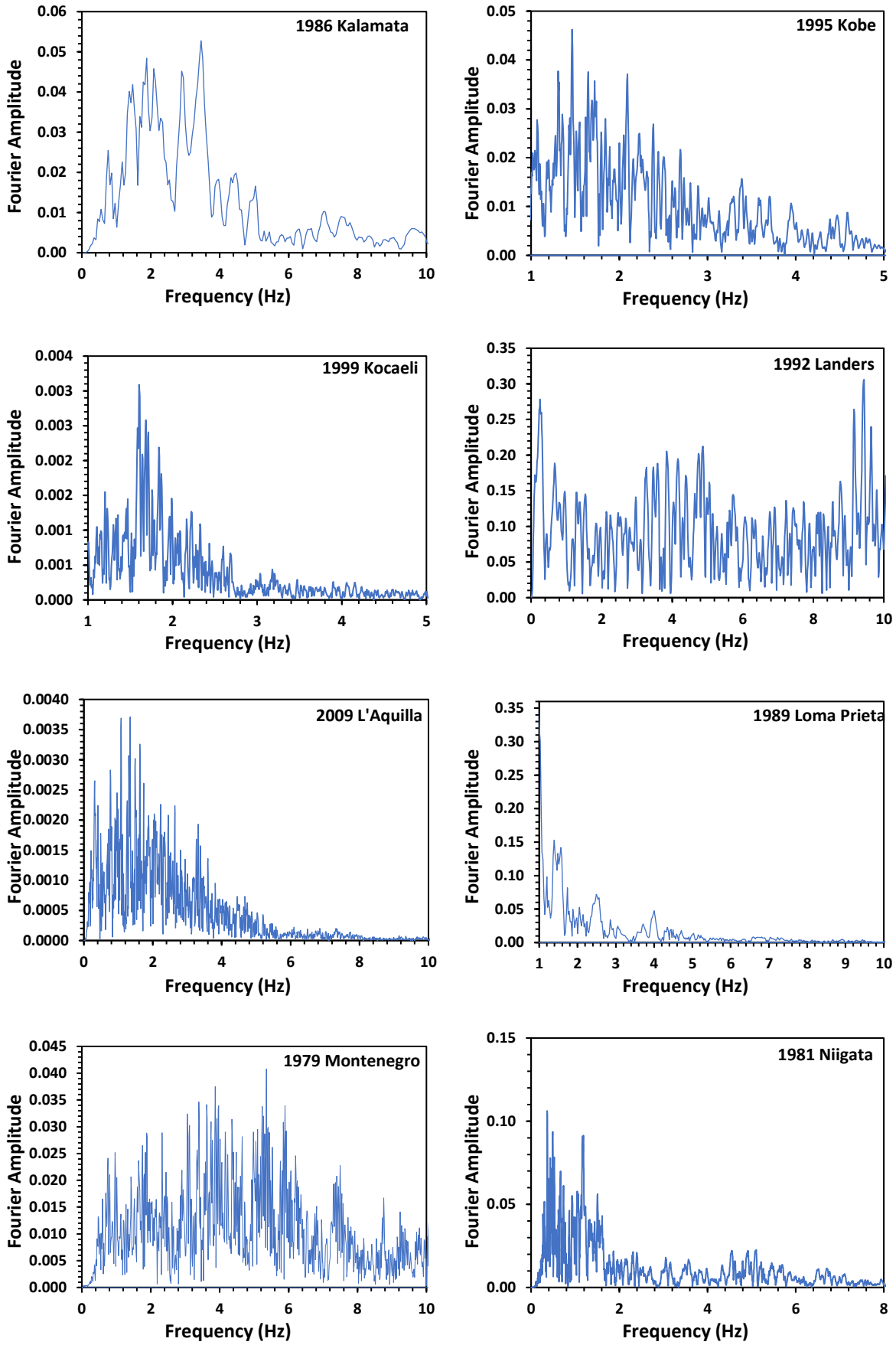
1986 Kalamata
Fourier Amplitude
Frequency (Hz)
1995 Kobe
Fourier Amplitude
Frequency (Hz)
1999 Kocaeli
Fourier Amplitude
Frequency (Hz)
1992 Landers
Fourier Amplitude
Frequency (Hz)
2009 L'Aquilla
Fourier Amplitude
Frequency (Hz)
1989 Loma Prieta
Fourier Amplitude
Frequency (Hz)
1979 Montenegro
Fourier Amplitude
Frequency (Hz)
1981 Niigata
Fourier Amplitude
Frequency (Hz)

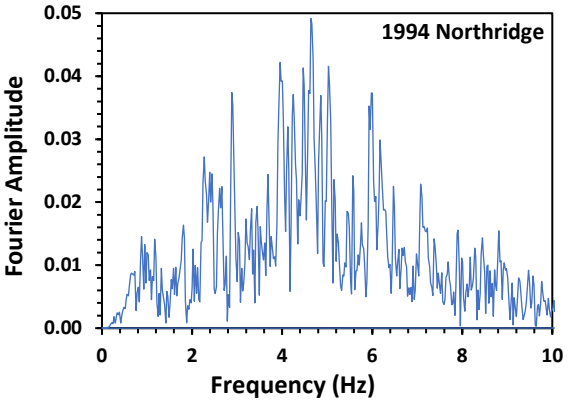
1994 Northridge
Fourier Amplitude
Frequency (Hz)

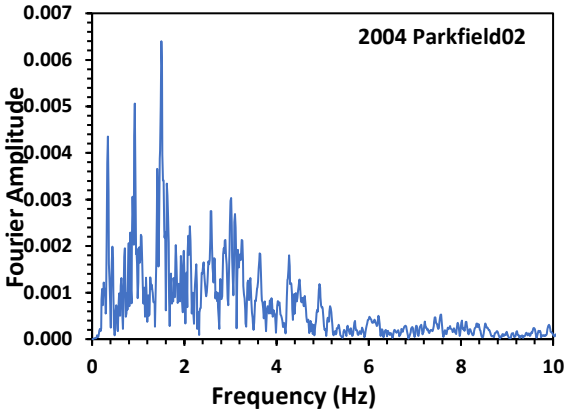
2004 Parkfield02
Fourier Amplitude
Frequency (Hz)

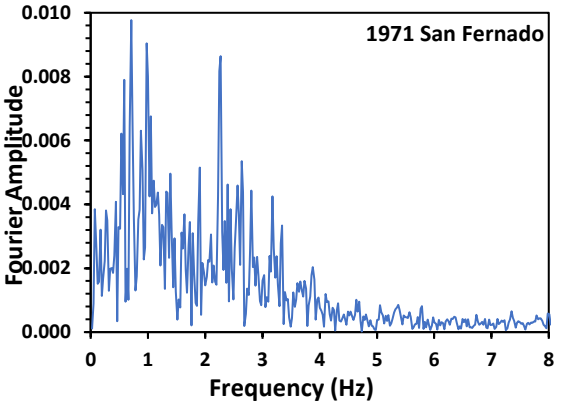
1971 San Fernado
Fourier Amplitude
Frequency (Hz)

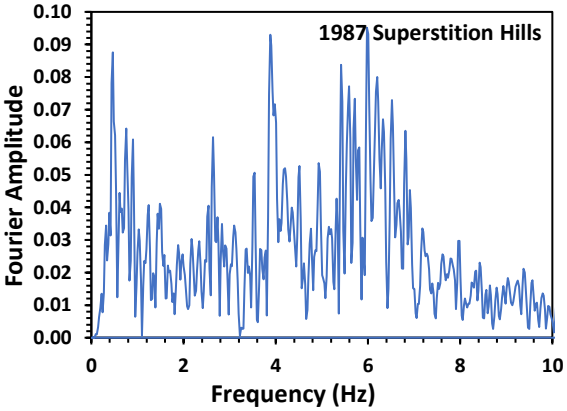
1987 Superstition Hills
Fourier Amplitude
Frequency (Hz)

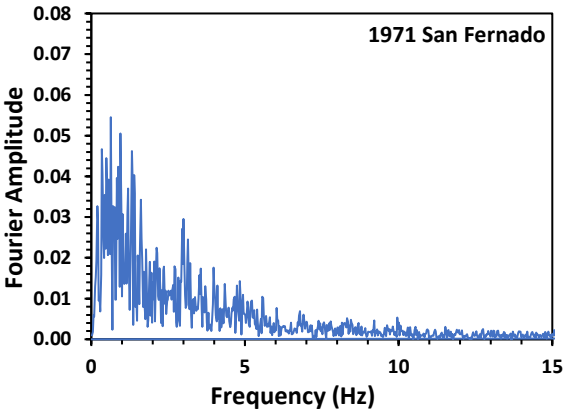
1971 San Fernado
Fourier Amplitude
Frequency (Hz)

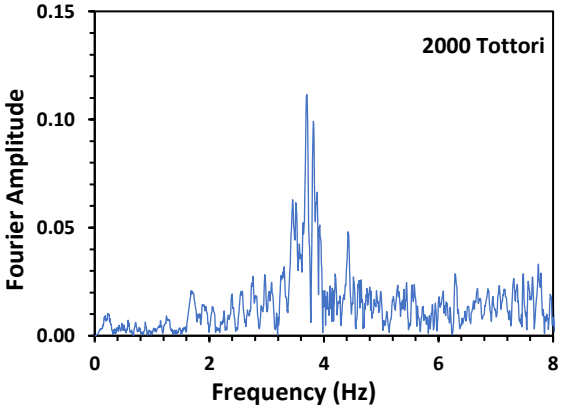
2000 Tottori
Fourier Amplitude
Frequency (Hz)

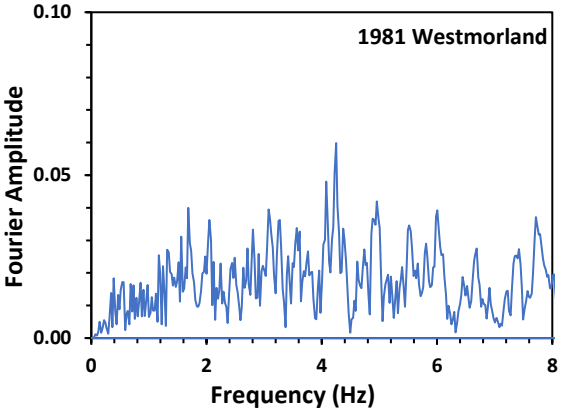
1981 Westmorland
Fourier Amplitude
Frequency (Hz)

Power Amplitude (NF):

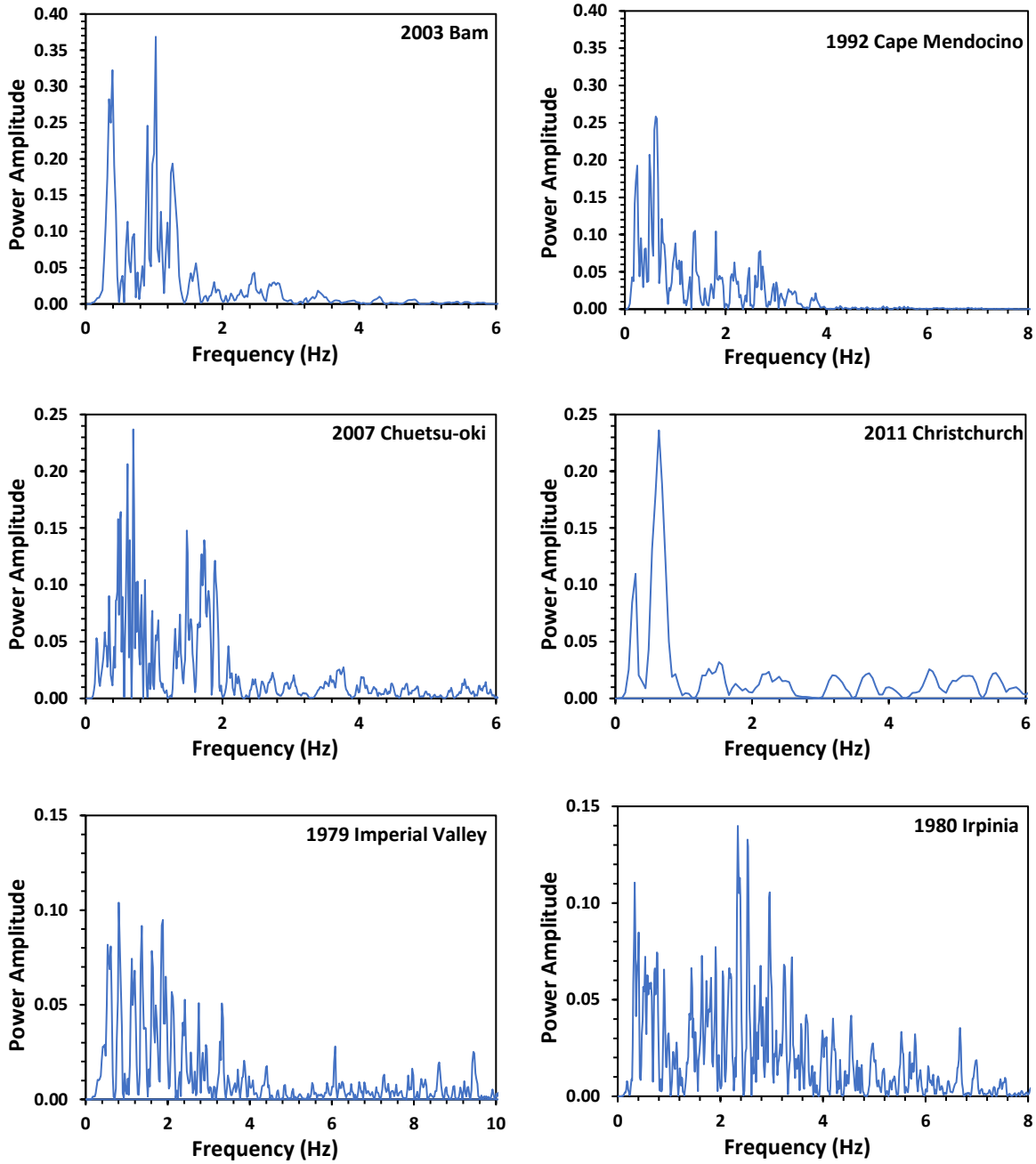

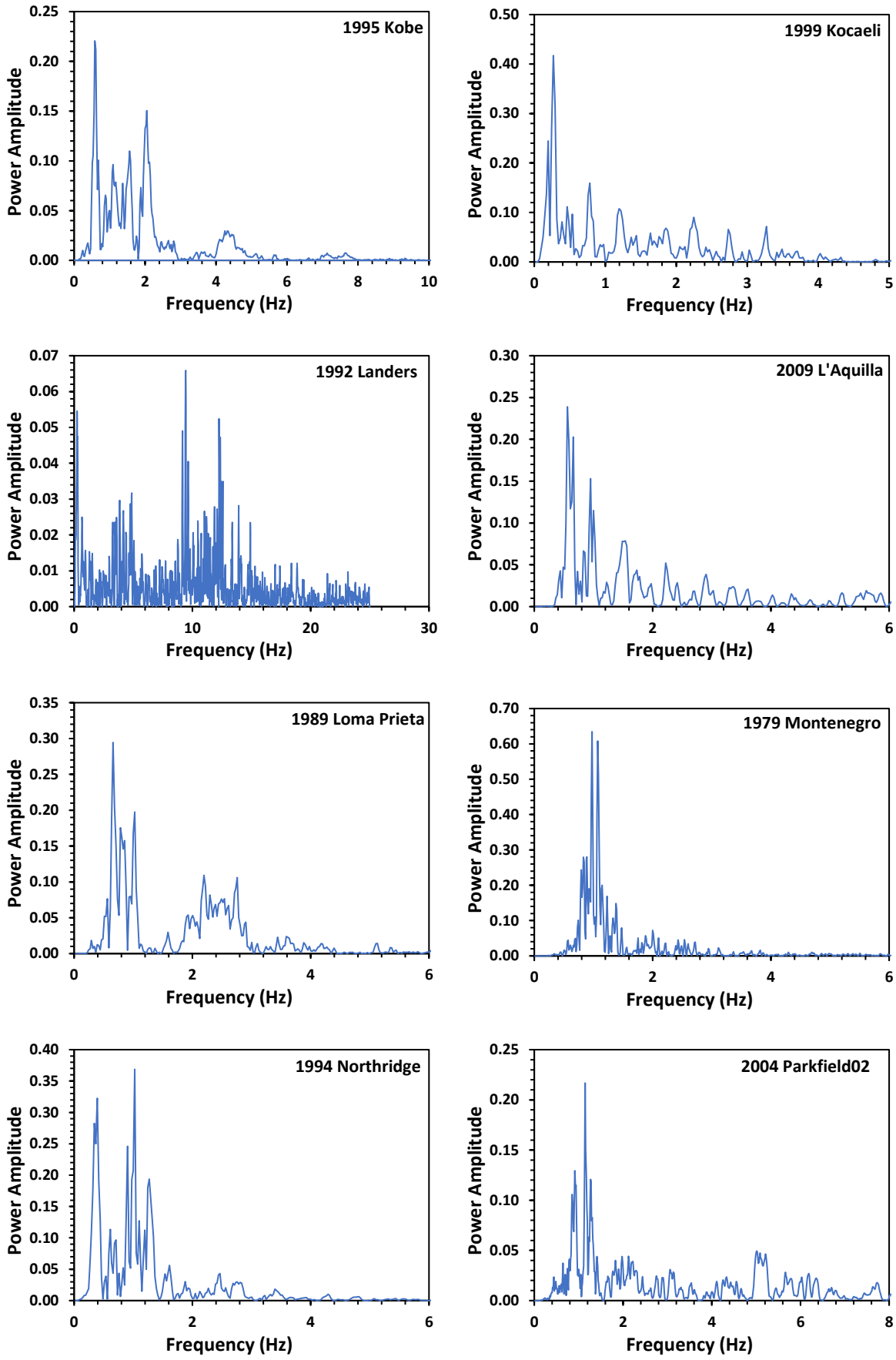
1995 Kobe
Power Amplitude
Frequency (Hz)
1999 Kocaeli
Power Amplitude
Frequency (Hz)
1992 Landers
Power Amplitude
Frequency (Hz)
2009 L'Aquilla
Power Amplitude
Frequency (Hz)
1989 Loma Prieta
Power Amplitude
Frequency (Hz)
1979 Montenegro
Power Amplitude
Frequency (Hz)
1994 Northridge
Power Amplitude
Frequency (Hz)
2004 Parkfield02
Power Amplitude
Frequency (Hz)

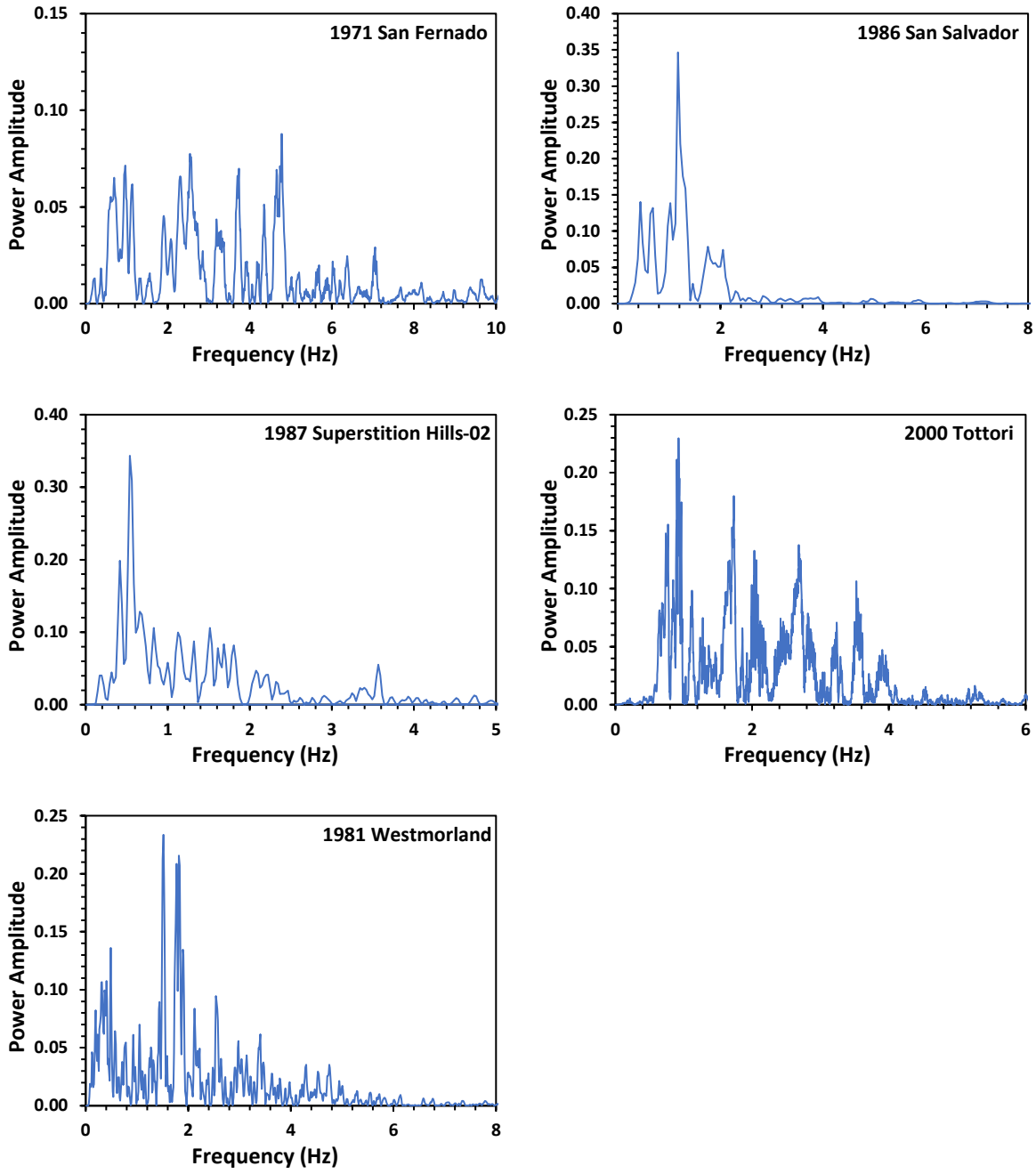

Power Amplitude (FF):

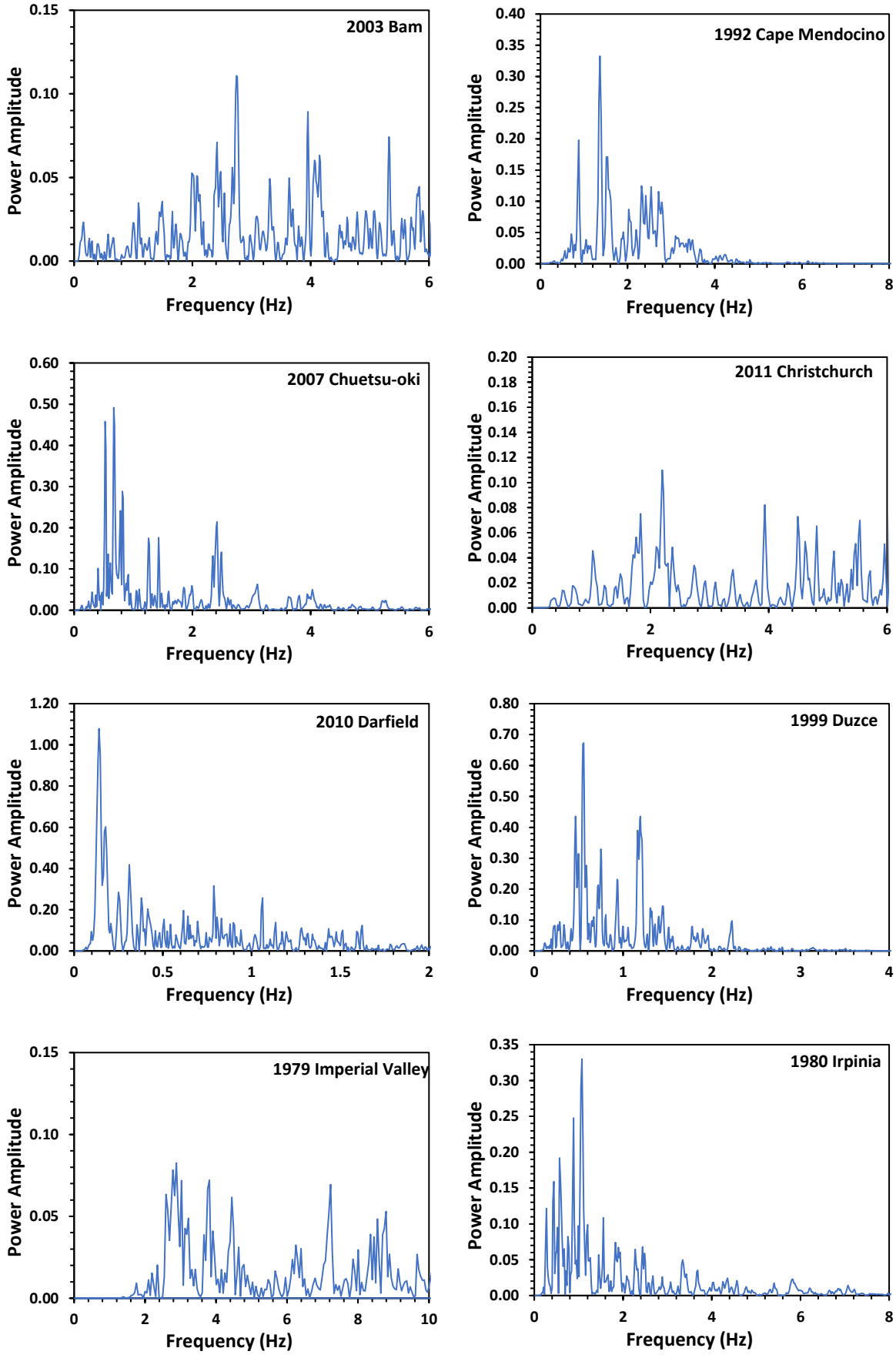
2003 Bam
Power Amplitude
Frequency (Hz)
1992 Cape Mendocino
Power Amplitude
Frequency (Hz)
2007 Chuetsu-oki
Power Amplitude
Frequency (Hz)
2011 Christchurch
Power Amplitude
Frequency (Hz)
2010 Darfield
Power Amplitude
Frequency (Hz)
1999 Duzce
Power Amplitude
Frequency (Hz)
1979 Imperial Valley
Power Amplitude
Frequency (Hz)
1980 Irpinia
Power Amplitude
Frequency (Hz)

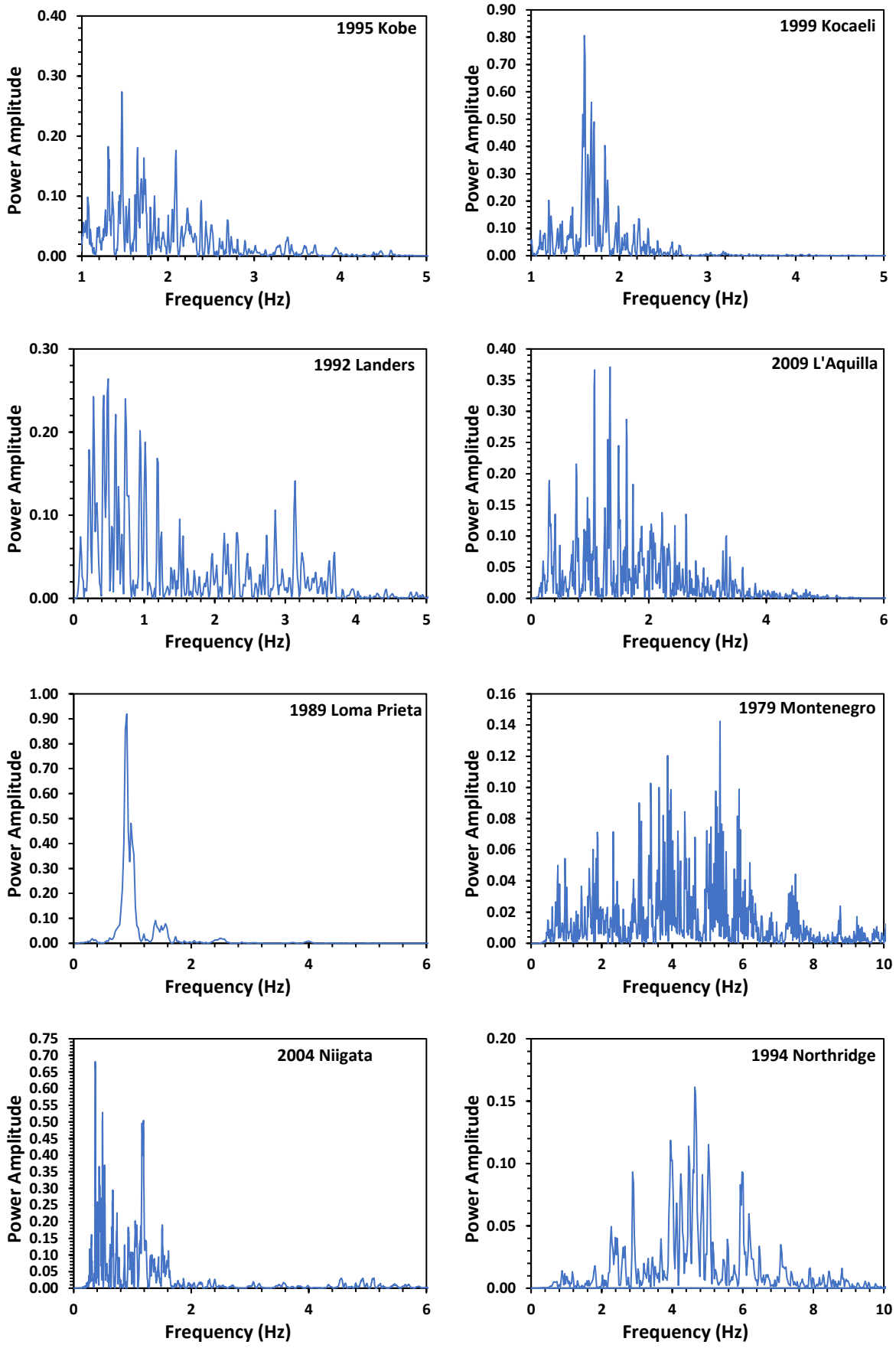
1995 Kobe
1999 Kocaeli
1992 Landers
2009 L'Aquilla
1989 Loma Prieta
1979 Montenegro
2004 Niigata
1994 Northridge
Power Amplitude
Frequency (Hz)

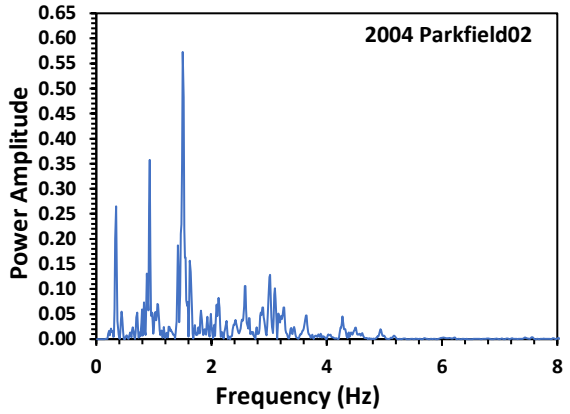
2004 Parkfield02
Power Amplitude
Frequency (Hz)

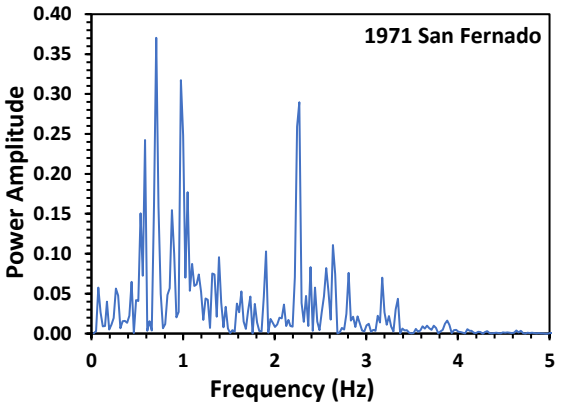
1971 San Fernado
Power Amplitude
Frequency (Hz)

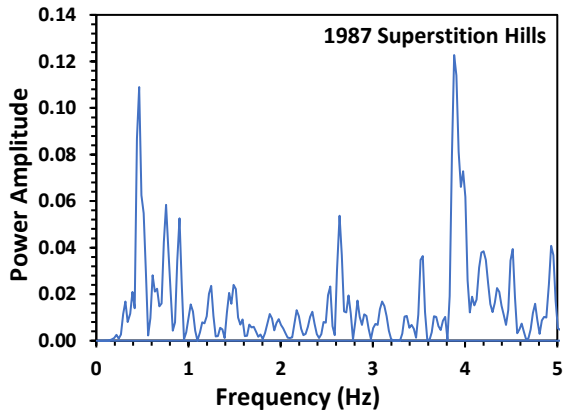
1987 Superstition Hills
Power Amplitude
Frequency (Hz)

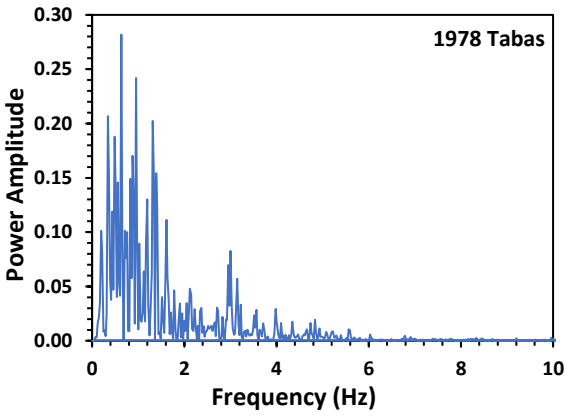
1978 Tabas
Power Amplitude
Frequency (Hz)

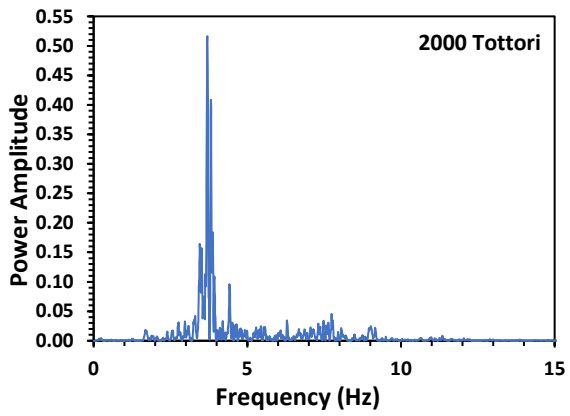
2000 Tottori
Power Amplitude
Frequency (Hz)

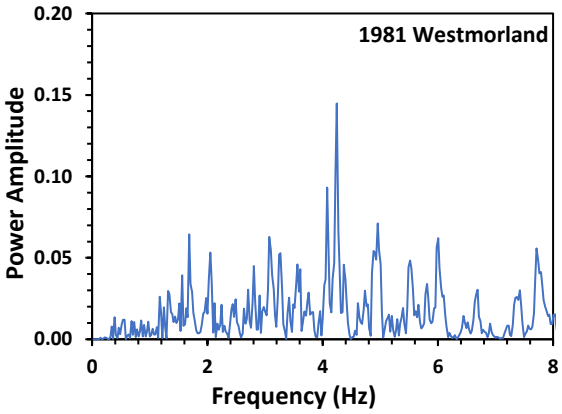
1981 Westmorland
Power Amplitude
Frequency (Hz)

APPENDIX-II

Displacement response (NLTHA)

Bam-NF:

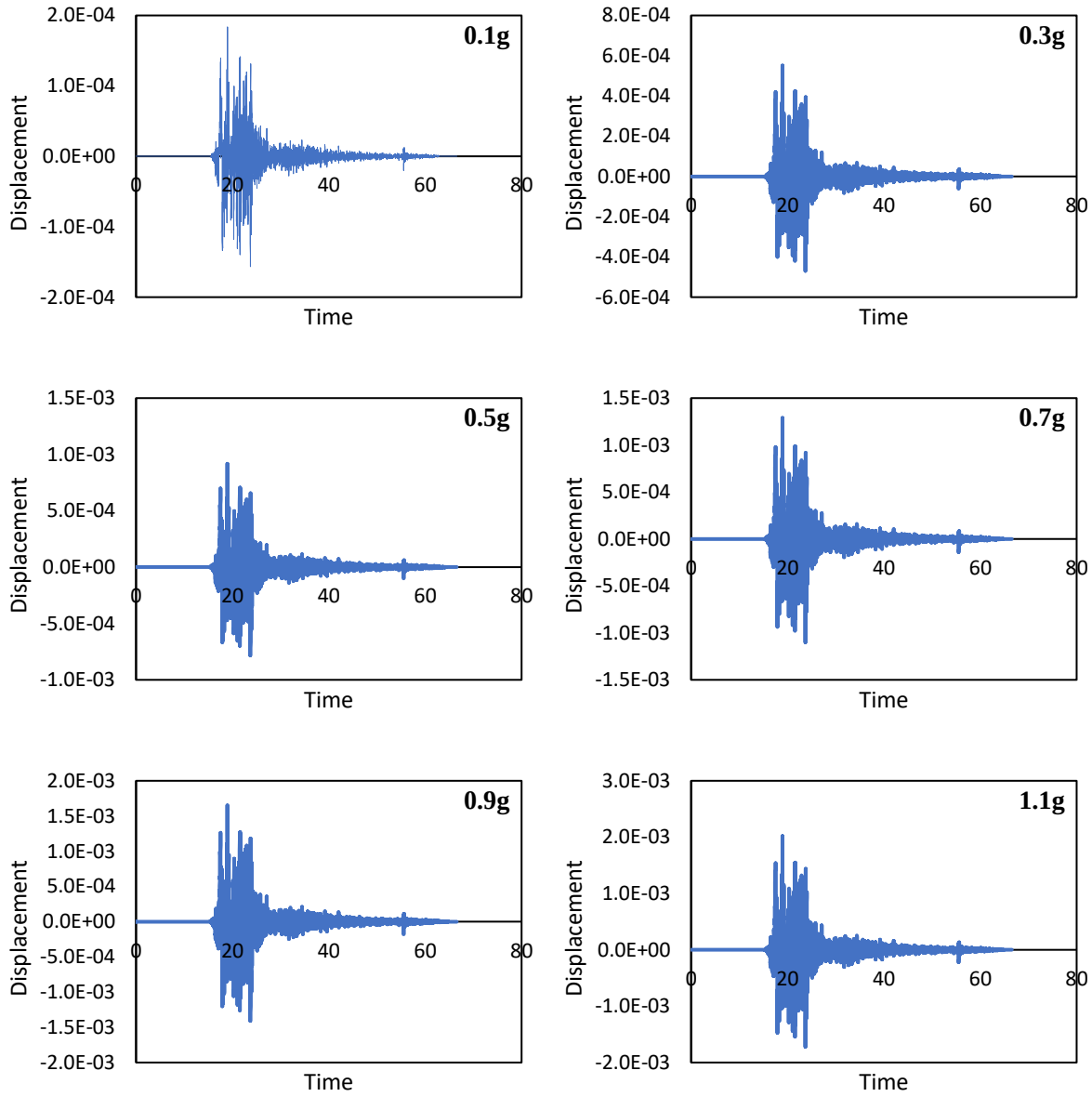

Bam-FF:

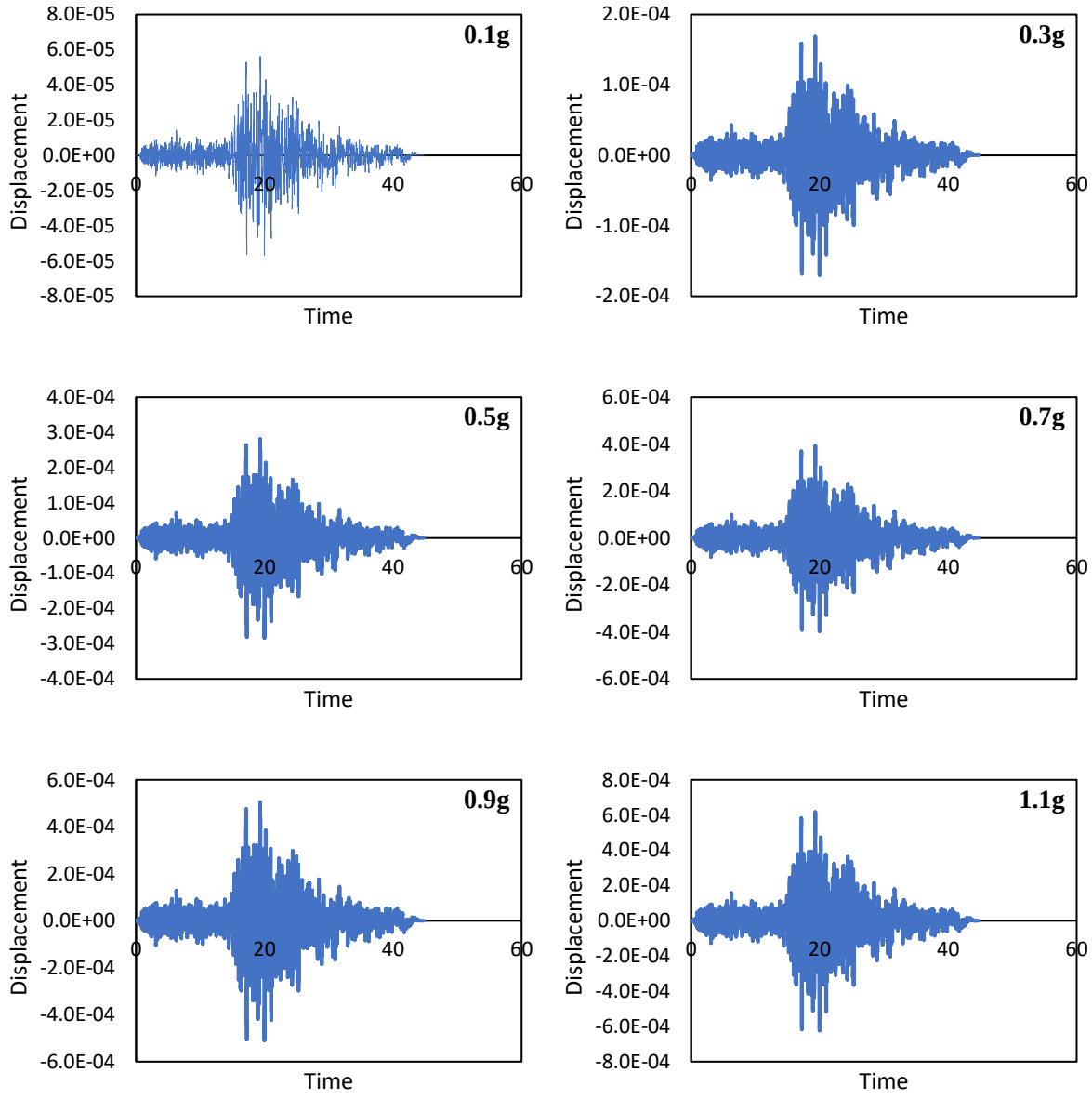

Cape Mendocino-NF

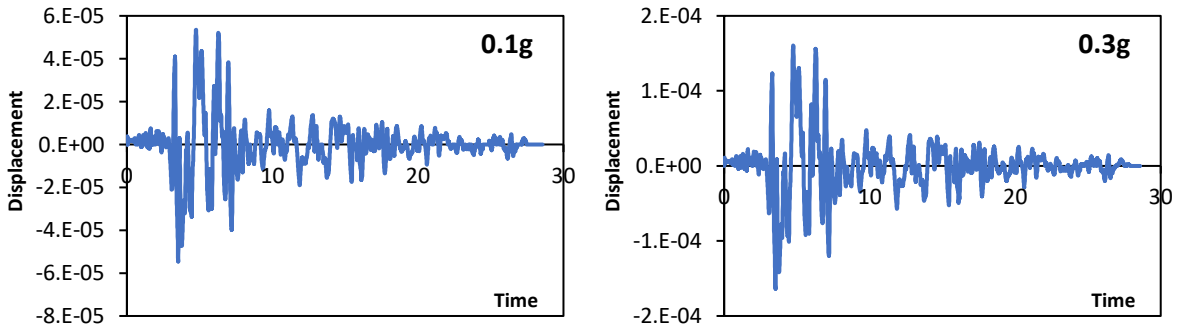

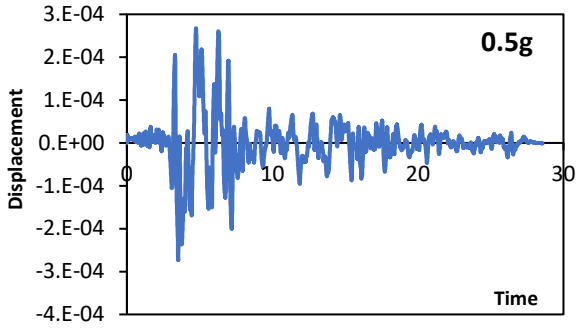

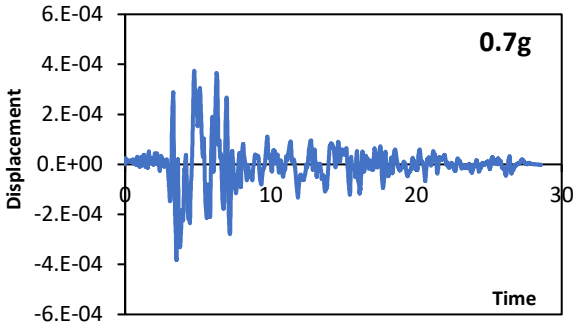

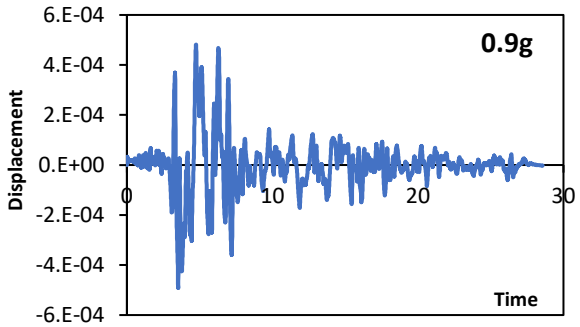

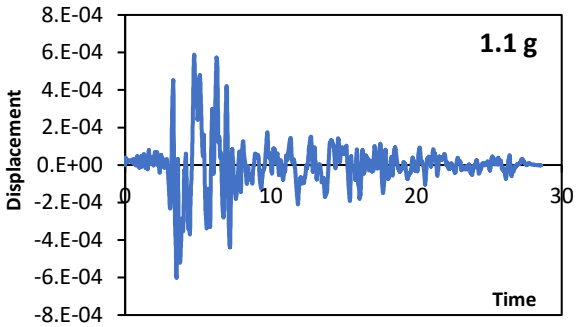

Cape Mendocino-FF

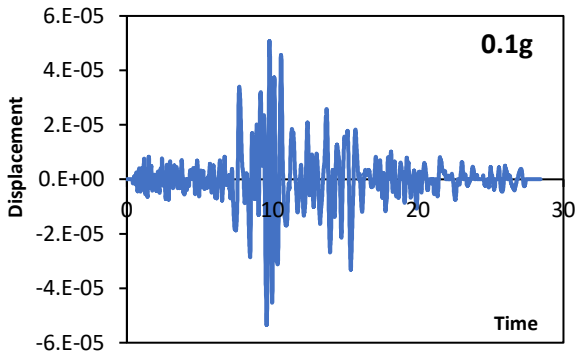

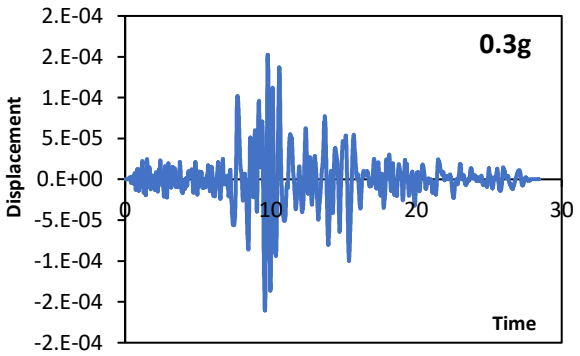

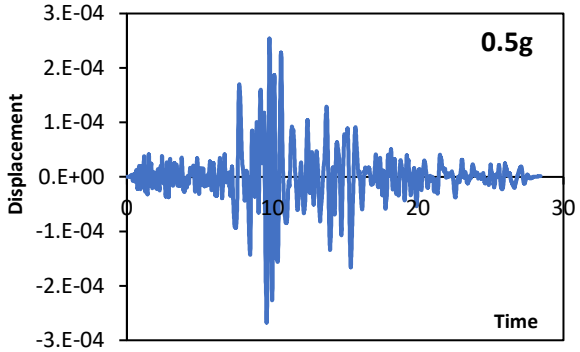

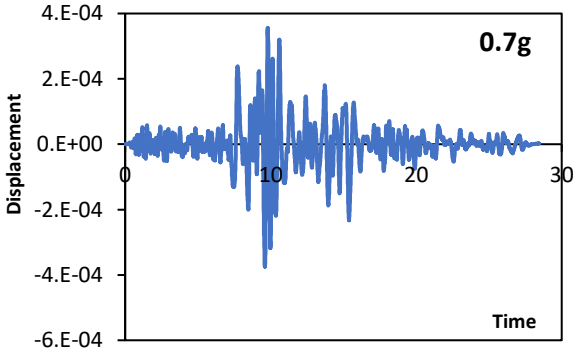

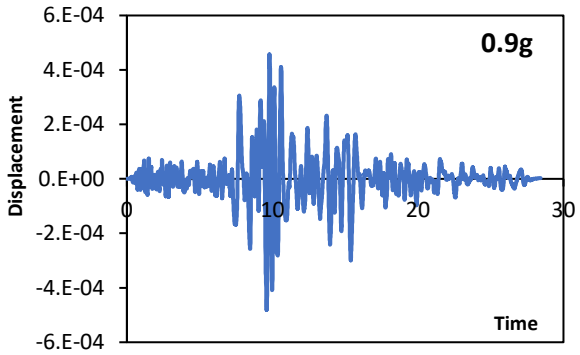

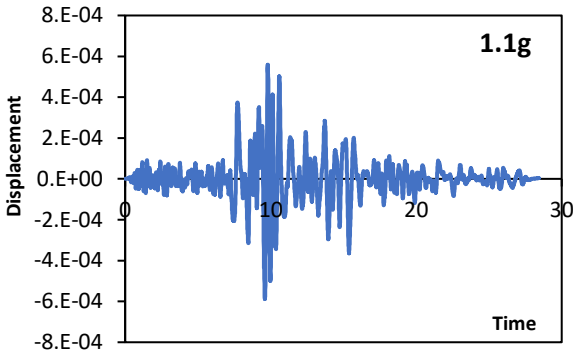

Christchurch-NF

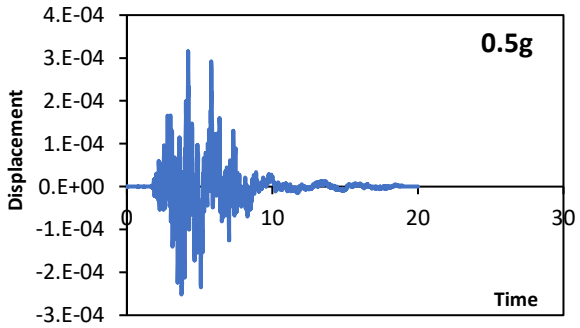

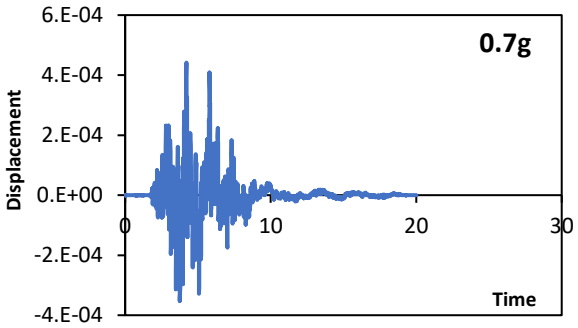

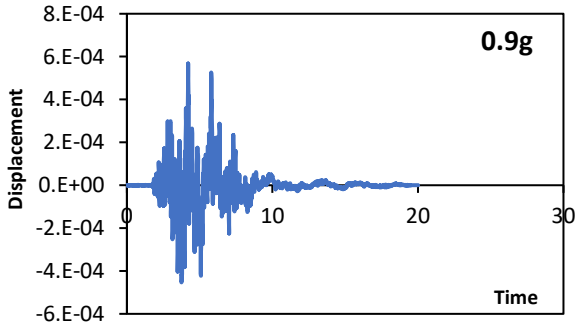

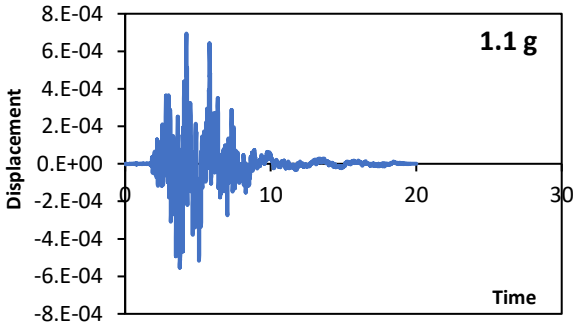

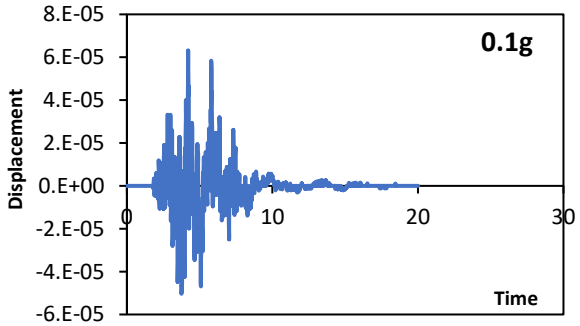

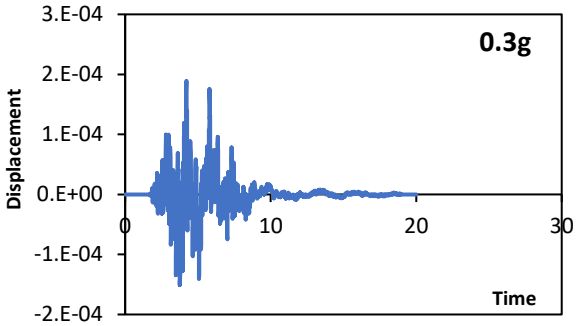

Christchurch-FF

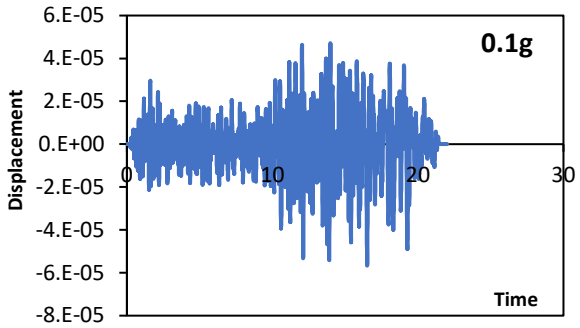

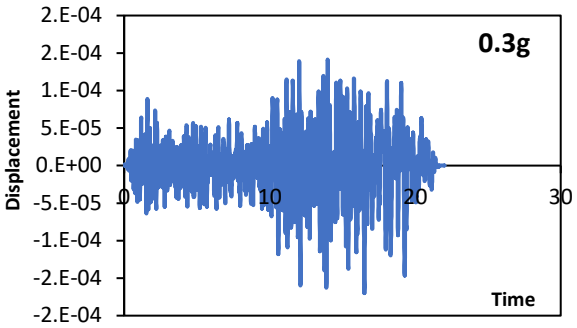

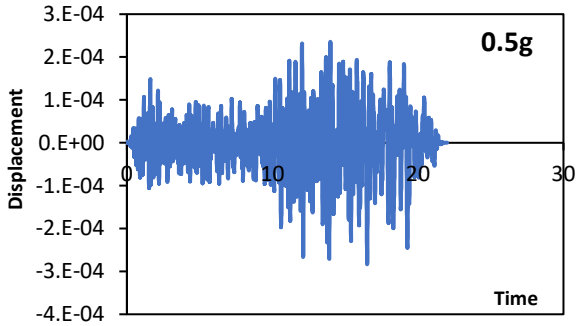

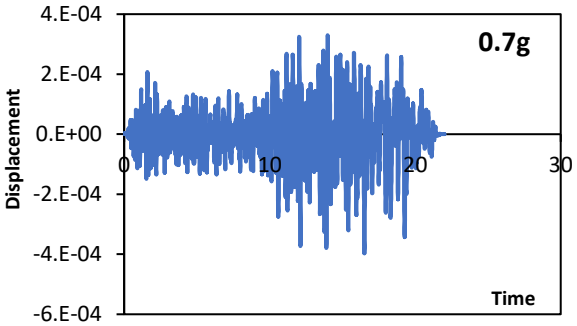

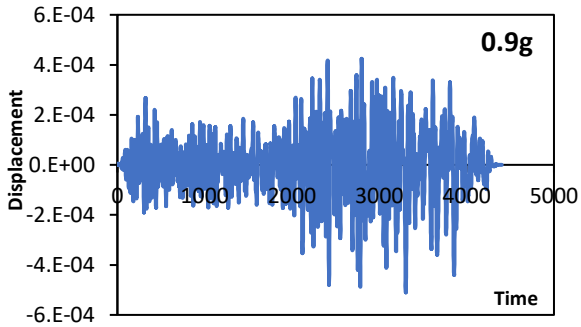

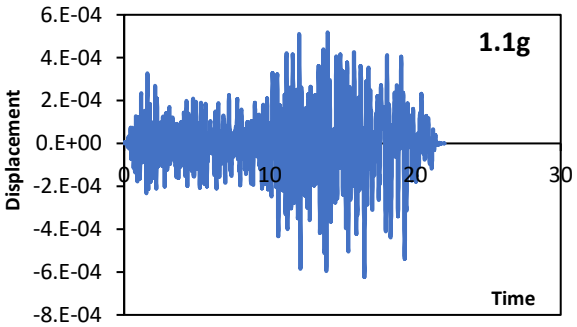

Chetsu-oki-NF

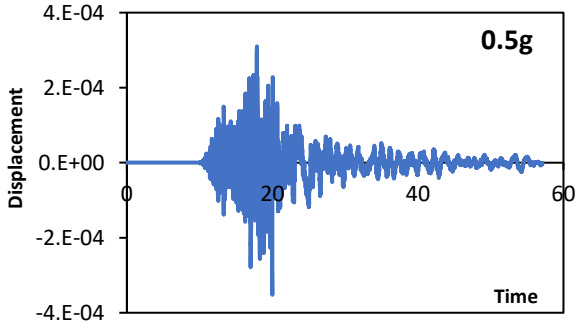

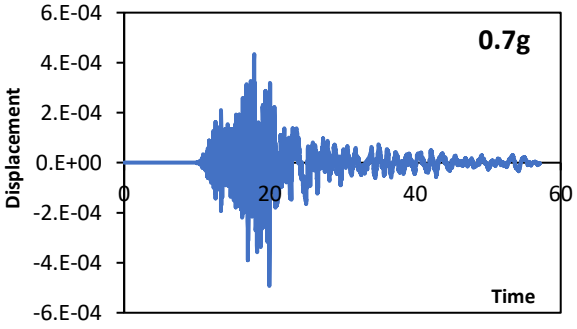

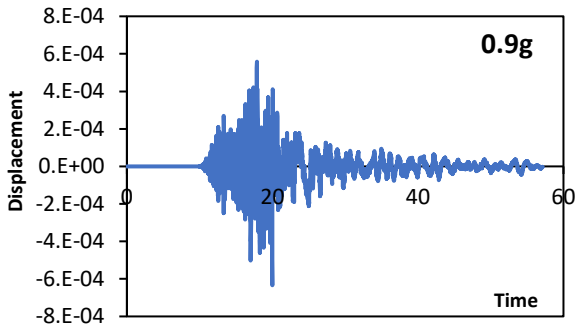

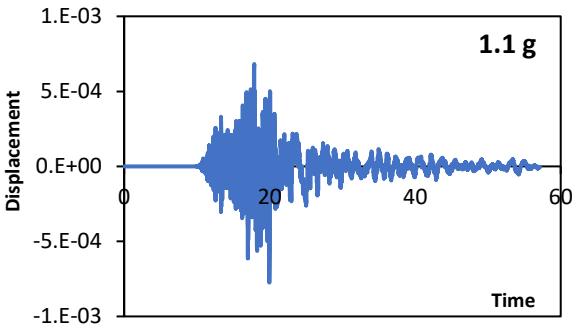

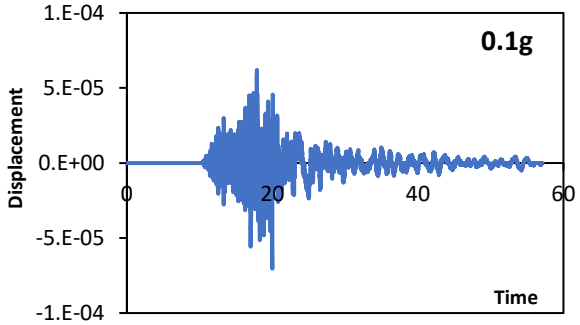

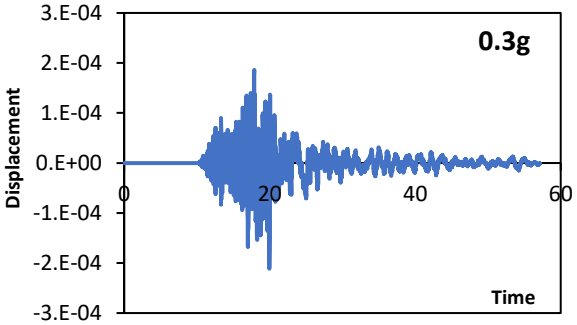

Chetsu-oki- FF

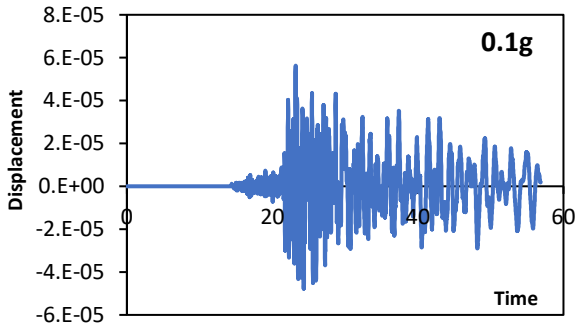

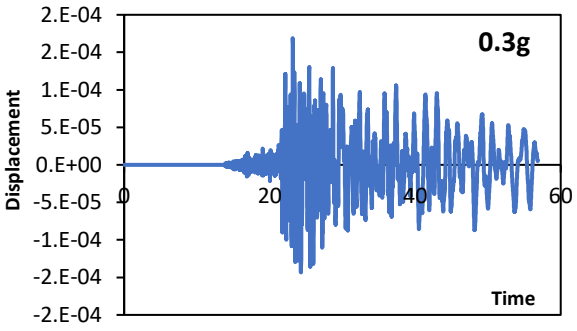

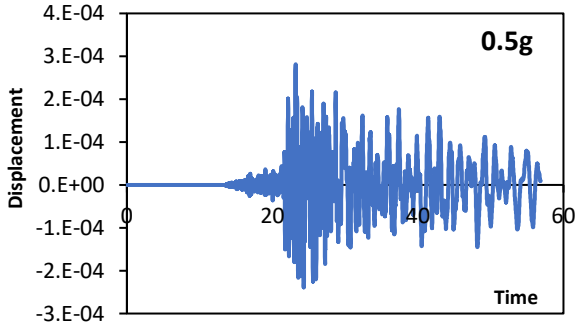

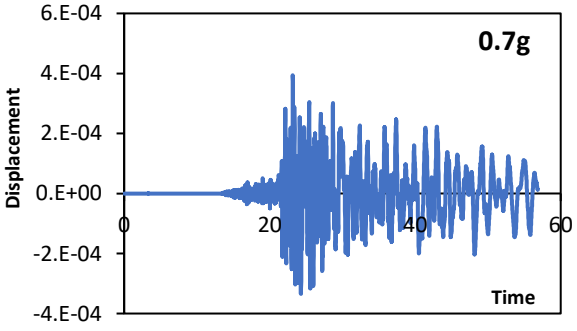

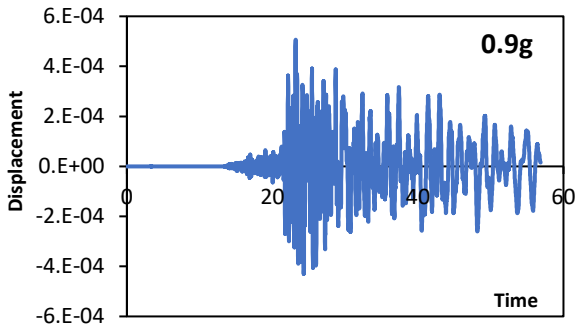

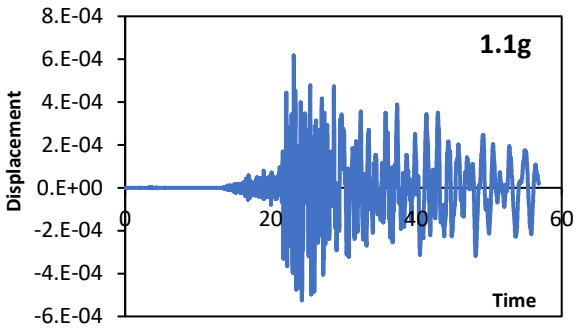

Imperial Valley-NF

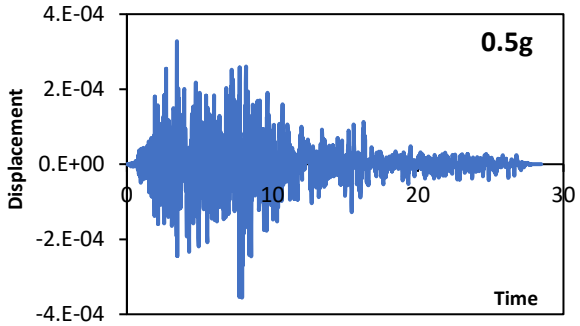

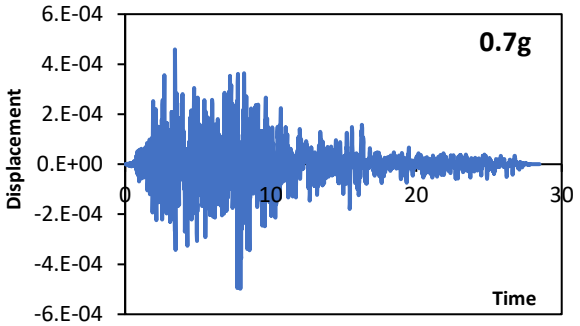

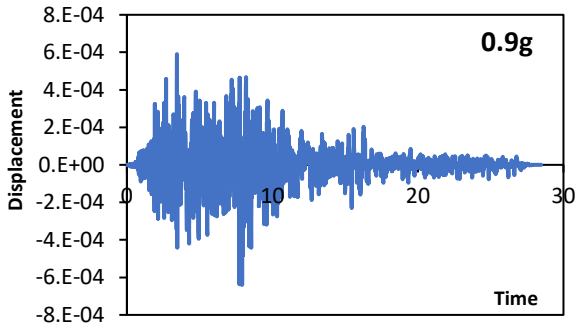

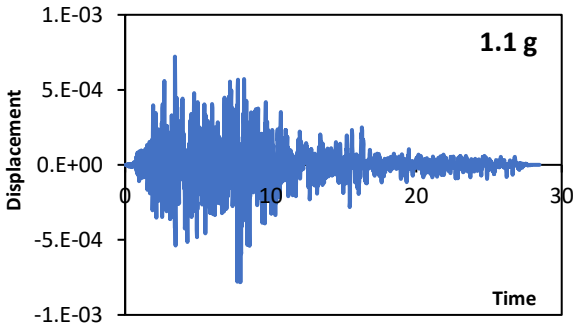

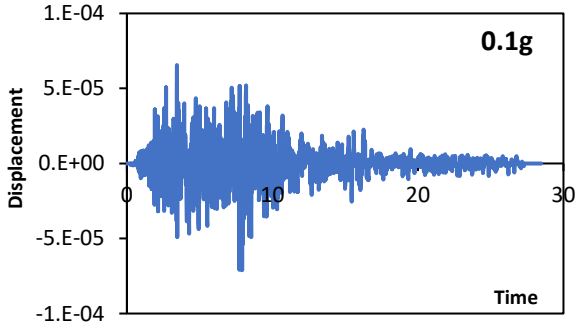

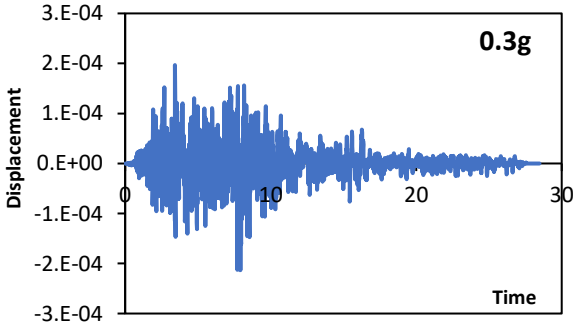

\

Imperial Valley-FF

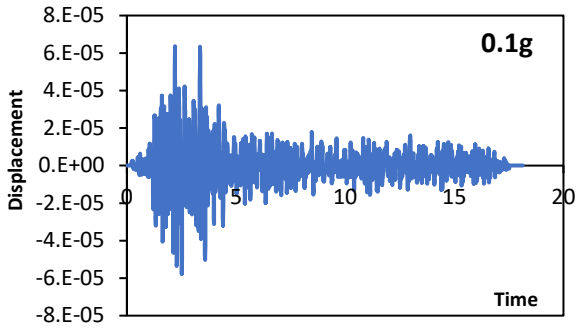

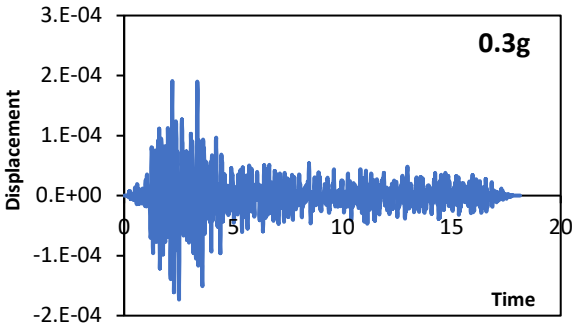

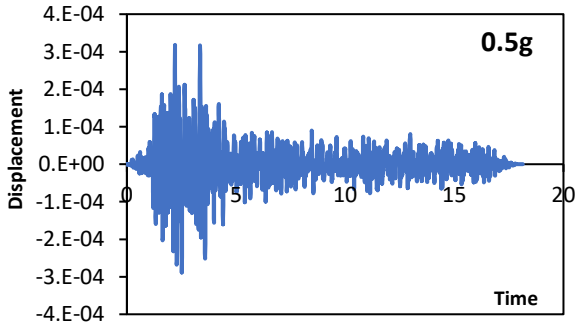

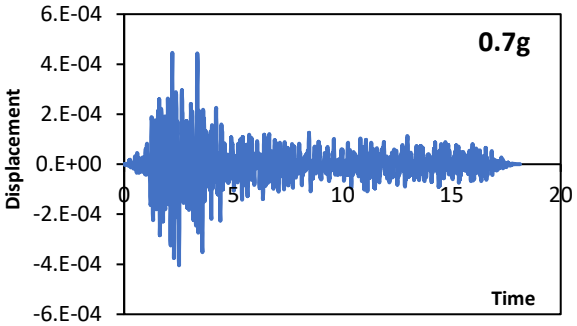

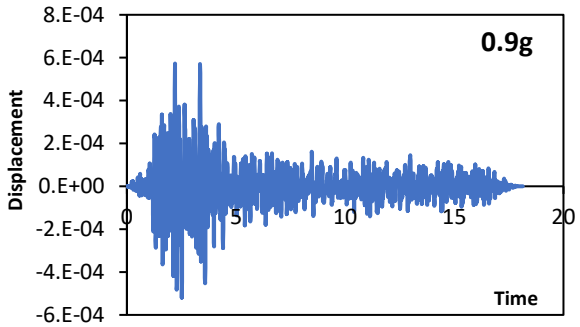

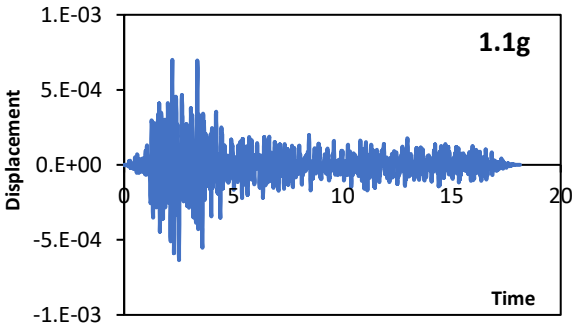

Irpinia-NF

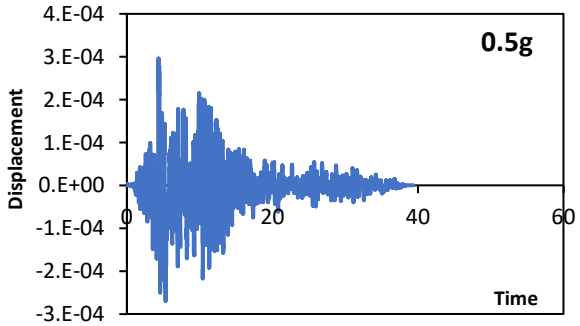

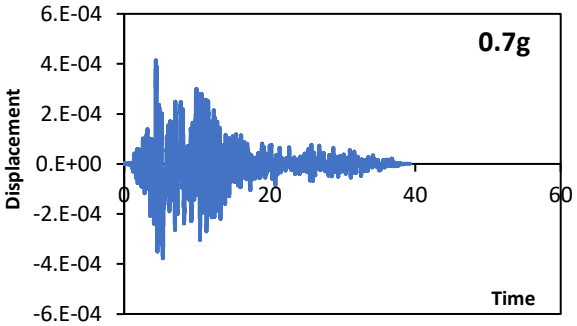

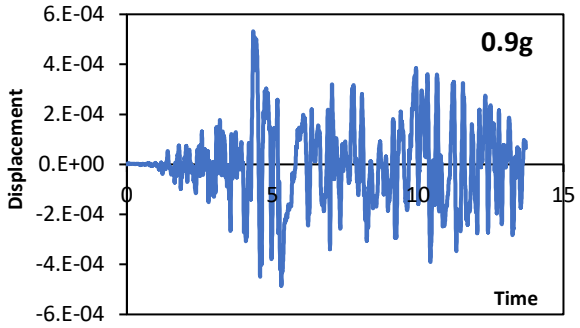
0.9g
Displacement
Time
6.E-04
4.E-04
2.E-04
0.E+00
-2.E-04
-4.E-04
-6.E-04
0
5
10
15

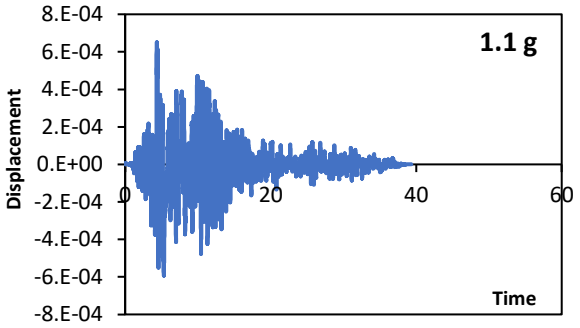
1.1 g
Displacement
Time
8.E-04
6.E-04
4.E-04
2.E-04
0.E+00
-2.E-04
-4.E-04
-6.E-04
-8.E-04
0
20
40
60

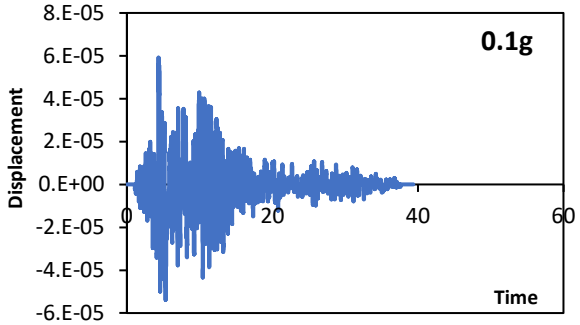
0.1g
Displacement
Time
8.E-05
6.E-05
4.E-05
2.E-05
0.E+00
-2.E-05
-4.E-05
-6.E-05
0
20
40
60

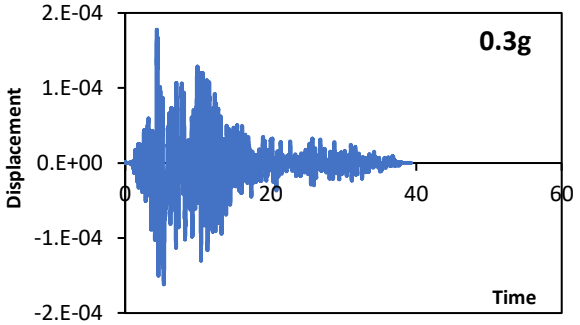
0.3g
Displacement
Time
2.E-04
1.E-04
0.E+00
-1.E-04
-2.E-04
0
20
40
60

Irpinia-FF

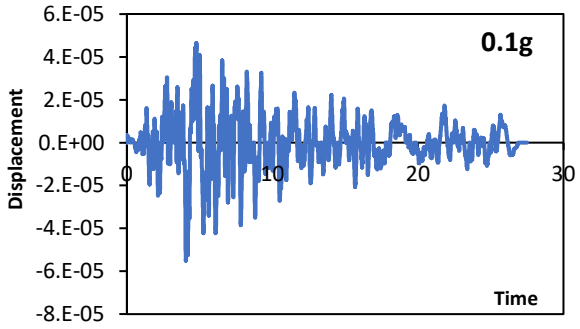
0.1g
Displacement
Time
6.E-05
4.E-05
2.E-05
0.E+00
-2.E-05
-4.E-05
-6.E-05
-8.E-05
0
10
20
30

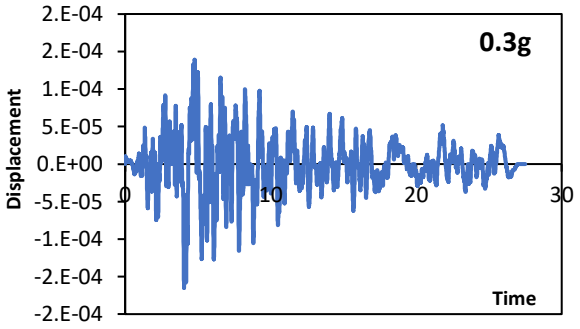
0.3g
Displacement
Time
2.E-04
2.E-04
1.E-04
5.E-05
0.E+00
-5.E-05
-1.E-04
-2.E-04
-2.E-04
0
10
20
30

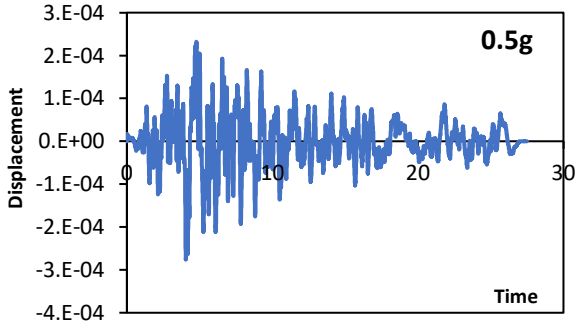
0.5g
Displacement
Time
3.E-04
2.E-04
1.E-04
0.E+00
-1.E-04
-2.E-04
-3.E-04
-4.E-04
0
10
20
30

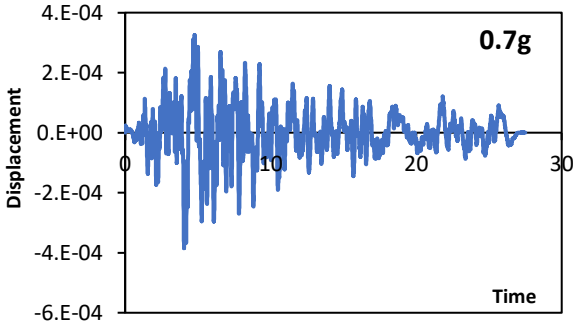
0.7g
Displacement
Time
4.E-04
2.E-04
0.E+00
-2.E-04
-4.E-04
-6.E-04
0
10
20
30

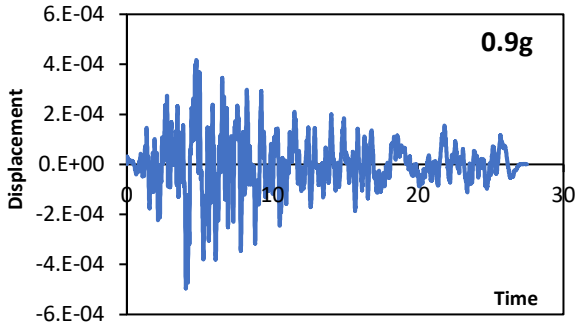
0.9g
Displacement
Time
6.E-04
4.E-04
2.E-04
0.E+00
-2.E-04
-4.E-04
-6.E-04
0
10
20
30

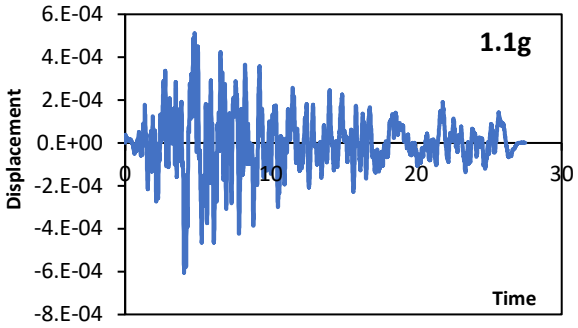
1.1g
Displacement
Time
6.E-04
4.E-04
2.E-04
0.E+00
-2.E-04
-4.E-04
-6.E-04
-8.E-04
0
10
20
30

Kalmata-NF

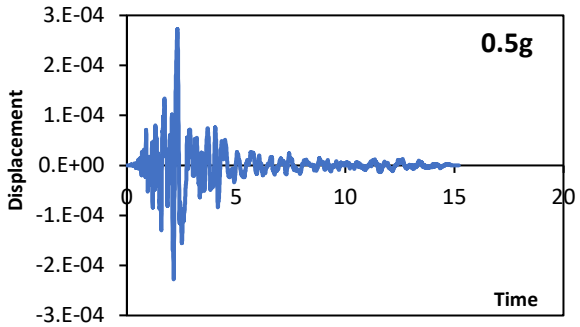
0.5g
Displacement
Time
3.E-04
2.E-04
1.E-04
0.E+00
-1.E-04
-2.E-04
-3.E-04
0
5
10
15
20

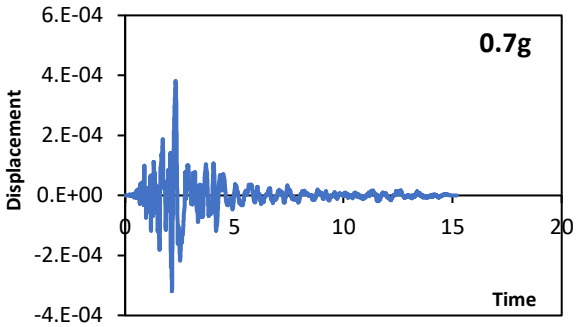
0.7g
Displacement
Time
6.E-04
4.E-04
2.E-04
0.E+00
-2.E-04
-4.E-04
0
5
10
15
20

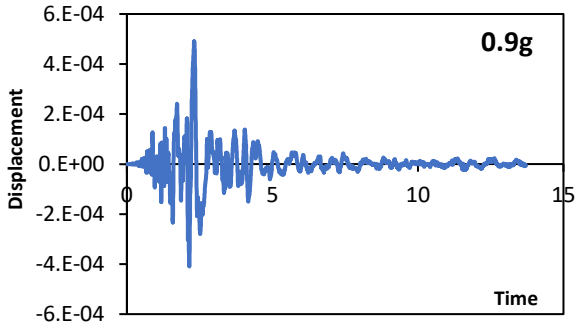
0.9g
Displacement
Time
6.E-04
4.E-04
2.E-04
0.E+00
-2.E-04
-4.E-04
-6.E-04
0
5
10
15

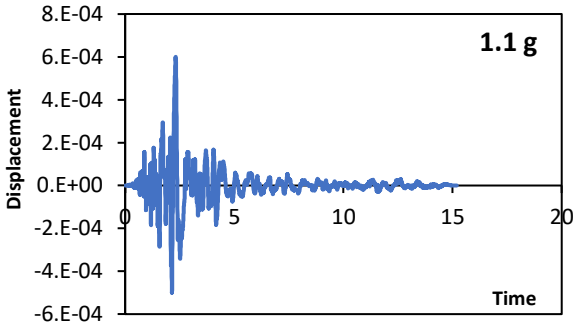
1.1 g
Displacement
Time
8.E-04
6.E-04
4.E-04
2.E-04
0.E+00
-2.E-04
-4.E-04
-6.E-04
0
5
10
15
20

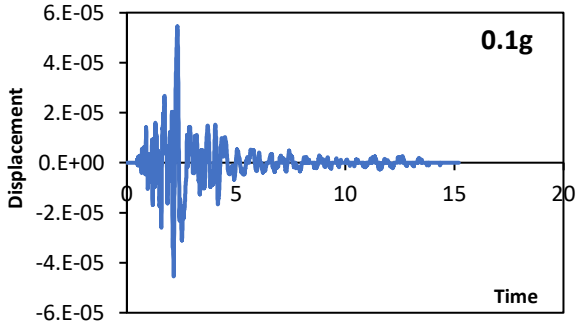
0.1g
Displacement
Time
6.E-05
4.E-05
2.E-05
0.E+00
-2.E-05
-4.E-05
-6.E-05
0
5
10
15
20

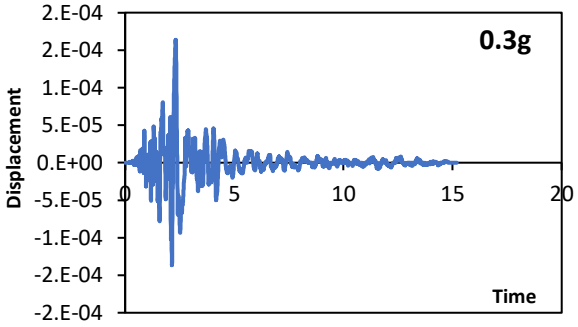
0.3g
Displacement
Time
2.E-04
2.E-04
1.E-04
5.E-05
0.E+00
-5.E-05
-1.E-04
-2.E-04
-2.E-04
0
5
10
15
20

Kobe-NF:

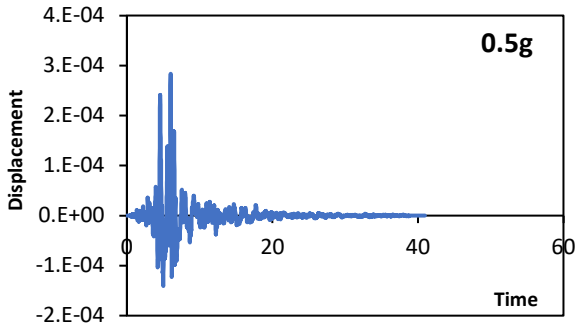

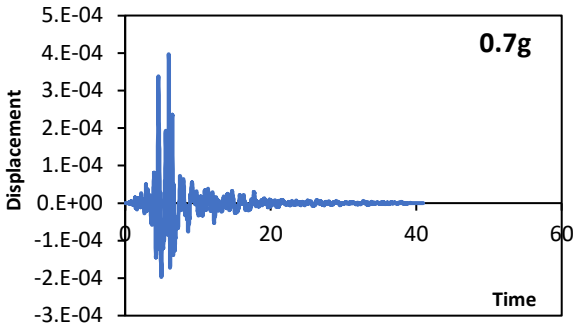

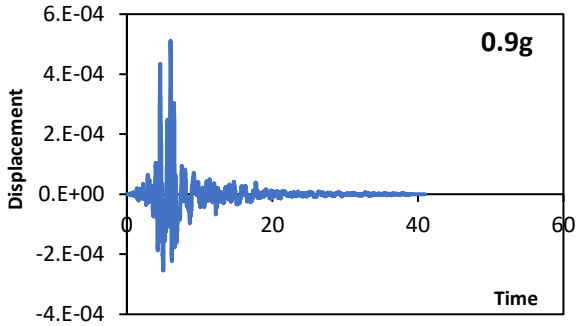

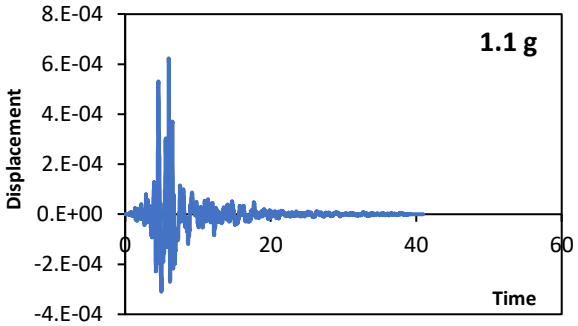

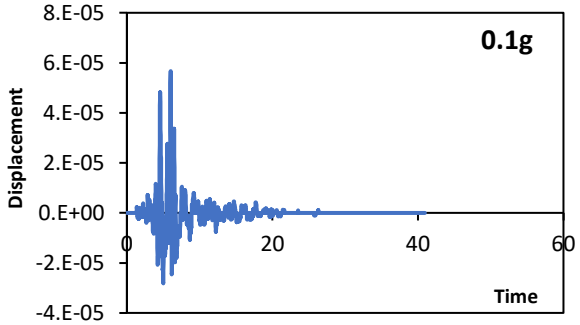

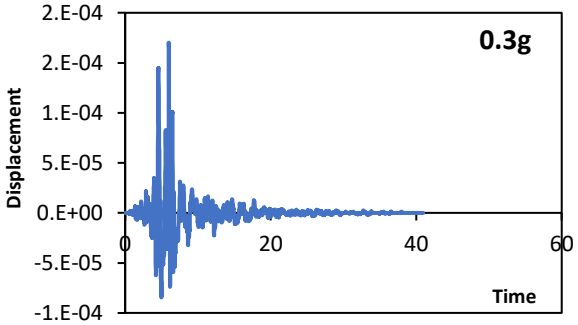

Kobe-FF:

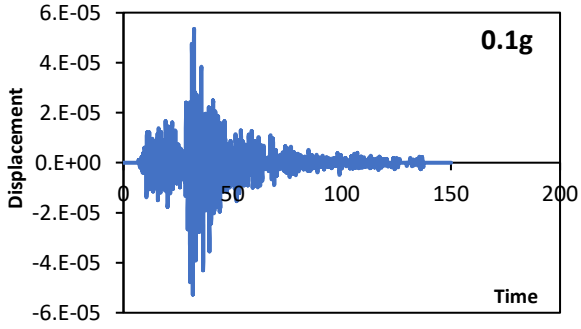

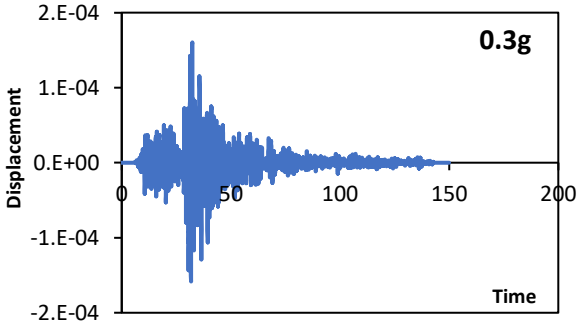

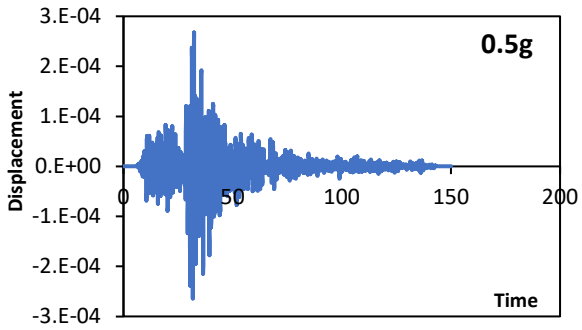
0.5g
Displacement
Time
3.E-04
2.E-04
1.E-04
0.E+00
-1.E-04
-2.E-04
-3.E-04
0
50
100
150
200

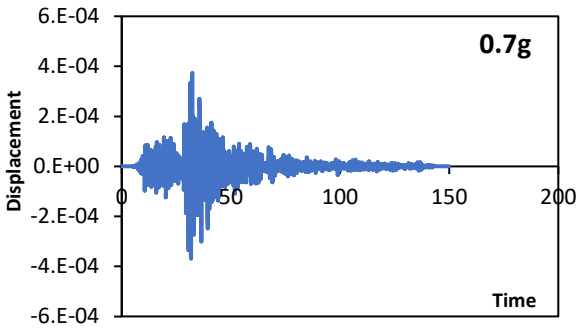
0.7g
Displacement
Time
6.E-04
4.E-04
2.E-04
0.E+00
-2.E-04
-4.E-04
-6.E-04
0
50
100
150
200

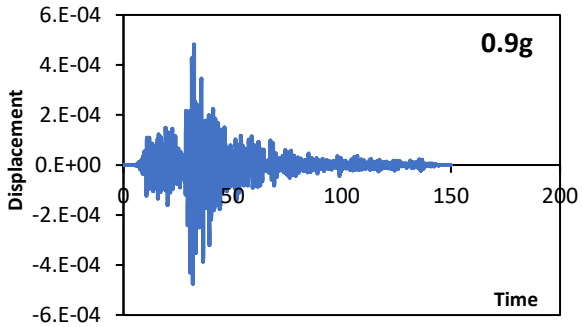
0.9g
Displacement
Time
6.E-04
4.E-04
2.E-04
0.E+00
-2.E-04
-4.E-04
-6.E-04
0
50
100
150
200

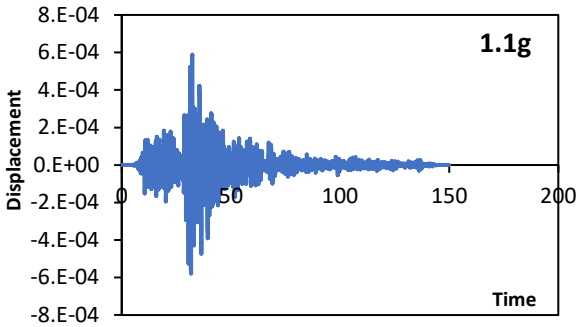
1.1g
Displacement
Time
8.E-04
6.E-04
4.E-04
2.E-04
0.E+00
-2.E-04
-4.E-04
-6.E-04
-8.E-04
0
50
100
150
200

Kocaeli-NF:

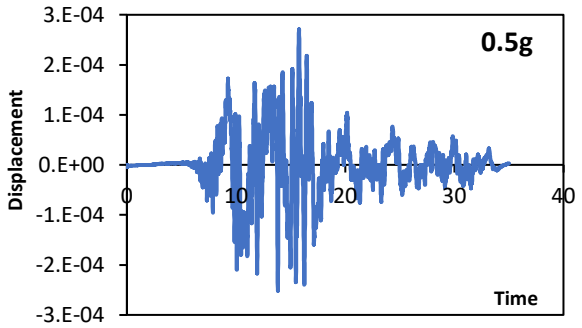
0.5g
Displacement
Time
3.E-04
2.E-04
1.E-04
0.E+00
-1.E-04
-2.E-04
-3.E-04
0
10
20
30
40

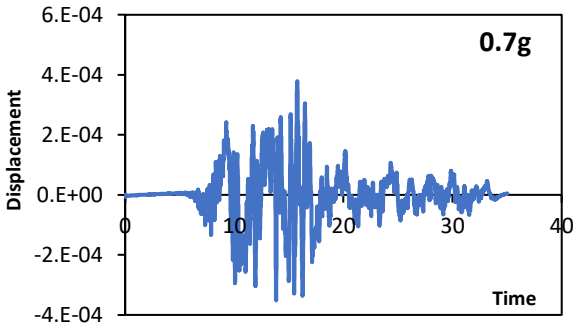
0.7g
Displacement
Time
6.E-04
4.E-04
2.E-04
0.E+00
-2.E-04
-4.E-04
0
10
20
30
40

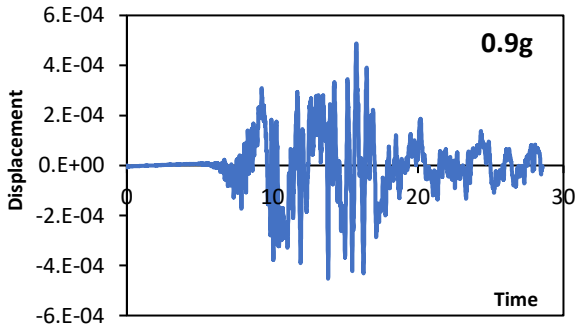
0.9g
Displacement
Time
6.E-04
4.E-04
2.E-04
0.E+00
-2.E-04
-4.E-04
-6.E-04
0
10
20
30

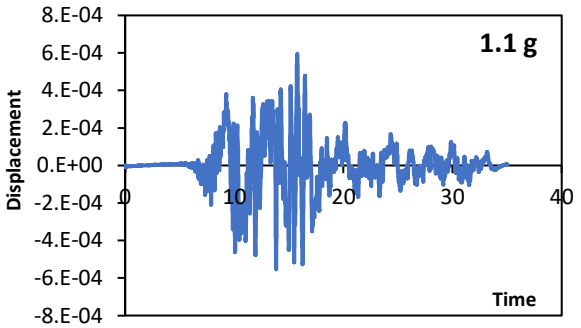
1.1 g
Displacement
Time
8.E-04
6.E-04
4.E-04
2.E-04
0.E+00
-2.E-04
-4.E-04
-6.E-04
-8.E-04
0
10
20
30
40

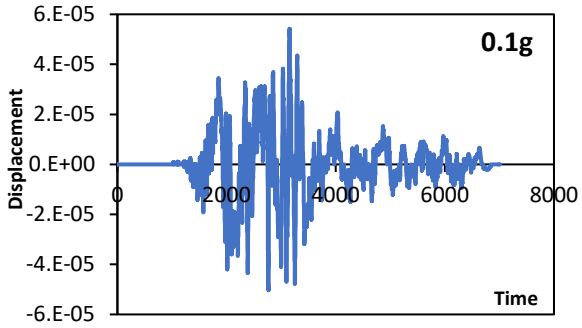
0.1g
Displacement
Time
6.E-05
4.E-05
2.E-05
0.E+00
-2.E-05
-4.E-05
-6.E-05
0
2000
4000
6000
8000

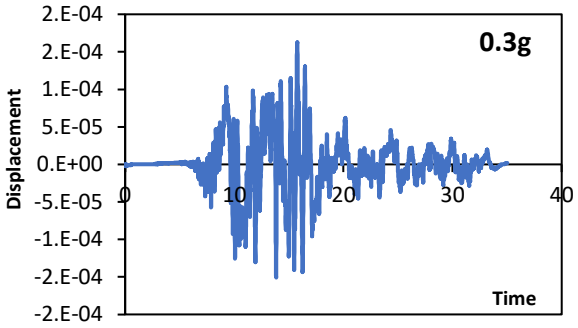
0.3g
Displacement
Time
2.E-04
2.E-04
1.E-04
5.E-05
0.E+00
-5.E-05
-1.E-04
-2.E-04
-2.E-04
0
10
20
30
40

Kocaeli-FF:

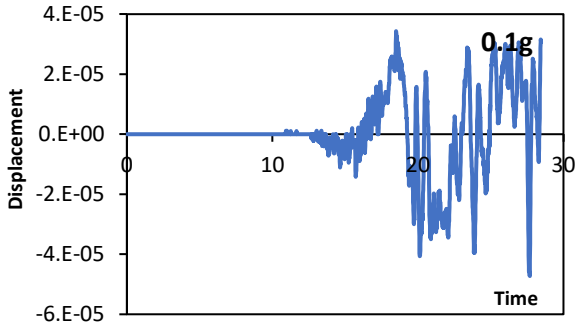
0.1g
Displacement
Time
4.E-05
2.E-05
0.E+00
-2.E-05
-4.E-05
-6.E-05
0
10
20
30

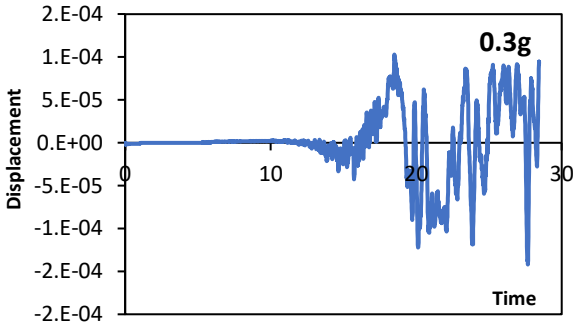
0.3g
Displacement
Time
2.E-04
1.E-04
5.E-05
0.E+00
-5.E-05
-1.E-04
-2.E-04
-2.E-04
0
10
20
30

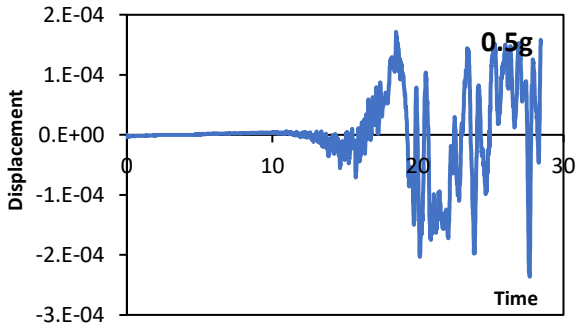
0.5g
Displacement
Time
2.E-04
1.E-04
0.E+00
-1.E-04
-2.E-04
-3.E-04
0
10
20
30

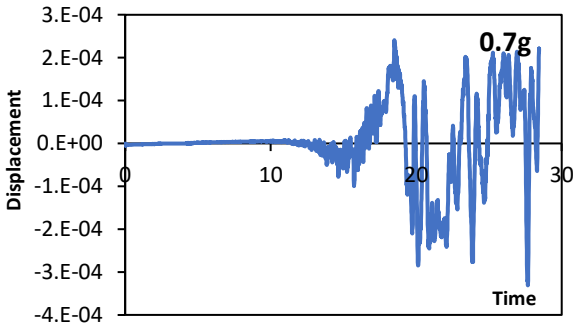
0.7g
Displacement
Time
3.E-04
2.E-04
1.E-04
0.E+00
-1.E-04
-2.E-04
-3.E-04
-4.E-04
0
10
20
30

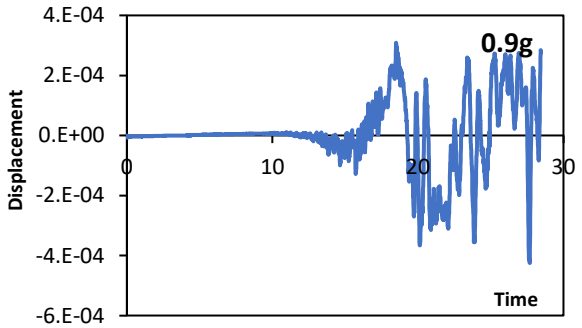
0.9g
Displacement
Time
4.E-04
2.E-04
0.E+00
-2.E-04
-4.E-04
-6.E-04
0
10
20
30

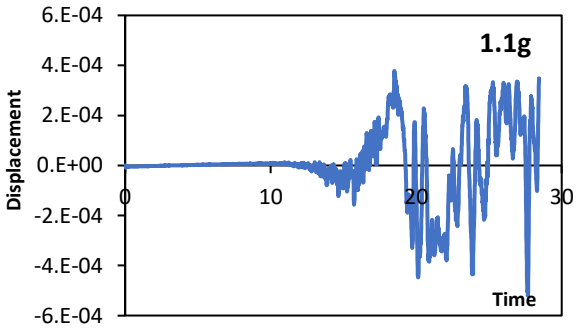
1.1g
Displacement
Time
6.E-04
4.E-04
2.E-04
0.E+00
-2.E-04
-4.E-04
-6.E-04
0
10
20
30

Landers-NF:

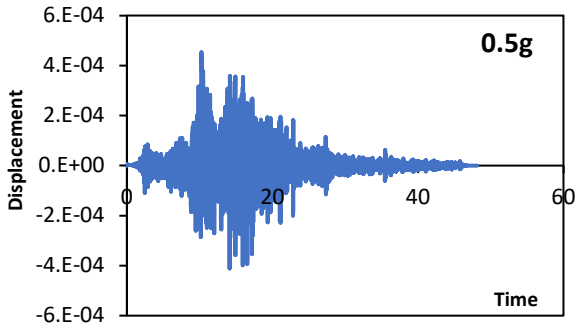

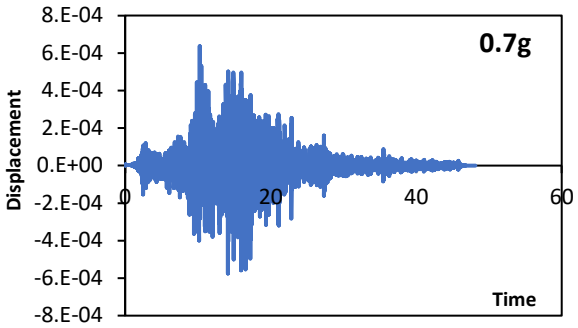

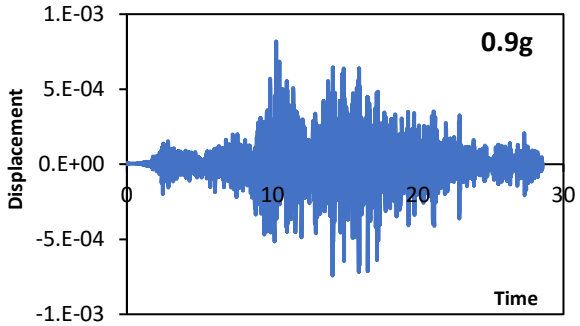

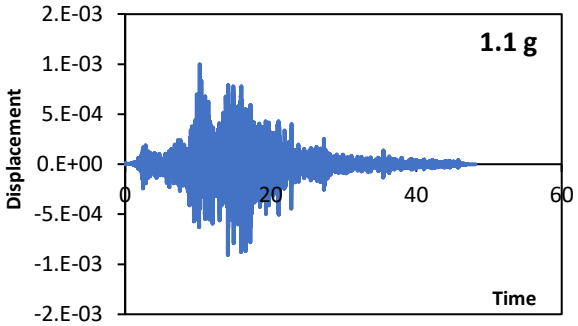

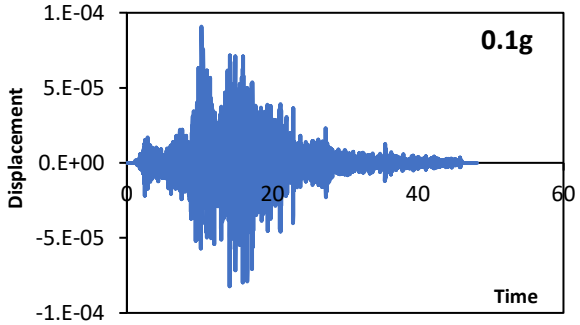

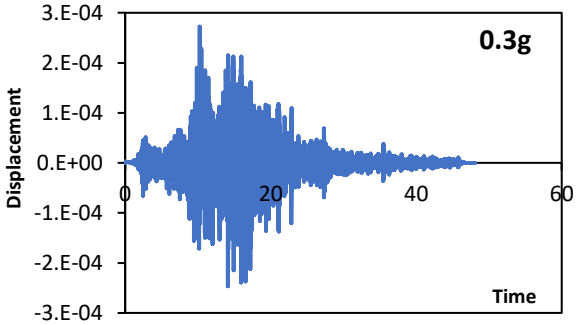

Landers-FF:

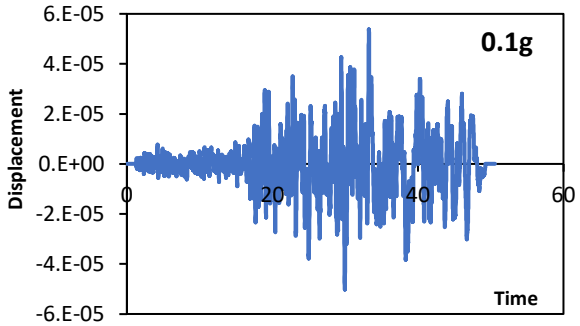

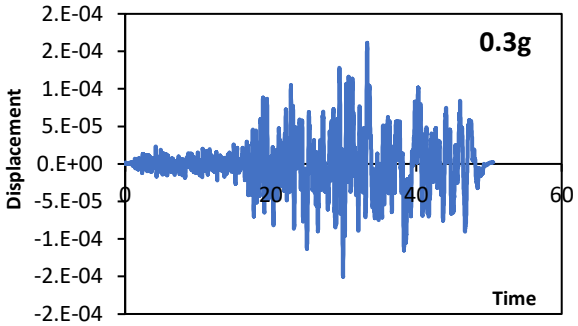

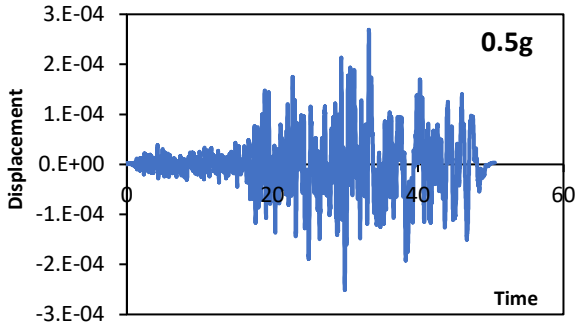
0.5g
Displacement
Time
3.E-04
2.E-04
1.E-04
0.E+00
-1.E-04
-2.E-04
-3.E-04
0
20
40
60

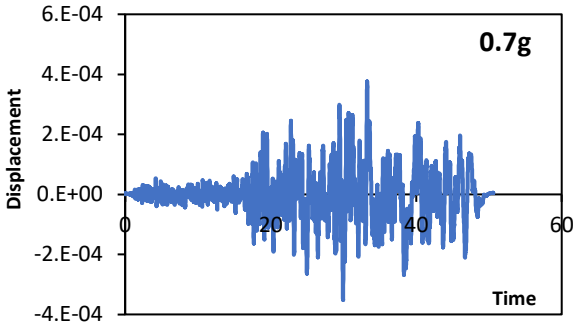
0.7g
Displacement
Time
6.E-04
4.E-04
2.E-04
0.E+00
-2.E-04
-4.E-04
0
20
40
60

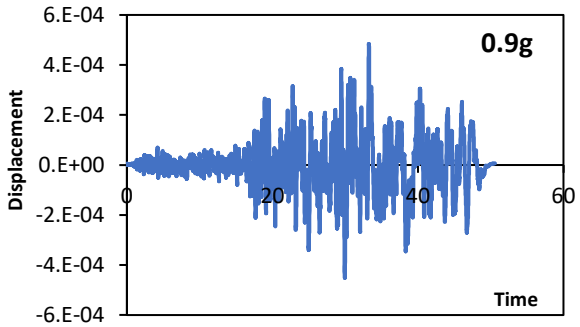
0.9g
Displacement
Time
6.E-04
4.E-04
2.E-04
0.E+00
-2.E-04
-4.E-04
-6.E-04
0
20
40
60

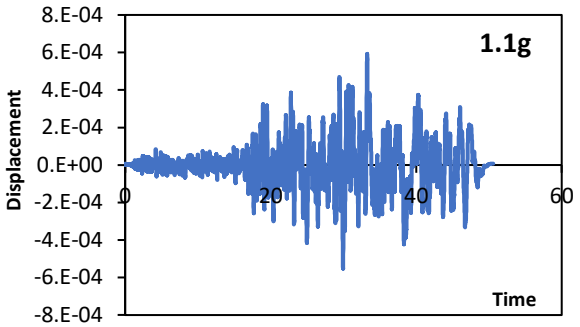
1.1g
Displacement
Time
8.E-04
6.E-04
4.E-04
2.E-04
0.E+00
-2.E-04
-4.E-04
-6.E-04
-8.E-04
0
20
40
60

L-Aquilla-NF:

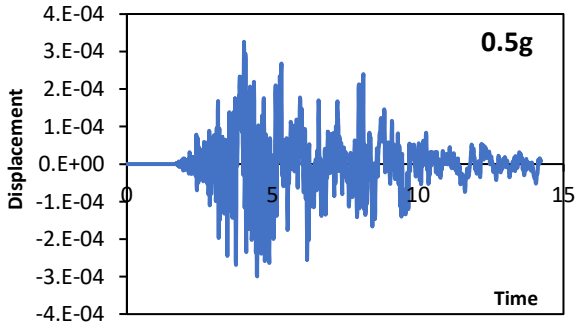
0.5g
Displacement
Time
4.E-04
3.E-04
2.E-04
1.E-04
0.E+00
-1.E-04
-2.E-04
-3.E-04
-4.E-04
0
5
10
15

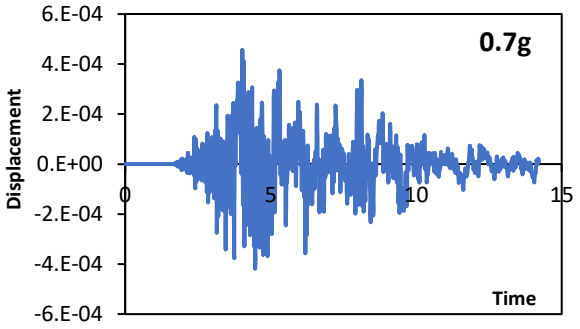
0.7g
Displacement
Time
6.E-04
4.E-04
2.E-04
0.E+00
-2.E-04
-4.E-04
-6.E-04
0
5
10
15

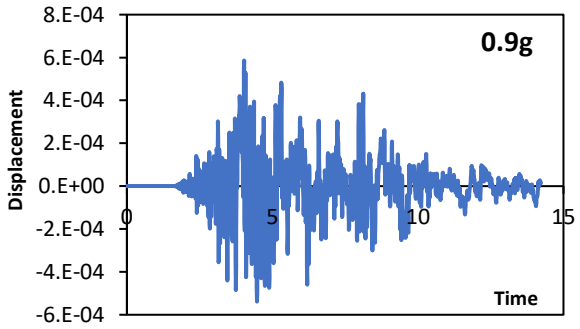
0.9g
Displacement
Time
8.E-04
6.E-04
4.E-04
2.E-04
0.E+00
-2.E-04
-4.E-04
-6.E-04
0
5
10
15

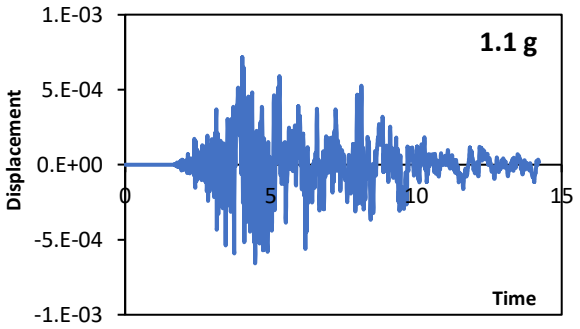
1.1 g
Displacement
Time
1.E-03
5.E-04
0.E+00
-5.E-04
-1.E-03
0
5
10
15

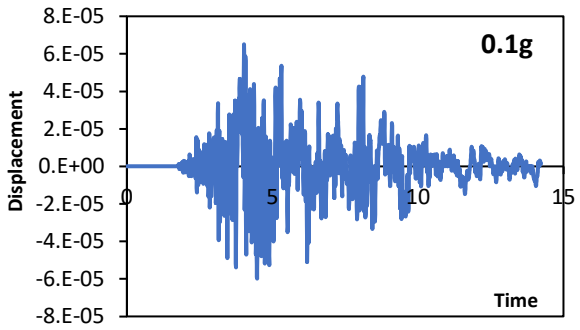
0.1g
Displacement
Time
8.E-05
6.E-05
4.E-05
2.E-05
0.E+00
-2.E-05
-4.E-05
-6.E-05
-8.E-05
0
5
10
15

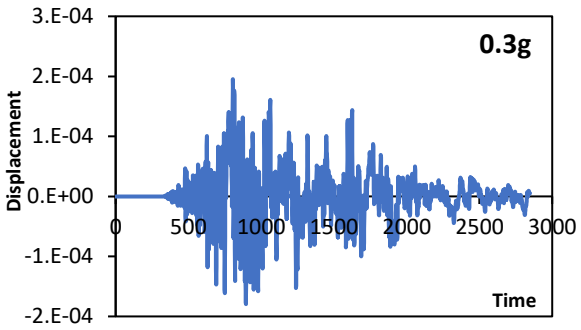
0.3g
Displacement
Time
3.E-04
2.E-04
1.E-04
0.E+00
-1.E-04
-2.E-04
0
500
1000
1500
2000
2500
3000

L-Aquilla-FF:

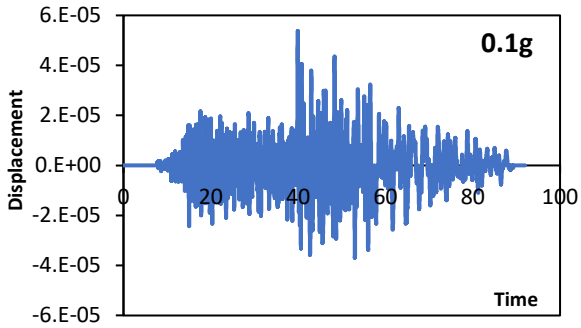
0.1g
Displacement
Time
6.E-05
4.E-05
2.E-05
0.E+00
-2.E-05
-4.E-05
-6.E-05
0
20
40
60
80
100

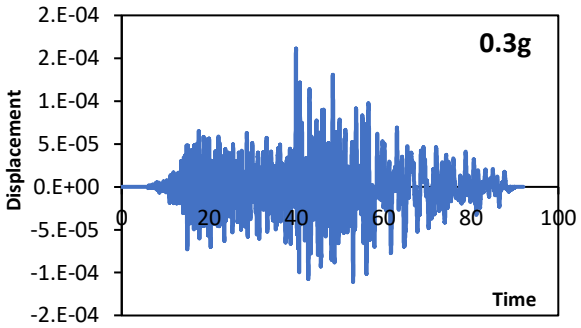
0.3g
Displacement
Time
2.E-04
2.E-04
1.E-04
5.E-05
0.E+00
-5.E-05
-1.E-04
-2.E-04
0
20
40
60
80
100

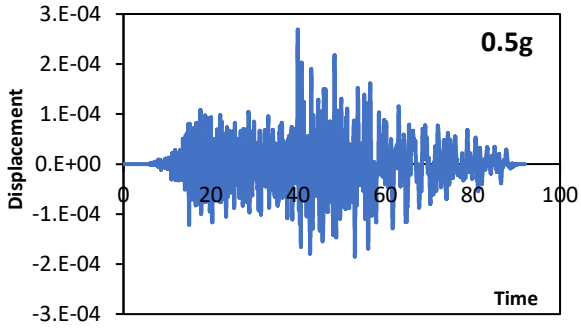
0.5g
Displacement
Time
3.E-04
2.E-04
1.E-04
0.E+00
-1.E-04
-2.E-04
-3.E-04
0
20
40
60
80
100

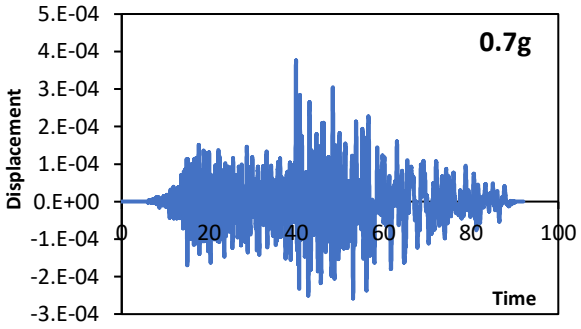
0.7g
Displacement
Time
5.E-04
4.E-04
3.E-04
2.E-04
1.E-04
0.E+00
-1.E-04
-2.E-04
-3.E-04
0
20
40
60
80
100

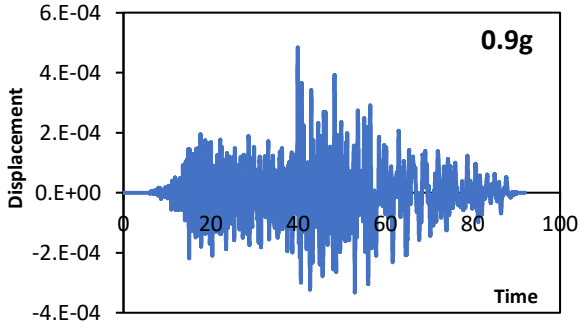
0.9g
Displacement
Time
6.E-04
4.E-04
2.E-04
0.E+00
-2.E-04
-4.E-04
0
20
40
60
80
100

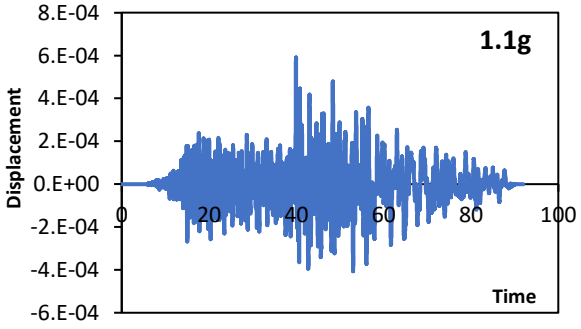
1.1g
Displacement
Time
8.E-04
6.E-04
4.E-04
2.E-04
0.E+00
-2.E-04
-4.E-04
-6.E-04
0
20
40
60
80
100

Loma Prieta-NF:

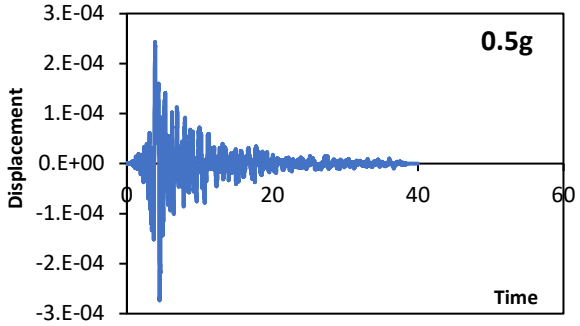

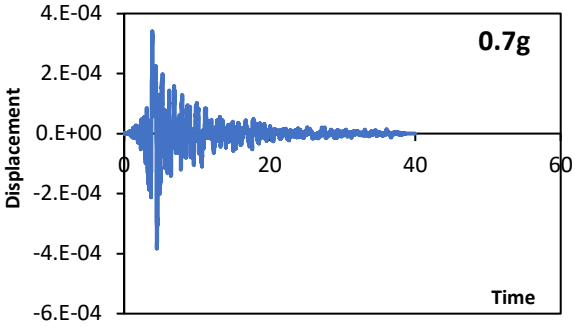

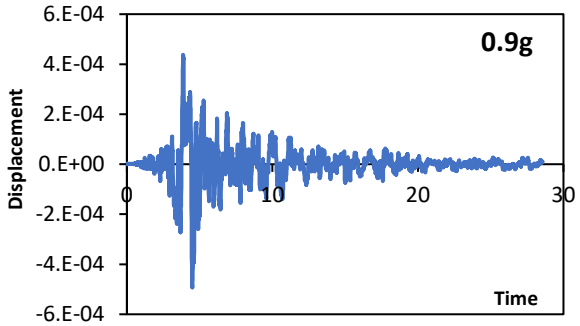

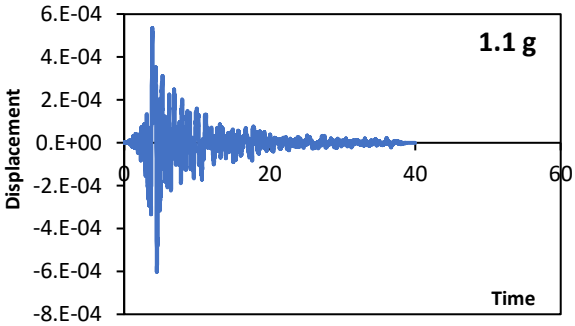

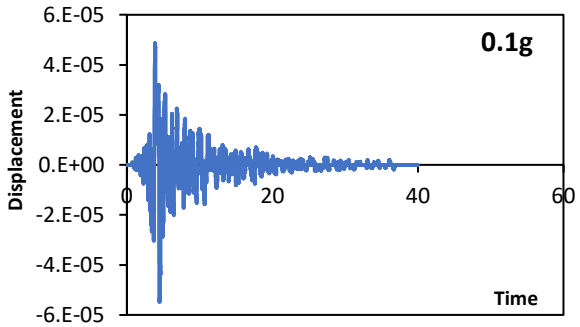

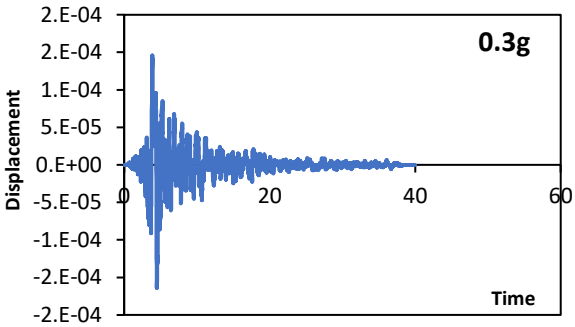

Loma Prieta-FF:

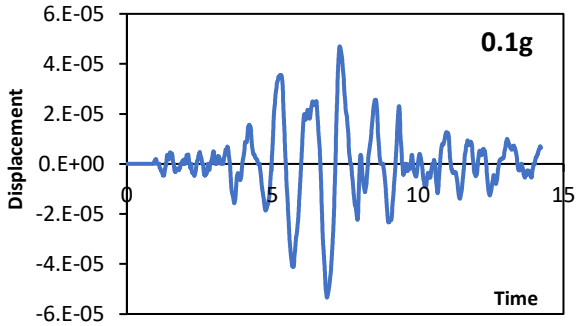

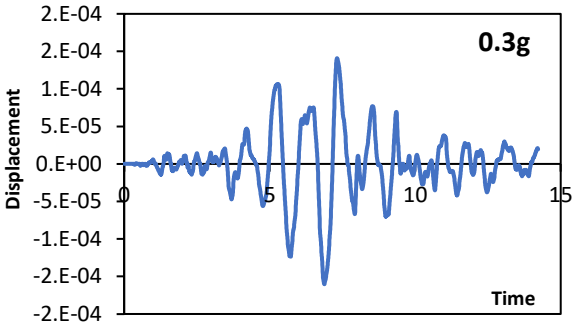

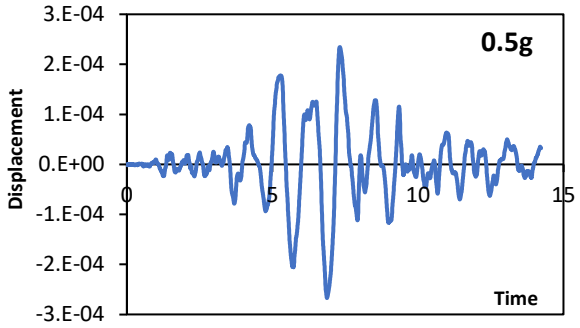

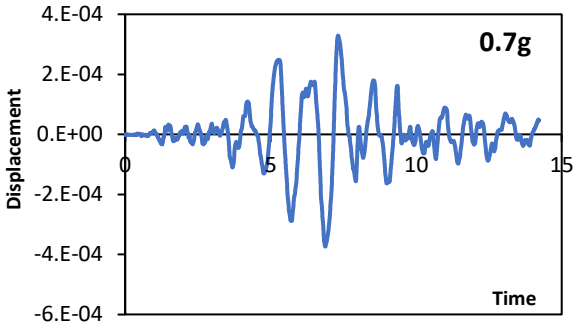

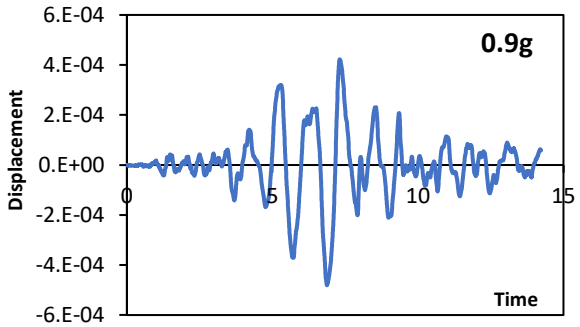

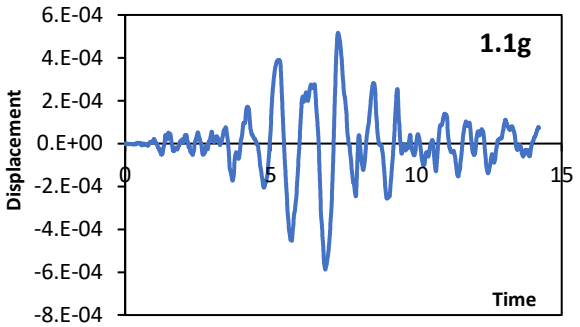

Montenegro-NF:

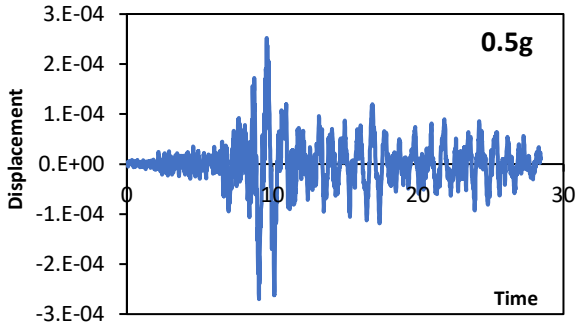

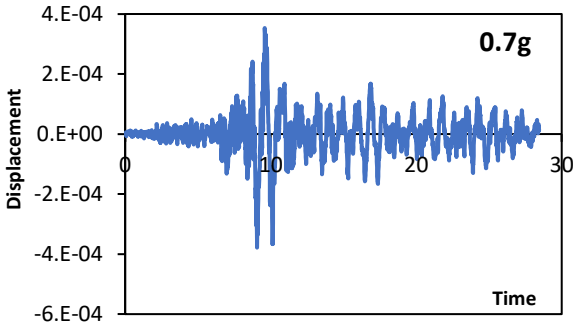

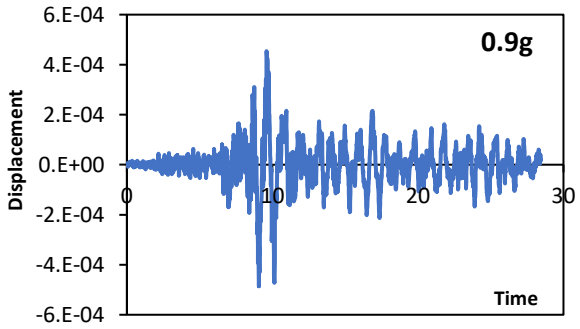

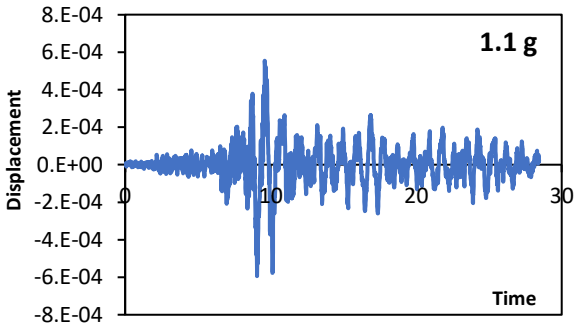

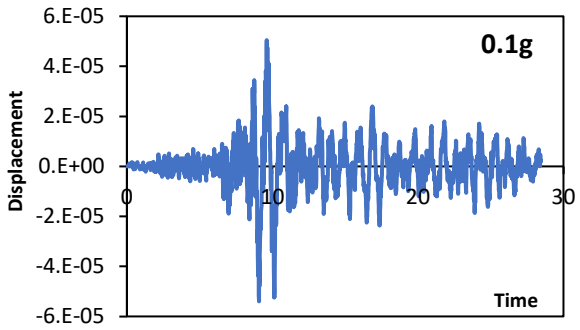

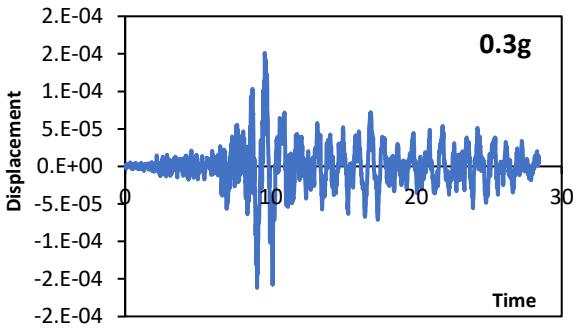

Montenegro-FF:

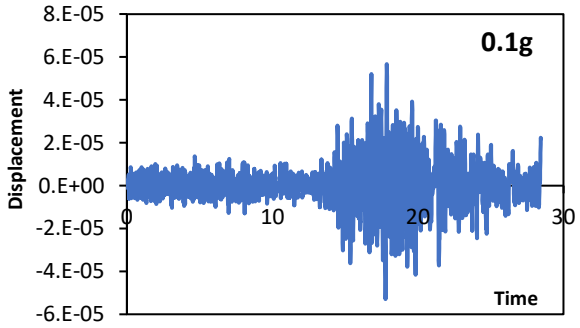

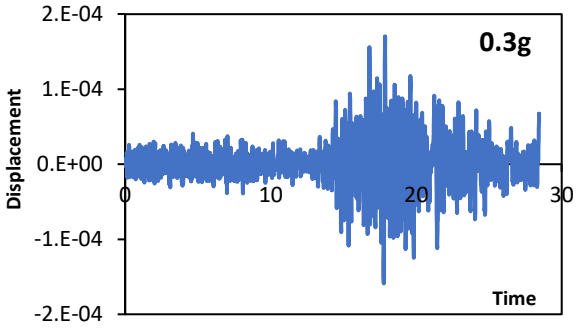

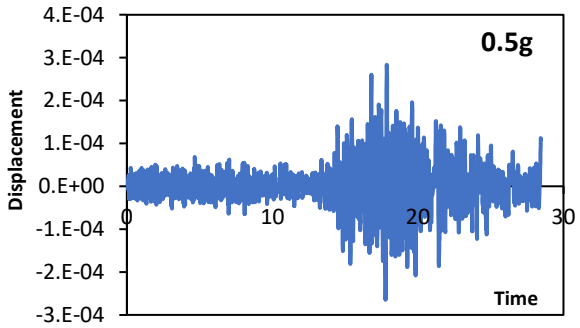

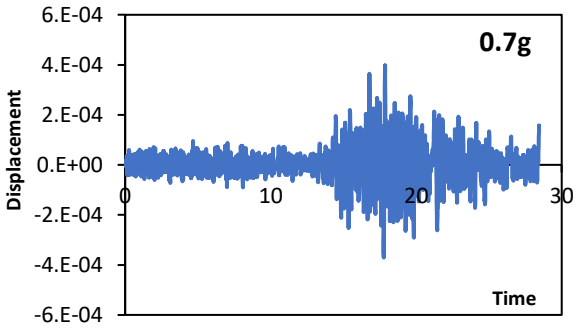

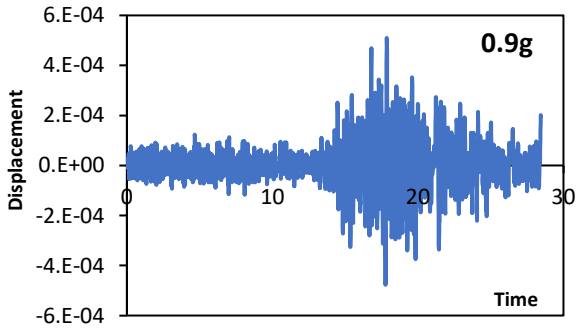

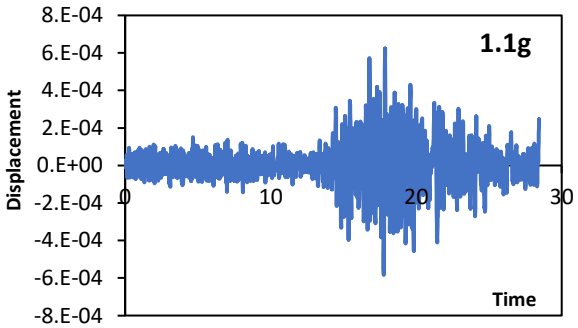

Niigata-FF:

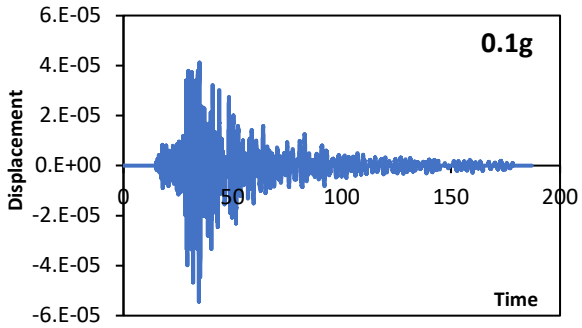

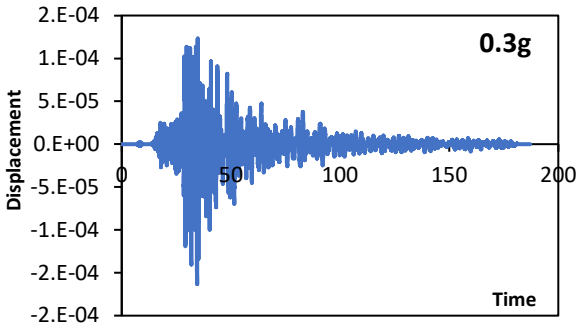

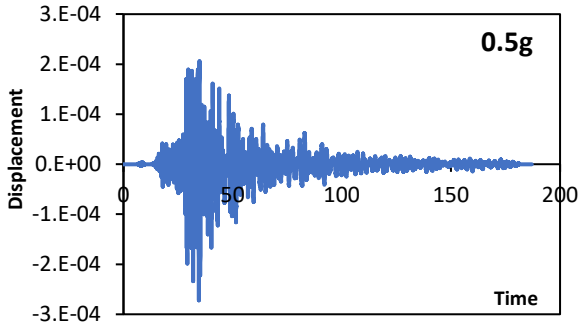

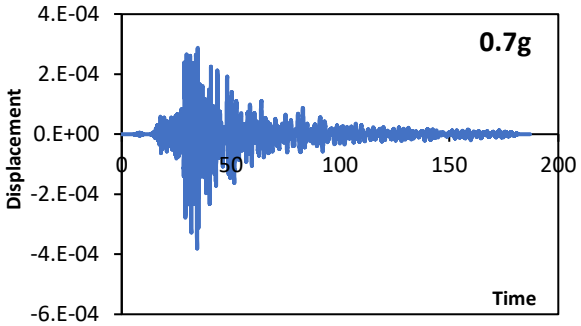

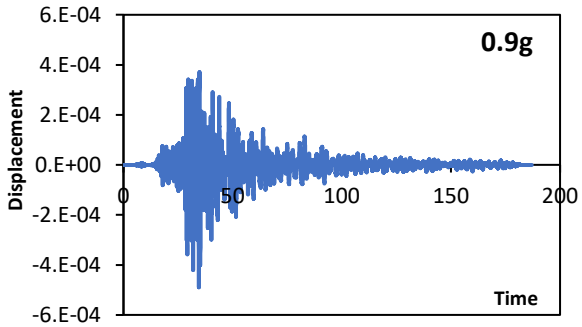

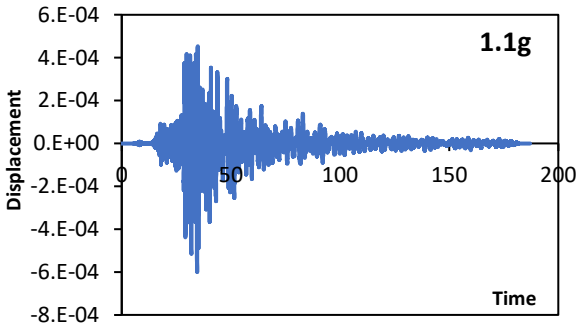

Northridge-NF:

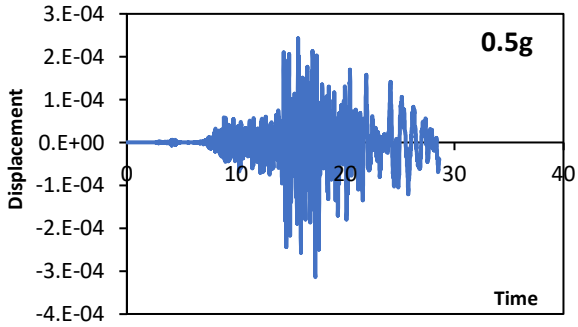

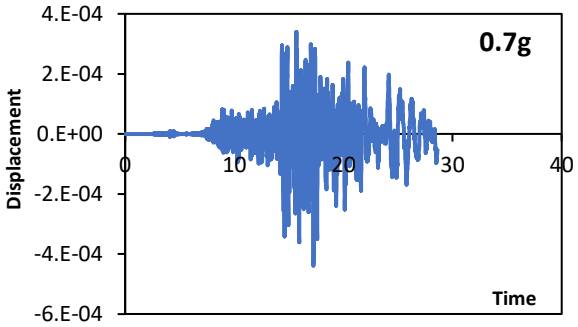

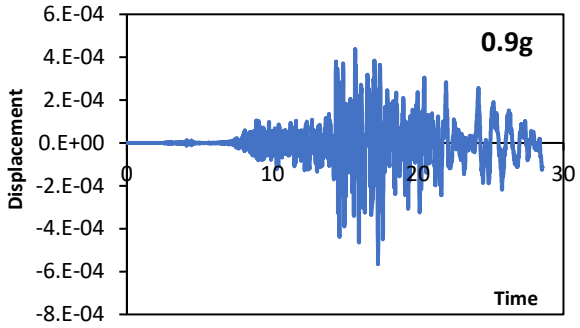

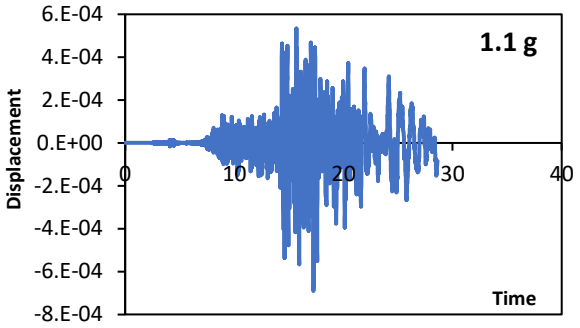

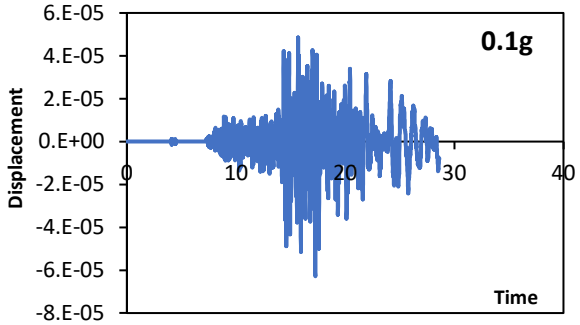

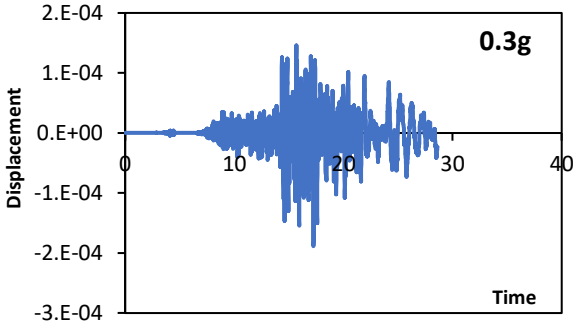

Northridge-FF:

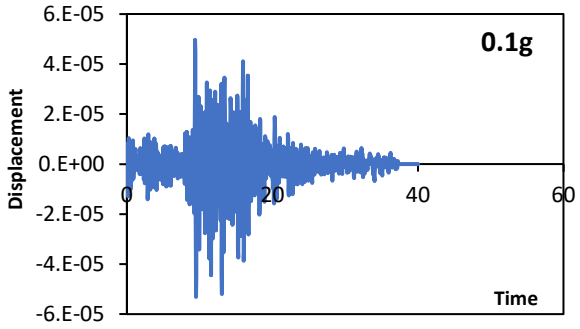

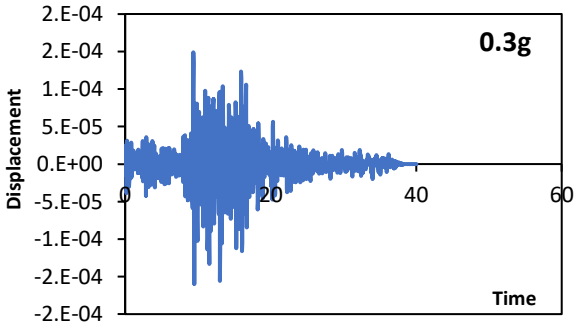

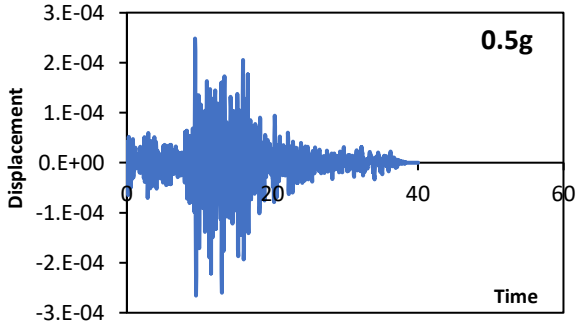

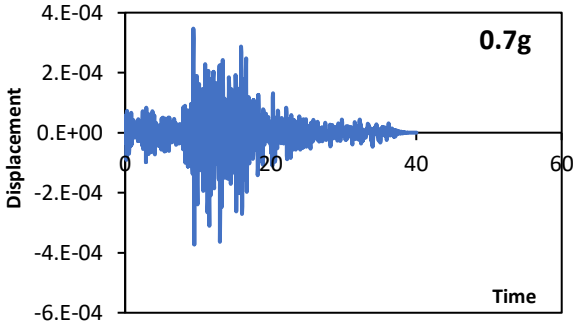

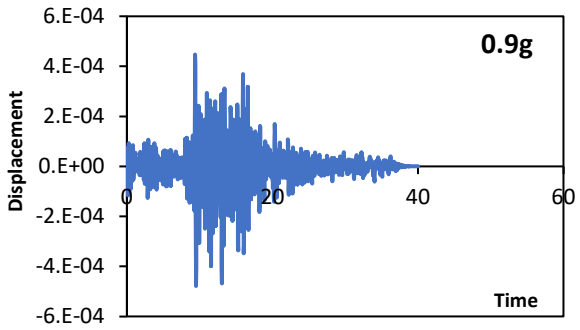

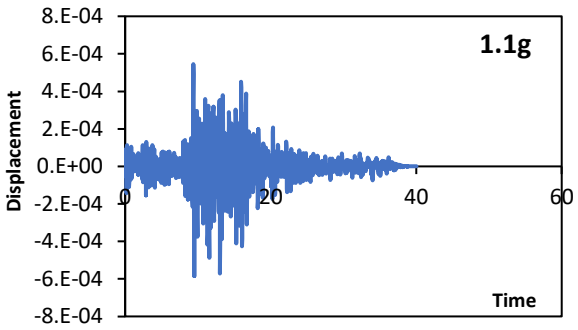

Parkfield-NF:

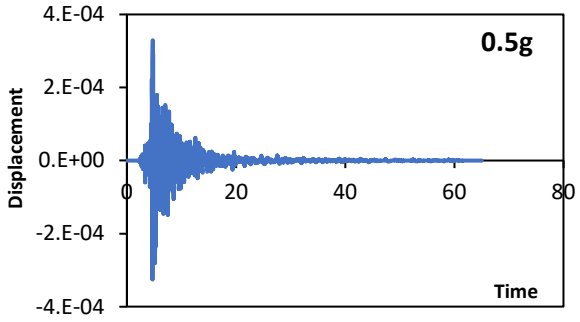

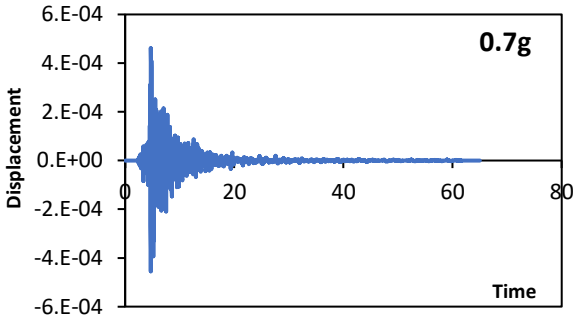

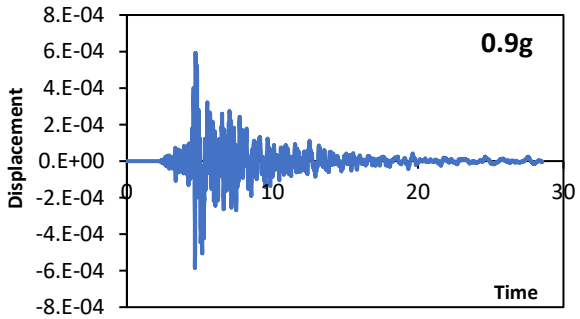

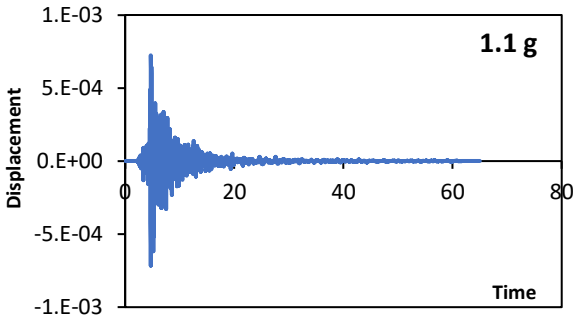

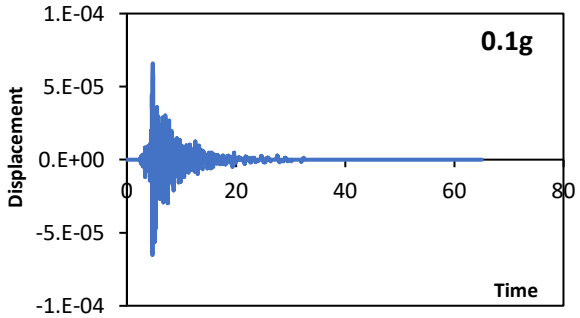

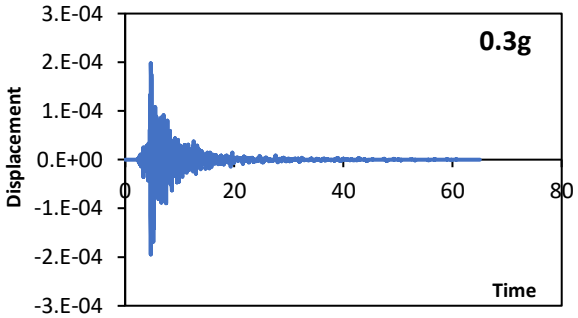

Parkfield-FF:

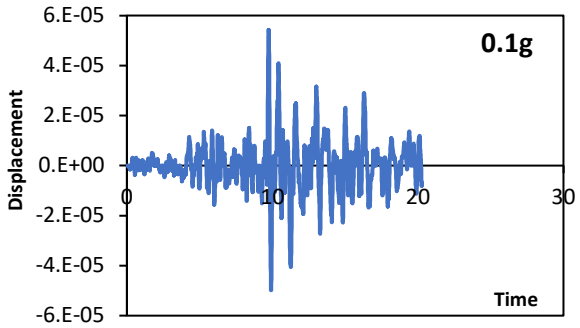

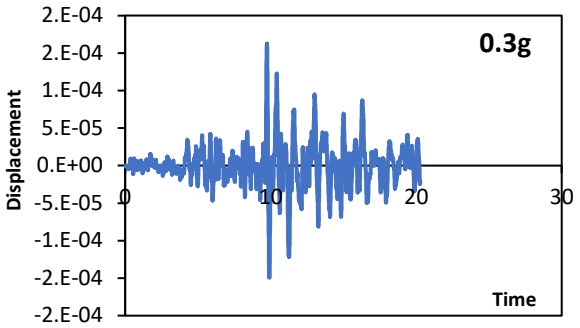

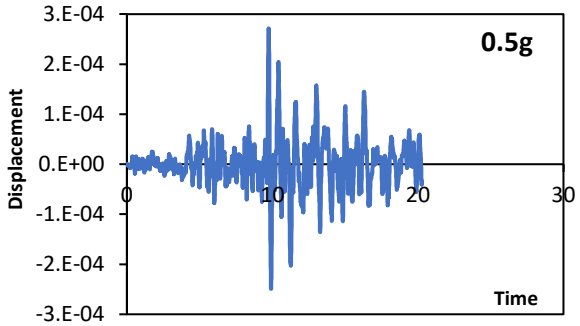

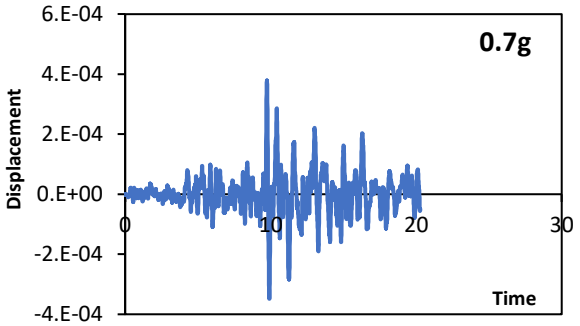

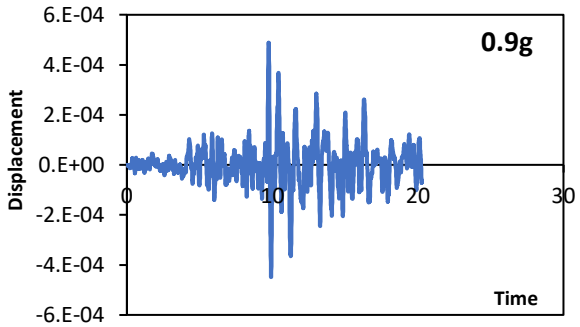

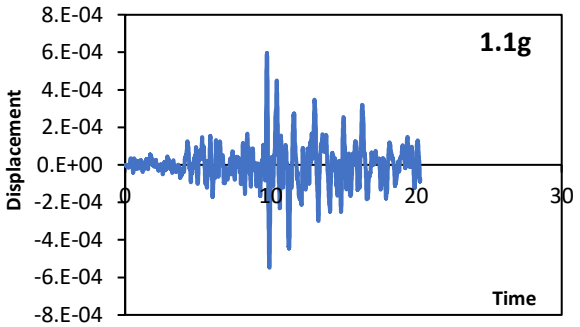

San Fernado-NF:

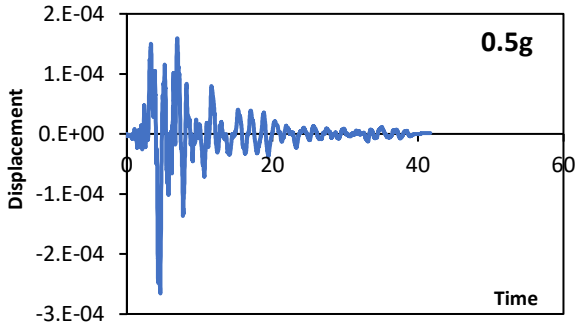

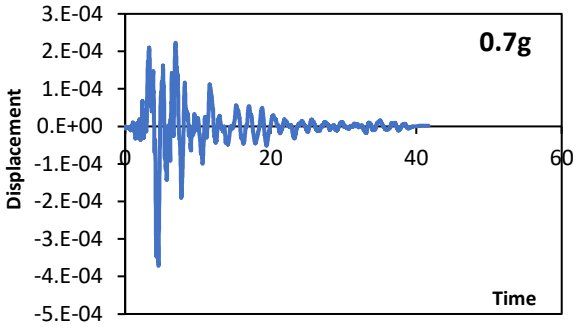

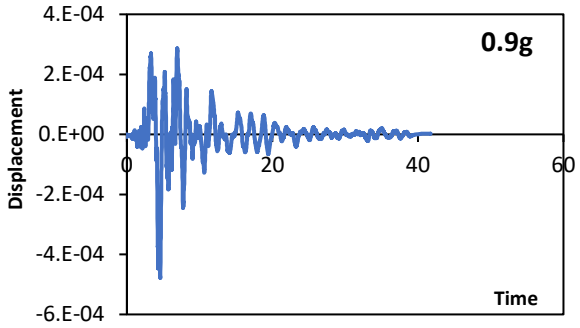

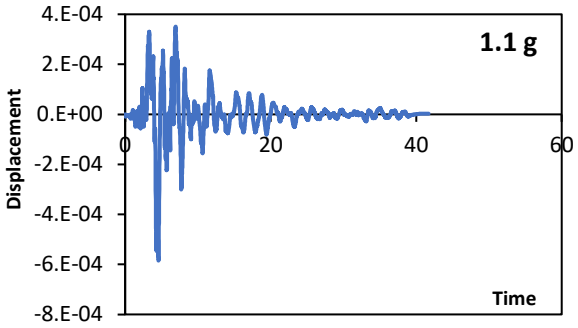

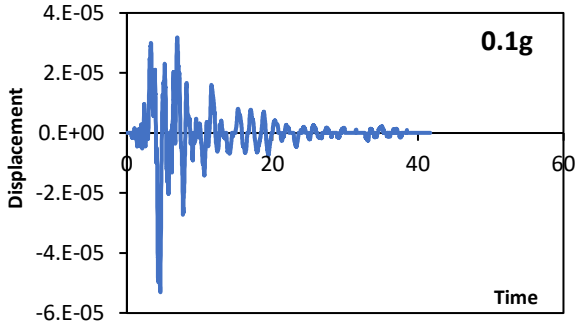

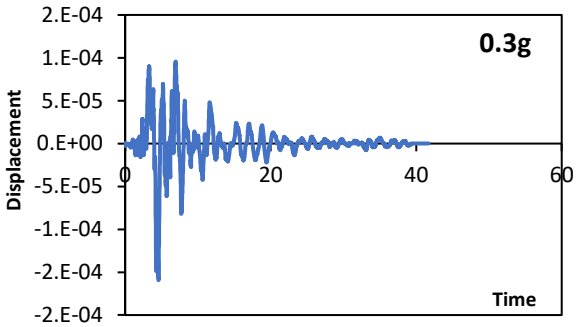

San Fernado-FF:

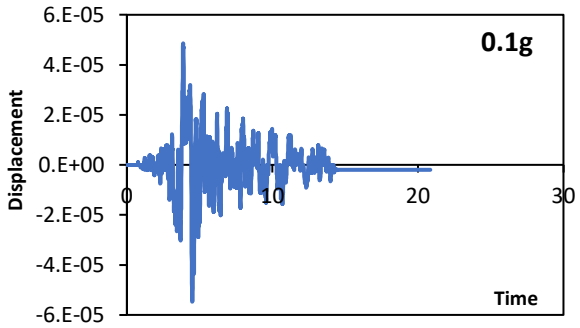

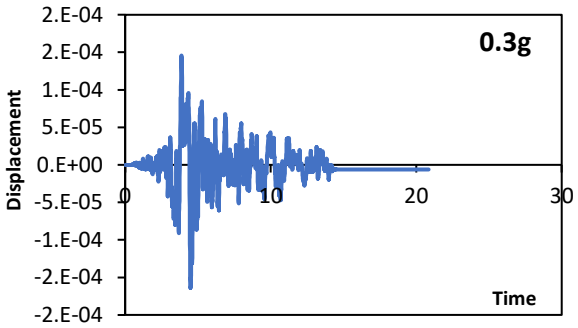

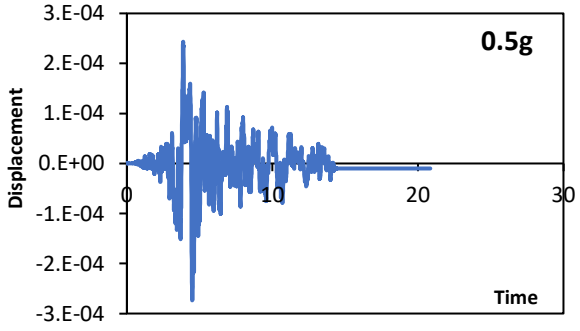

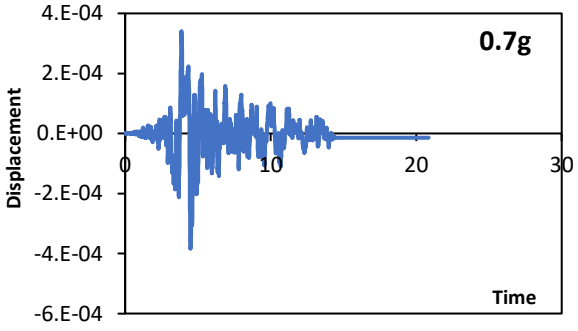

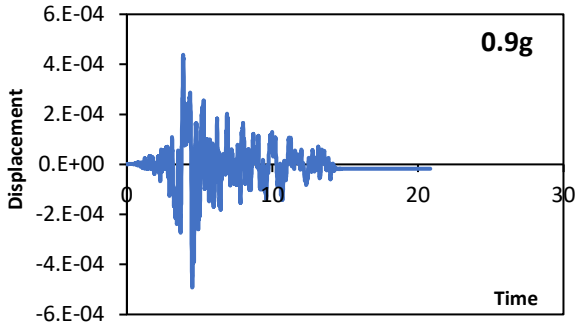

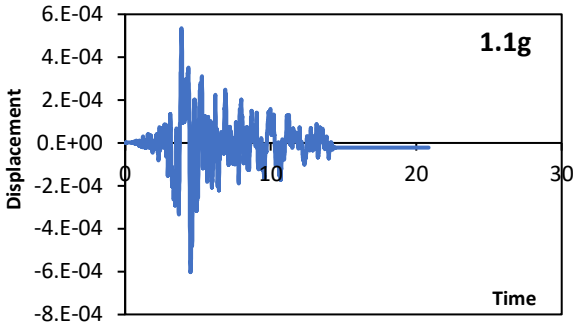

San Salvador-NF:

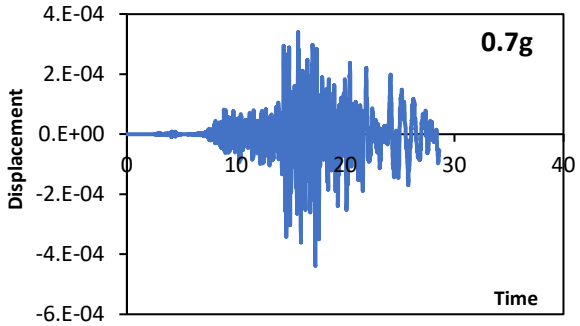

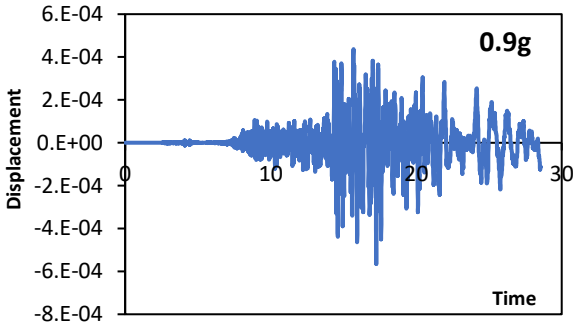

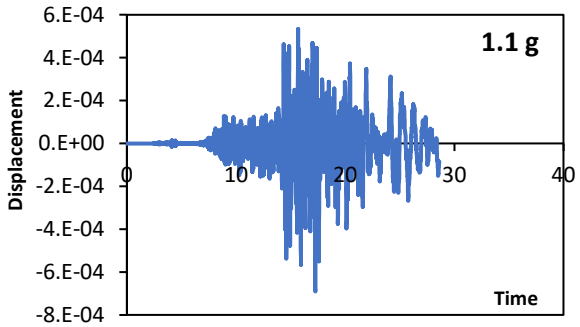

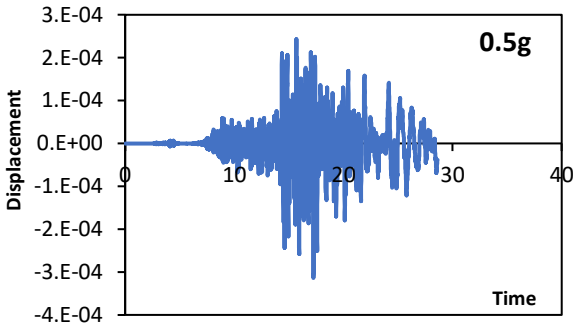

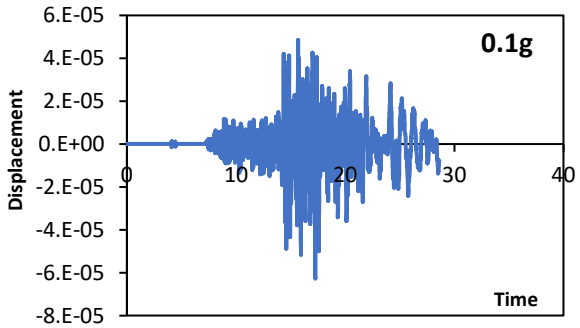

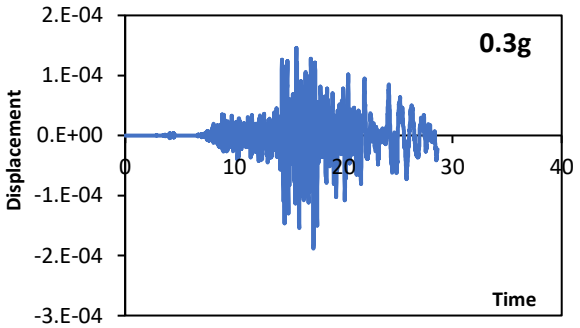

San Salvador-FF:

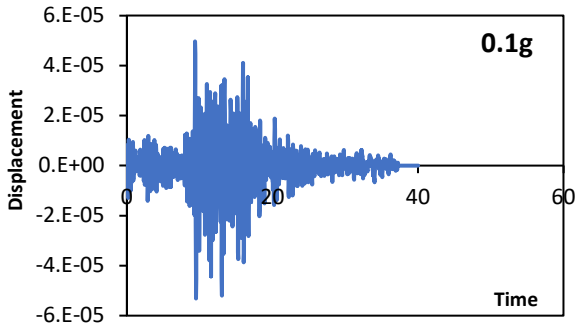

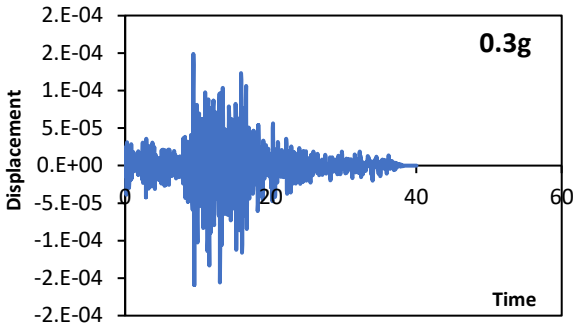

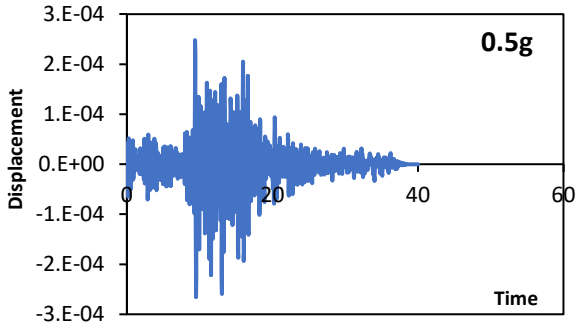

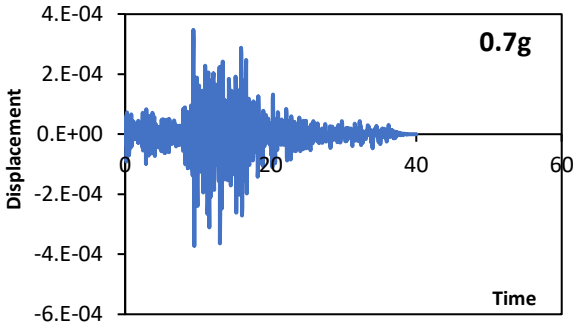

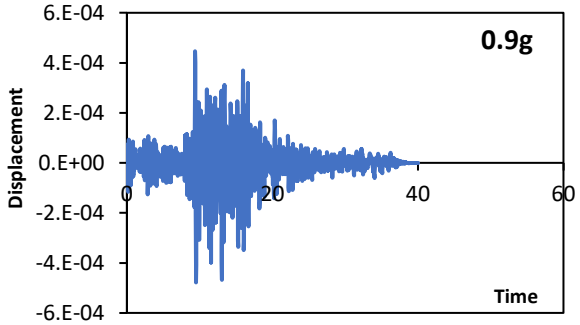

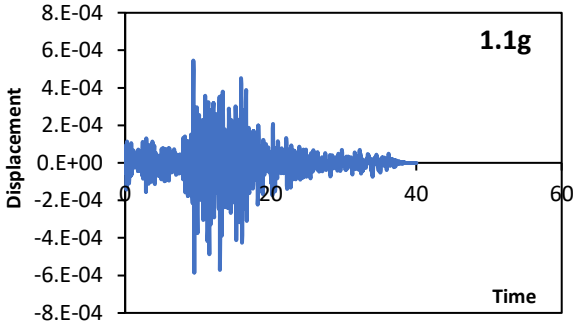

Superstition Hills-NF:

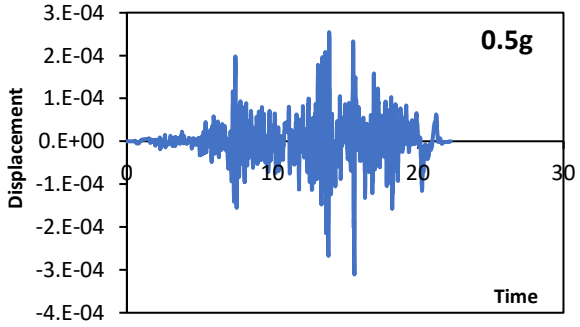

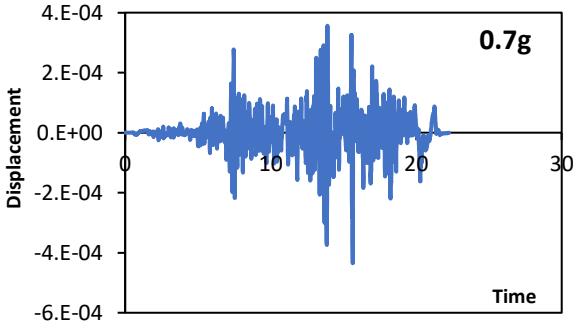

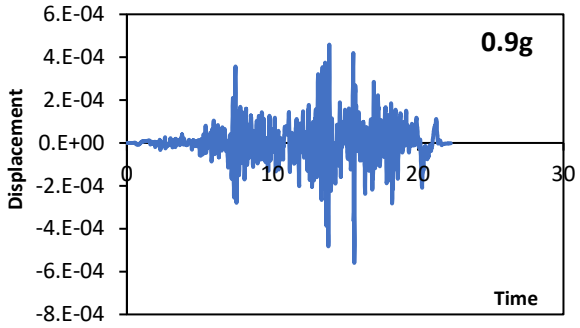

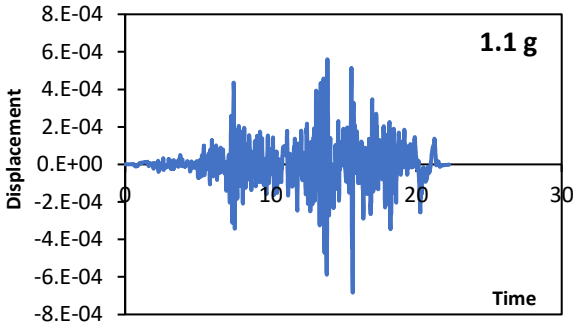

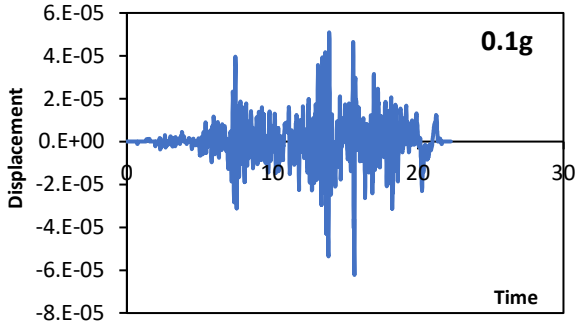

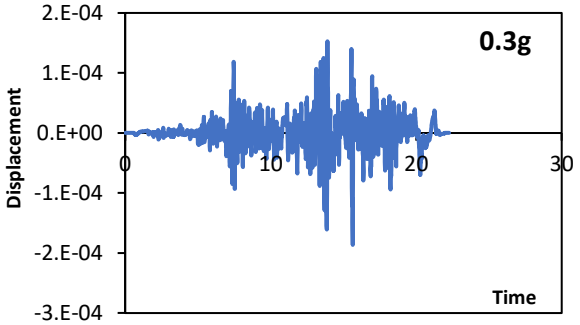

Superstition Hills-FF:

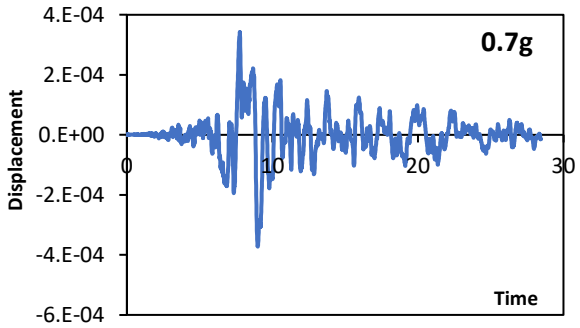

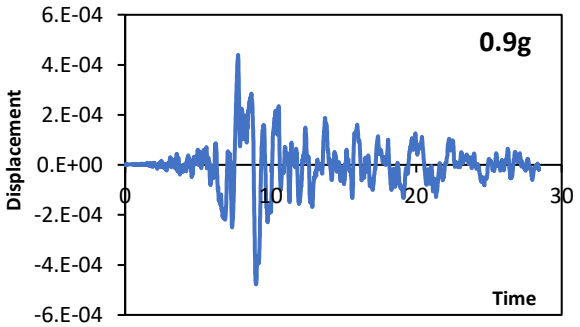

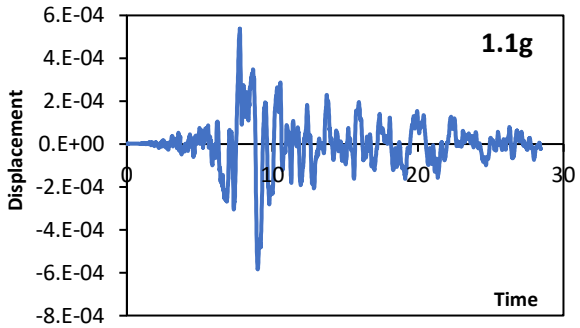

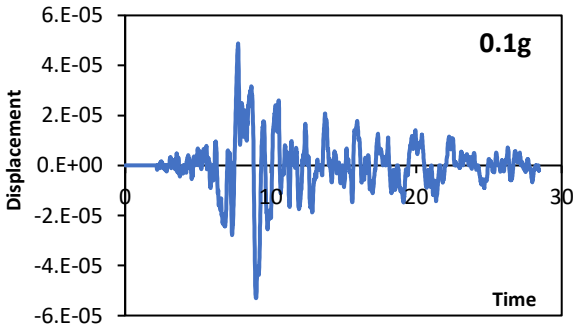

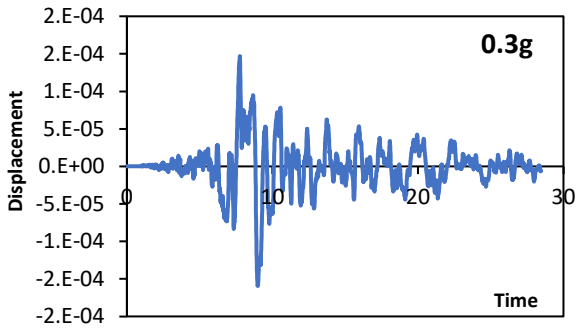
0.3g
Displacement
Time
2.E-04
2.E-04
1.E-04
5.E-05
0.E+00
-5.E-05
-1.E-04
-2.E-04
-2.E-04
0
10
20
30

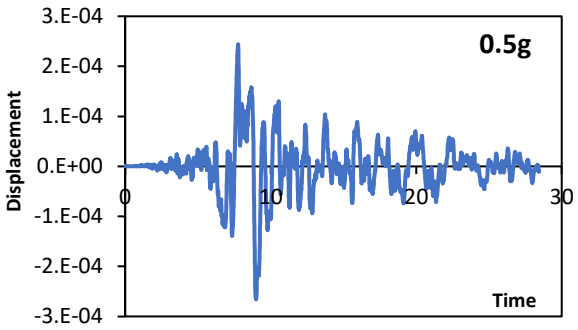
0.5g
Displacement
Time
3.E-04
2.E-04
1.E-04
0.E+00
-1.E-04
-2.E-04
-3.E-04
0
10
20
30

Tottori-NF:

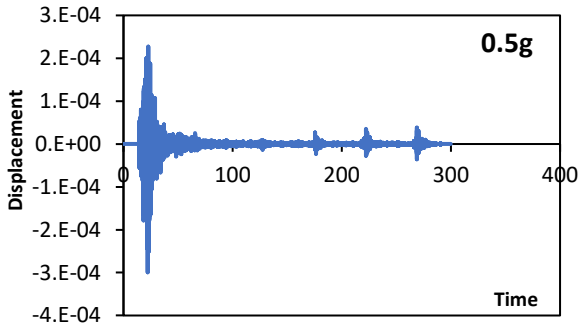
0.5g
Displacement
Time
3.E-04
2.E-04
1.E-04
0.E+00
-1.E-04
-2.E-04
-3.E-04
-4.E-04
0
100
200
300
400

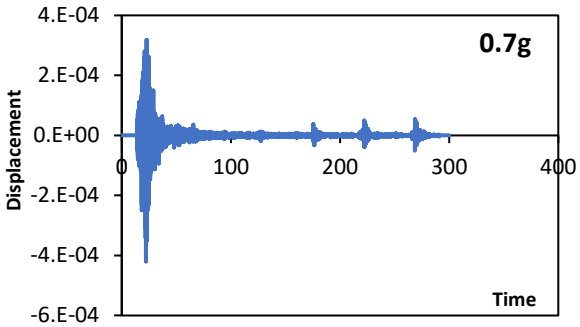
0.7g
Displacement
Time
4.E-04
2.E-04
0.E+00
-2.E-04
-4.E-04
-6.E-04
0
100
200
300
400

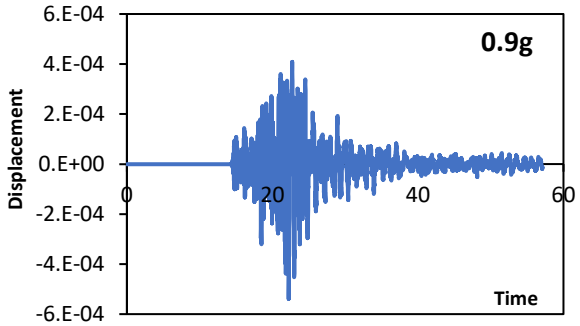
0.9g
Displacement
Time
6.E-04
4.E-04
2.E-04
0.E+00
-2.E-04
-4.E-04
-6.E-04
0
20
40
60

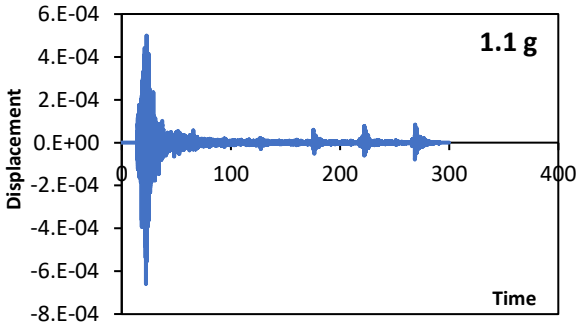
1.1 g
Displacement
Time
6.E-04
4.E-04
2.E-04
0.E+00
-2.E-04
-4.E-04
-6.E-04
-8.E-04
0
100
200
300
400

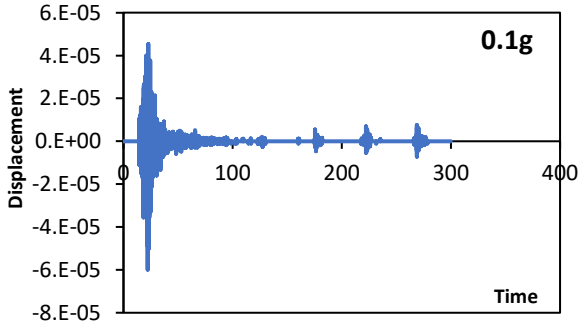
0.1g
Displacement
Time
6.E-05
4.E-05
2.E-05
0.E+00
-2.E-05
-4.E-05
-6.E-05
-8.E-05
0
100
200
300
400

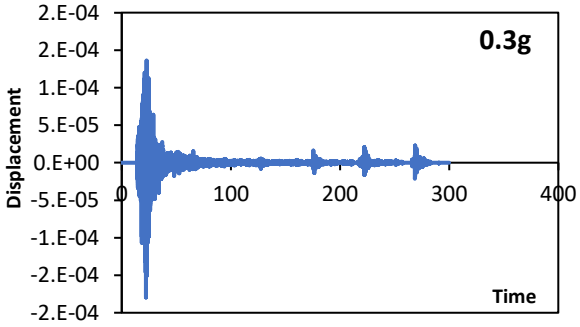
0.3g
Displacement
Time
2.E-04
2.E-04
1.E-04
5.E-05
0.E+00
-5.E-05
-1.E-04
-2.E-04
-2.E-04
0
100
200
300
400

Tottori-FF:

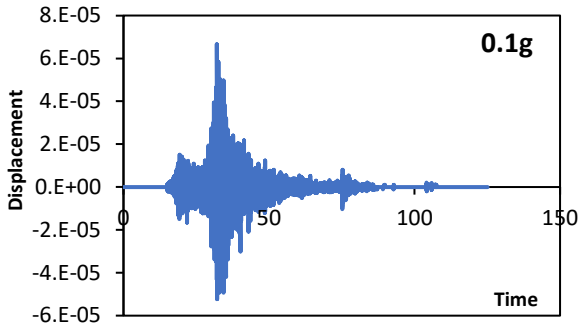

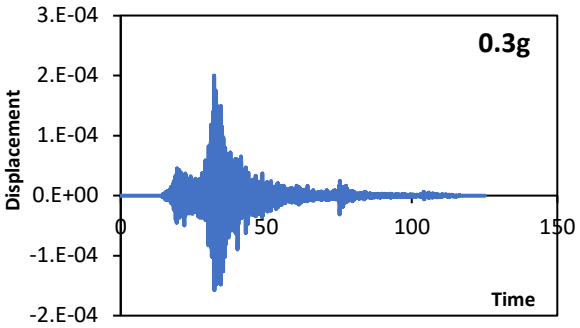

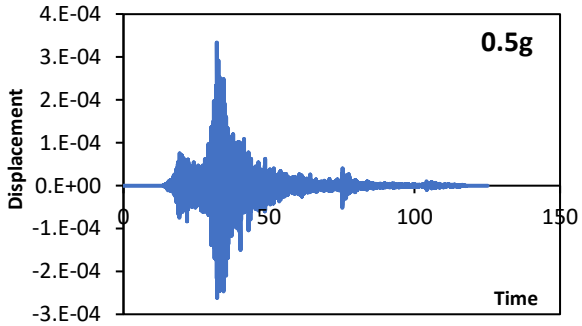

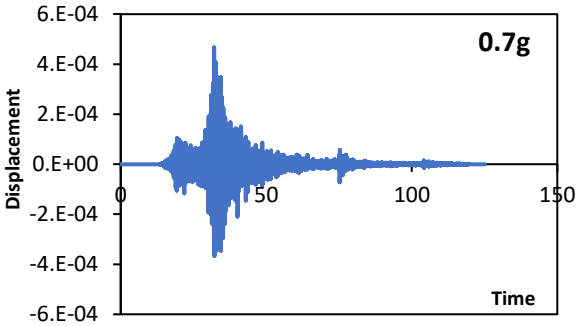

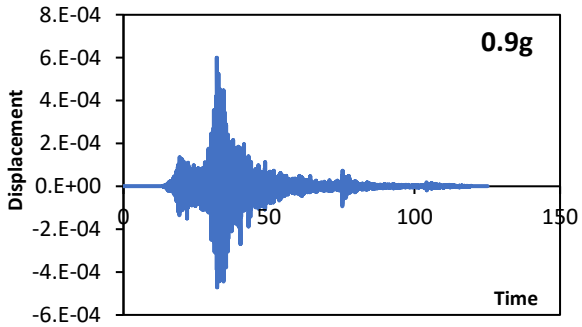

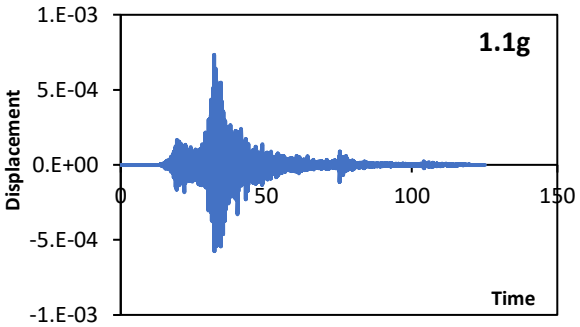

Westmorland-NF:

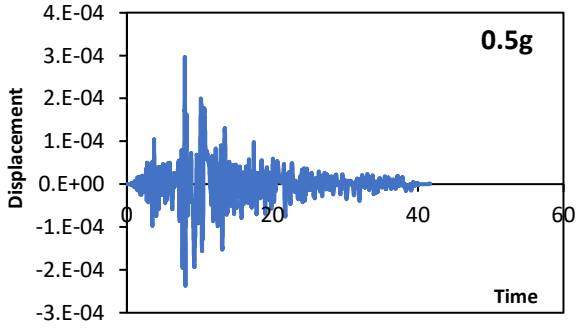

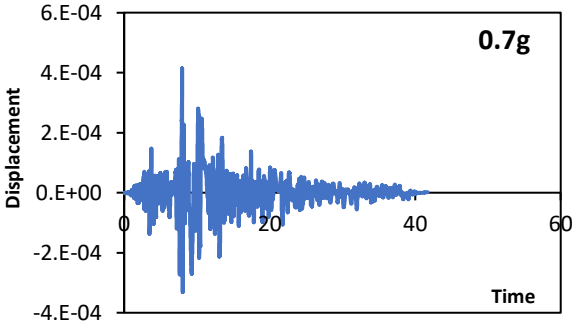

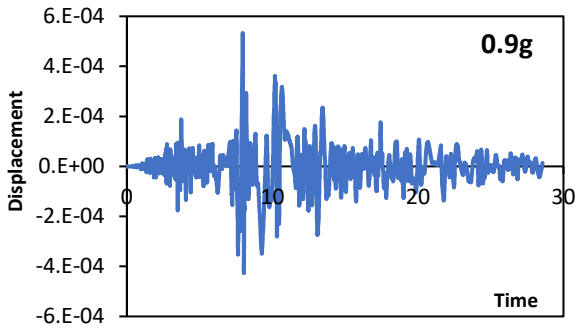

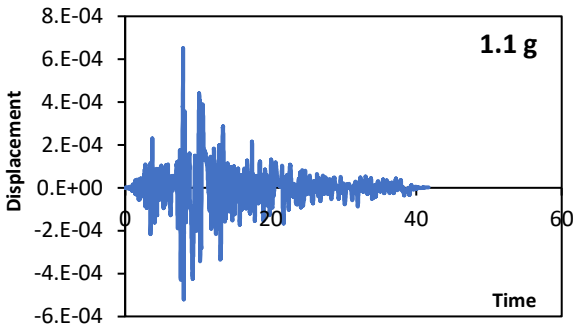

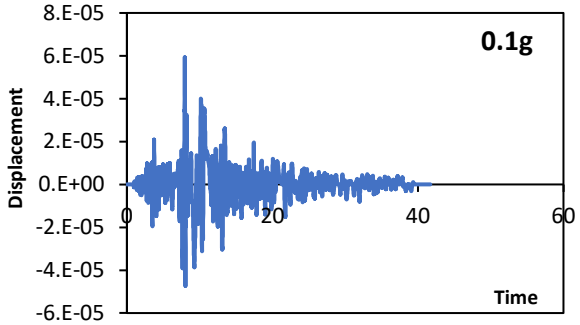

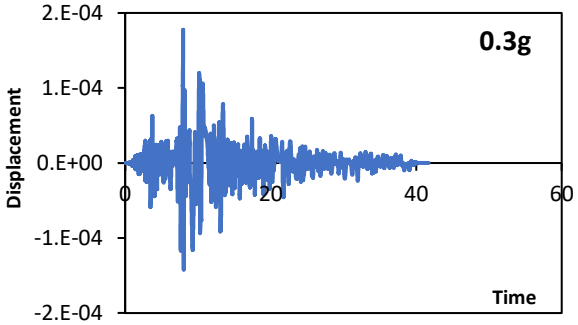

Westmorland-FF:

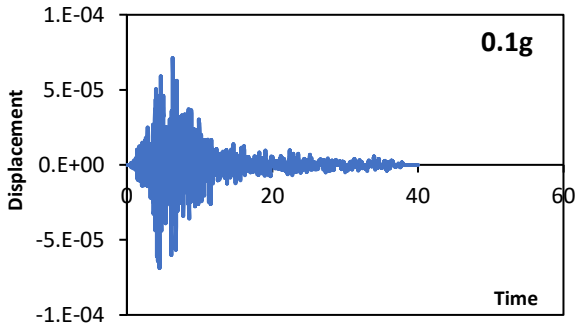

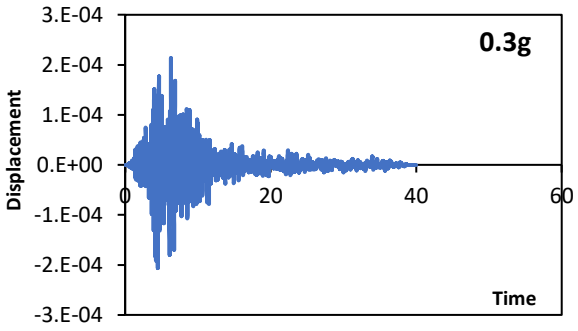

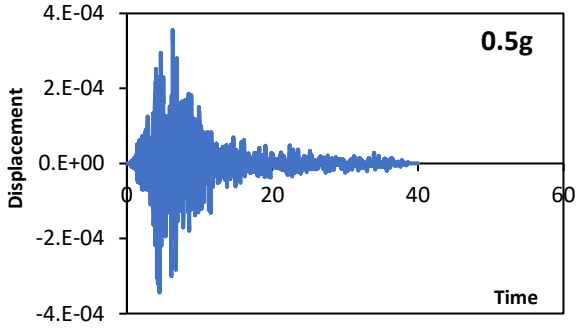

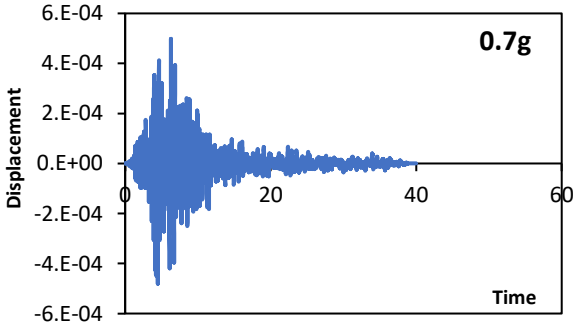

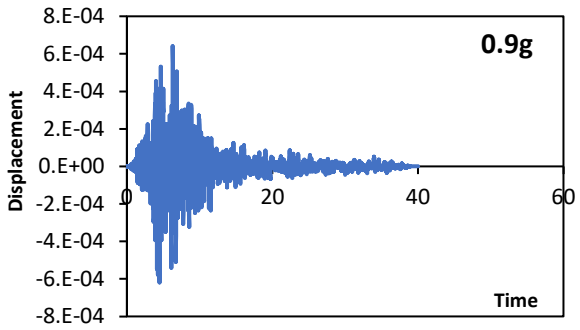

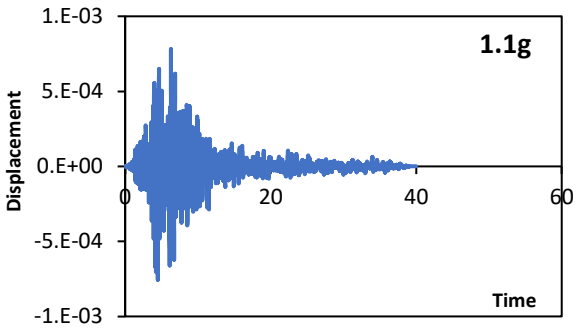

Potential Energy

Bam-NF

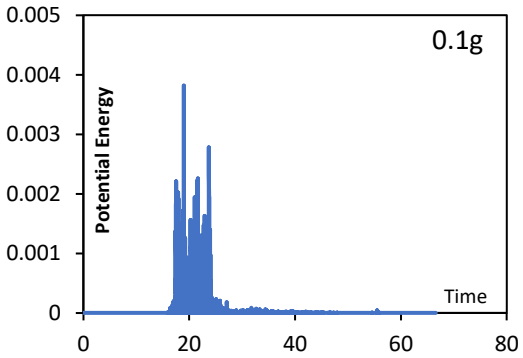

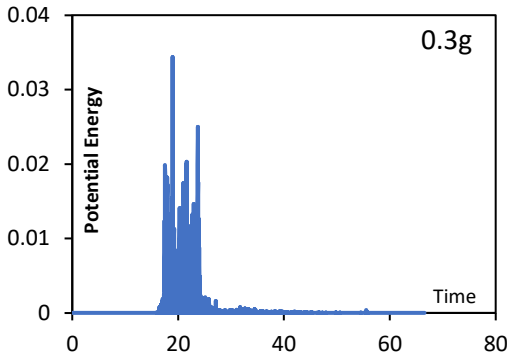

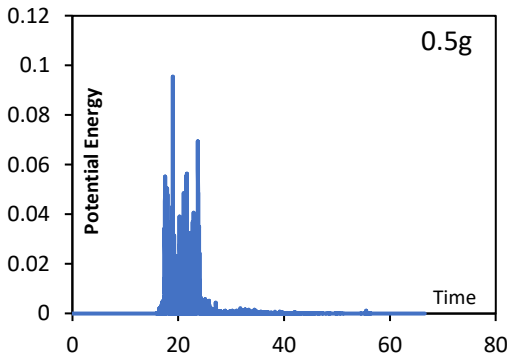

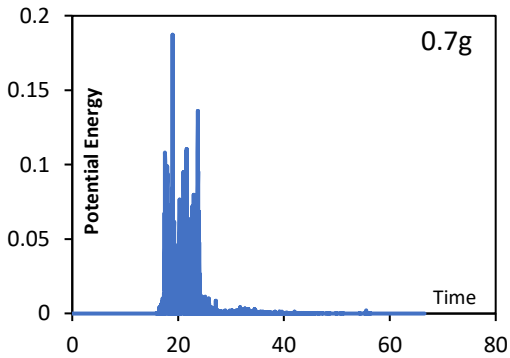

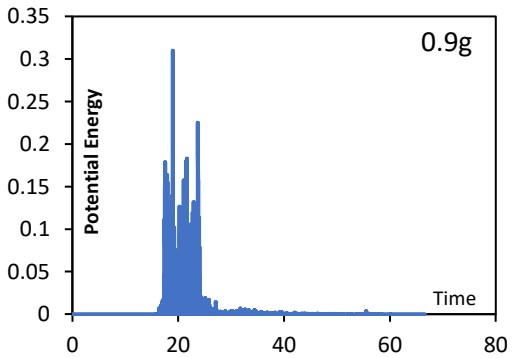

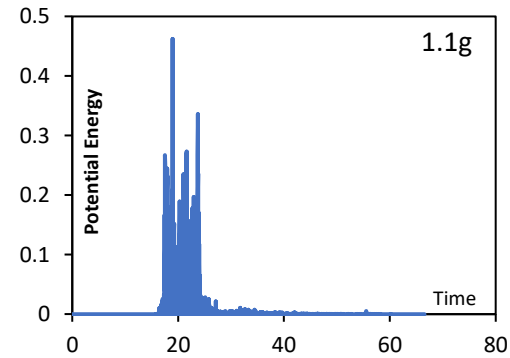

Bam-FF

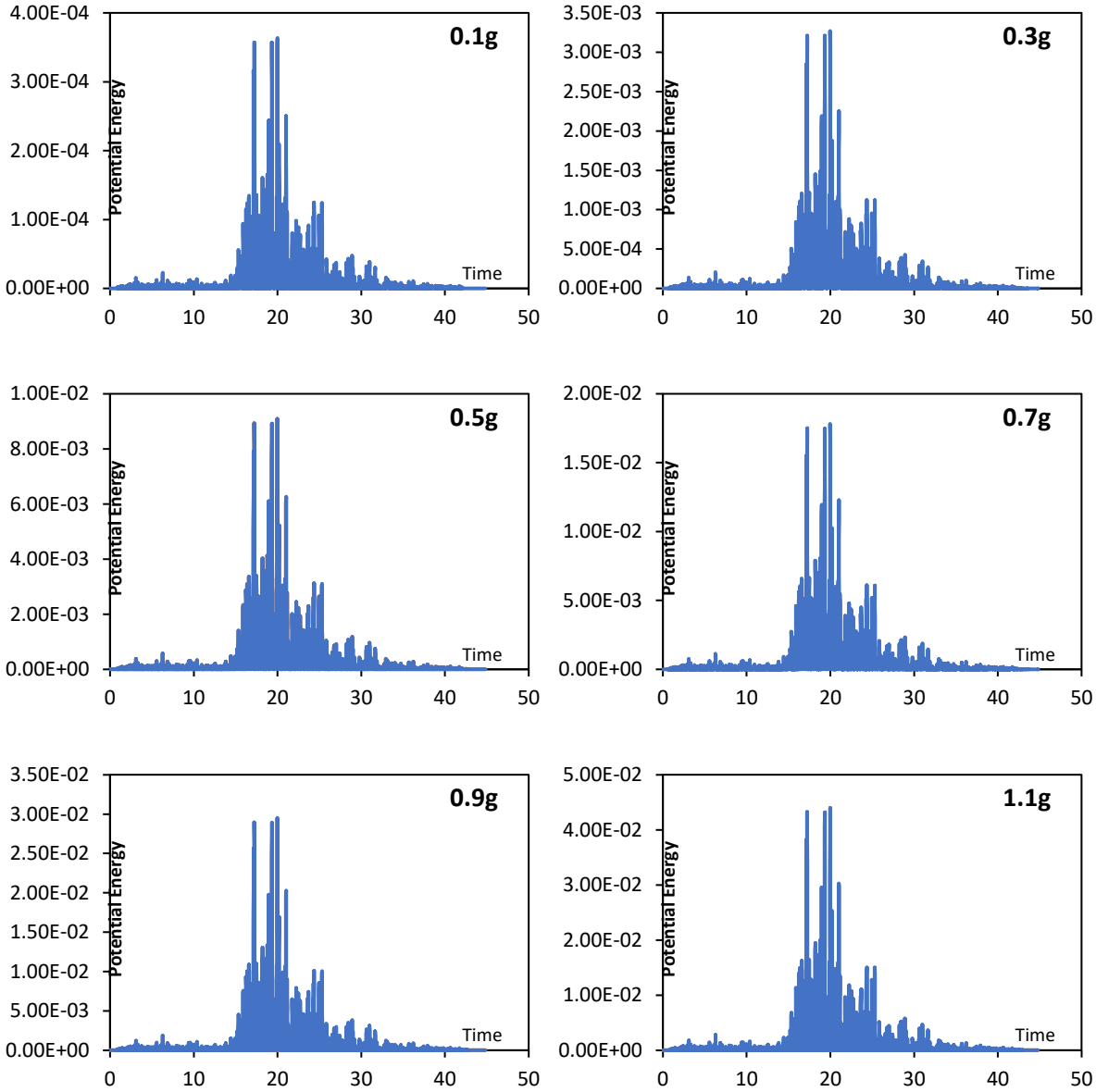

Cape Mendocino-NF

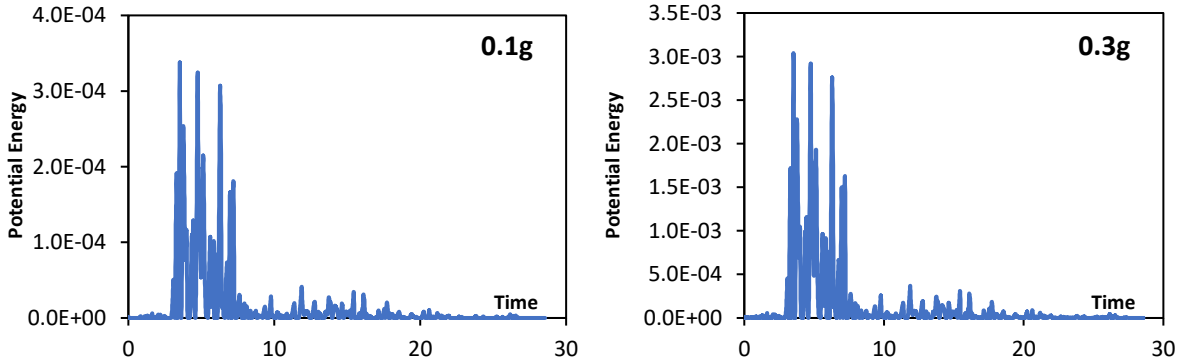

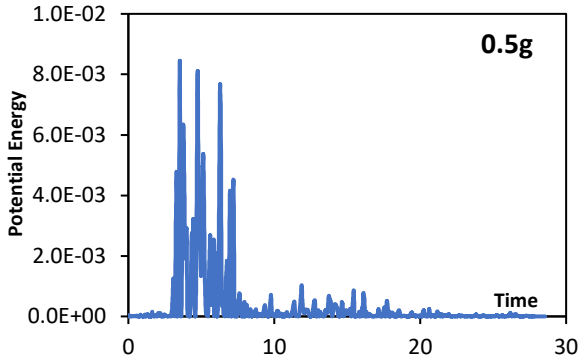

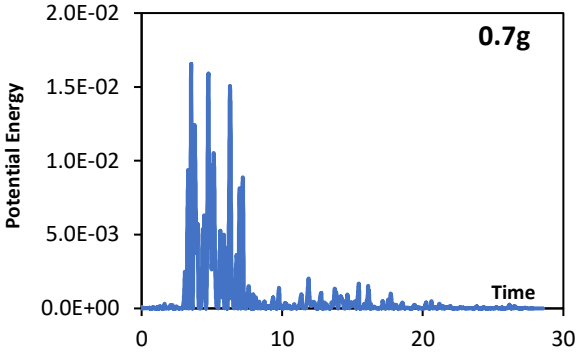

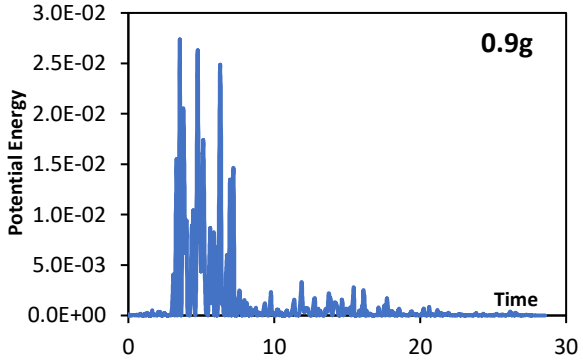

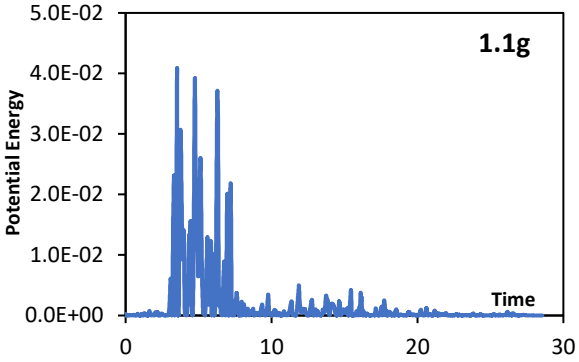

Cape Mendocino-NF

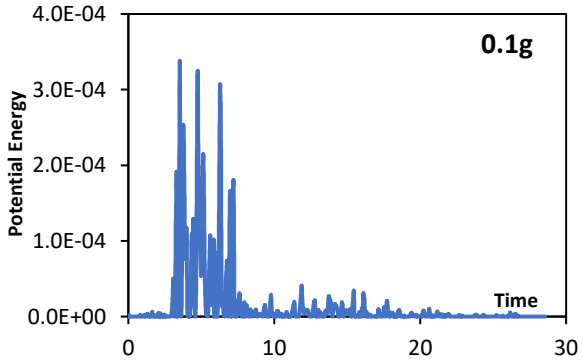

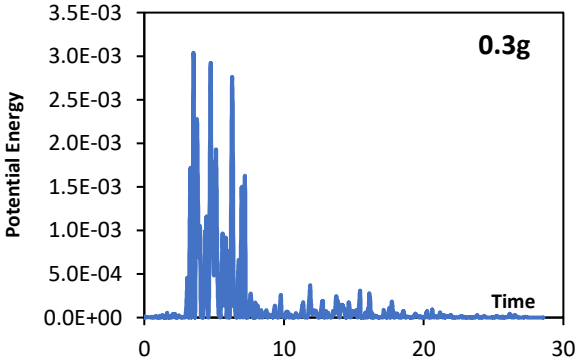

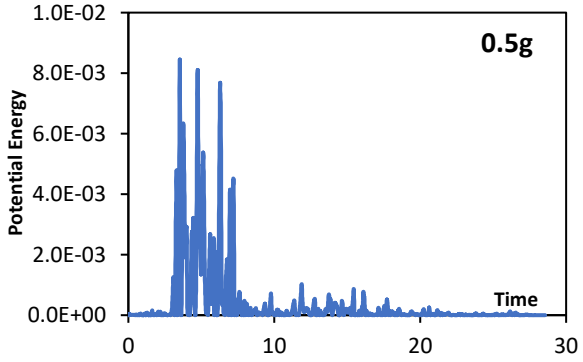

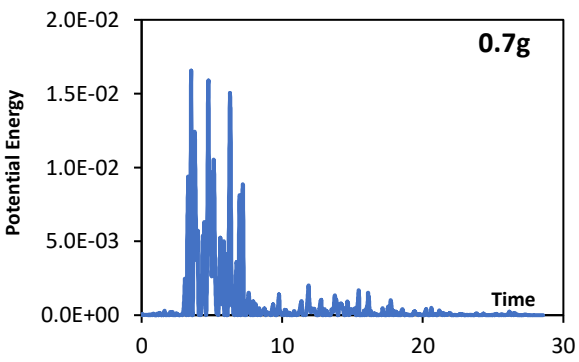

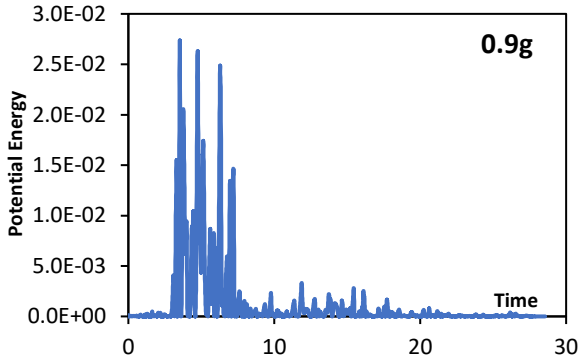

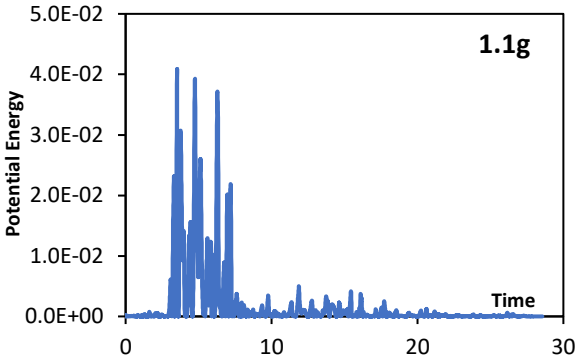

Cape Mendocino-FF

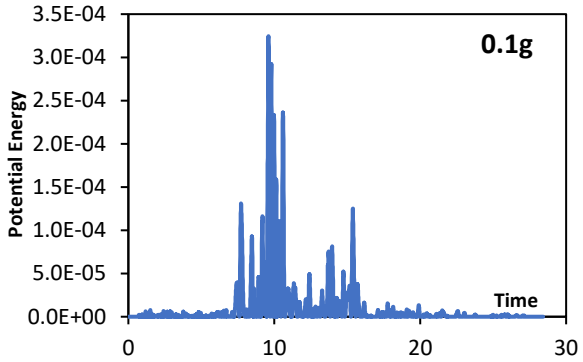

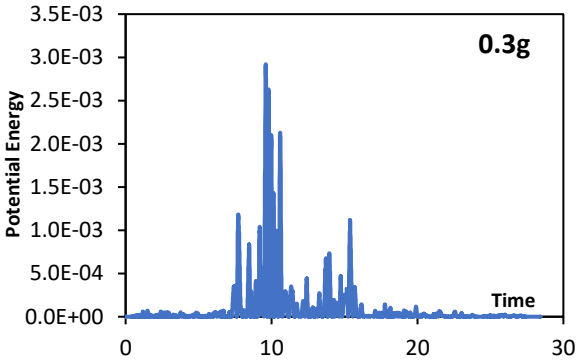

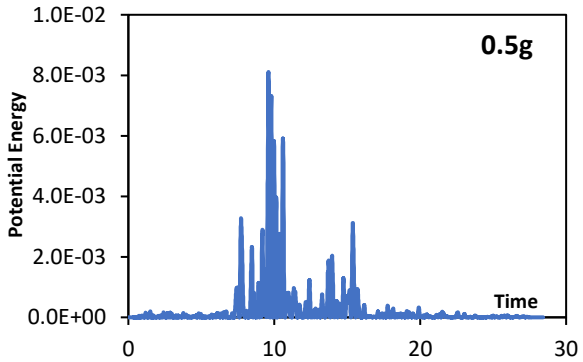

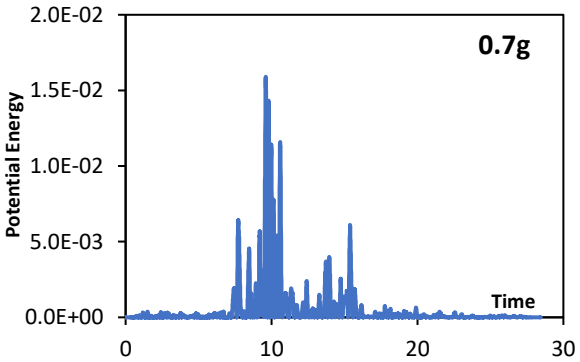

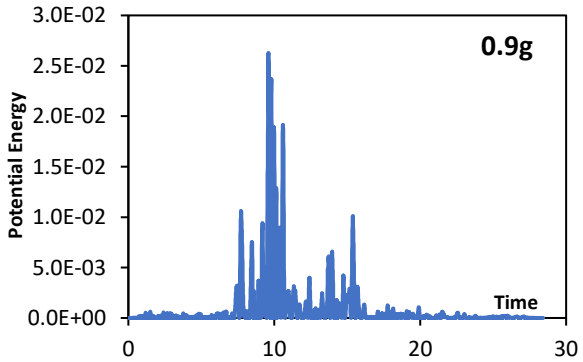

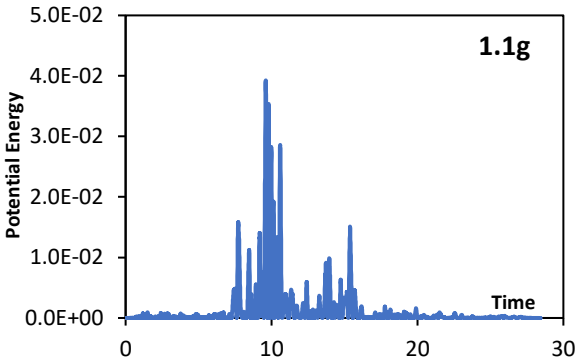

Christchurch-NF

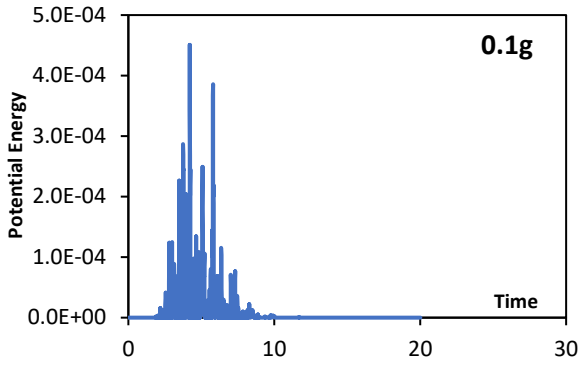

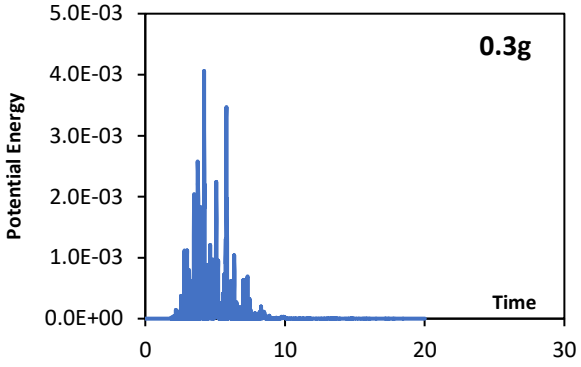

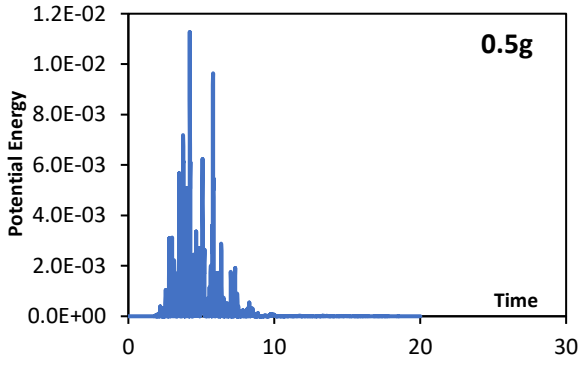

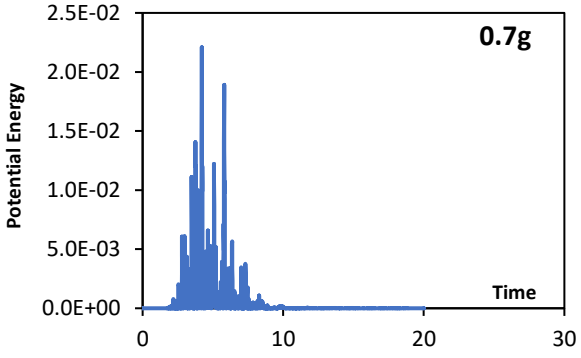

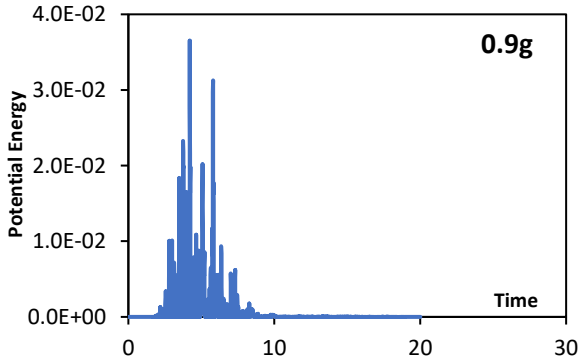

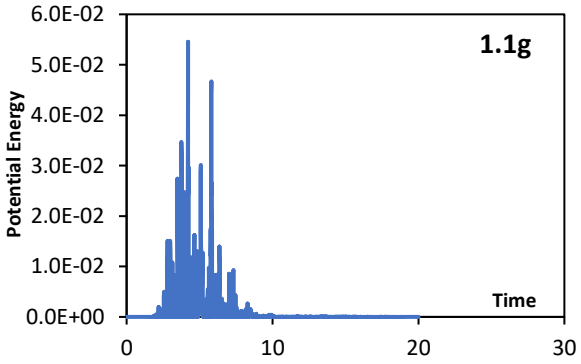

Christchurch-FF

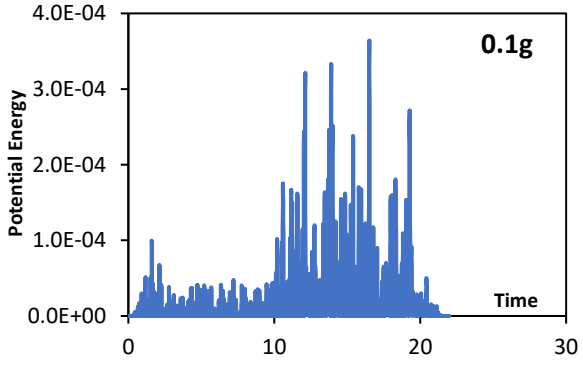

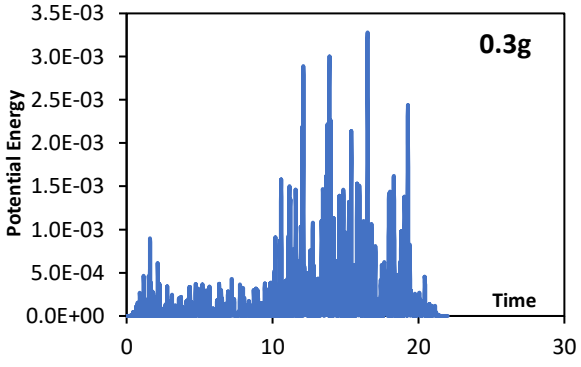

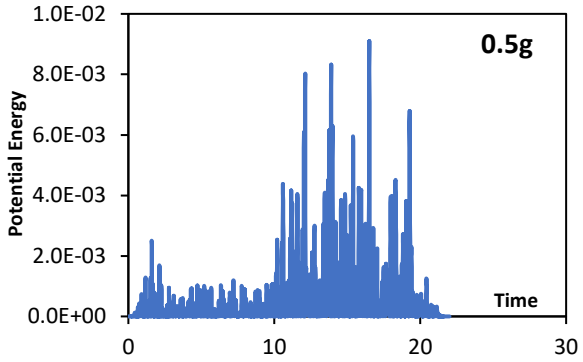

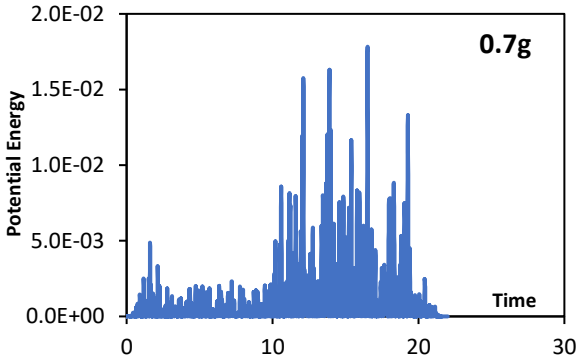

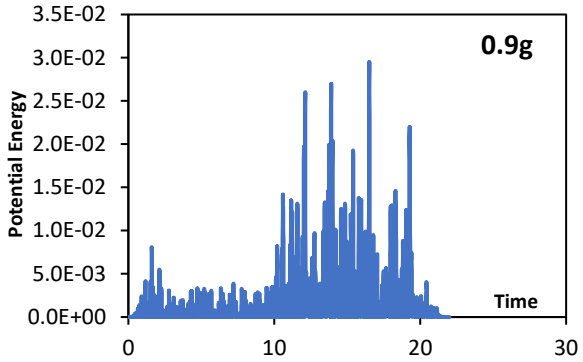

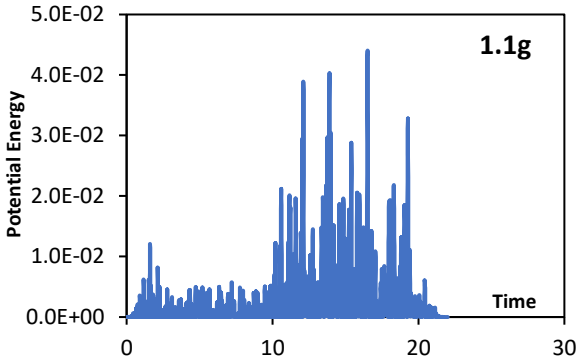

Chetsu-oki-NF

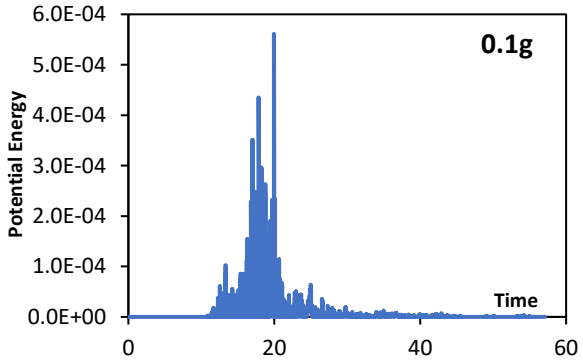

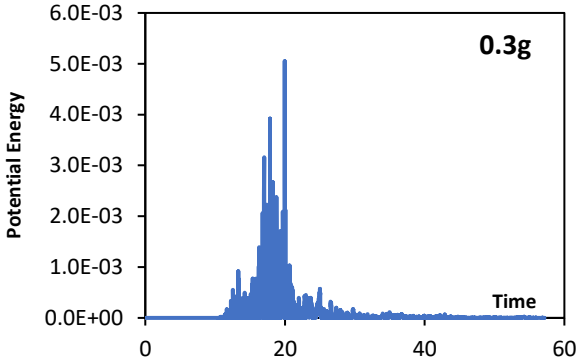

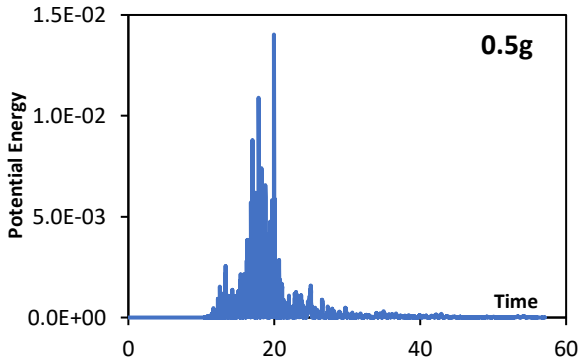

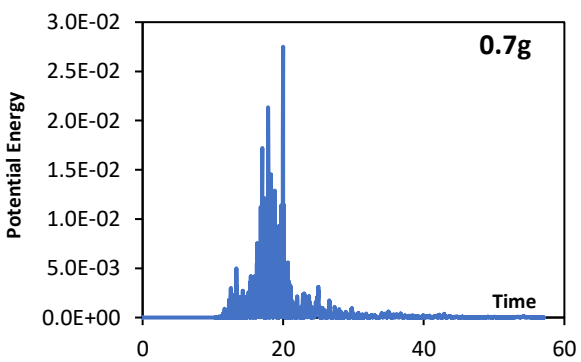

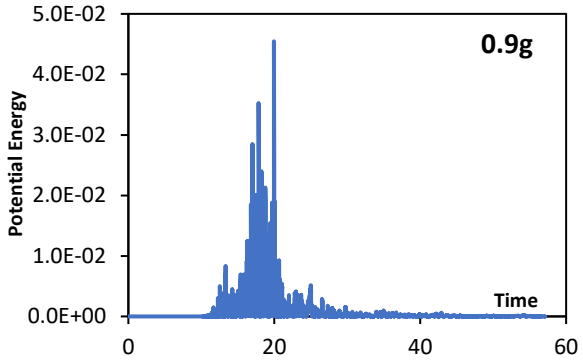

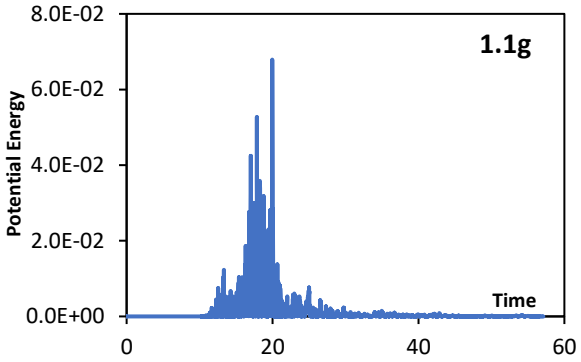

Chetsu-oki-FF

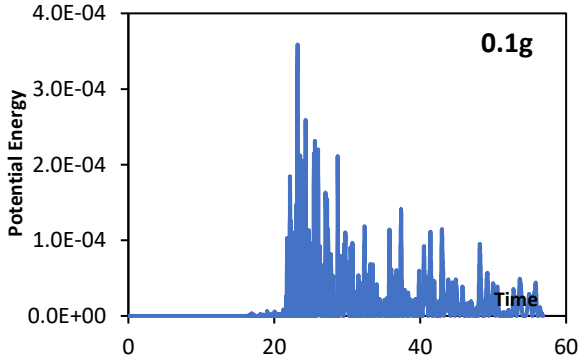

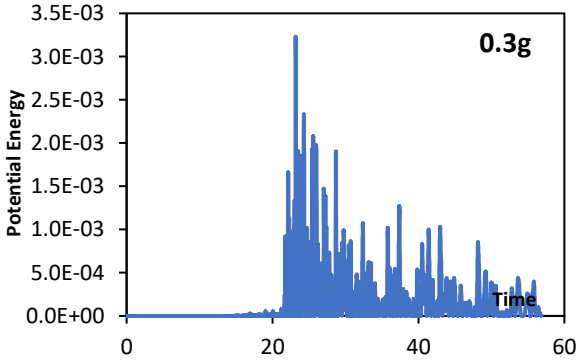

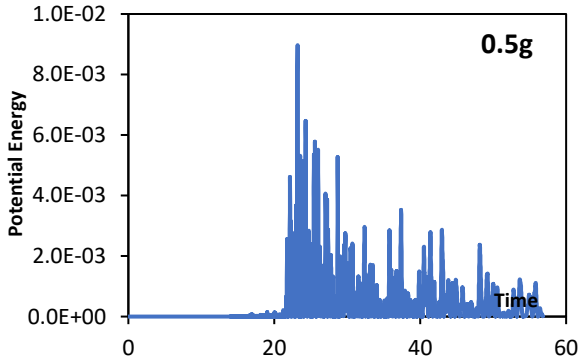

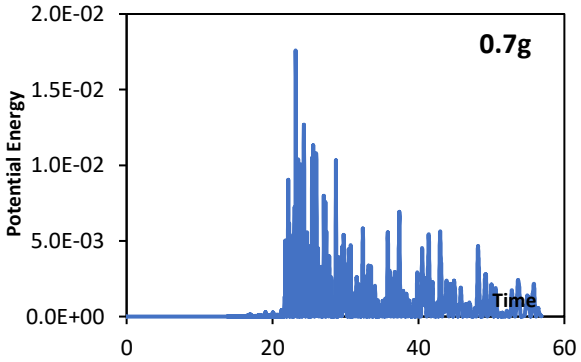

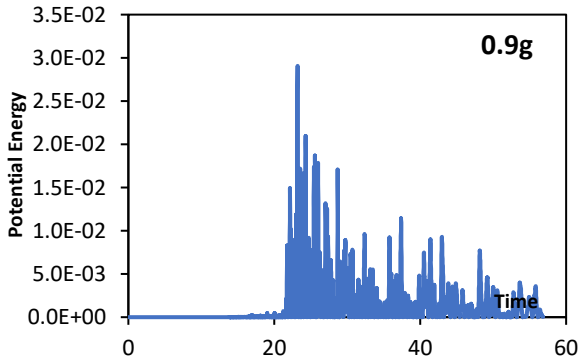

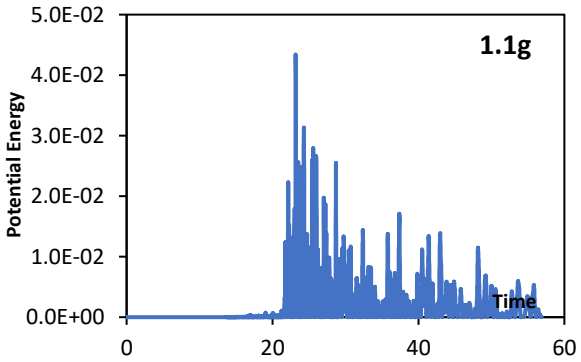

Imperial Valley-NF

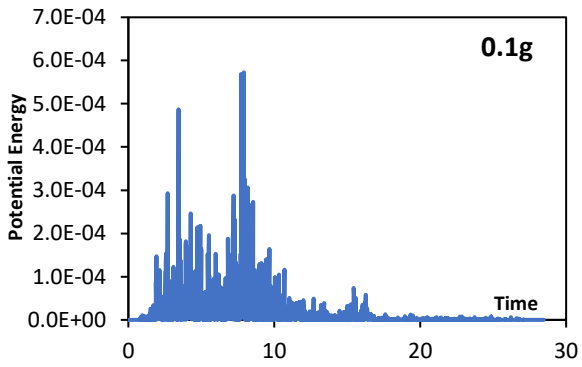

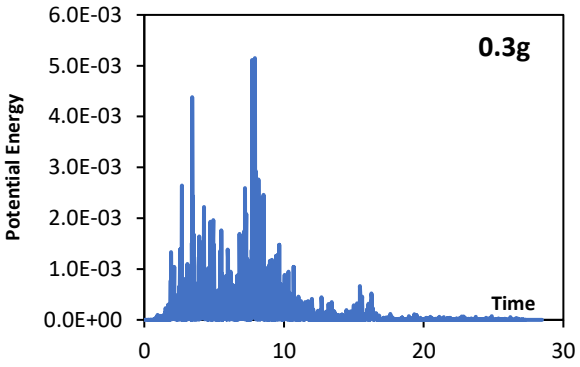

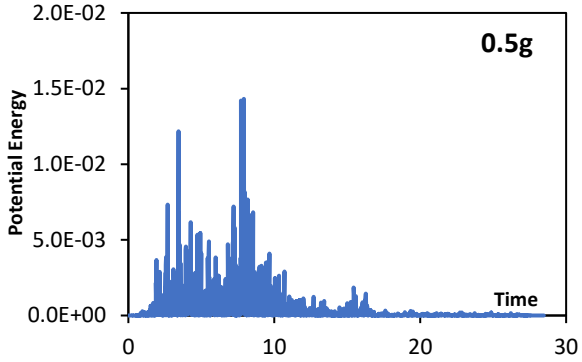

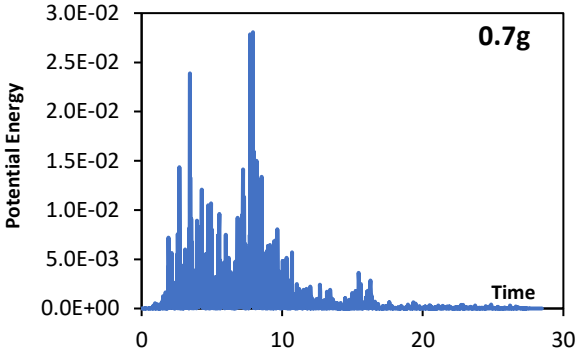

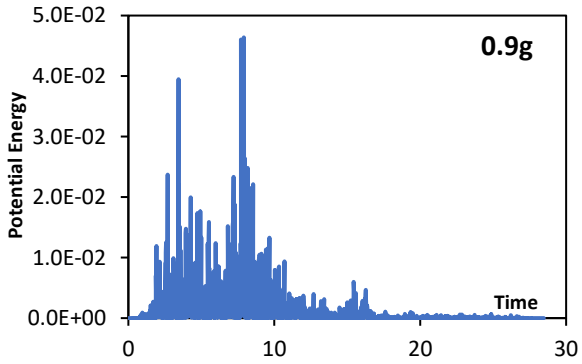

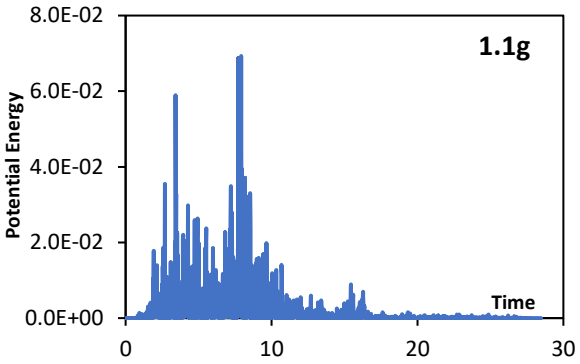

Imperial Valley-FF

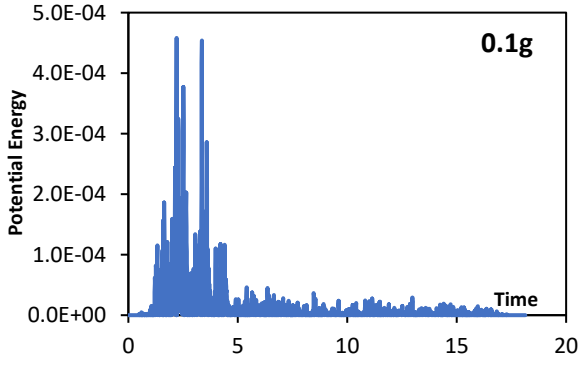

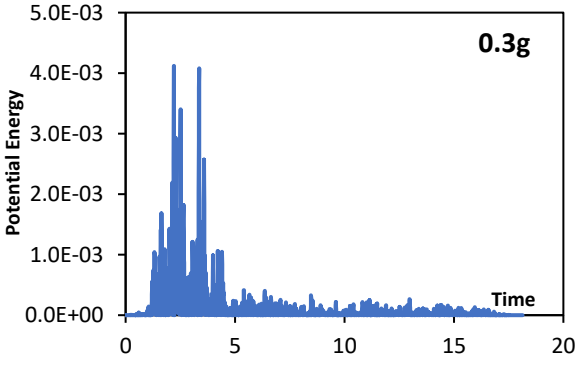

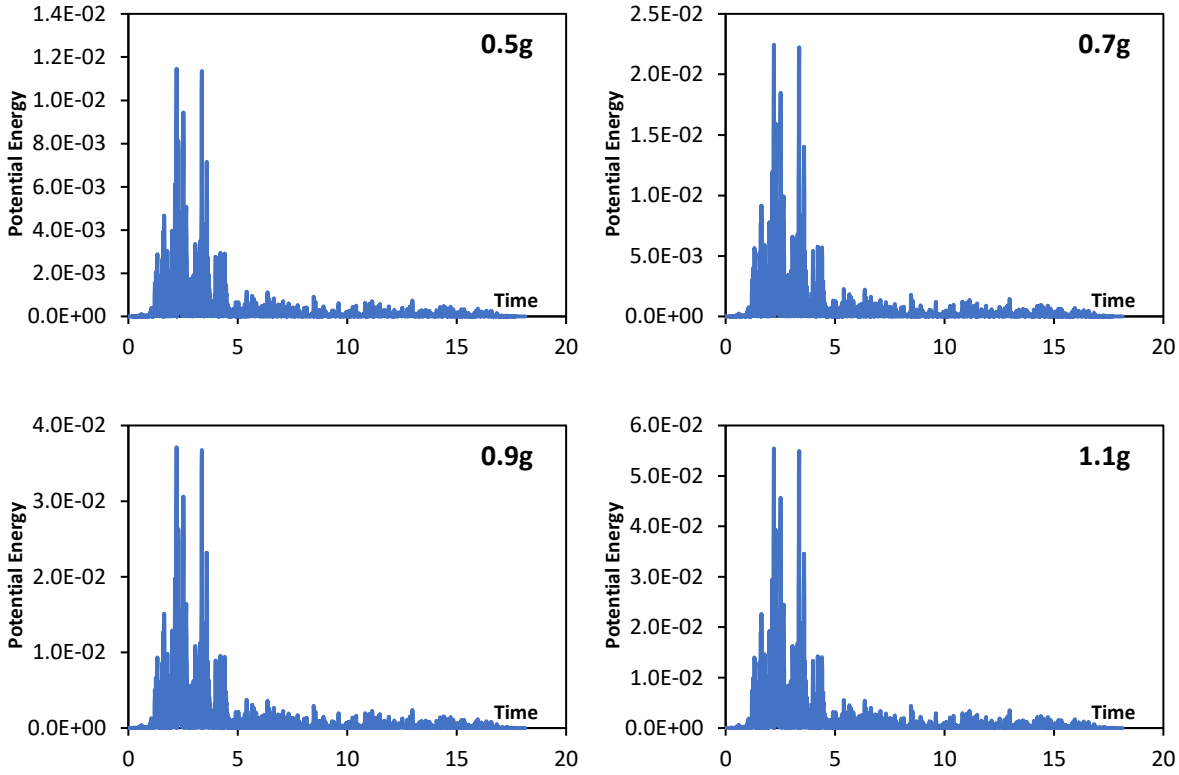
0.5g
0.7g
0.9g
1.1g
Potential Energy
Time

Irpinia-NF

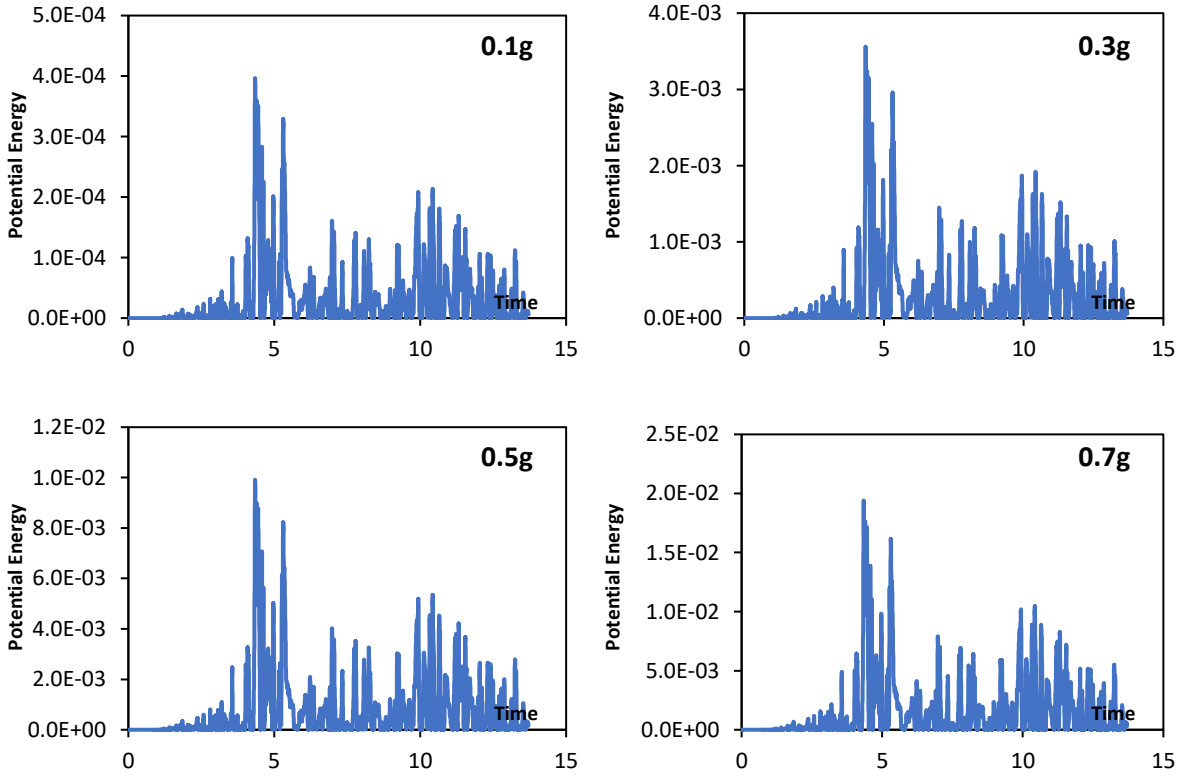
0.1g
0.3g
0.5g
0.7g
Potential Energy
Time

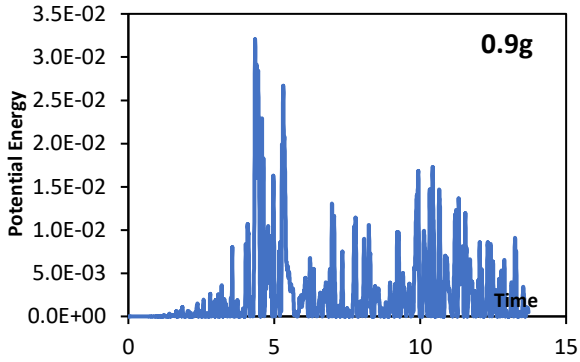
0.9g
Potential Energy
Time
3.5E-02
3.0E-02
2.5E-02
2.0E-02
1.5E-02
1.0E-02
5.0E-03
0.0E+00
0
5
10
15

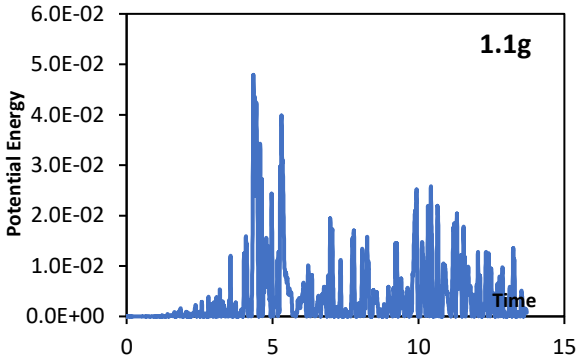
1.1g
Potential Energy
Time
6.0E-02
5.0E-02
4.0E-02
3.0E-02
2.0E-02
1.0E-02
0.0E+00
0
5
10
15

Irpinia-FF

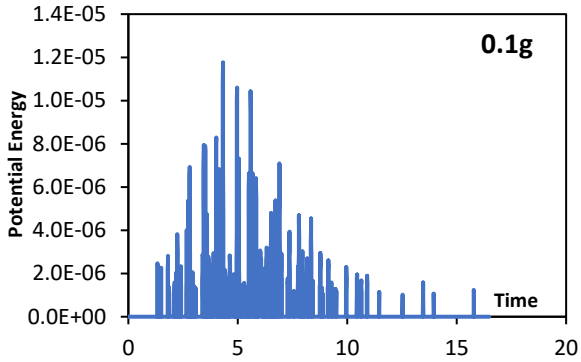
0.1g
Potential Energy
Time
1.4E-05
1.2E-05
1.0E-05
8.0E-06
6.0E-06
4.0E-06
2.0E-06
0.0E+00
0
5
10
15
20

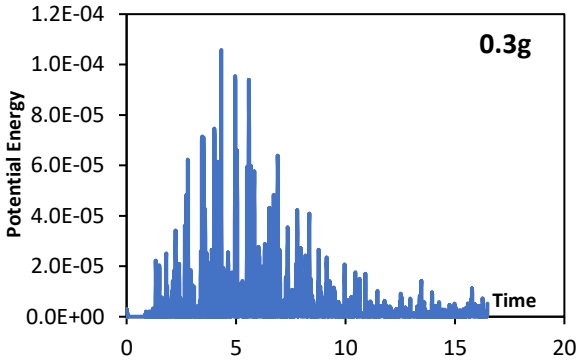
0.3g
Potential Energy
Time
1.2E-04
1.0E-04
8.0E-05
6.0E-05
4.0E-05
2.0E-05
0.0E+00
0
5
10
15
20

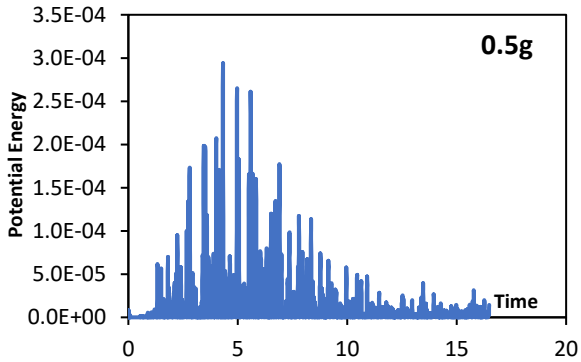
0.5g
Potential Energy
Time
3.5E-04
3.0E-04
2.5E-04
2.0E-04
1.5E-04
1.0E-04
5.0E-05
0.0E+00
0
5
10
15
20

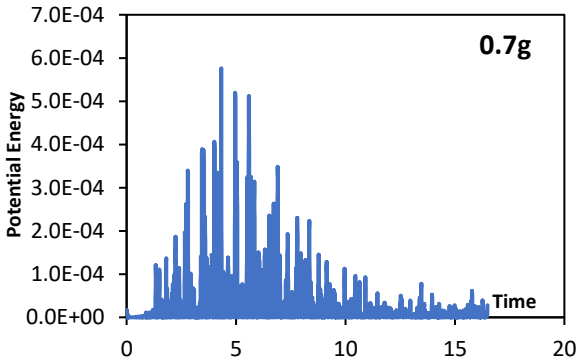
0.7g
Potential Energy
Time
7.0E-04
6.0E-04
5.0E-04
4.0E-04
3.0E-04
2.0E-04
1.0E-04
0.0E+00
0
5
10
15
20

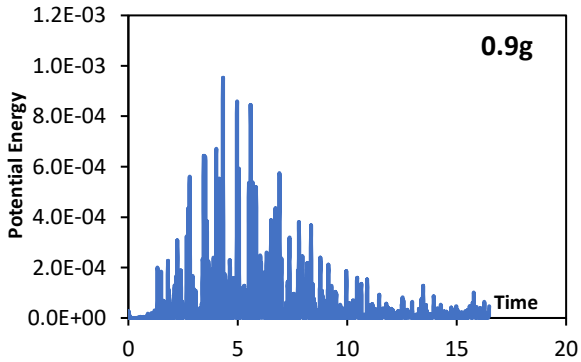
0.9g
Potential Energy
Time
1.2E-03
1.0E-03
8.0E-04
6.0E-04
4.0E-04
2.0E-04
0.0E+00
0
5
10
15
20

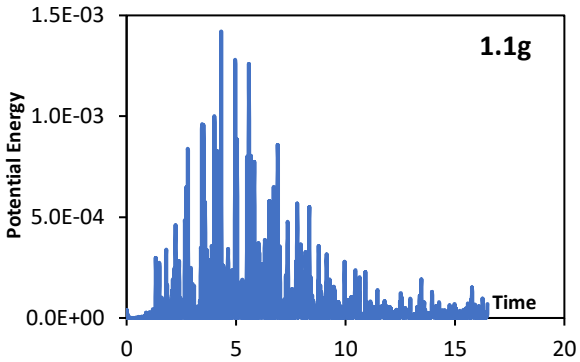
1.1g
Potential Energy
Time
1.5E-03
1.0E-03
5.0E-04
0.0E+00
0
5
10
15
20

Kalamata-NF

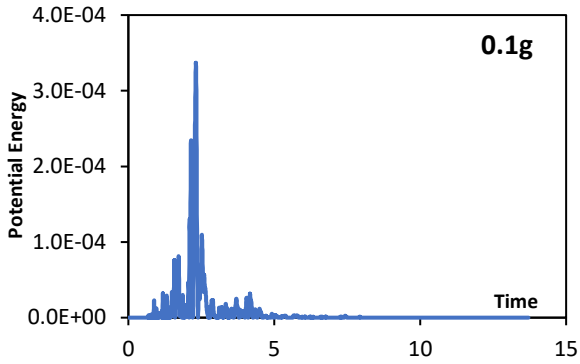

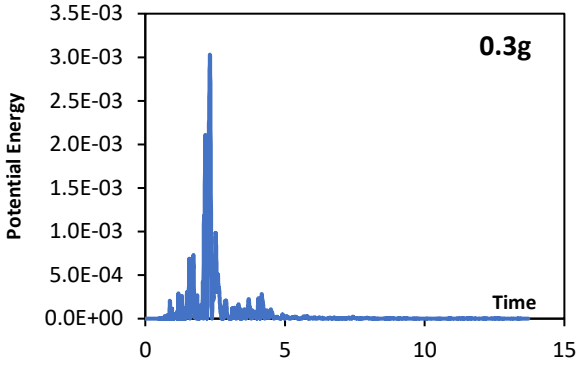

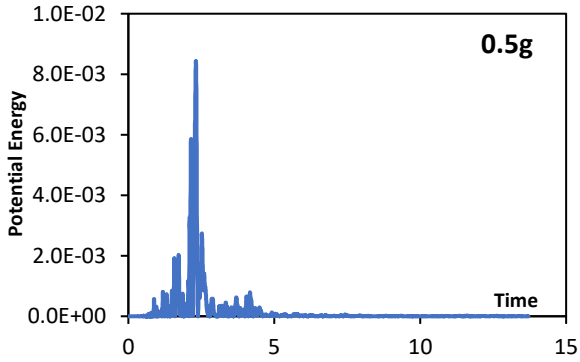

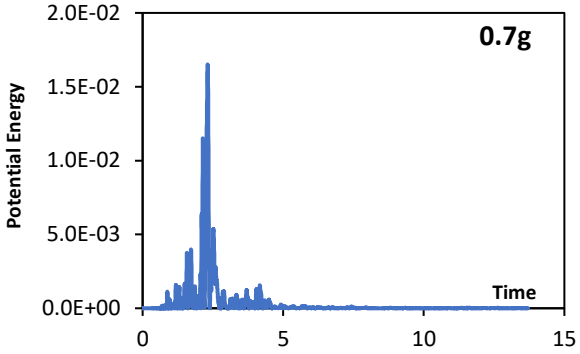

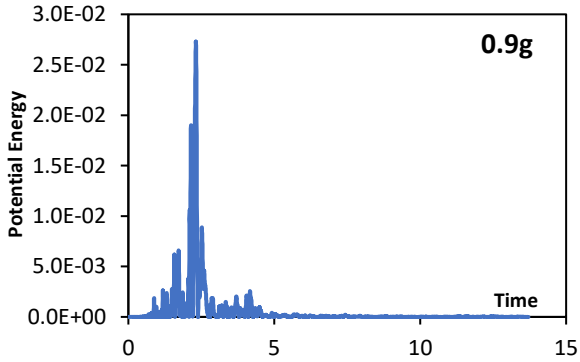

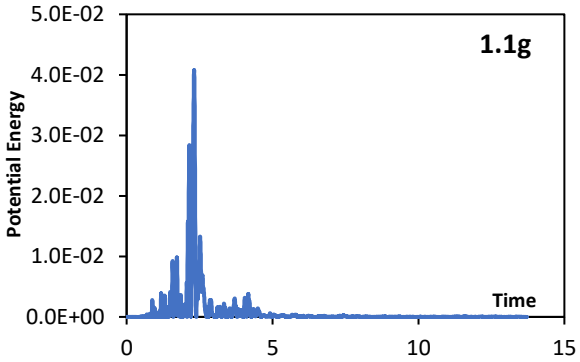

Kobe-NF

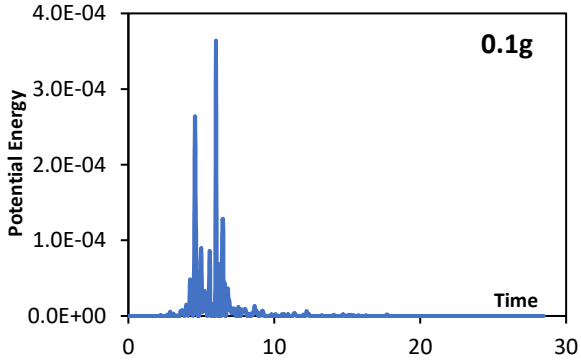

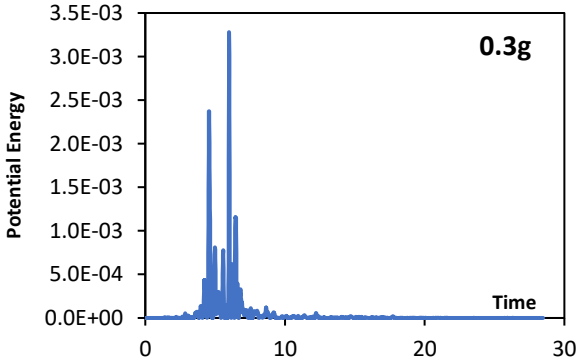

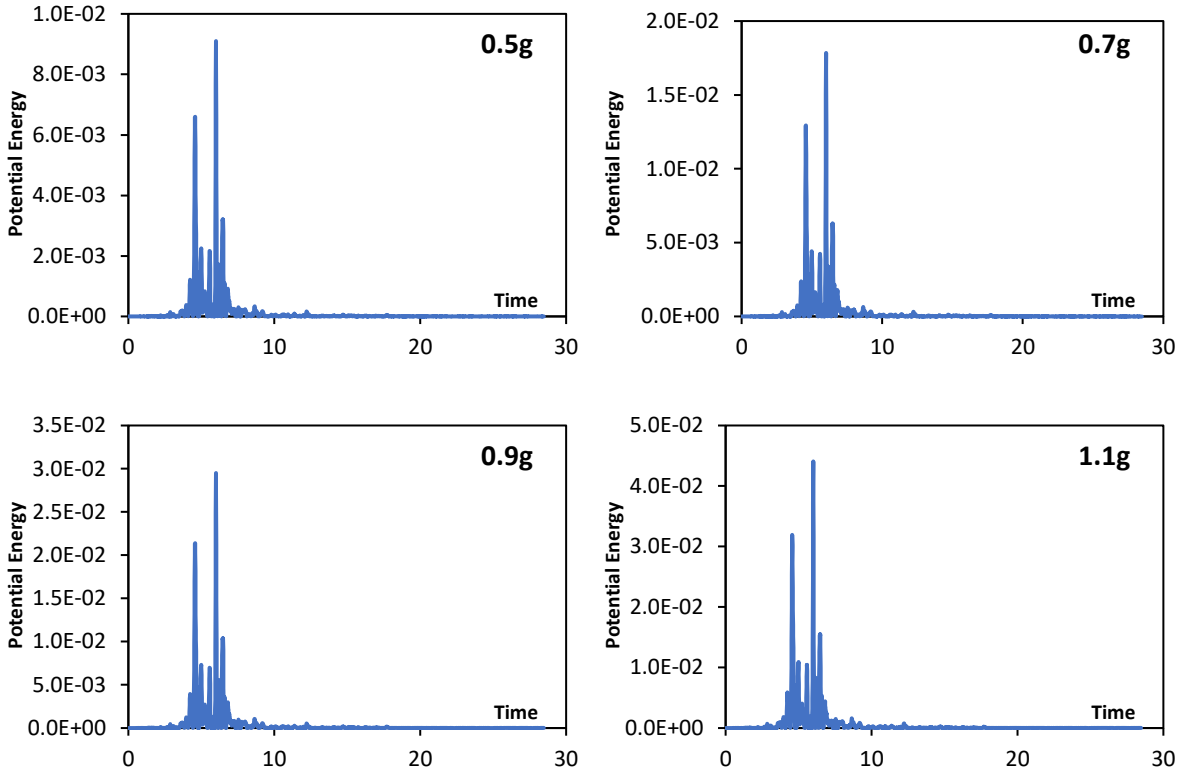
0.5g
0.7g
0.9g
1.1g
Potential Energy
Time
1.0E-02
8.0E-03
6.0E-03
4.0E-03
2.0E-03
0.0E+00
2.0E-02
1.5E-02
1.0E-02
5.0E-03
3.5E-02
3.0E-02
2.5E-02
2.0E-02
1.5E-02
1.0E-02
5.0E-03
5.0E-02
4.0E-02
3.0E-02
2.0E-02
1.0E-02
0
10
20
30

Kobe-FF

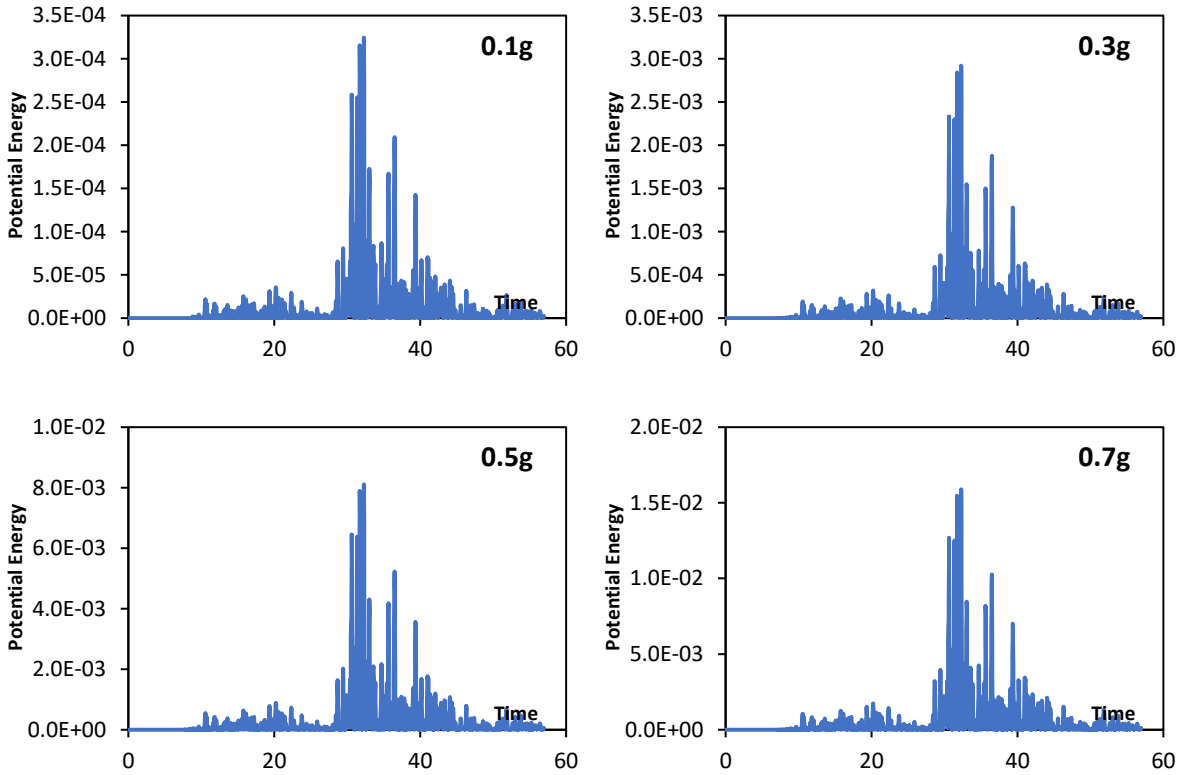
0.1g
0.3g
0.5g
0.7g
Potential Energy
Time
3.5E-04
3.0E-04
2.5E-04
2.0E-04
1.5E-04
1.0E-04
5.0E-05
0.0E+00
3.5E-03
3.0E-03
2.5E-03
2.0E-03
1.5E-03
1.0E-03
5.0E-04
1.0E-02
8.0E-03
6.0E-03
4.0E-03
2.0E-03
2.0E-02
1.5E-02
1.0E-02
5.0E-03
0
20
40
60

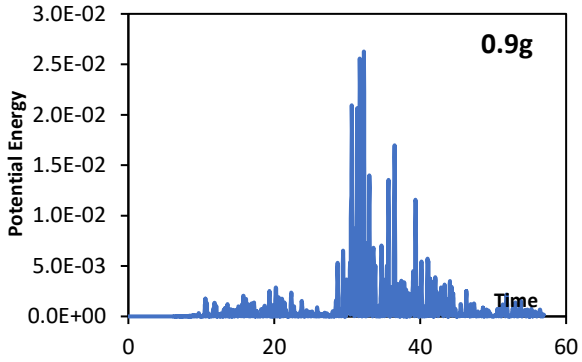
0.9g
Potential Energy
Time
3.0E-02
2.5E-02
2.0E-02
1.5E-02
1.0E-02
5.0E-03
0.0E+00
0
20
40
60

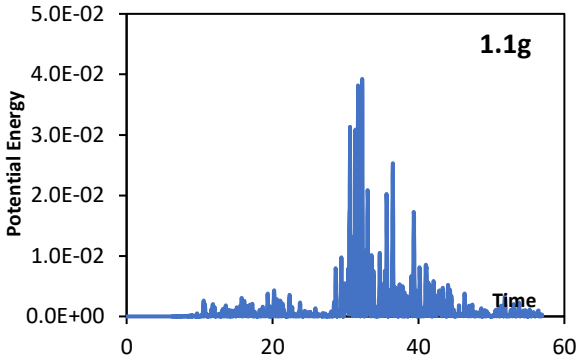
1.1g
Potential Energy
Time
5.0E-02
4.0E-02
3.0E-02
2.0E-02
1.0E-02
0.0E+00
0
20
40
60

Kocaeli-NF

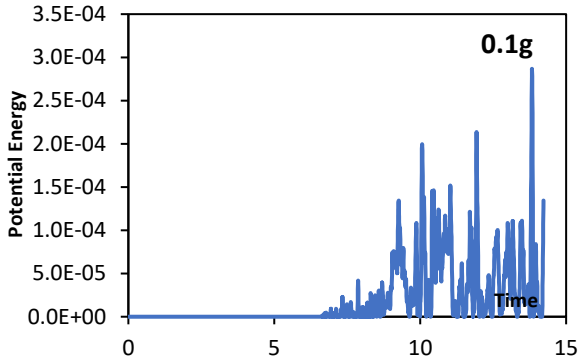
0.1g
Potential Energy
Time
3.5E-04
3.0E-04
2.5E-04
2.0E-04
1.5E-04
1.0E-04
5.0E-05
0.0E+00
0
5
10
15

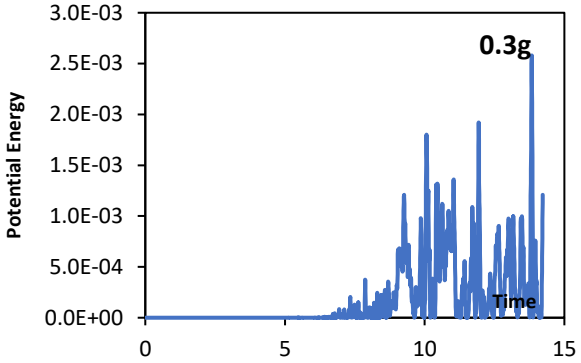
0.3g
Potential Energy
Time
3.0E-03
2.5E-03
2.0E-03
1.5E-03
1.0E-03
5.0E-04
0.0E+00
0
5
10
15

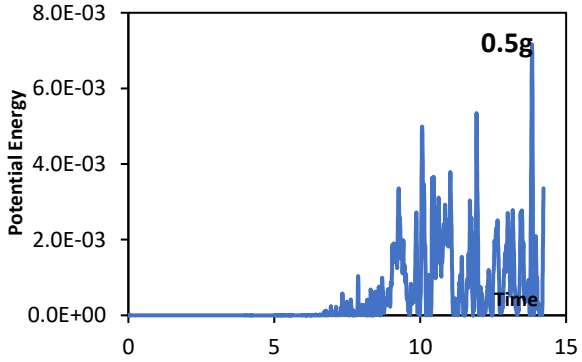
0.5g
Potential Energy
Time
8.0E-03
6.0E-03
4.0E-03
2.0E-03
0.0E+00
0
5
10
15

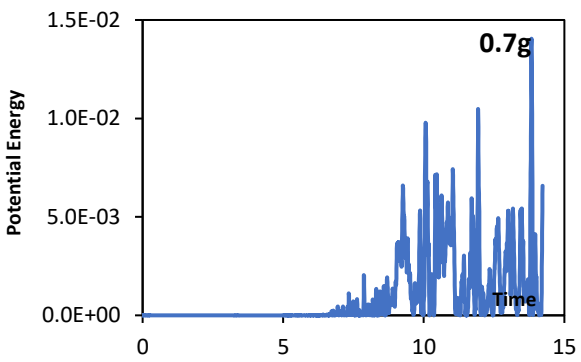
0.7g
Potential Energy
Time
1.5E-02
1.0E-02
5.0E-03
0.0E+00
0
5
10
15

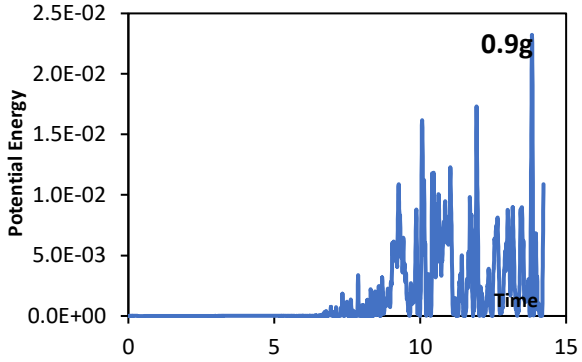
0.9g
Potential Energy
Time
2.5E-02
2.0E-02
1.5E-02
1.0E-02
5.0E-03
0.0E+00
0
5
10
15

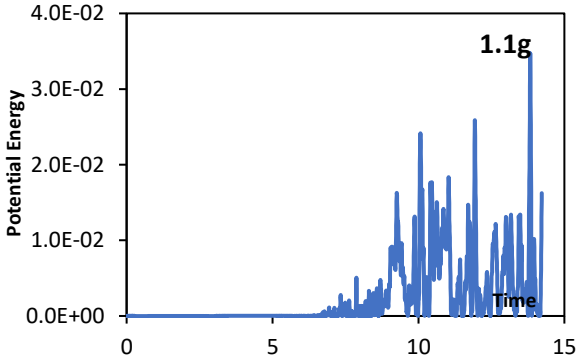
1.1g
Potential Energy
Time
4.0E-02
3.0E-02
2.0E-02
1.0E-02
0.0E+00
0
5
10
15

Kocaeli-FF

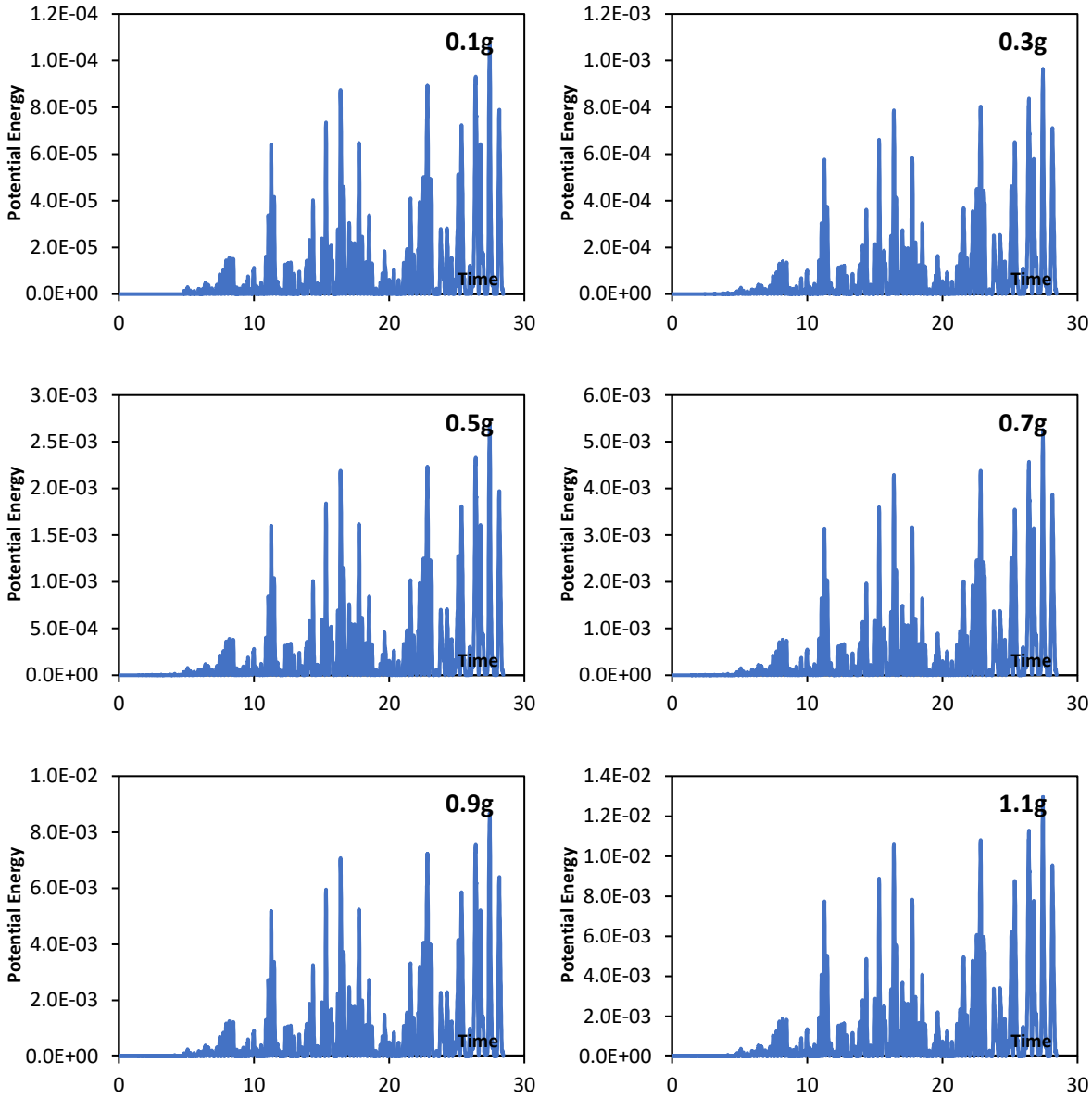

Landers-NF

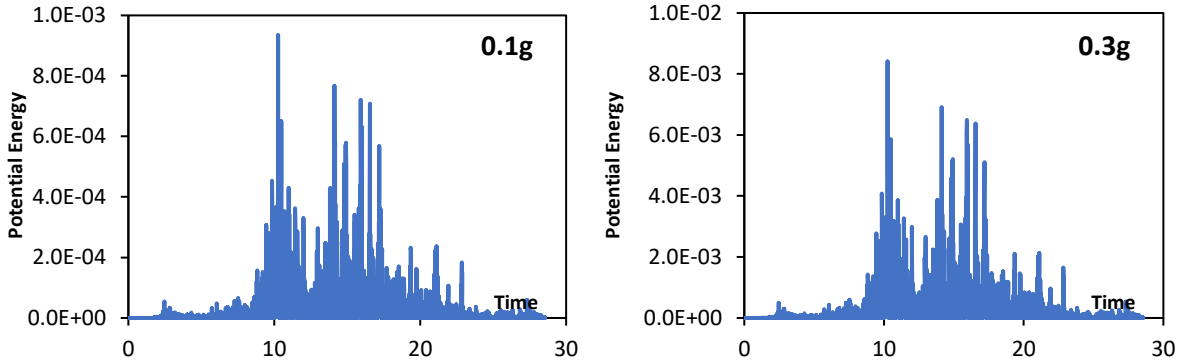

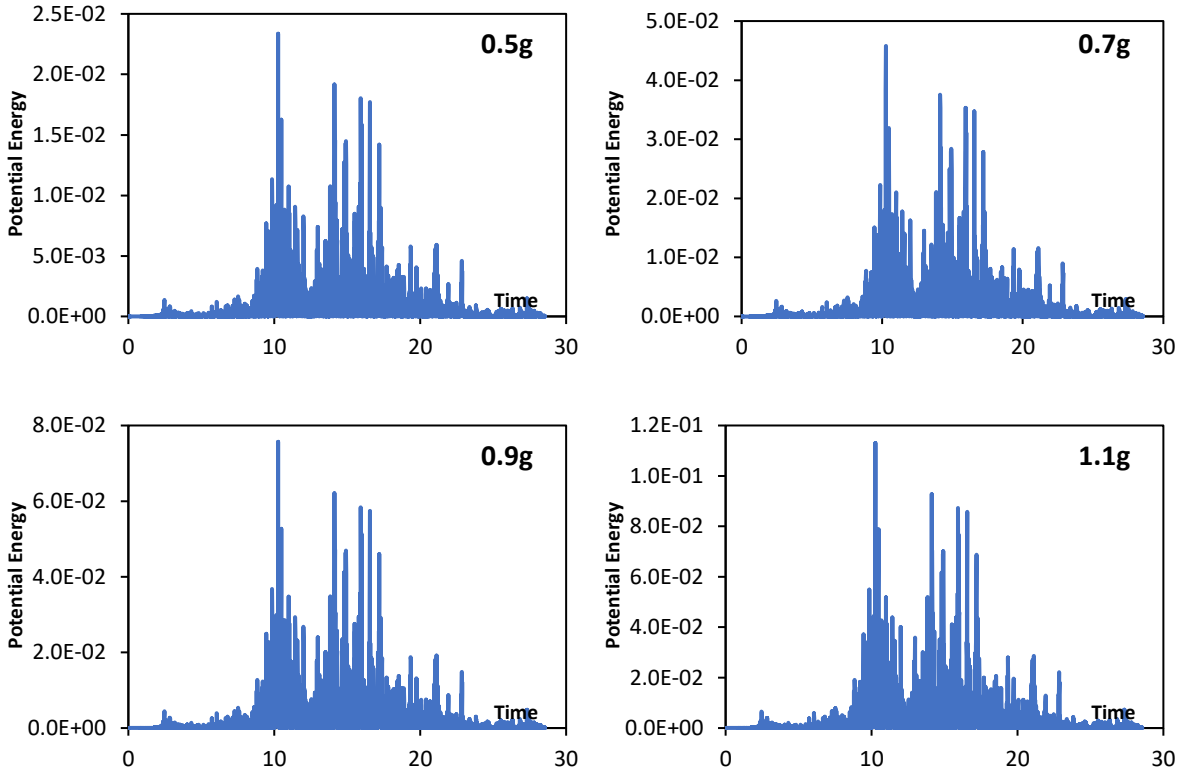
0.5g
0.7g
0.9g
1.1g
Potential Energy
Time
2.5E-02
2.0E-02
1.5E-02
1.0E-02
5.0E-03
0.0E+00
5.0E-02
4.0E-02
3.0E-02
2.0E-02
1.0E-02
8.0E-02
6.0E-02
4.0E-02
2.0E-02
1.2E-01
1.0E-01
8.0E-02
6.0E-02
4.0E-02
2.0E-02
0
10
20
30

Landers-FF

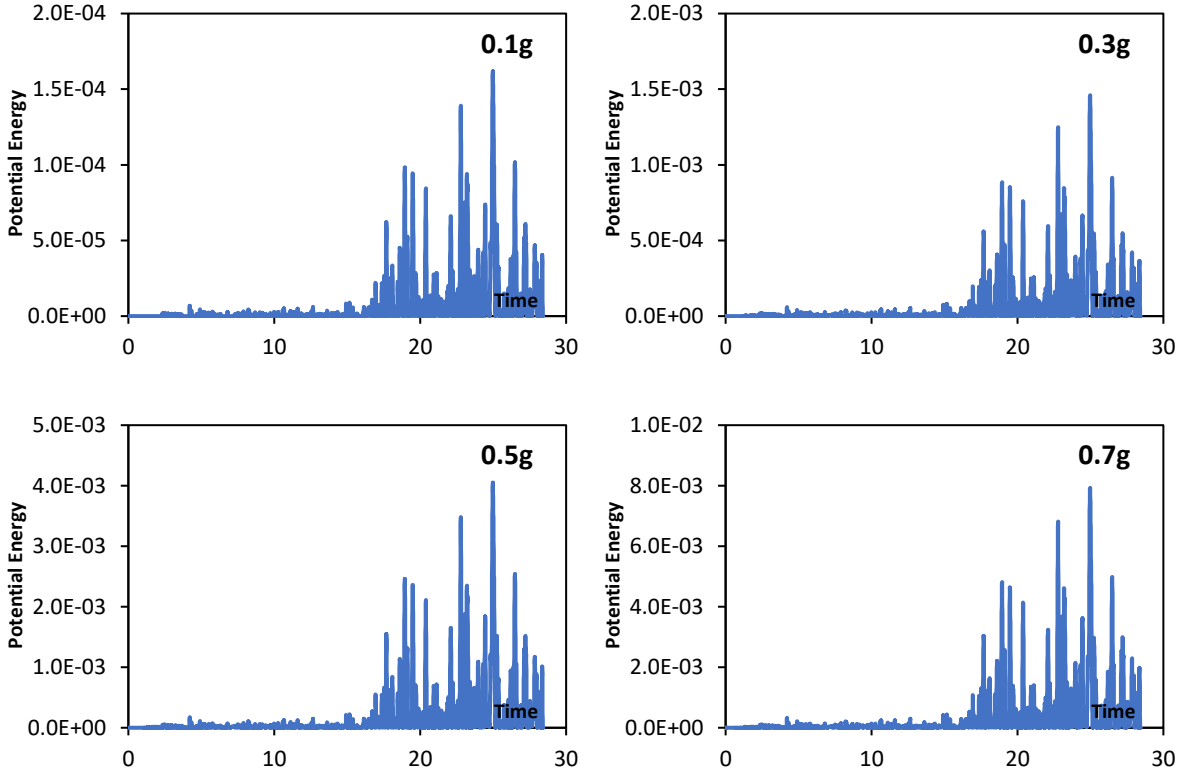
0.1g
0.3g
0.5g
0.7g
Potential Energy
Time
2.0E-04
1.5E-04
1.0E-04
5.0E-05
0.0E+00
2.0E-03
1.5E-03
1.0E-03
5.0E-04
5.0E-03
4.0E-03
3.0E-03
2.0E-03
1.0E-03
1.0E-02
8.0E-03
6.0E-03
4.0E-03
2.0E-03
0
10
20
30

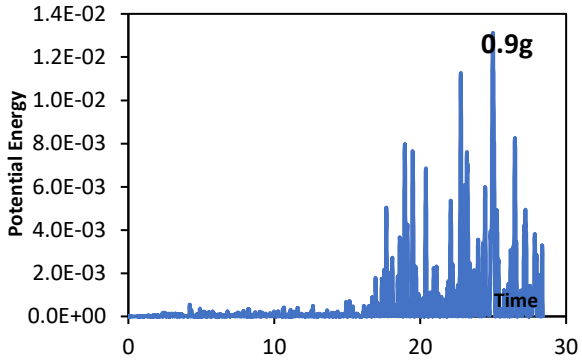
0.9g
Potential Energy
Time
1.4E-02
1.2E-02
1.0E-02
8.0E-03
6.0E-03
4.0E-03
2.0E-03
0.0E+00
0
10
20
30

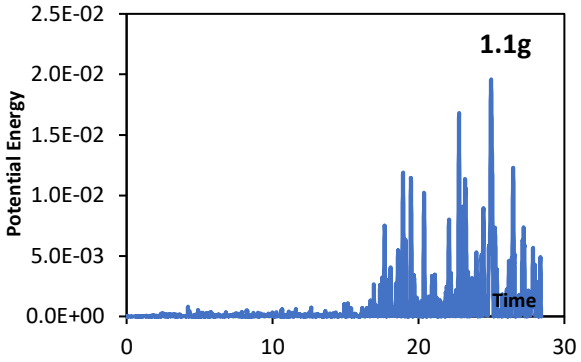
1.1g
Potential Energy
Time
2.5E-02
2.0E-02
1.5E-02
1.0E-02
5.0E-03
0.0E+00
0
10
20
30

L-Aquilla -NF

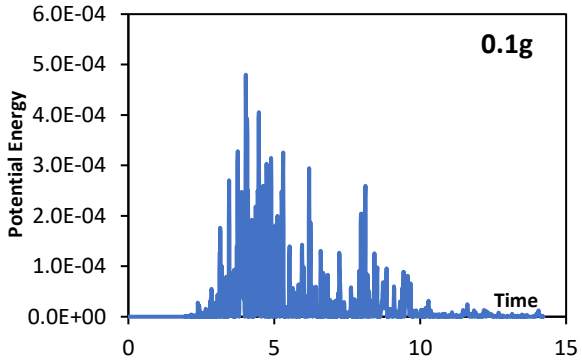
0.1g
Potential Energy
Time
6.0E-04
5.0E-04
4.0E-04
3.0E-04
2.0E-04
1.0E-04
0.0E+00
0
5
10
15

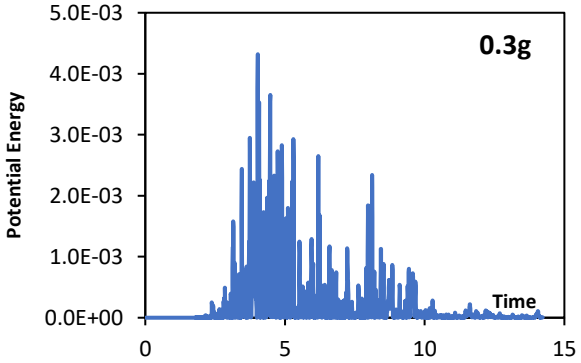
0.3g
Potential Energy
Time
5.0E-03
4.0E-03
3.0E-03
2.0E-03
1.0E-03
0.0E+00
0
5
10
15

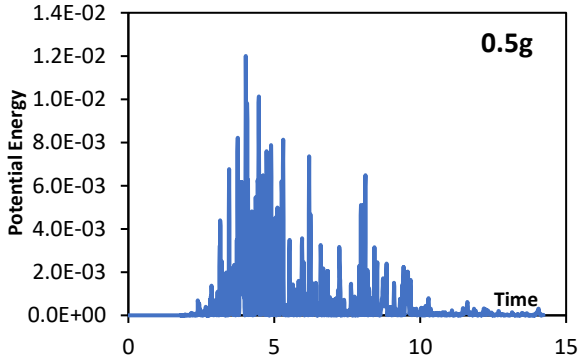
0.5g
Potential Energy
Time
1.4E-02
1.2E-02
1.0E-02
8.0E-03
6.0E-03
4.0E-03
2.0E-03
0.0E+00
0
5
10
15

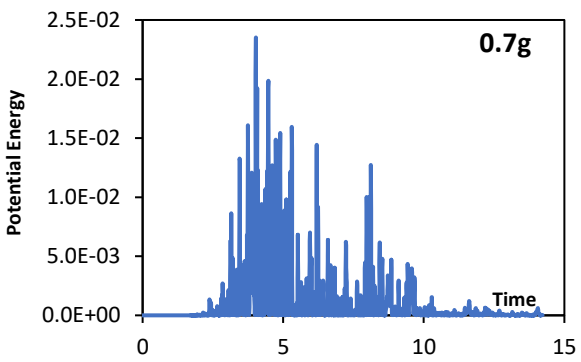
0.7g
Potential Energy
Time
2.5E-02
2.0E-02
1.5E-02
1.0E-02
5.0E-03
0.0E+00
0
5
10
15

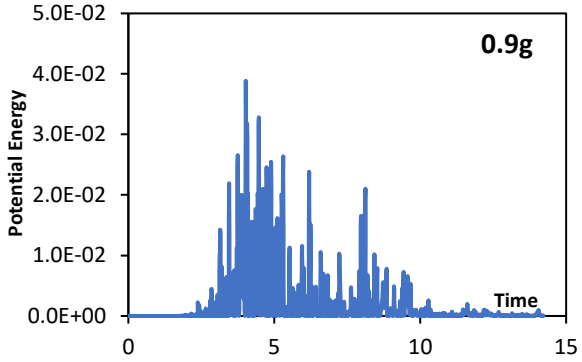
0.9g
Potential Energy
Time
5.0E-02
4.0E-02
3.0E-02
2.0E-02
1.0E-02
0.0E+00
0
5
10
15

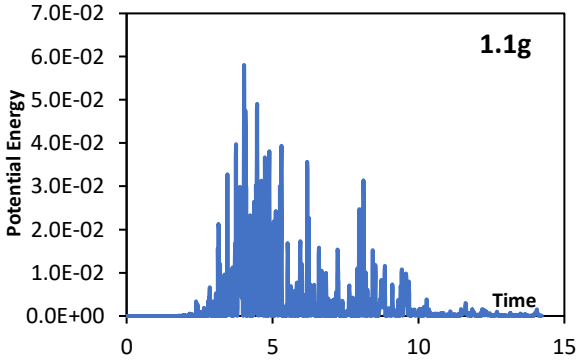
1.1g
Potential Energy
Time
7.0E-02
6.0E-02
5.0E-02
4.0E-02
3.0E-02
2.0E-02
1.0E-02
0.0E+00
0
5
10
15

L-Aquilla--FF

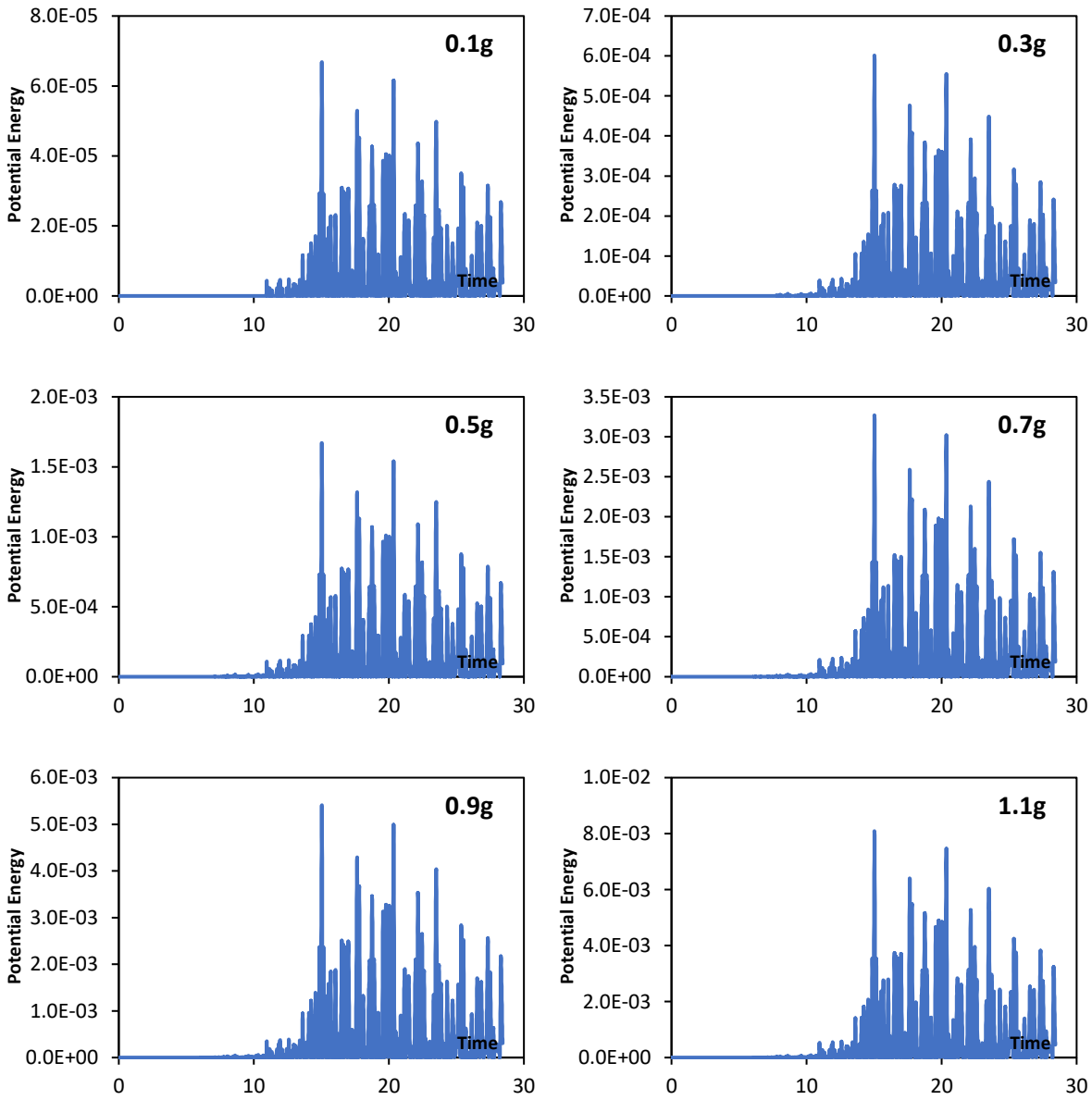

Loma Prieta-NF

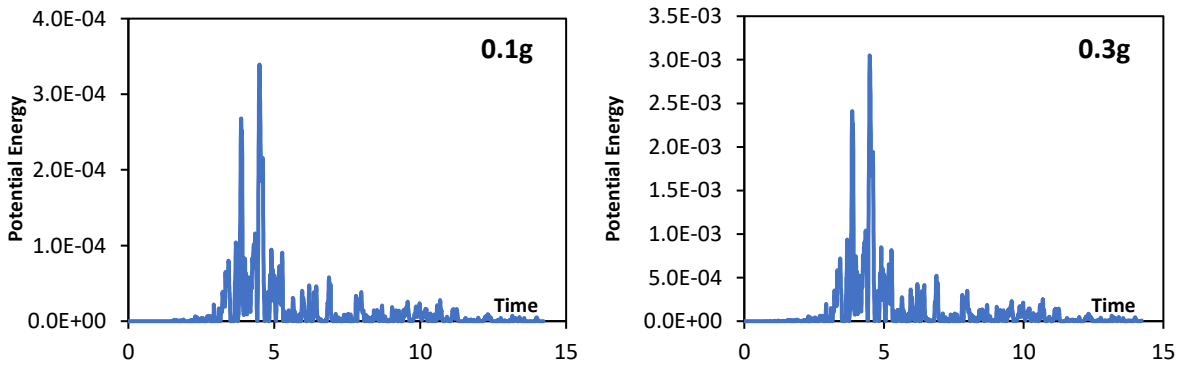

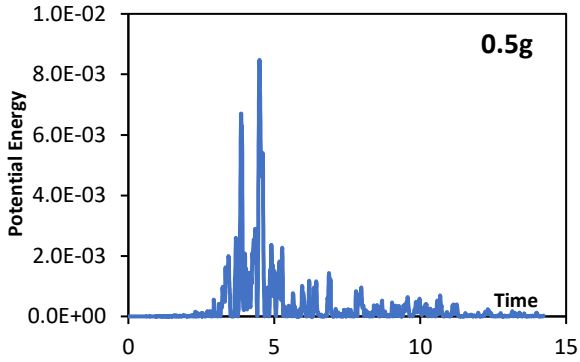

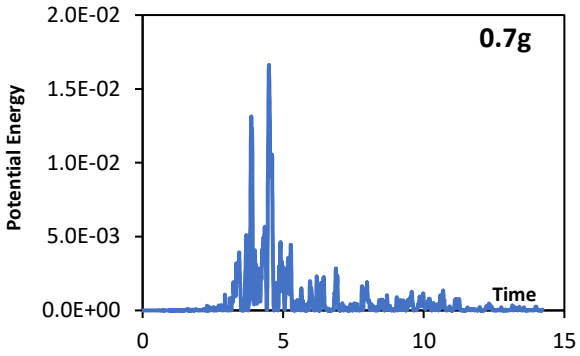

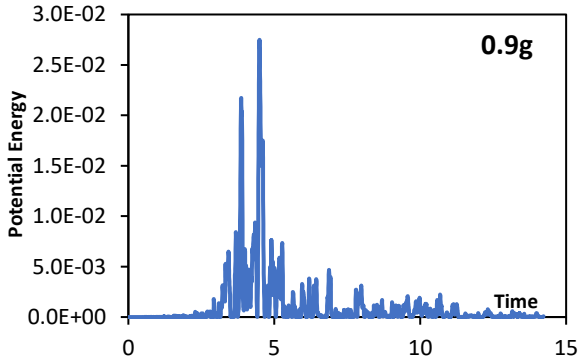

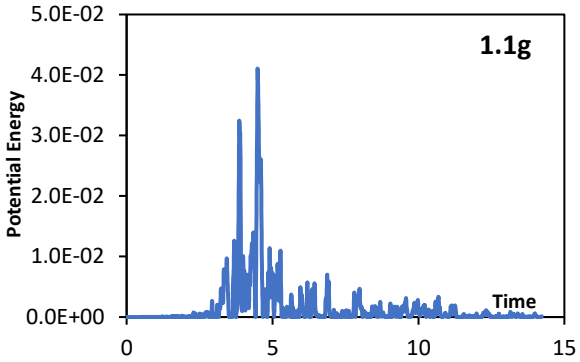

Loma Prieta-FF

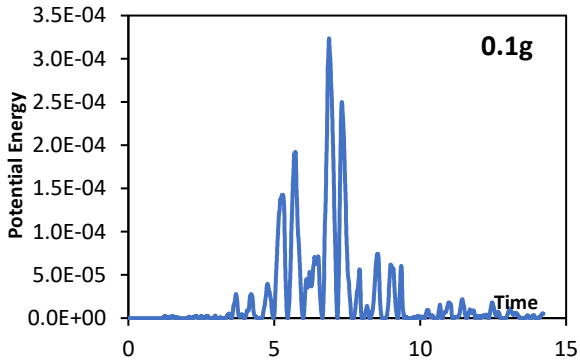

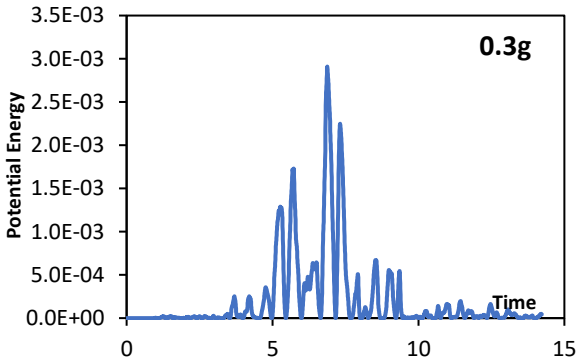

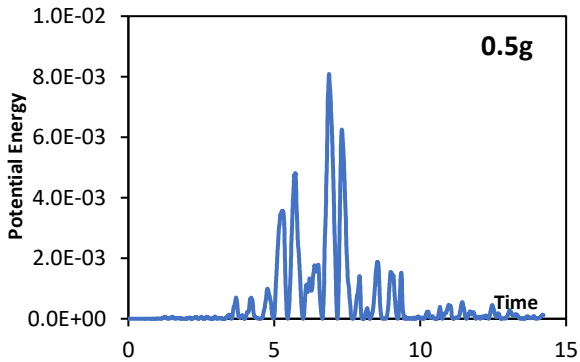

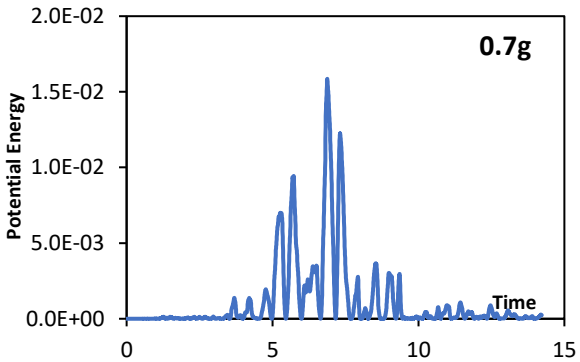

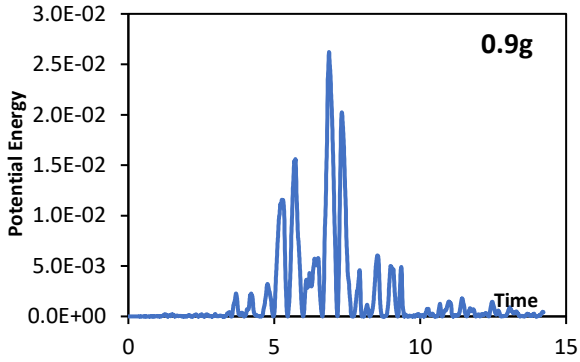

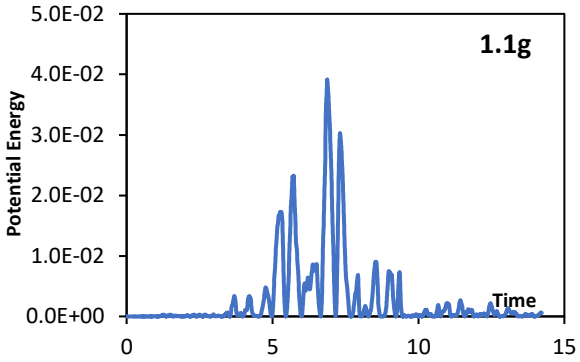

Montenegro-NF

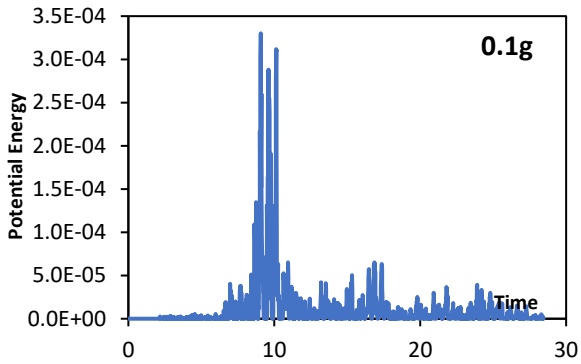

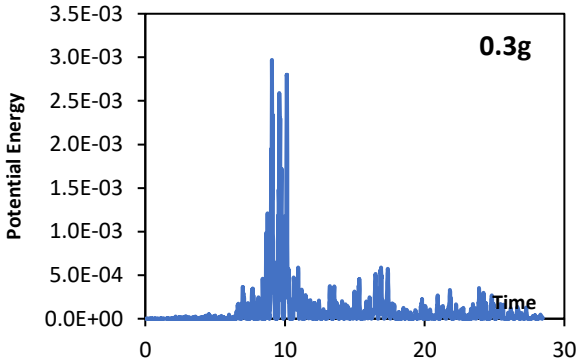

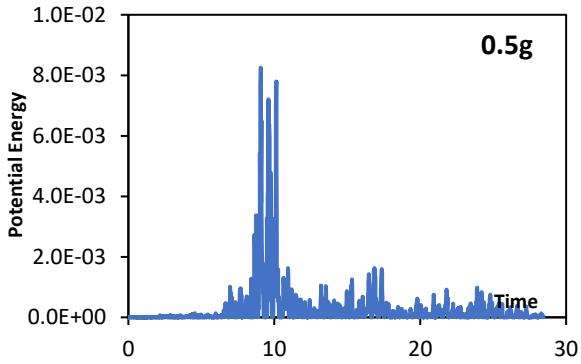

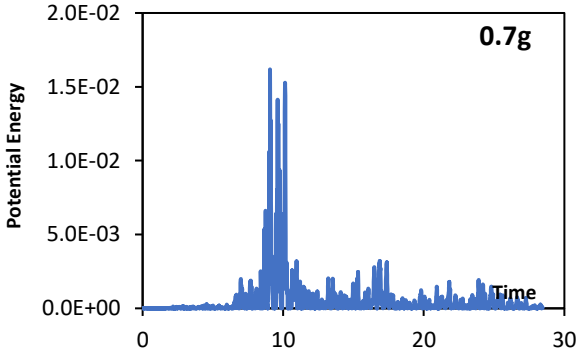

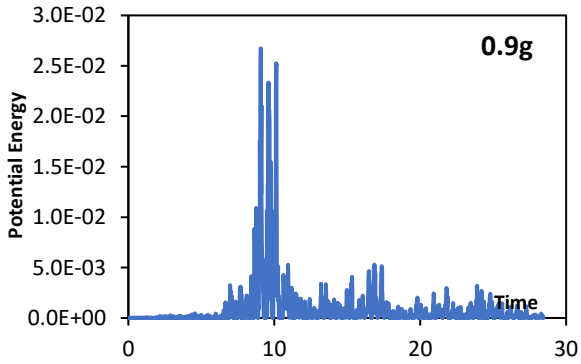

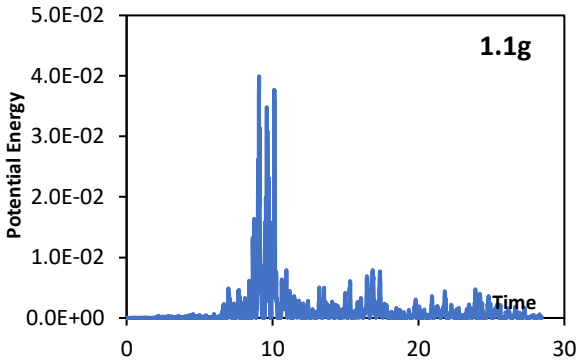

Montenegro-FF

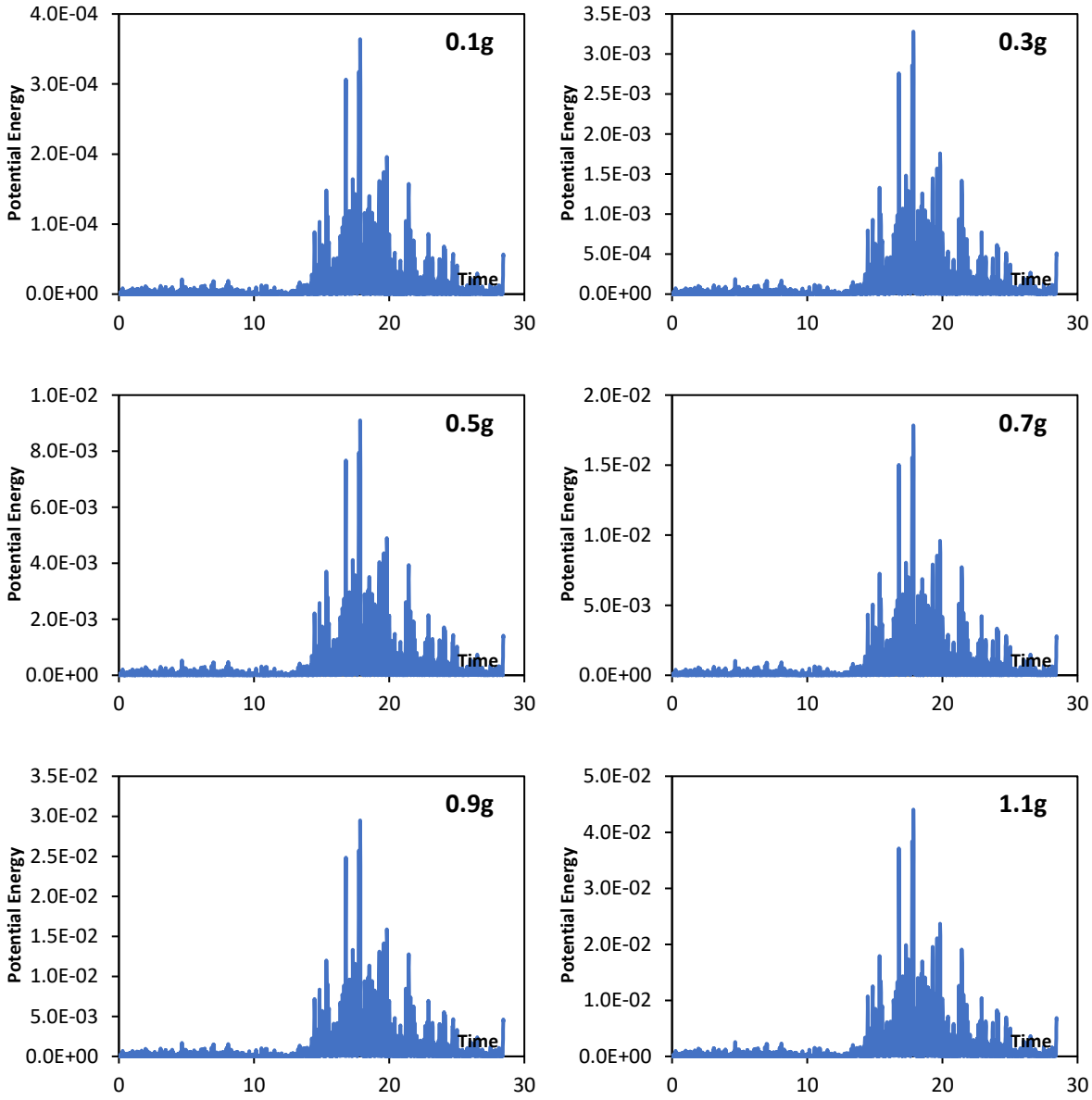

Niigata-FF

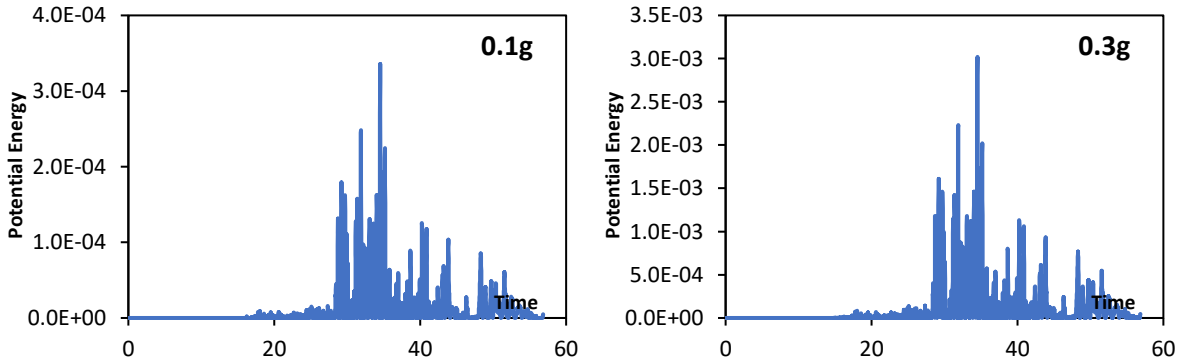

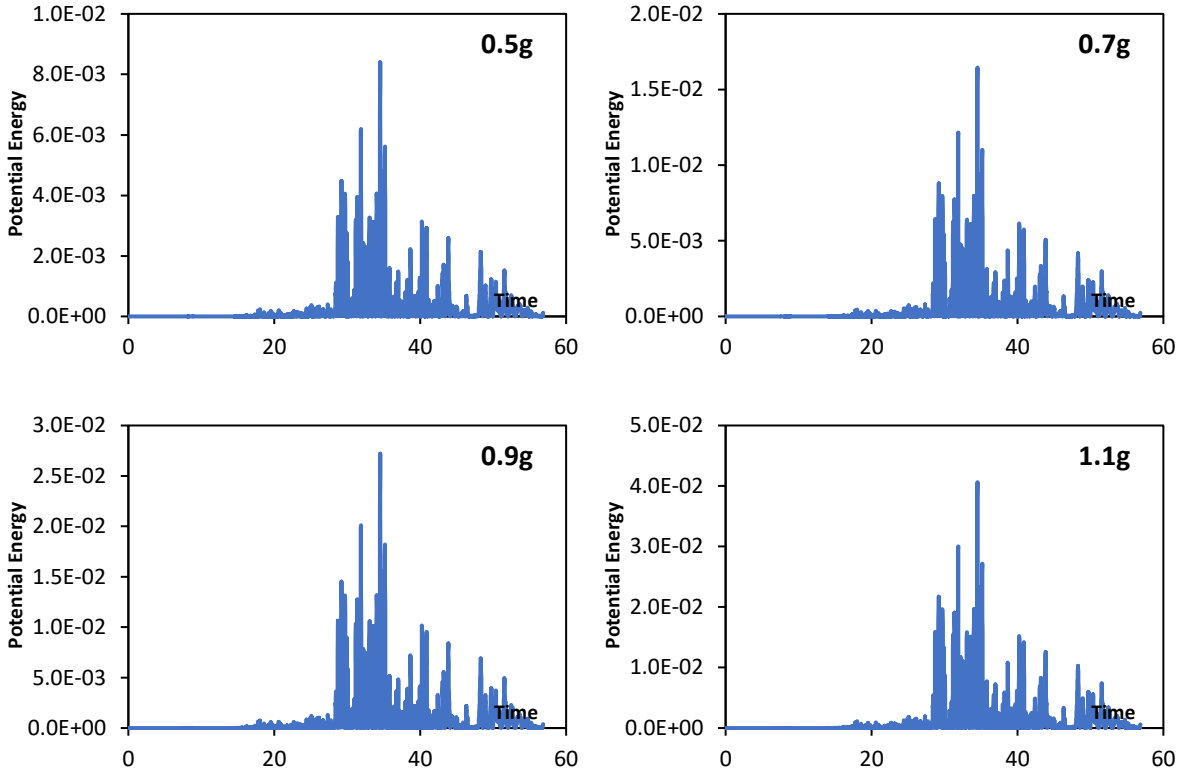

Northridge-NF

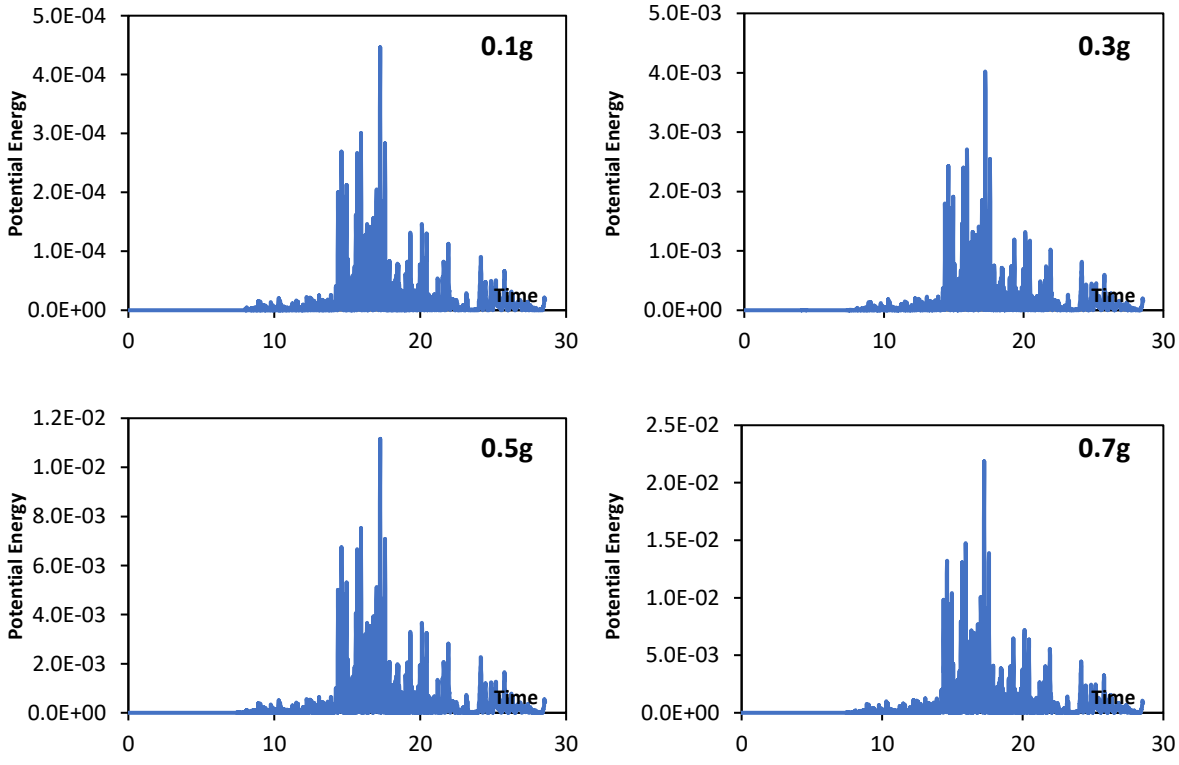

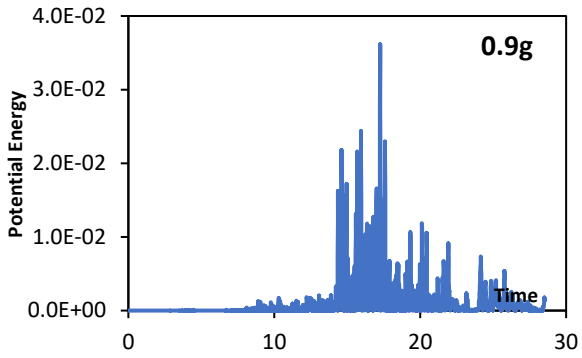

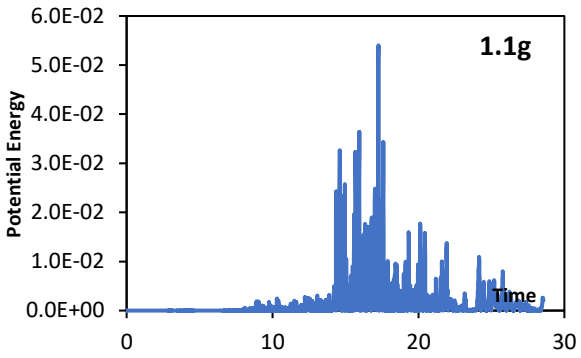

Northridge-FF

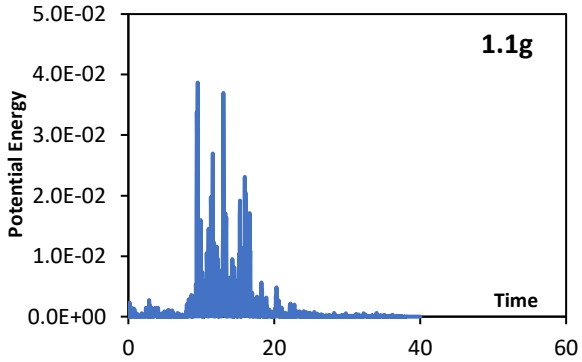

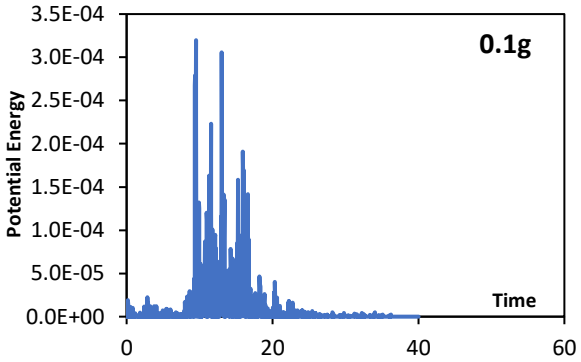

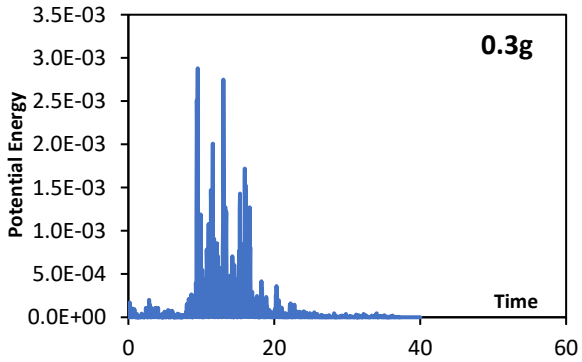

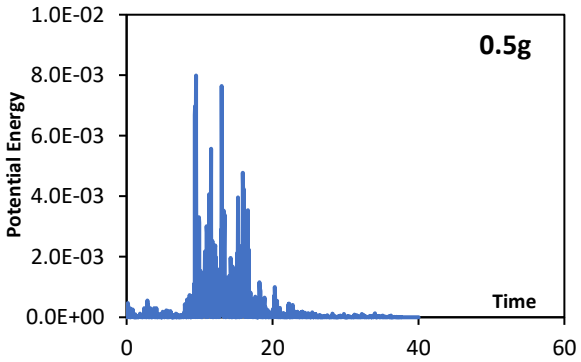

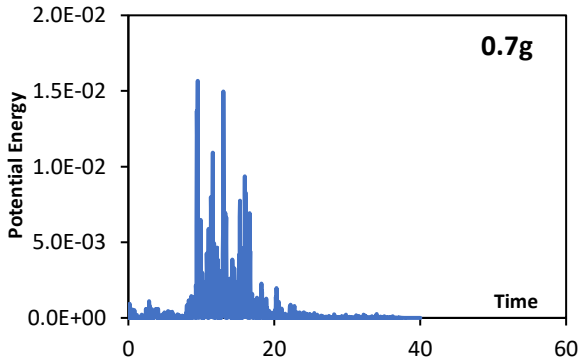

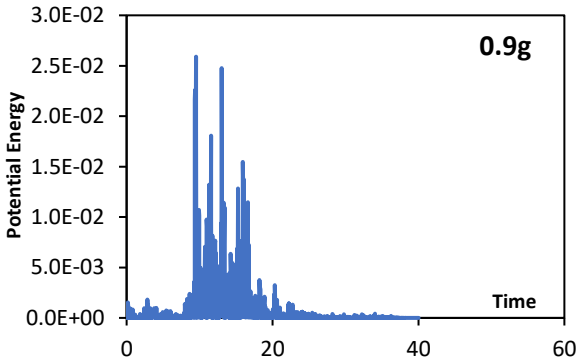

Parkfield-NF

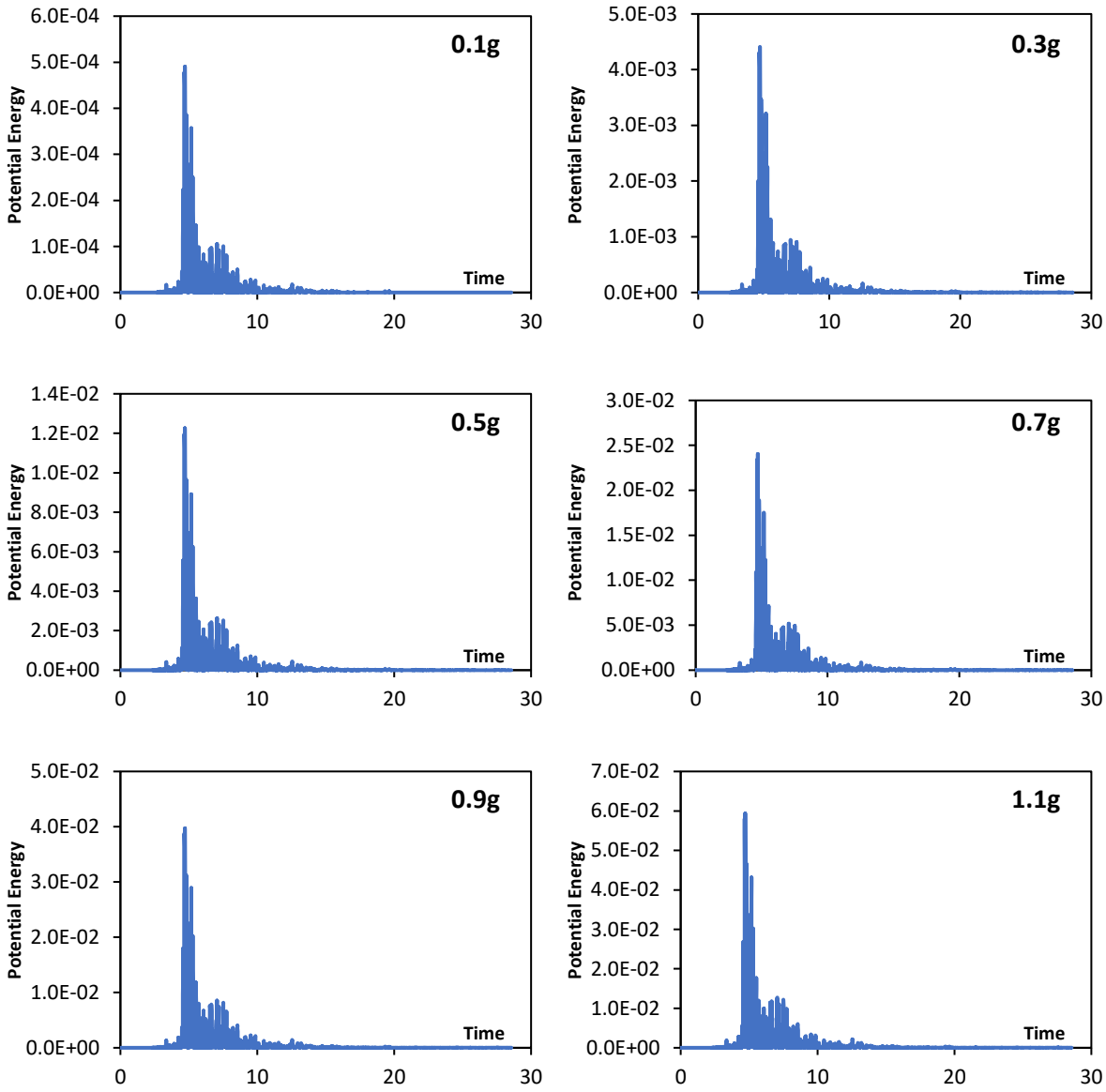

Parkfield-FF

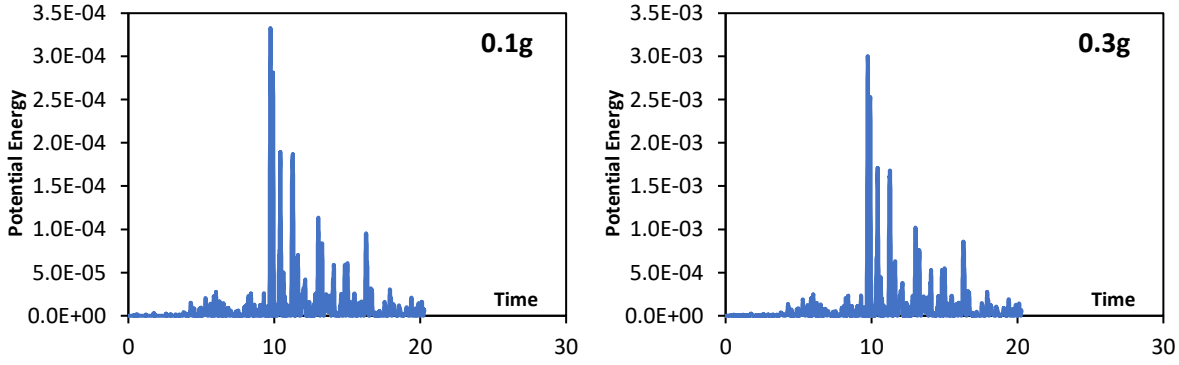

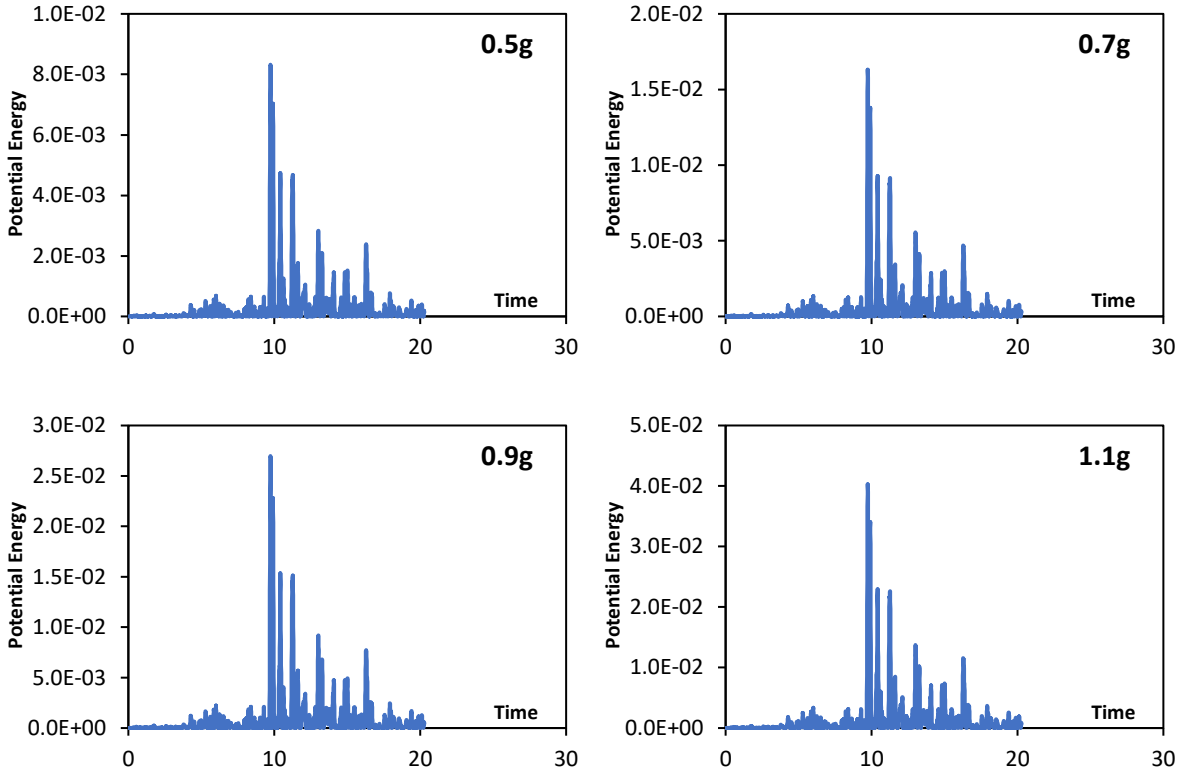

San Fernado-NF

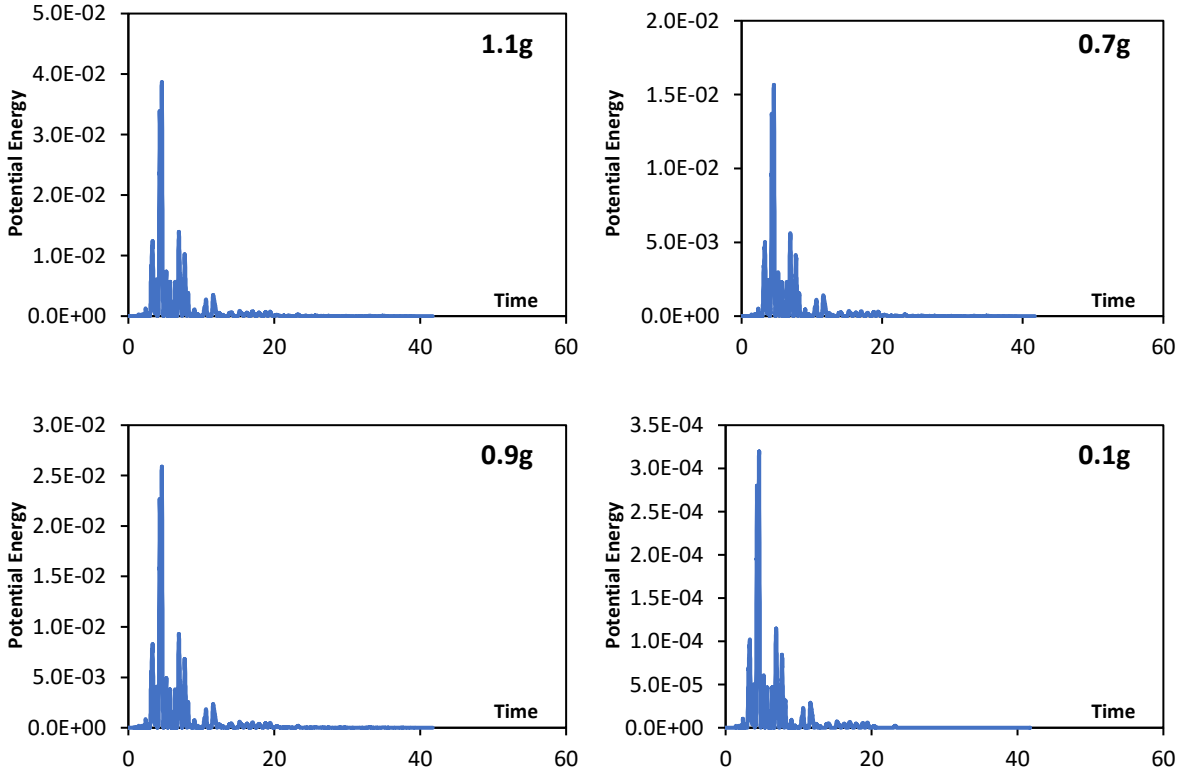

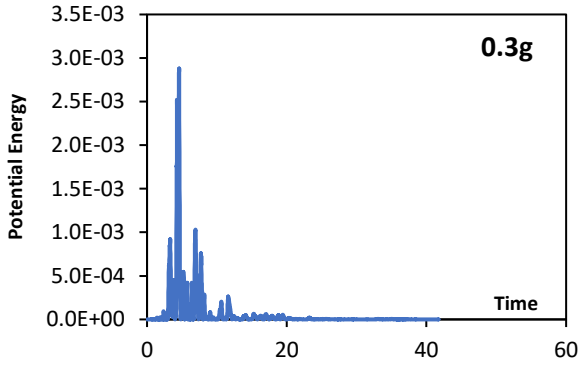

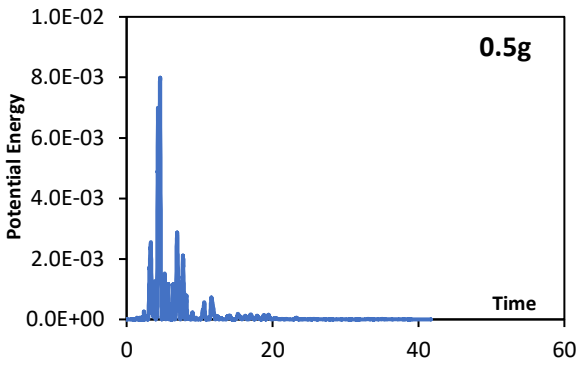

San Fernado-FF

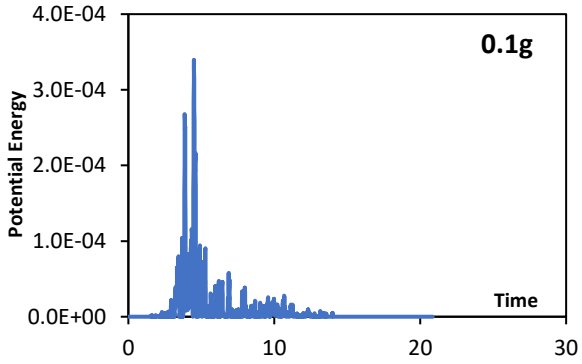

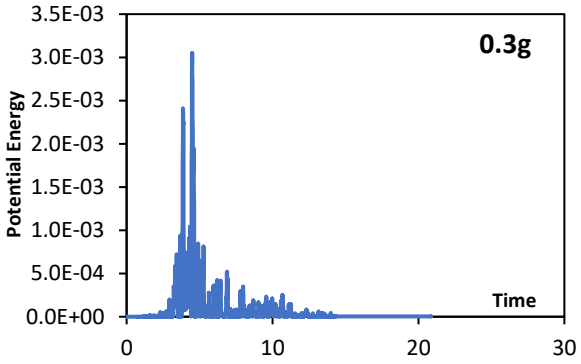

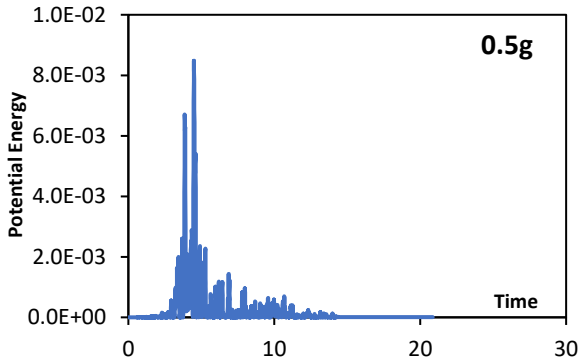

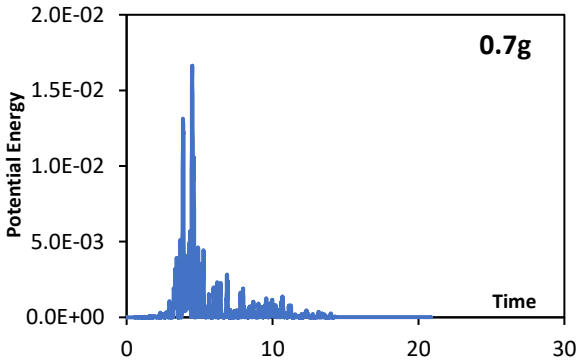

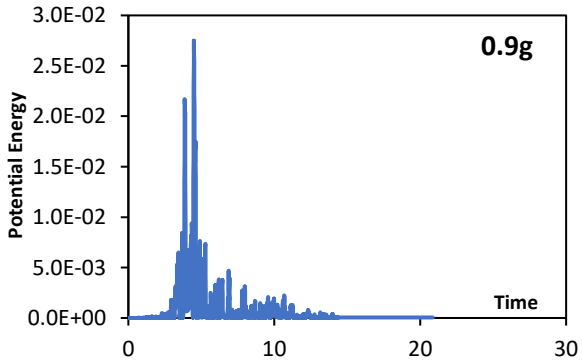

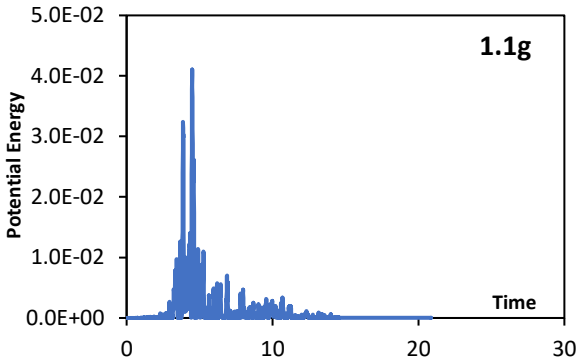

San Salvador-NF

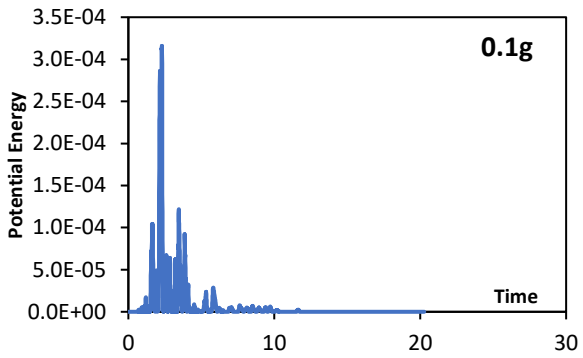

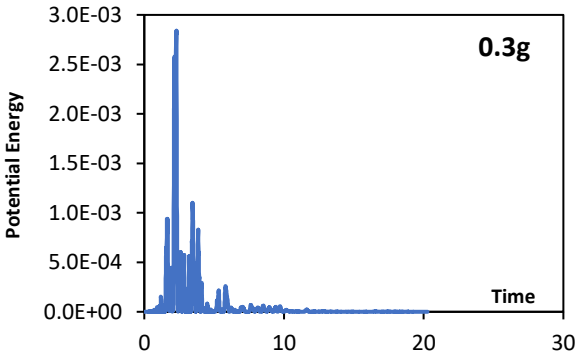

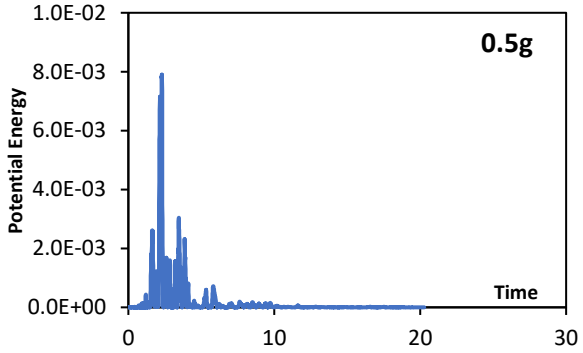

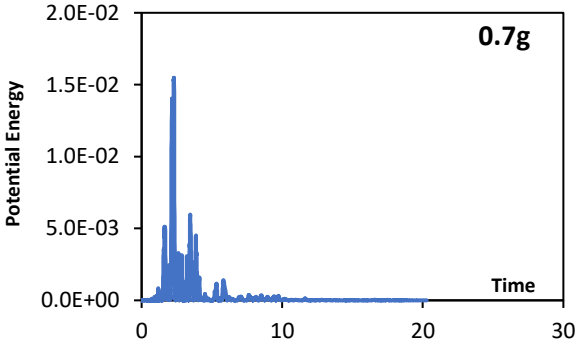

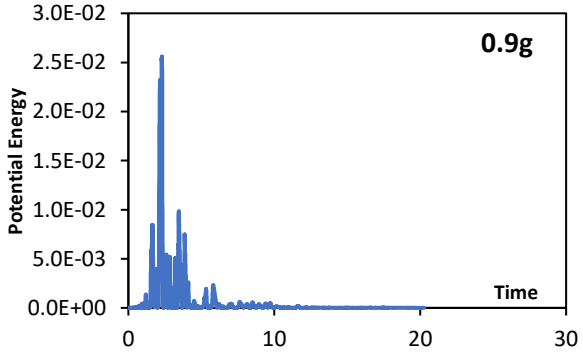

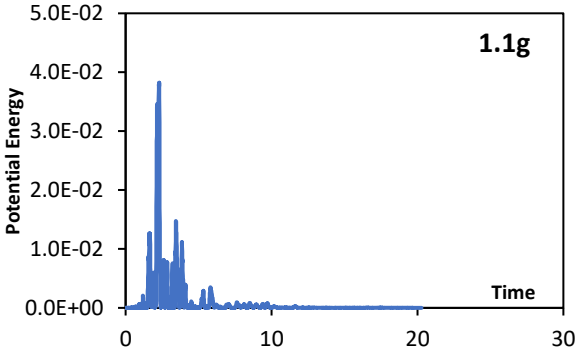

Superstition Hills-NF

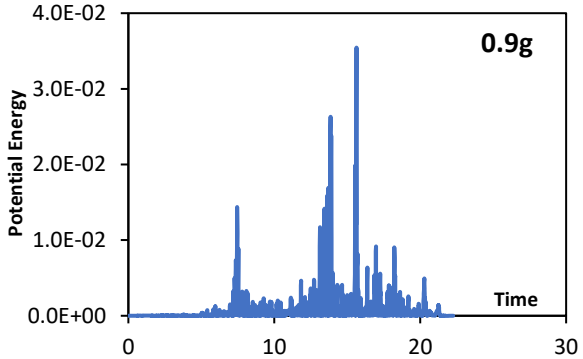

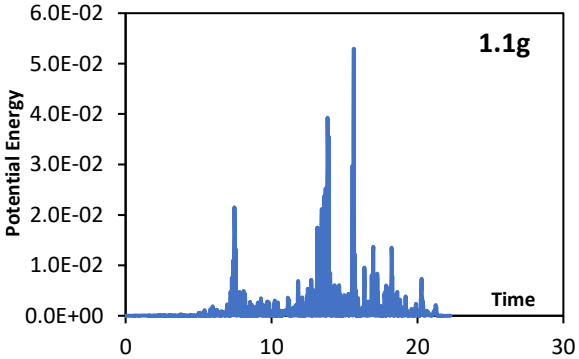

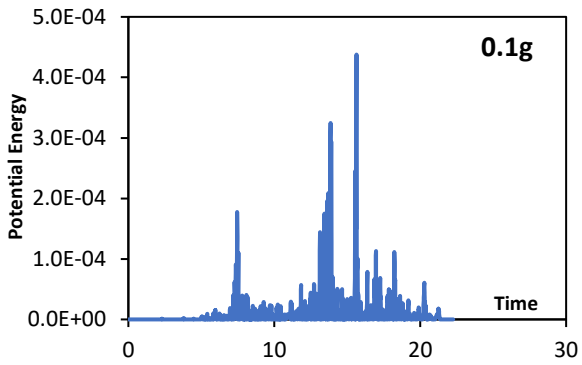

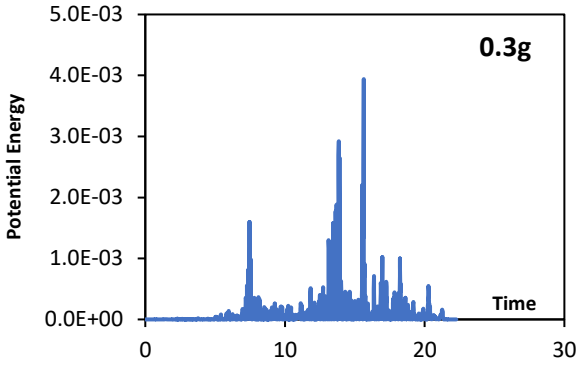

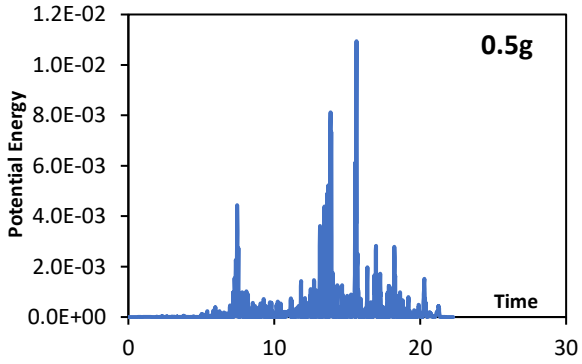

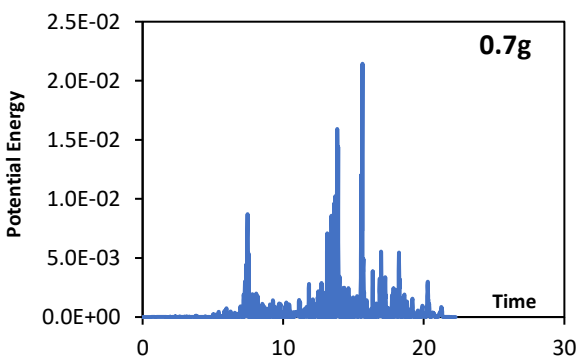

Superstition Hills-FF

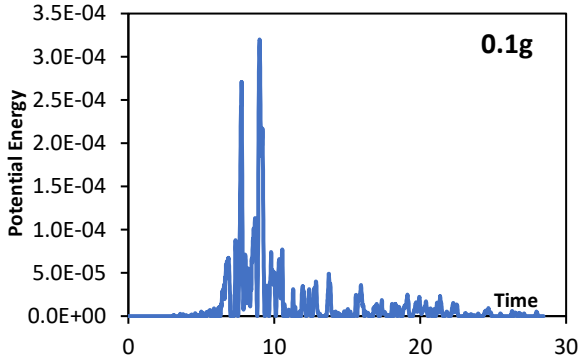

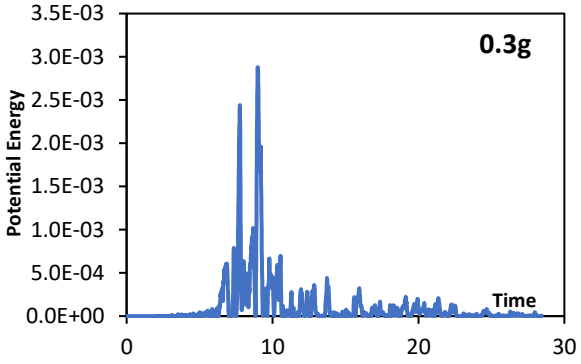

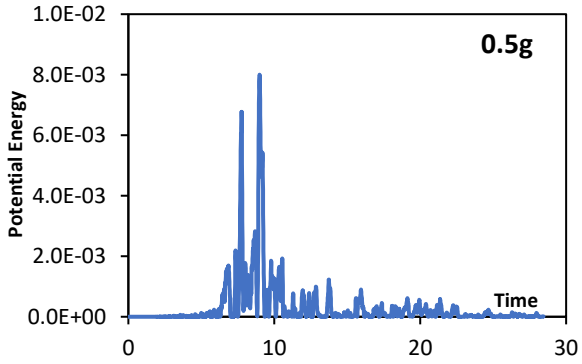

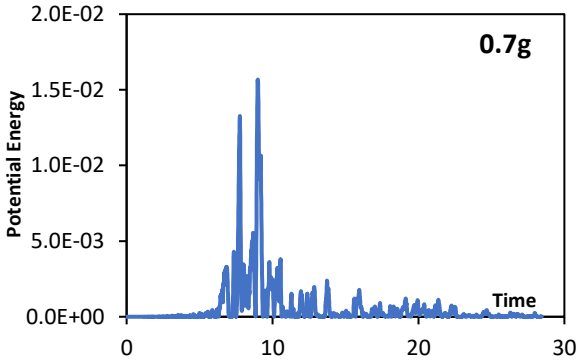

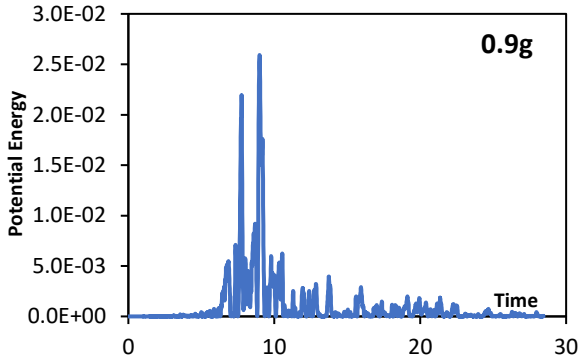
0.9g
Potential Energy
Time
3.0E-02
2.5E-02
2.0E-02
1.5E-02
1.0E-02
5.0E-03
0.0E+00
0
10
20
30

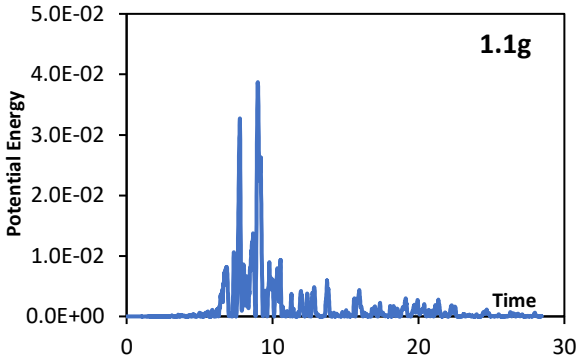
1.1g
Potential Energy
Time
5.0E-02
4.0E-02
3.0E-02
2.0E-02
1.0E-02
0.0E+00
0
10
20
30

Tottori-NF

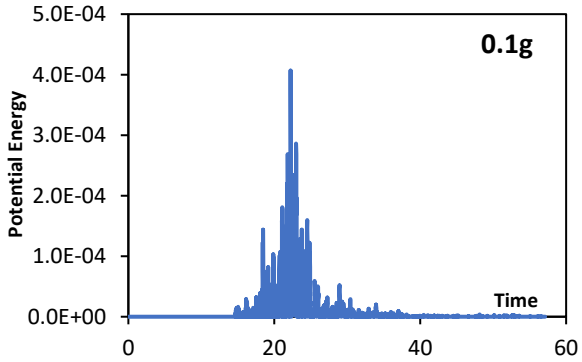
0.1g
Potential Energy
Time
5.0E-04
4.0E-04
3.0E-04
2.0E-04
1.0E-04
0.0E+00
0
20
40
60

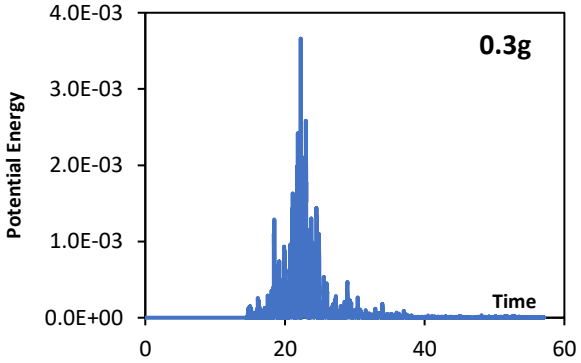
0.3g
Potential Energy
Time
4.0E-03
3.0E-03
2.0E-03
1.0E-03
0.0E+00
0
20
40
60

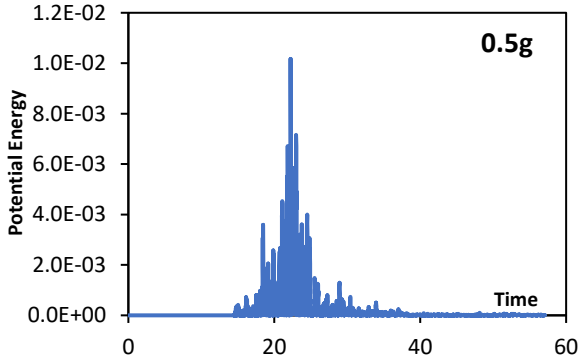
0.5g
Potential Energy
Time
1.2E-02
1.0E-02
8.0E-03
6.0E-03
4.0E-03
2.0E-03
0.0E+00
0
20
40
60

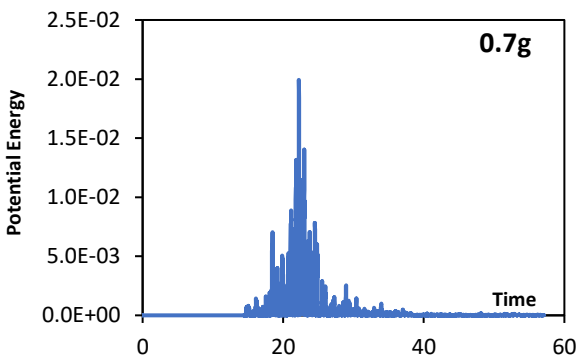
0.7g
Potential Energy
Time
2.5E-02
2.0E-02
1.5E-02
1.0E-02
5.0E-03
0.0E+00
0
20
40
60

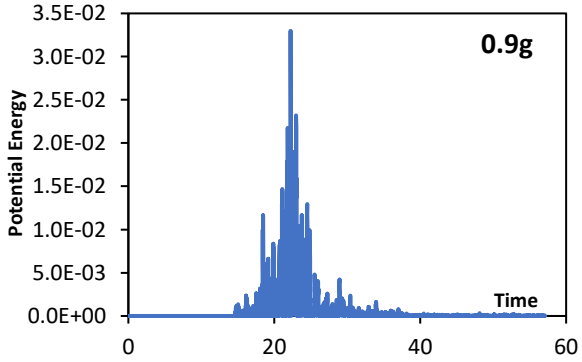
0.9g
Potential Energy
Time
3.5E-02
3.0E-02
2.5E-02
2.0E-02
1.5E-02
1.0E-02
5.0E-03
0.0E+00
0
20
40
60

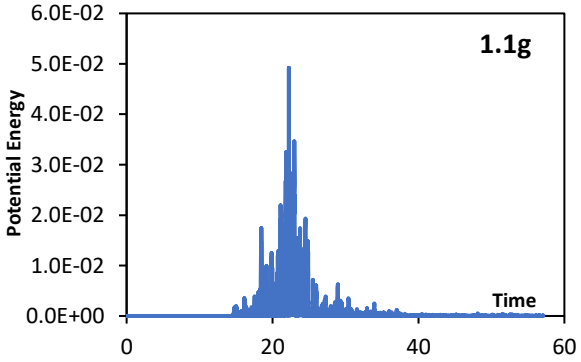
1.1g
Potential Energy
Time
6.0E-02
5.0E-02
4.0E-02
3.0E-02
2.0E-02
1.0E-02
0.0E+00
0
20
40
60

Tottori-FF

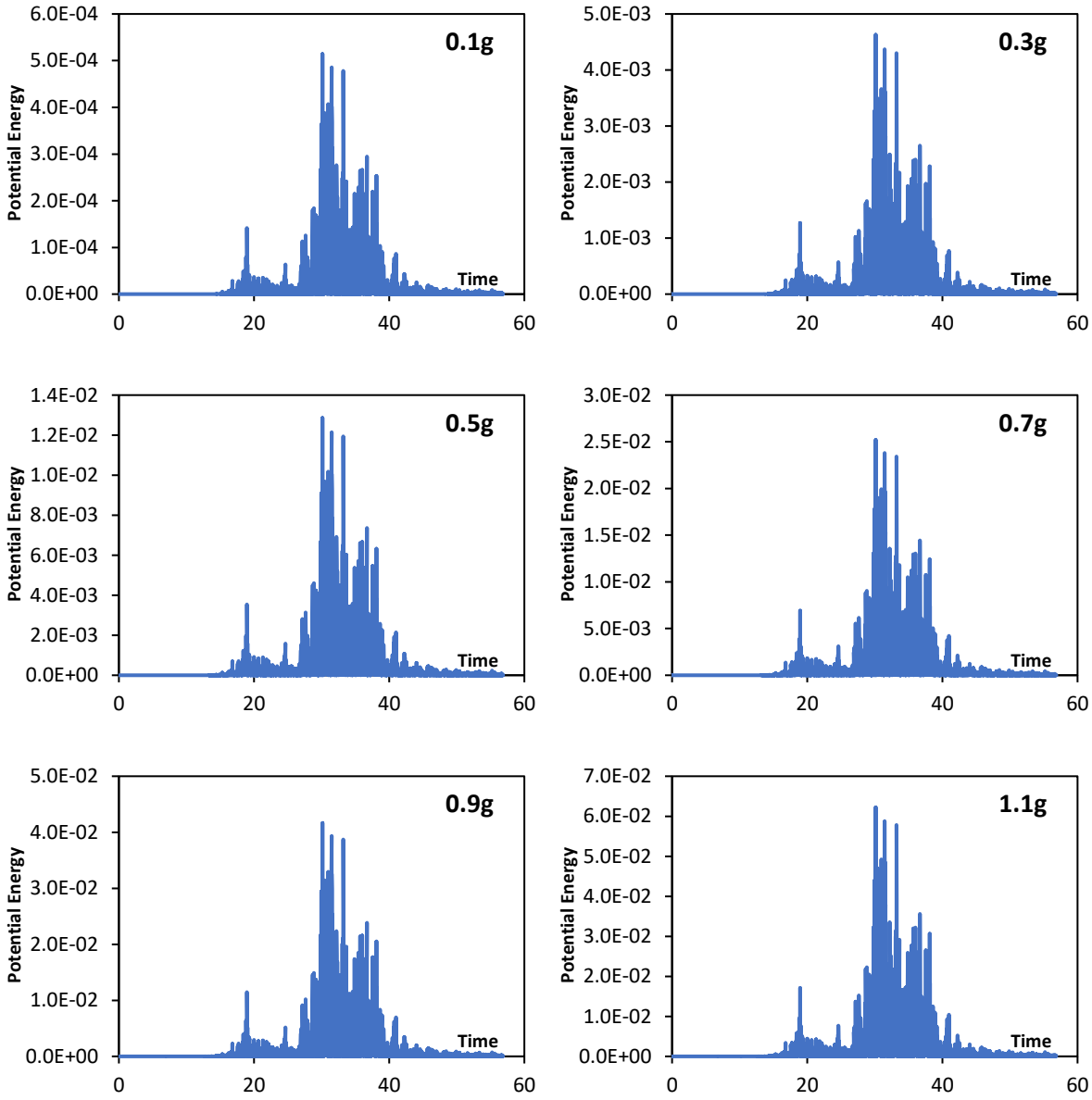

Westmorland-NF

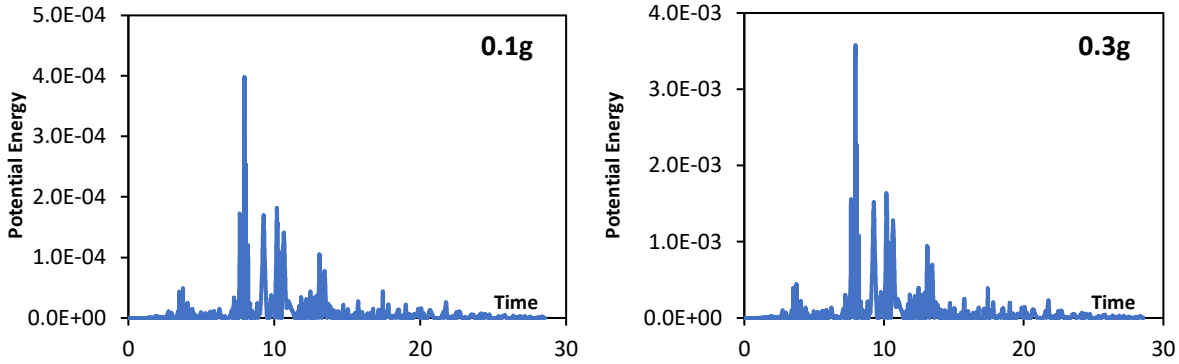

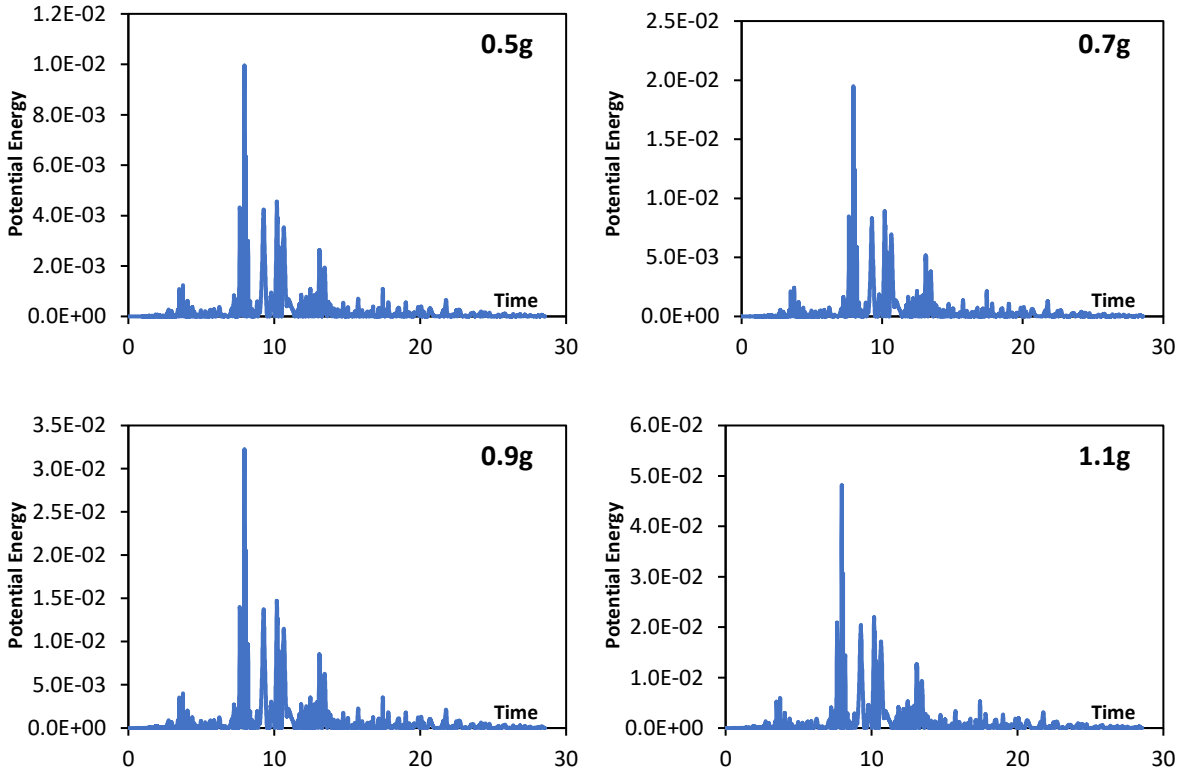

Westmorland-FF

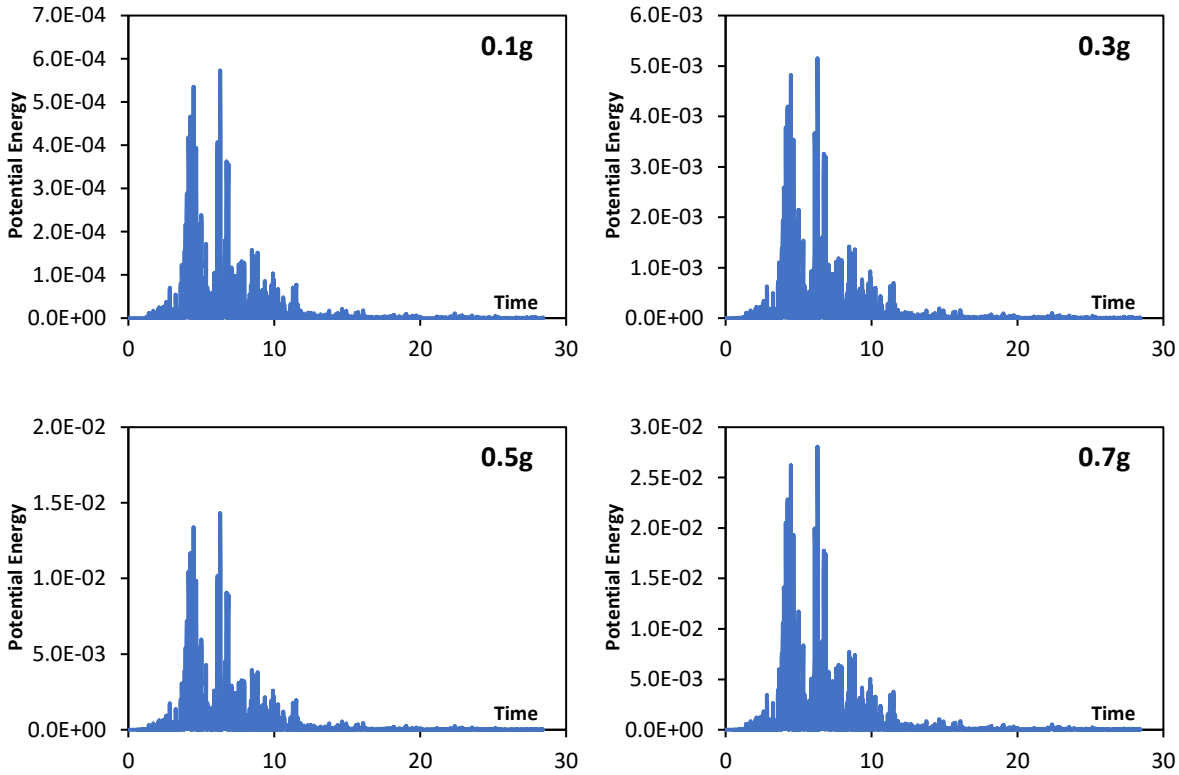

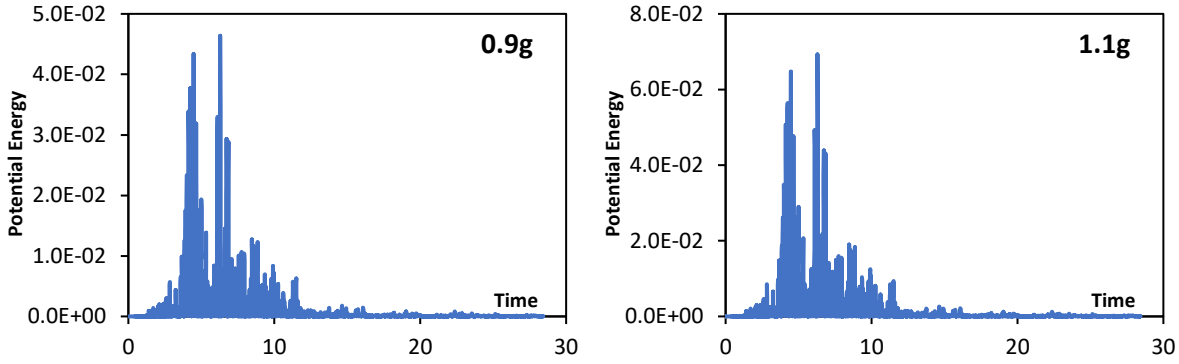

Base Shear

Bam-NF

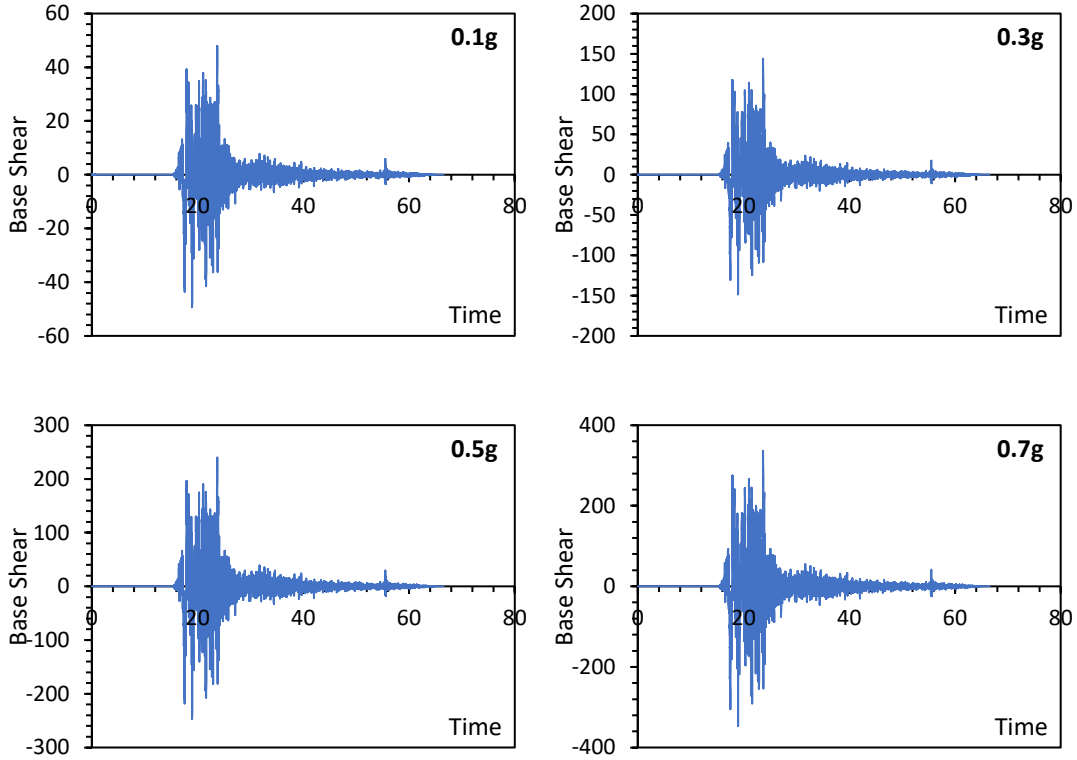

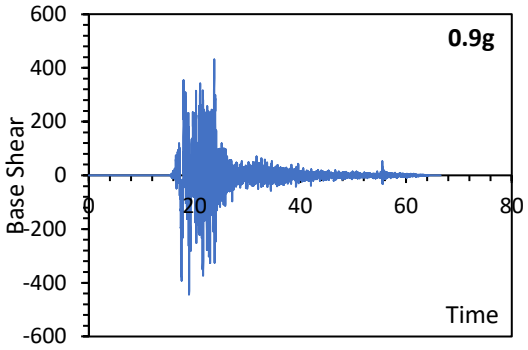
0.9g
Base Shear
Time
600
400
200
0
-200
-400
-600
0
20
40
60
80

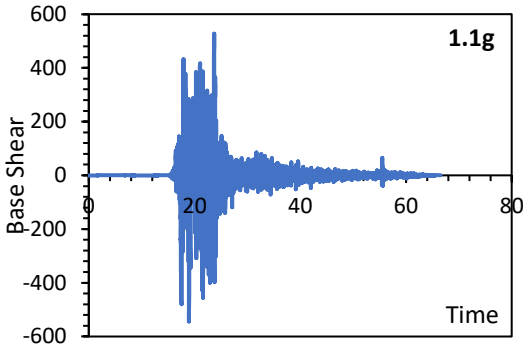
1.1g
Base Shear
Time
600
400
200
0
-200
-400
-600
0
20
40
60
80

Bam-FF

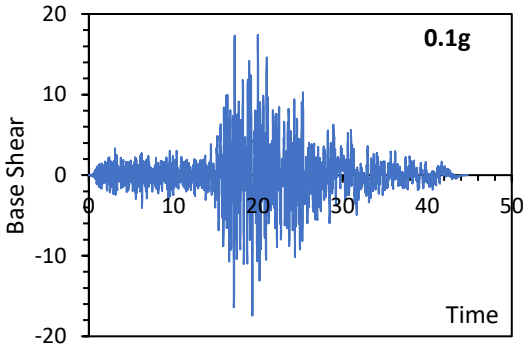
0.1g
Base Shear
Time
20
10
0
-10
-20
0
10
20
30
40
50

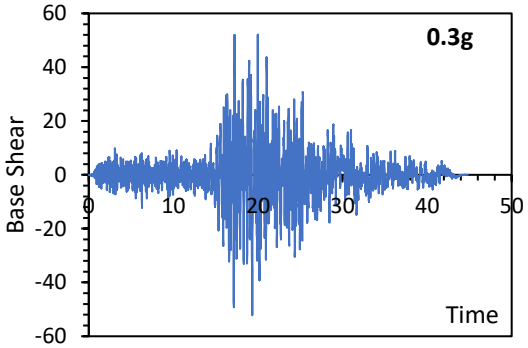
0.3g
Base Shear
Time
60
40
20
0
-20
-40
-60
0
10
20
30
40
50

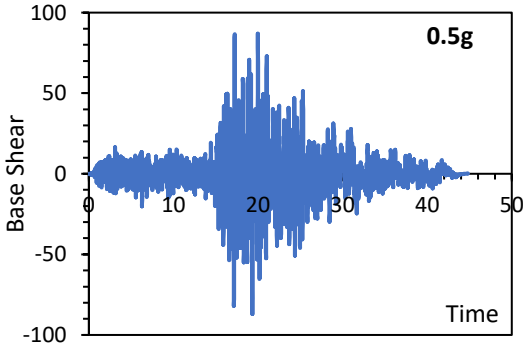
0.5g
Base Shear
Time
100
50
0
-50
-100
0
10
20
30
40
50

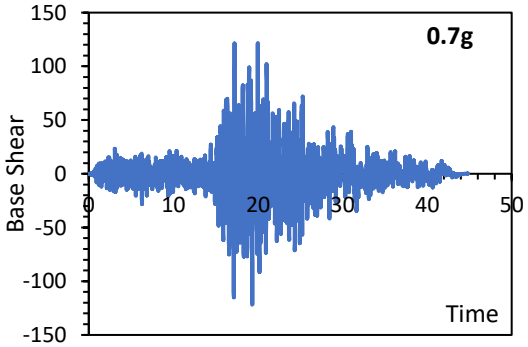
0.7g
Base Shear
Time
150
100
50
0
-50
-100
-150
0
10
20
30
40
50

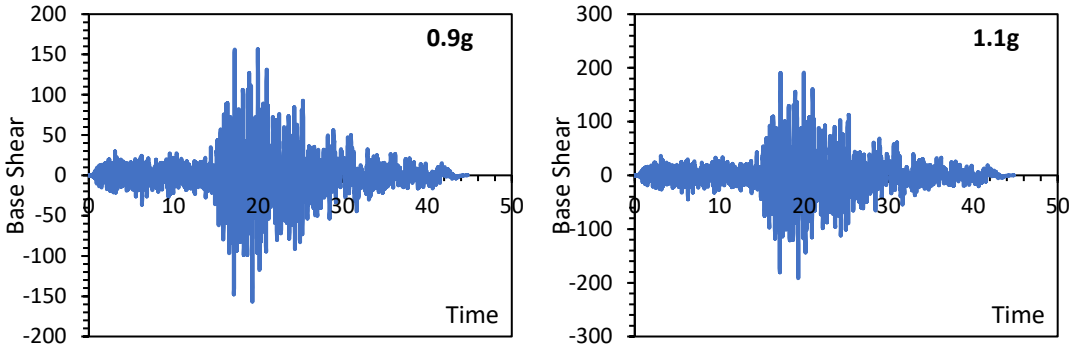

Cape Mendocino-NF

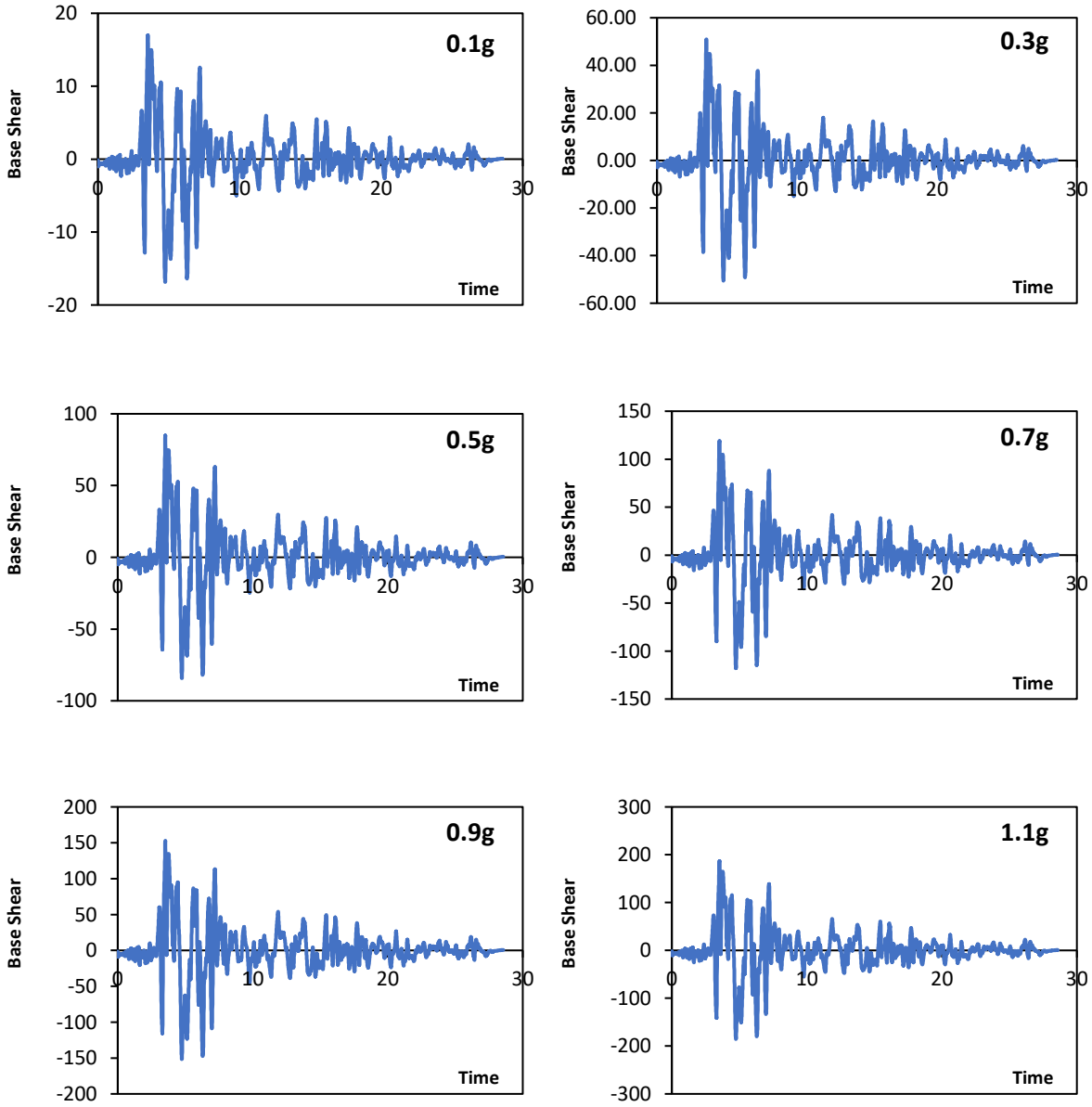

Cape Mendocino-FF

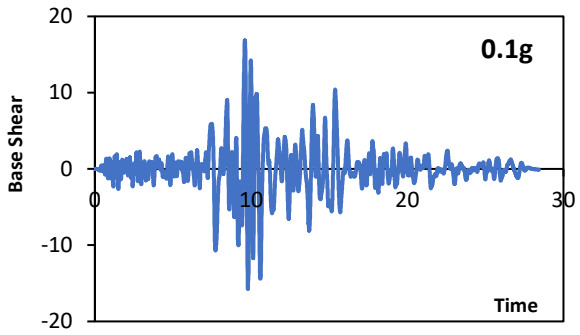

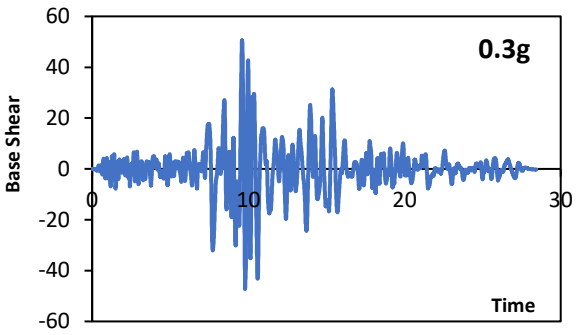

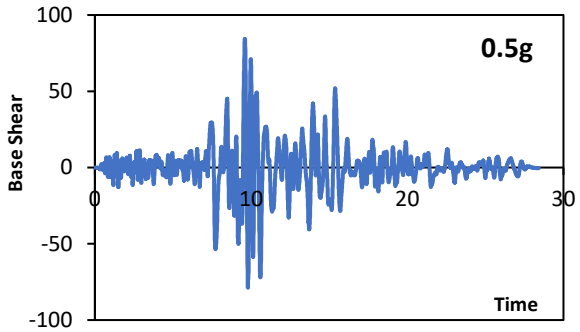

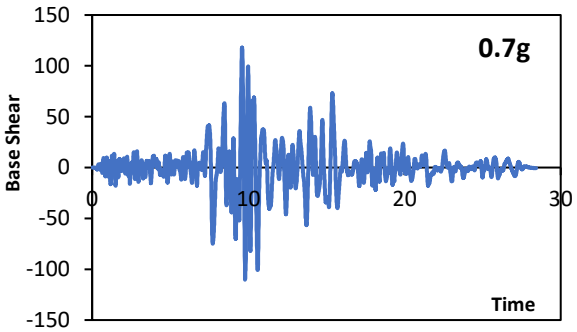

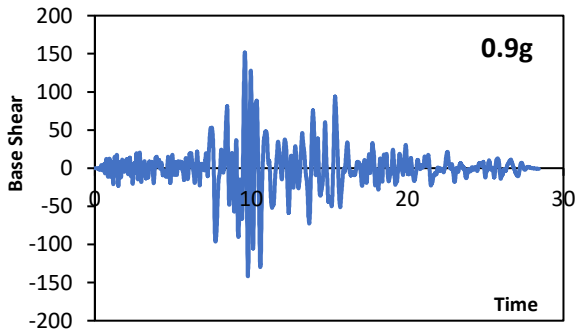

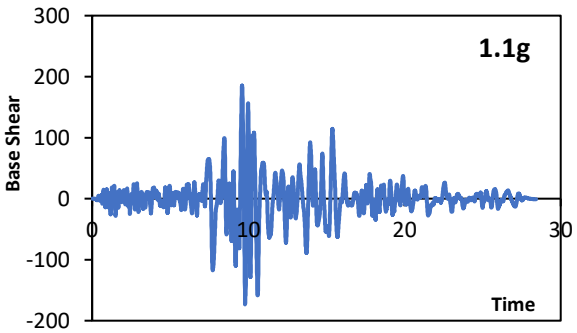

Christchurch-NF

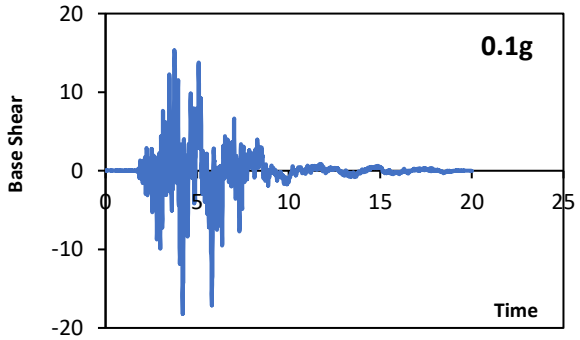

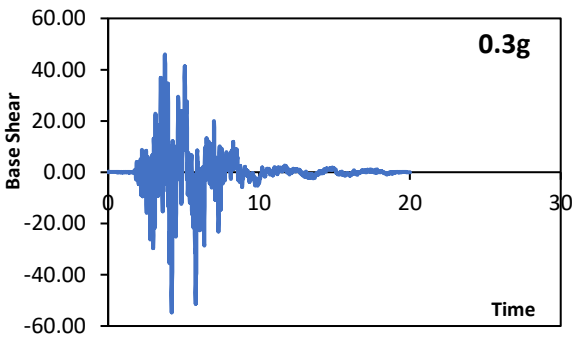

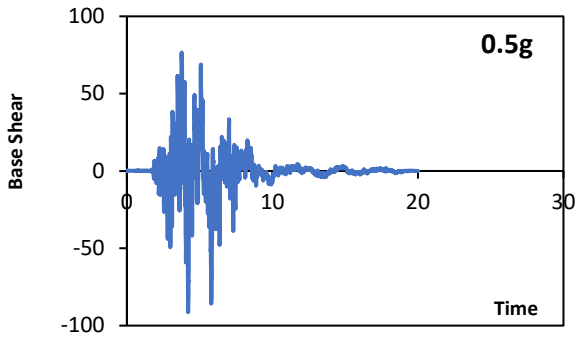

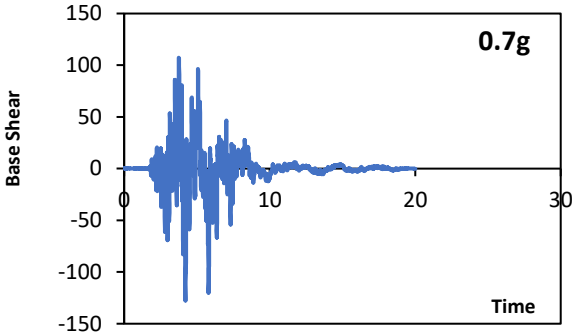

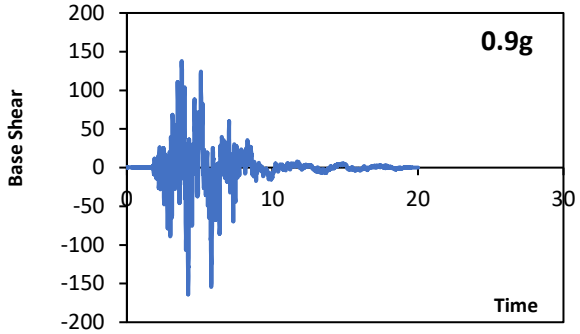

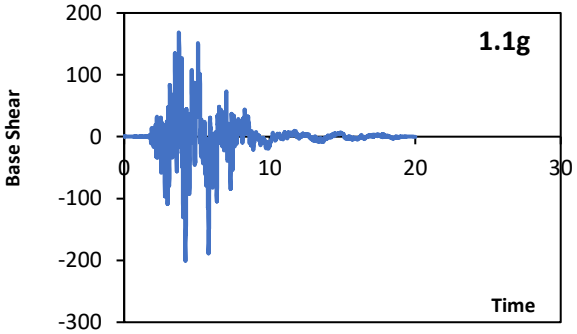

Christchurch-FF

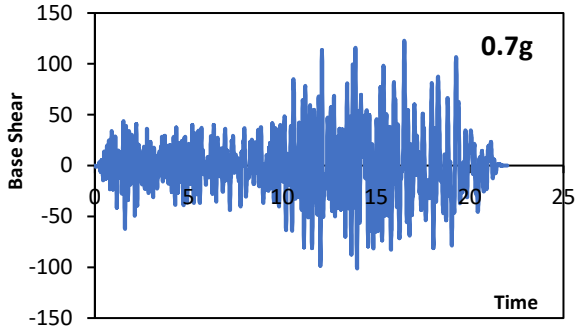

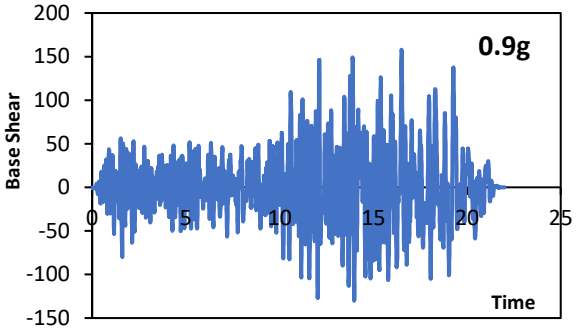

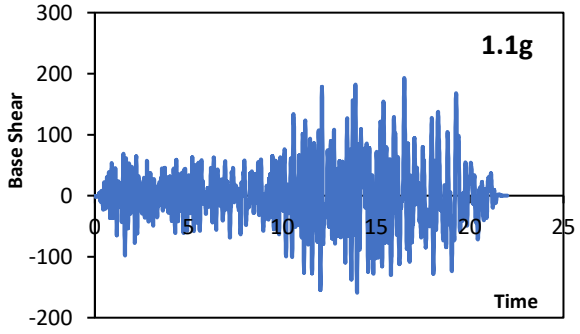

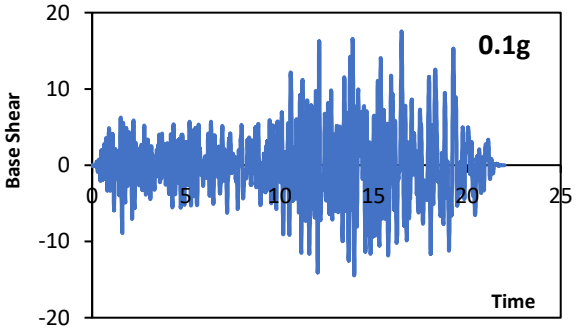

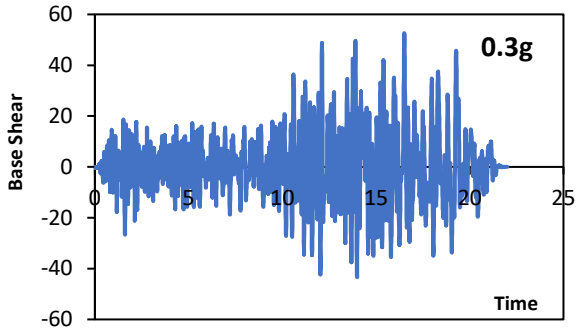

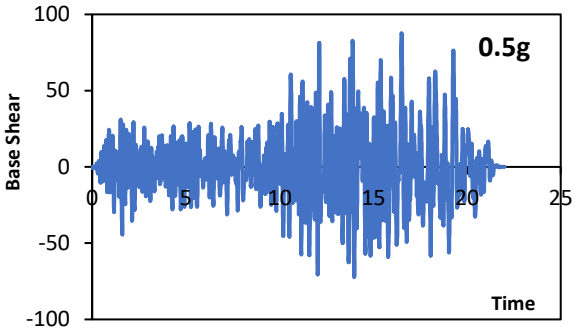

Chetsu-oki-NF

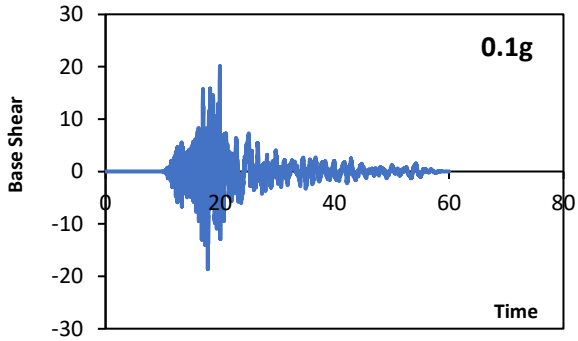

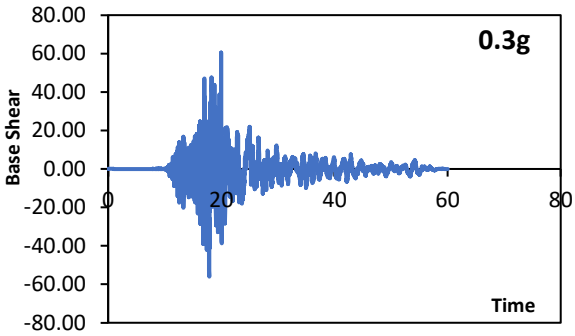

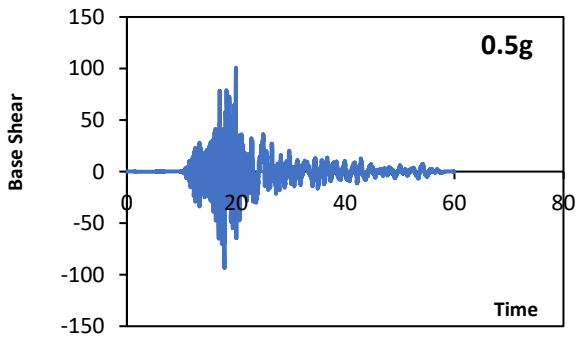

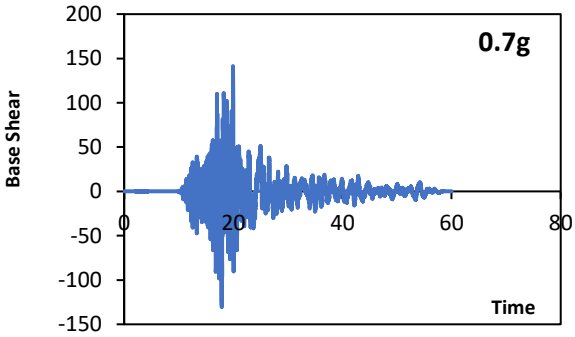

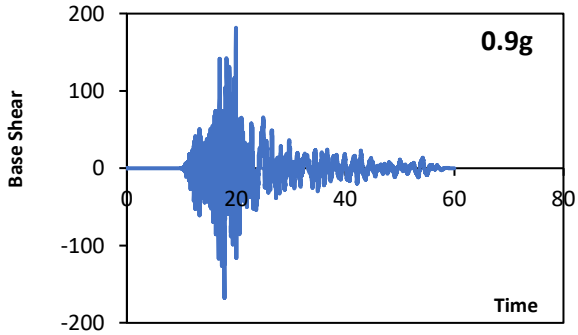

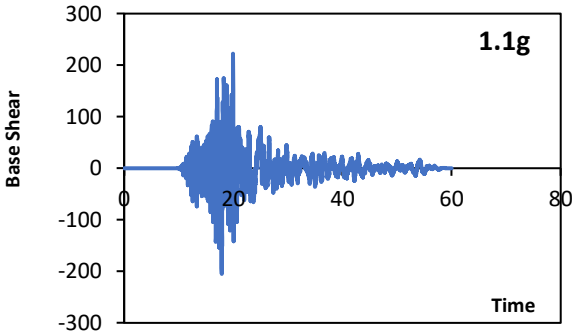

Chetsu-oki-FF

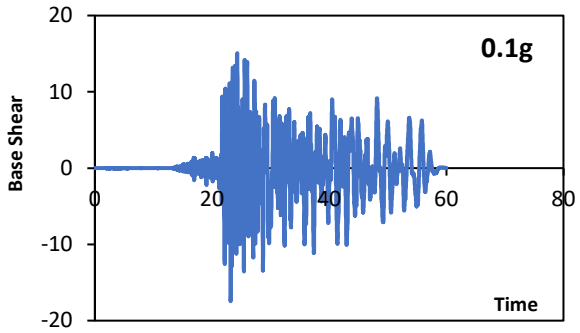

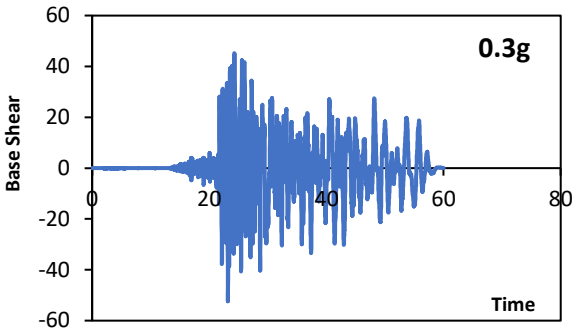

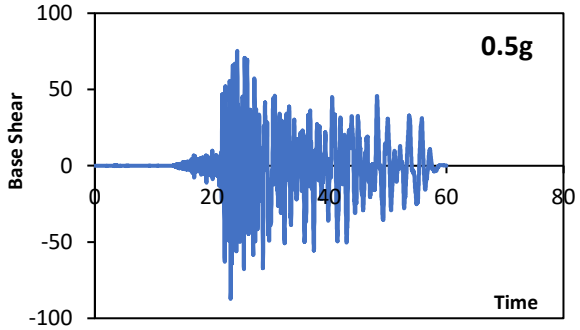

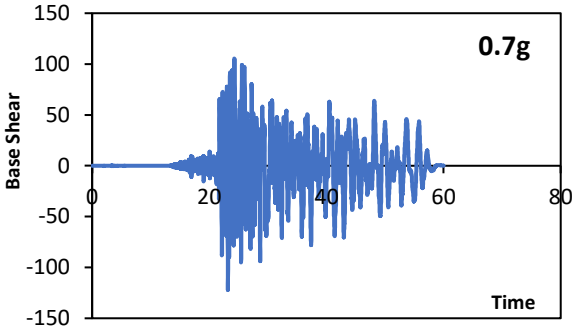

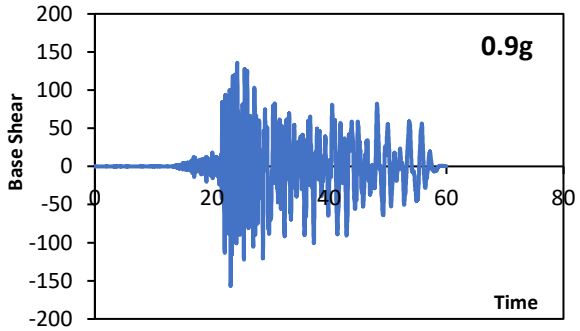

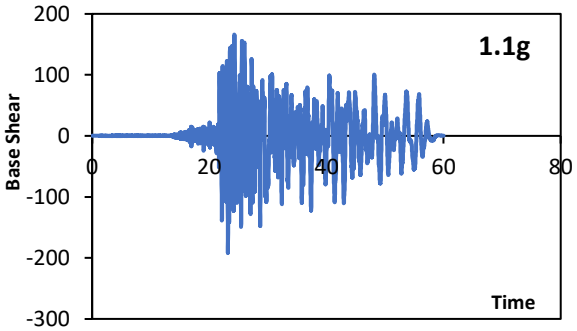

Imperial Valley-NF

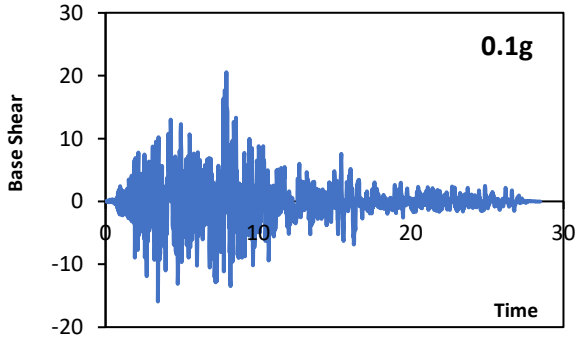

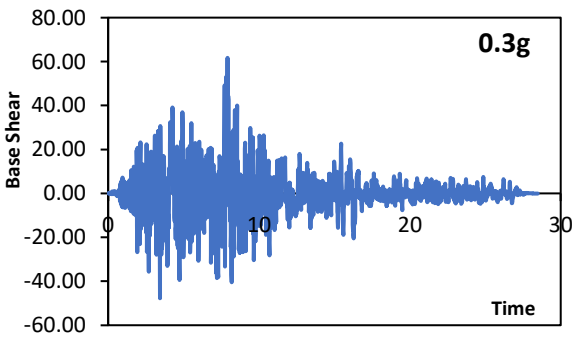

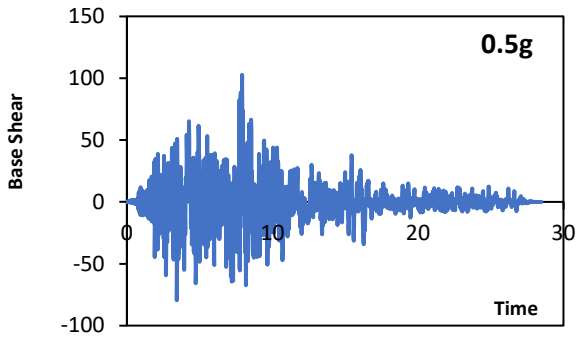

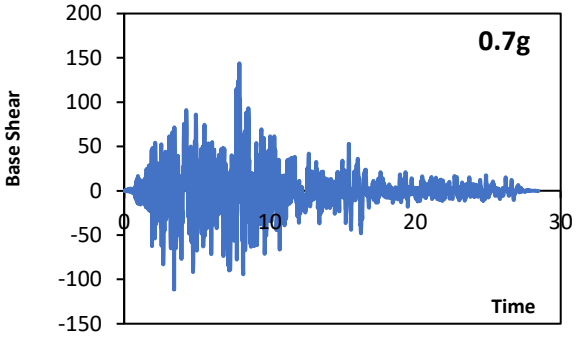

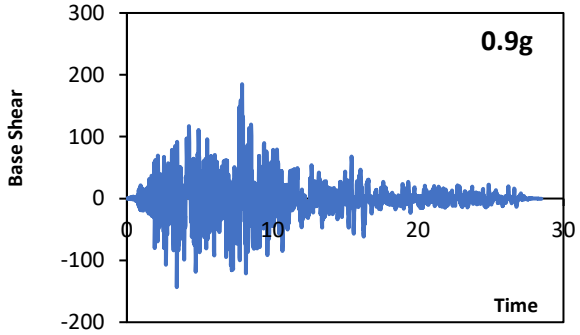

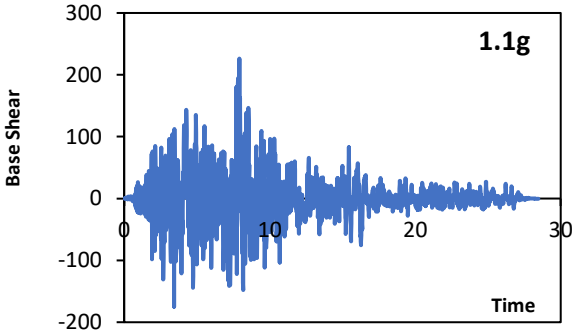

Imperial Valley-FF

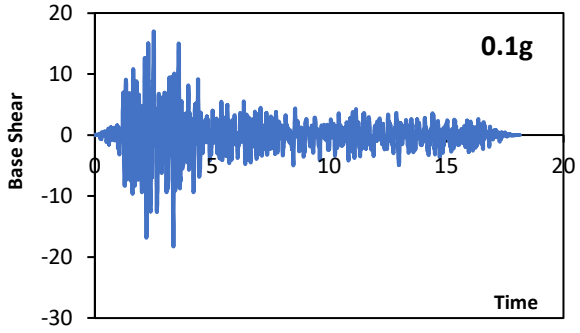

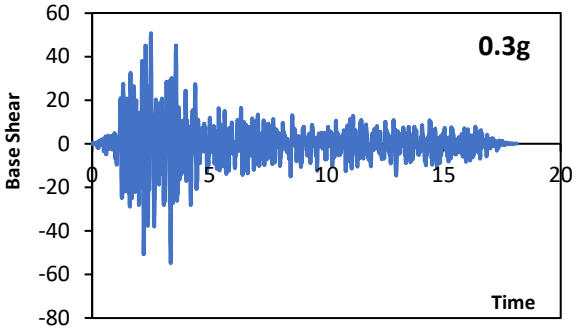

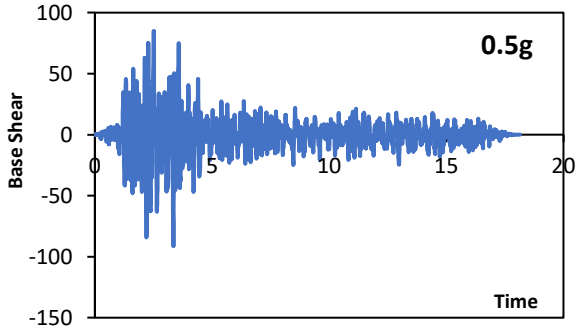

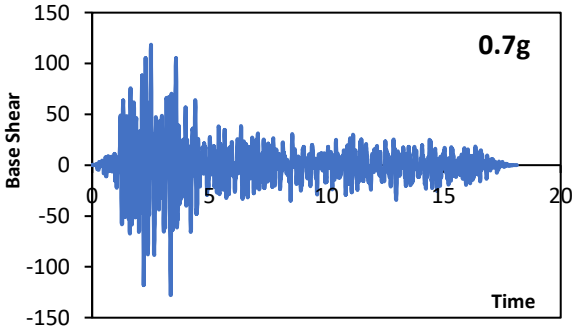

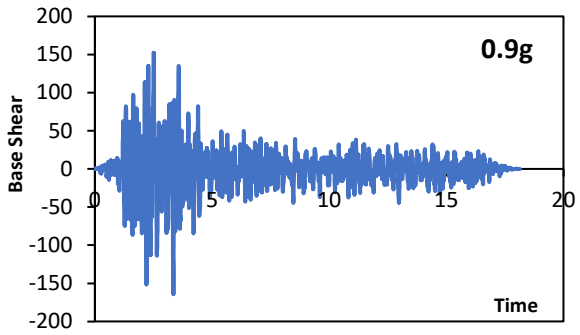
0.9g
Base Shear
Time
200
150
100
50
0
-50
-100
-150
-200
0
5
10
15
20

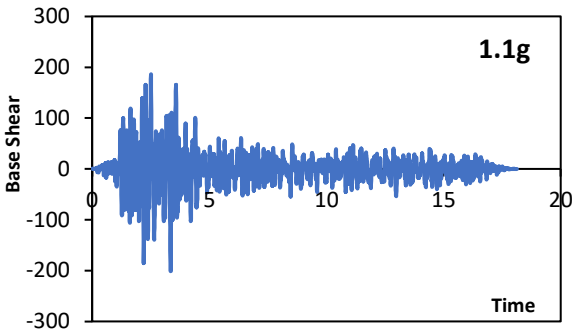
1.1g
Base Shear
Time
300
200
100
0
-100
-200
-300
0
5
10
15
20

Irpinia-NF

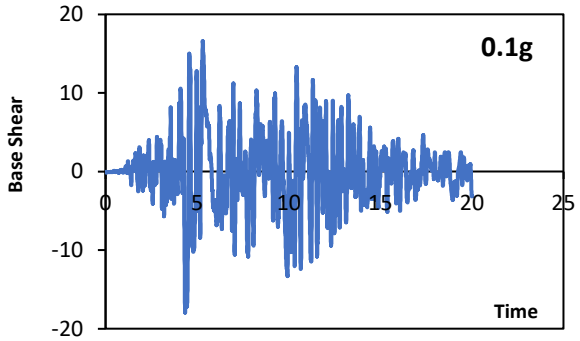
0.1g
Base Shear
Time
20
10
0
-10
-20
0
5
10
15
20
25

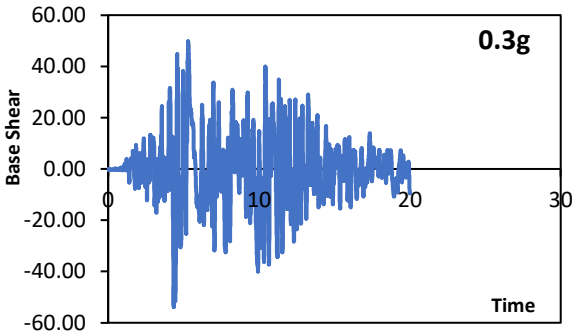
0.3g
Base Shear
Time
60.00
40.00
20.00
0.00
-20.00
-40.00
-60.00
0
10
20
30

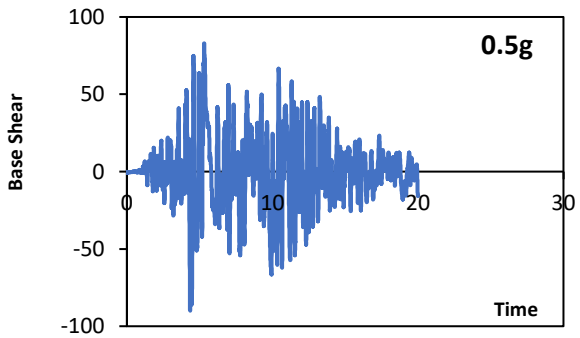
0.5g
Base Shear
Time
100
50
0
-50
-100
0
10
20
30

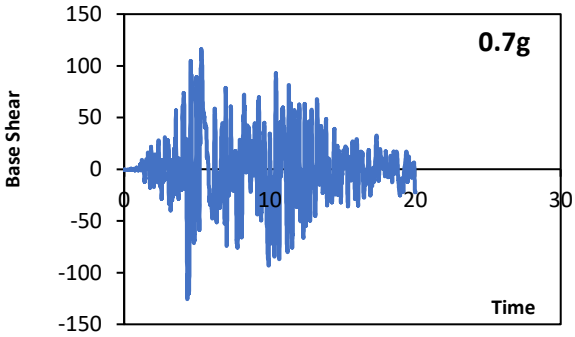
0.7g
Base Shear
Time
150
100
50
0
-50
-100
-150
0
10
20
30

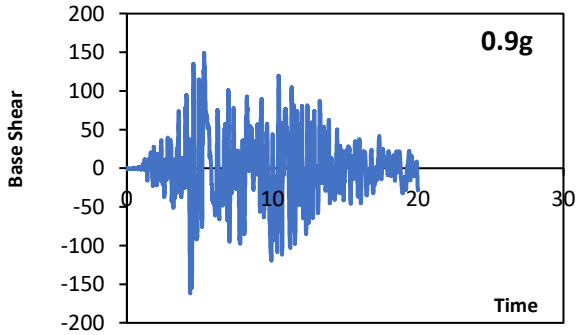
0.9g
Base Shear
Time
200
150
100
50
0
-50
-100
-150
-200
0
10
20
30

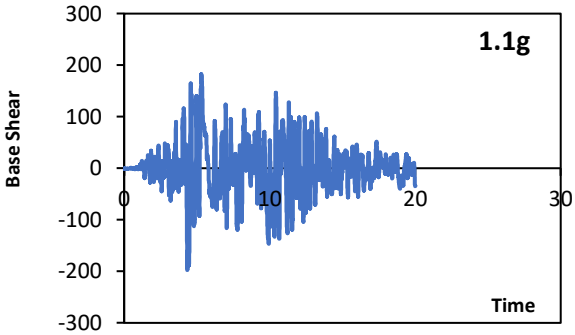
1.1g
Base Shear
Time
300
200
100
0
-100
-200
-300
0
10
20
30

Irpinia-FF

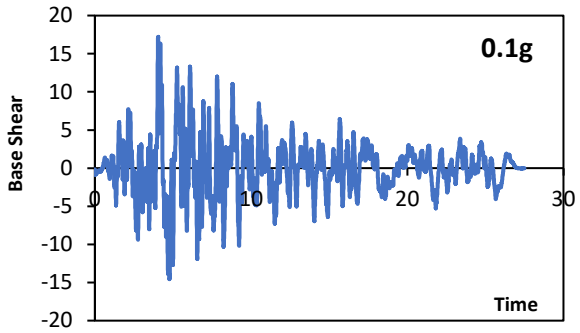

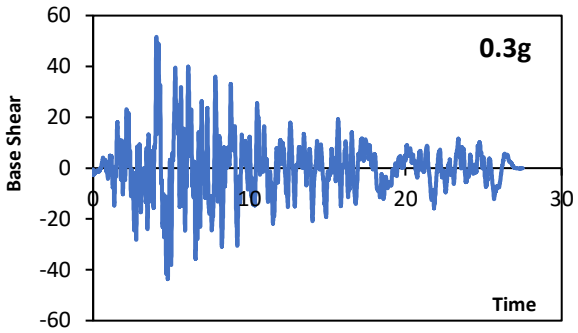

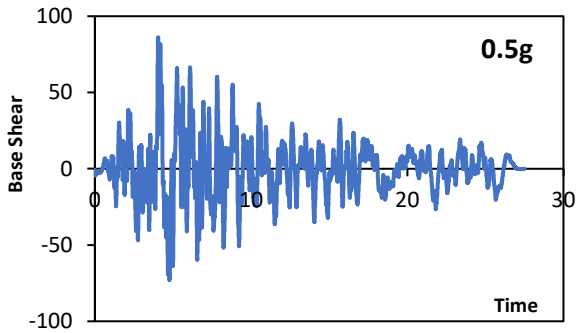

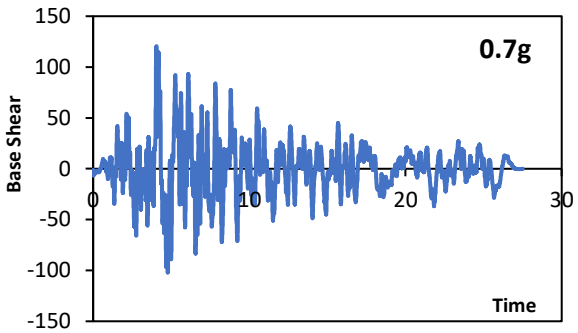

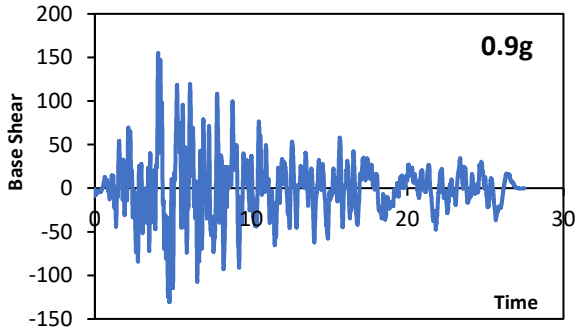

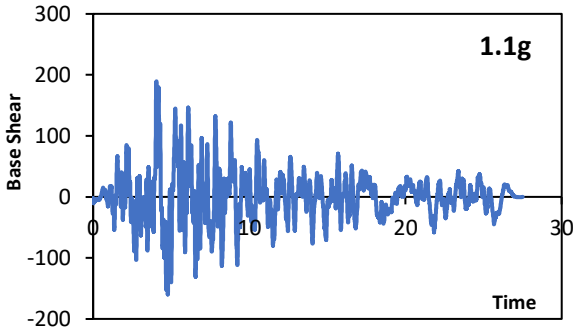

Kalamata-NF

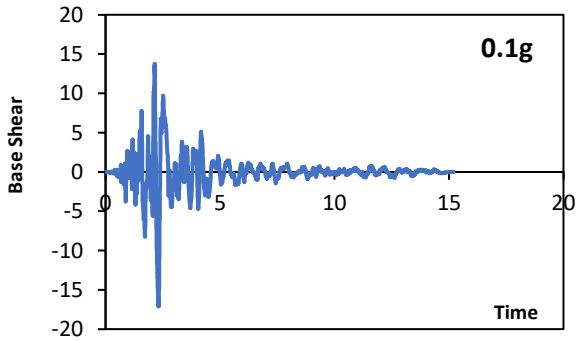

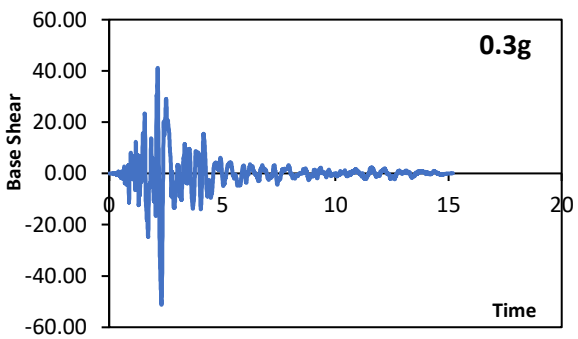

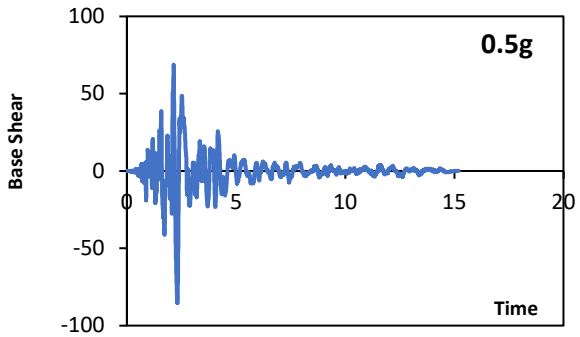
0.5g
Base Shear
Time
100
50
0
-50
-100
0
5
10
15
20

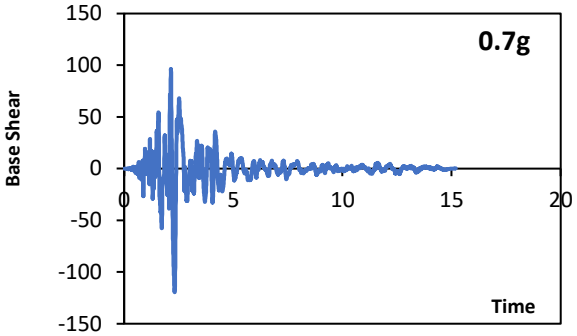
0.7g
Base Shear
Time
150
100
50
0
-50
-100
-150
0
5
10
15
20

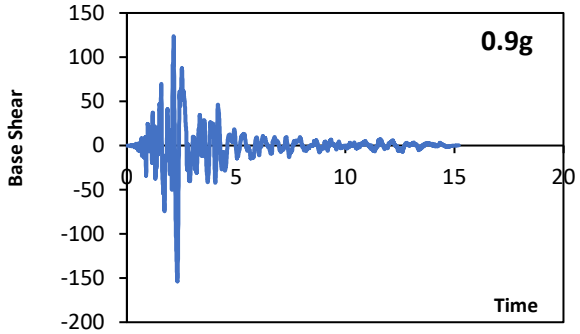
0.9g
Base Shear
Time
150
100
50
0
-50
-100
-150
-200
0
5
10
15
20

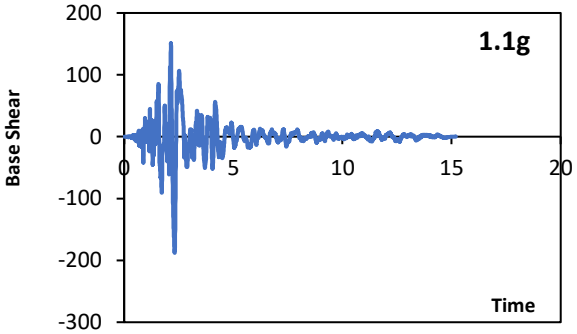
1.1g
Base Shear
Time
200
100
0
-100
-200
-300
0
5
10
15
20

Kobe-NF

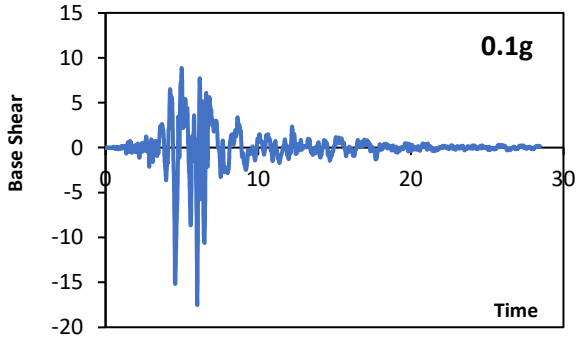
0.1g
Base Shear
Time
15
10
5
0
-5
-10
-15
-20
0
10
20
30

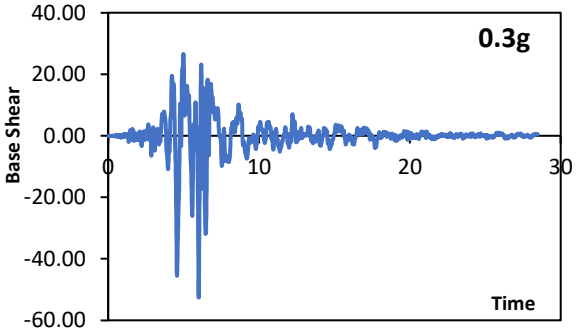
0.3g
Base Shear
Time
40.00
20.00
0.00
-20.00
-40.00
-60.00
0
10
20
30

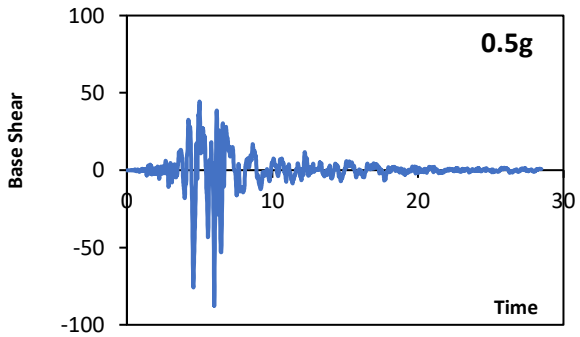
0.5g
Base Shear
Time
100
50
0
-50
-100
0
10
20
30

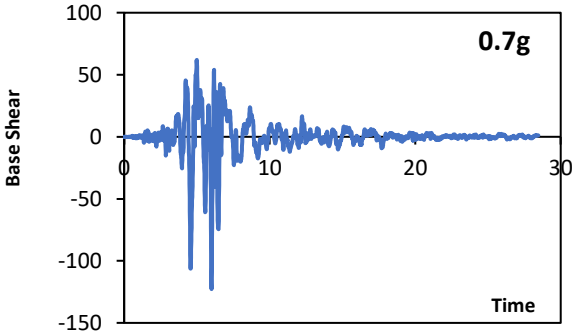
0.7g
Base Shear
Time
100
50
0
-50
-100
-150
0
10
20
30

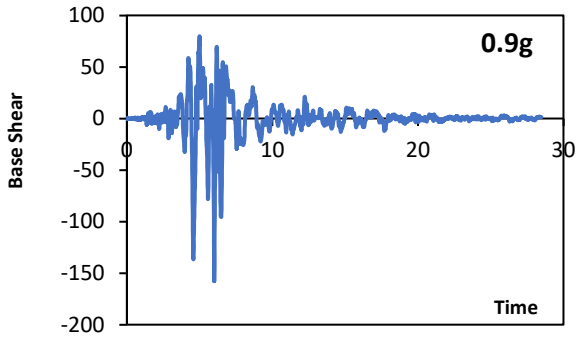
0.9g
Base Shear
Time
100
50
0
-50
-100
-150
-200
0
10
20
30

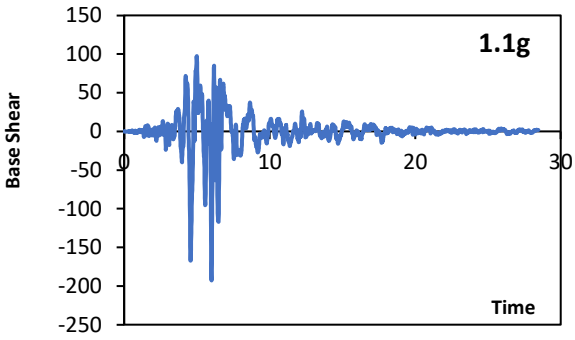
1.1g
Base Shear
Time
150
100
50
0
-50
-100
-150
-200
-250
0
10
20
30

Kobe-FF

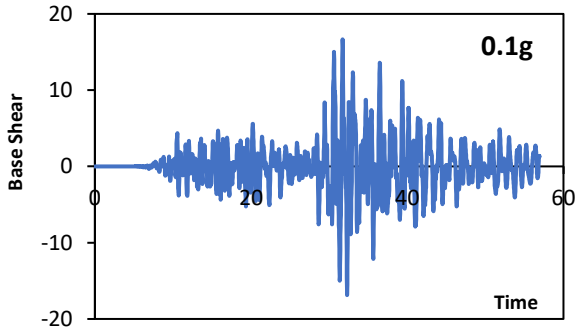
0.1g
Base Shear
Time
20
10
0
-10
-20
0
20
40
60

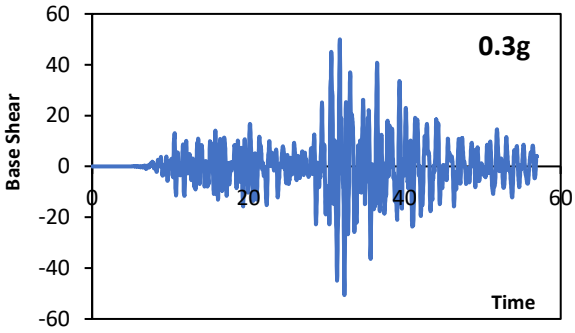
0.3g
Base Shear
Time
60
40
20
0
-20
-40
-60
0
20
40
60

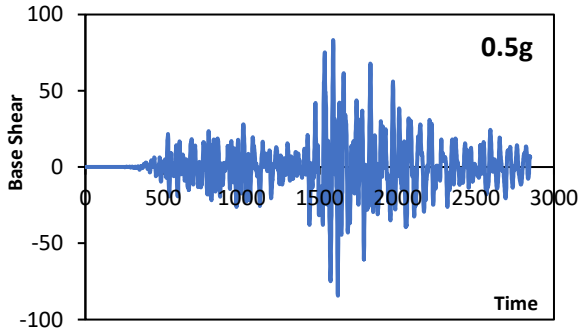
0.5g
Base Shear
Time
100
50
0
-50
-100
0
500
1000
1500
2000
2500
3000

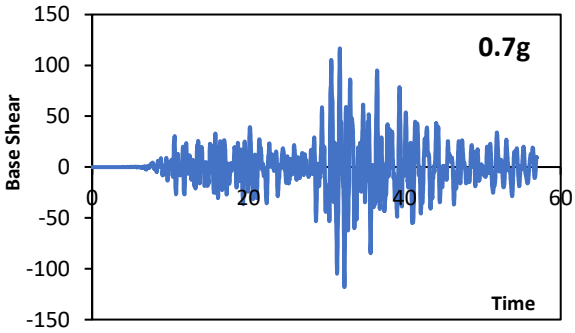
0.7g
Base Shear
Time
150
100
50
0
-50
-100
-150
0
20
40
60

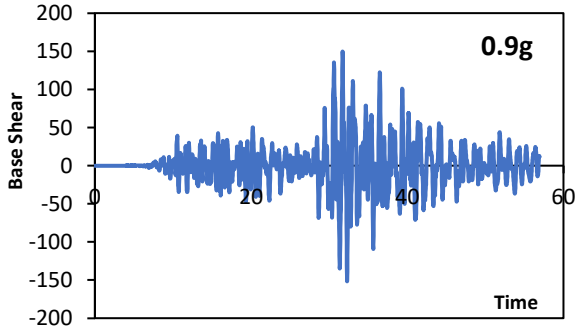
0.9g
Base Shear
Time
200
150
100
50
0
-50
-100
-150
-200
0
20
40
60

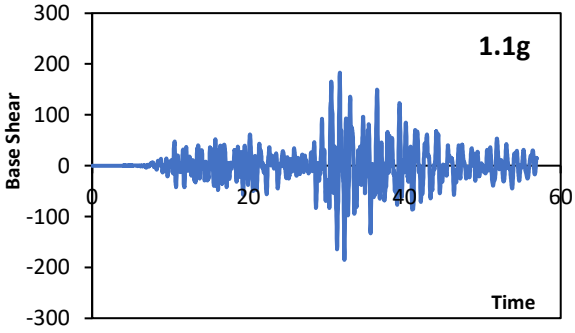
1.1g
Base Shear
Time
300
200
100
0
-100
-200
-300
0
20
40
60

Kocaeli-NF

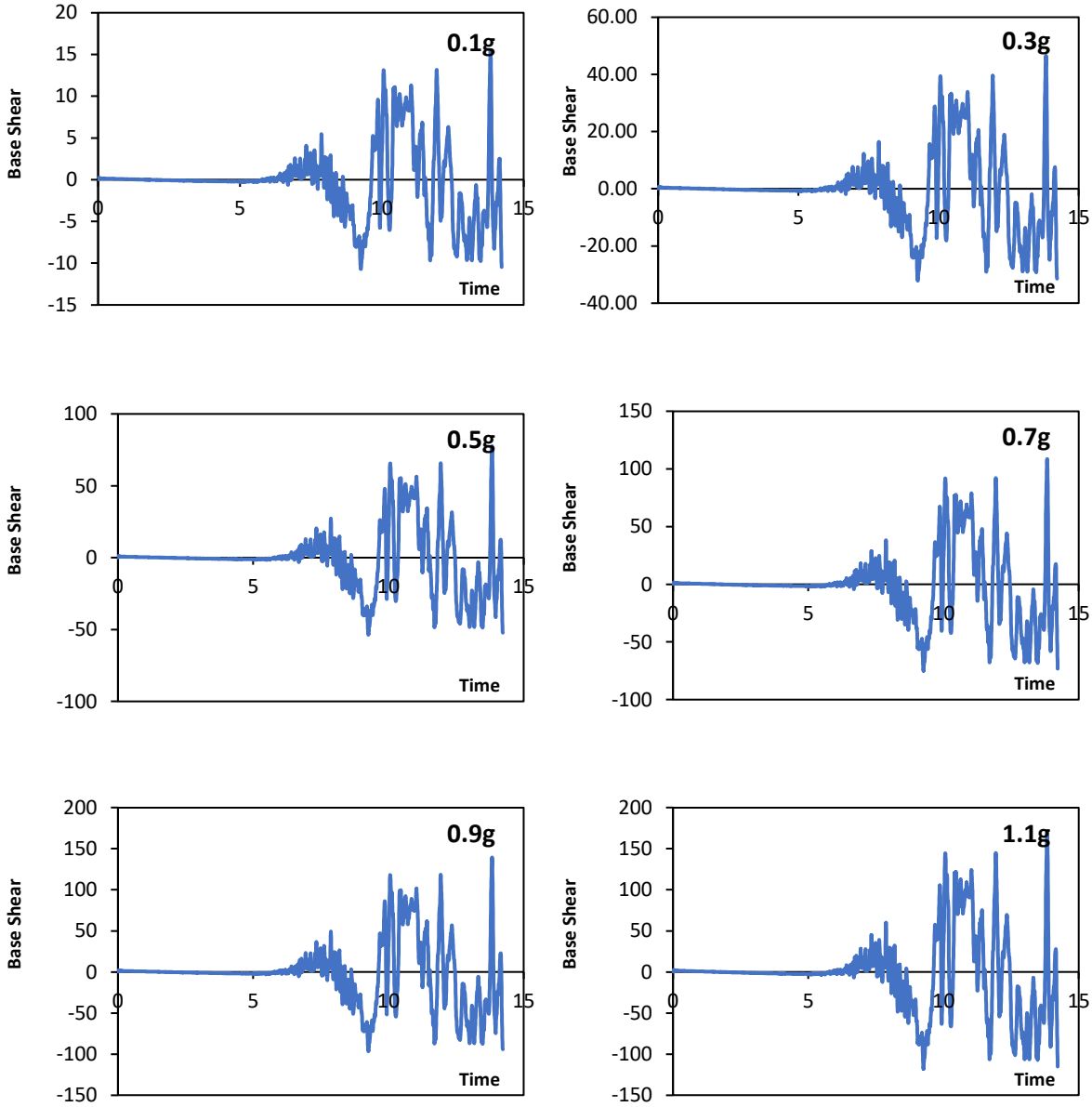

Kocaeli-FF

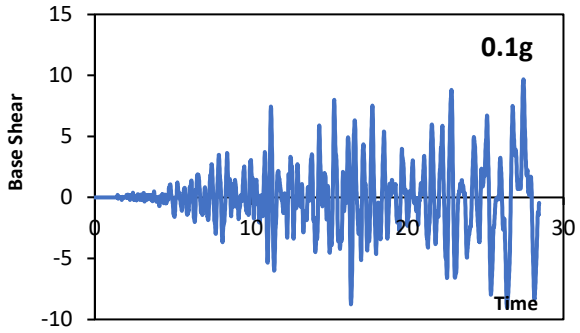
0.1g
Base Shear
Time
15
10
5
0
-5
-10
0
10
20
30

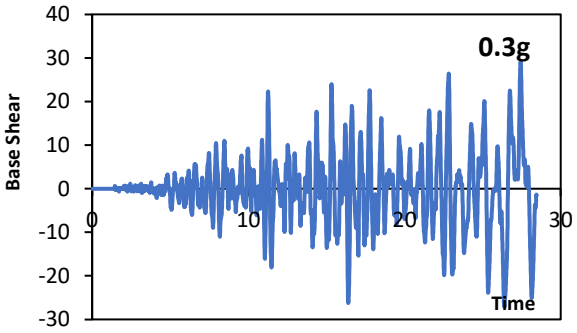
0.3g
Base Shear
Time
40
30
20
10
0
-10
-20
-30
0
10
20
30

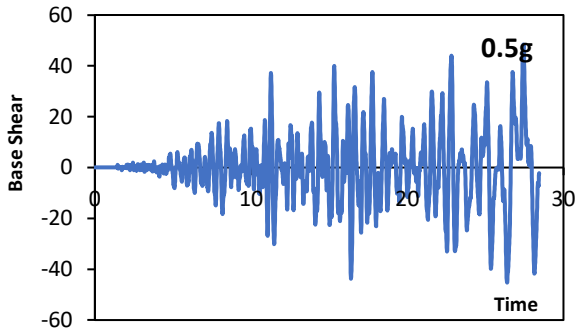
0.5g
Base Shear
Time
60
40
20
0
-20
-40
-60
0
10
20
30

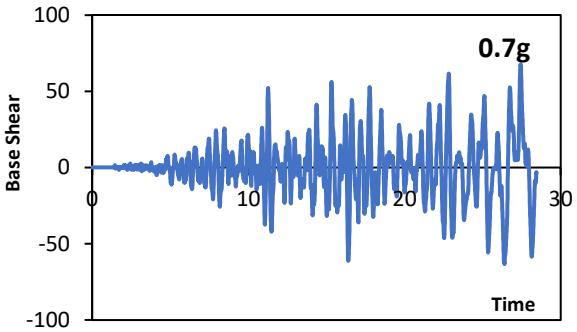
0.7g
Base Shear
Time
100
50
0
-50
-100
0
10
20
30

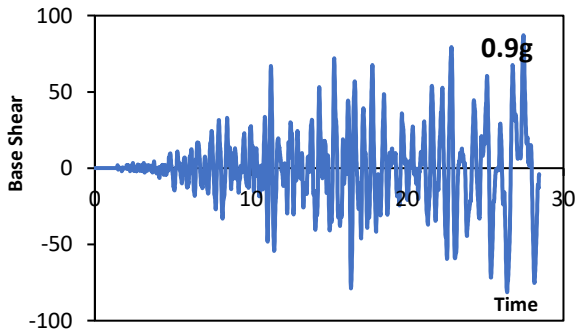
0.9g
Base Shear
Time
100
50
0
-50
-100
0
10
20
30

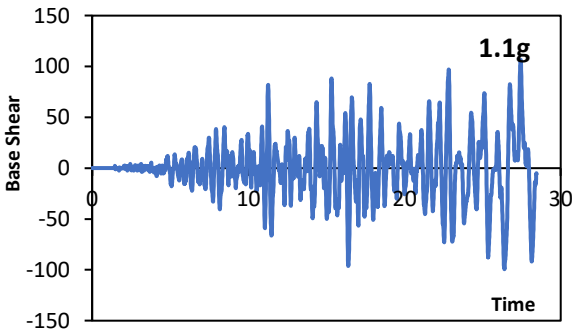
1.1g
Base Shear
Time
150
100
50
0
-50
-100
-150
0
10
20
30

Landers-NF

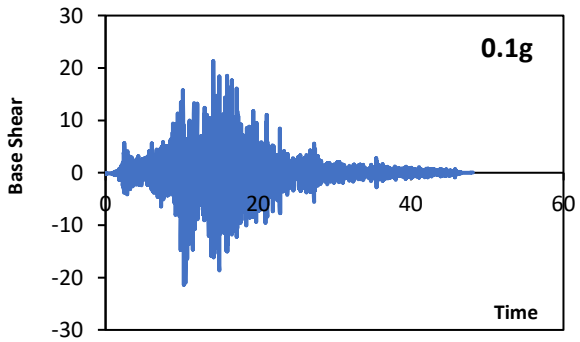
0.1g
Base Shear
Time
30
20
10
0
-10
-20
-30
0
20
40
60

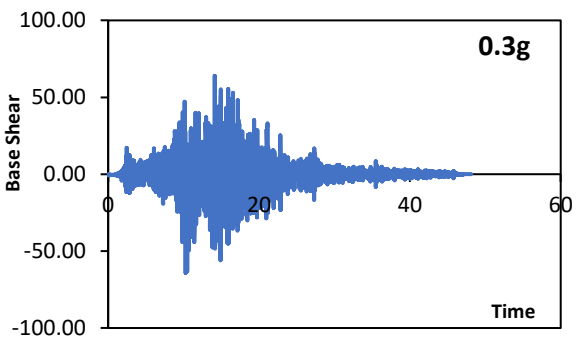
0.3g
Base Shear
Time
100.00
50.00
0.00
-50.00
-100.00
0
20
40
60

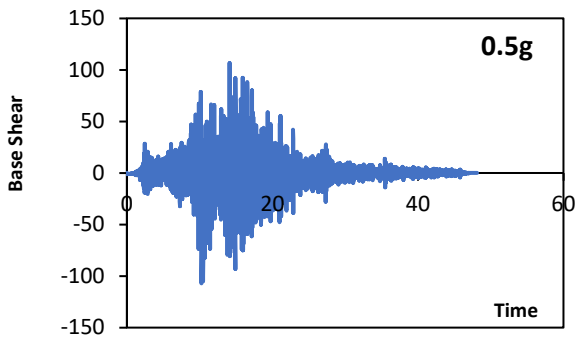
0.5g
Base Shear
Time
150
100
50
0
-50
-100
-150
0
20
40
60

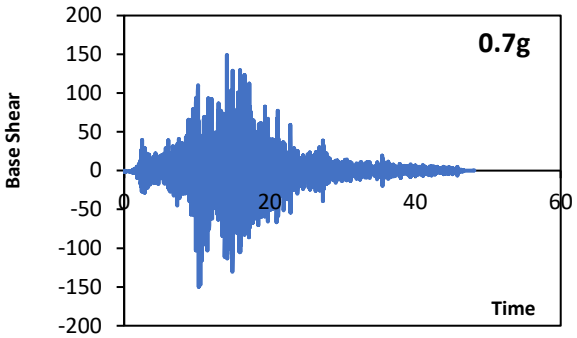
0.7g
Base Shear
Time
200
150
100
50
0
-50
-100
-150
-200
0
20
40
60

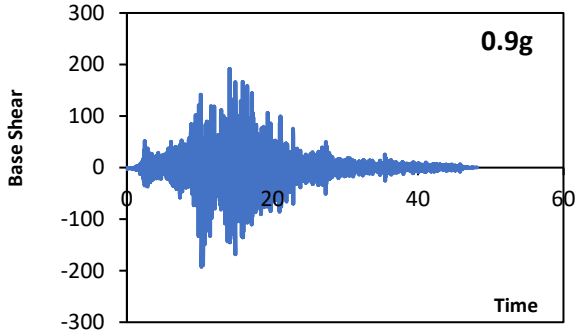
0.9g
Base Shear
Time
300
200
100
0
-100
-200
-300
0
20
40
60

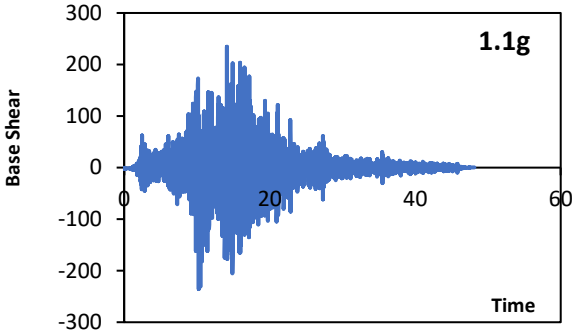
1.1g
Base Shear
Time
300
200
100
0
-100
-200
-300
0
20
40
60

Landers-FF

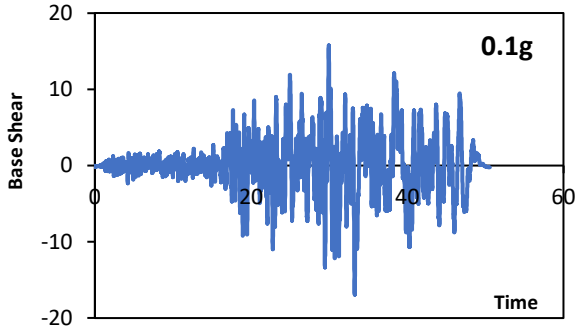
0.1g
Base Shear
Time
20
10
0
-10
-20
0
20
40
60

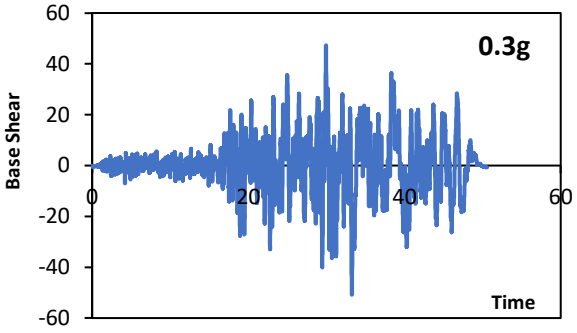
0.3g
Base Shear
Time
60
40
20
0
-20
-40
-60
0
20
40
60

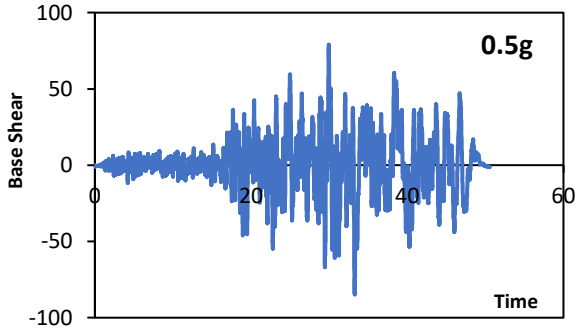
0.5g
Base Shear
Time
100
50
0
-50
-100
0
20
40
60

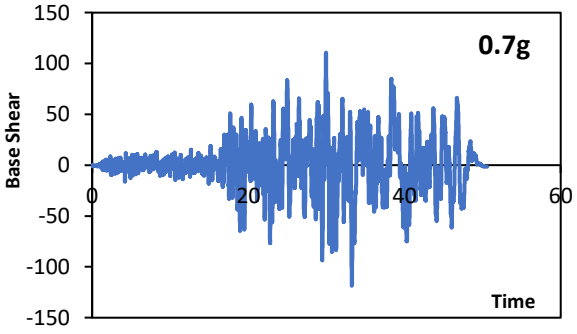
0.7g
Base Shear
Time
150
100
50
0
-50
-100
-150
0
20
40
60

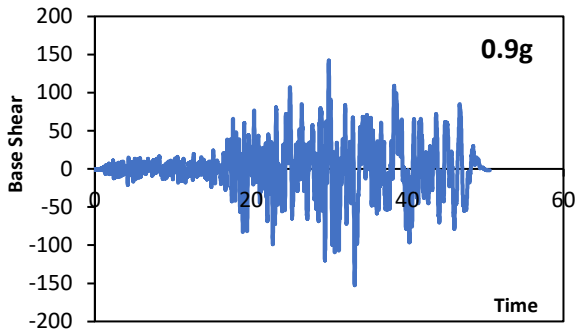
0.9g
Base Shear
Time
200
150
100
50
0
-50
-100
-150
-200
0
20
40
60

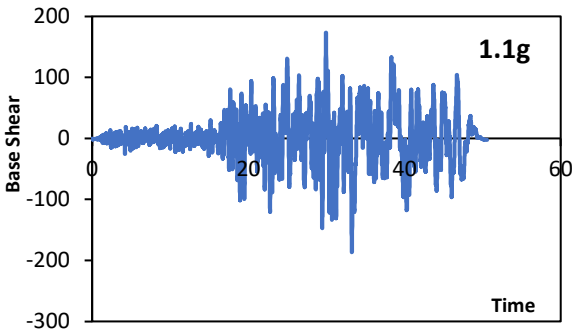
1.1g
Base Shear
Time
200
100
0
-100
-200
-300
0
20
40
60

L-Aquilla-NF

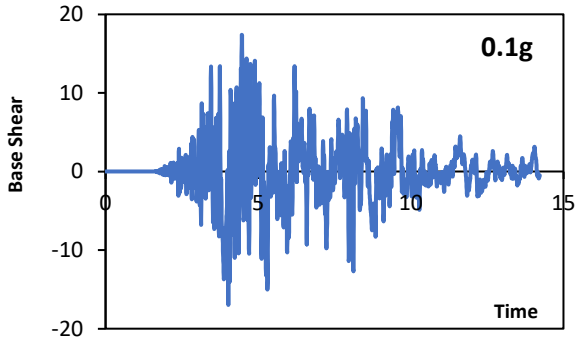
0.1g
Base Shear
Time
20
10
0
-10
-20
0
5
10
15

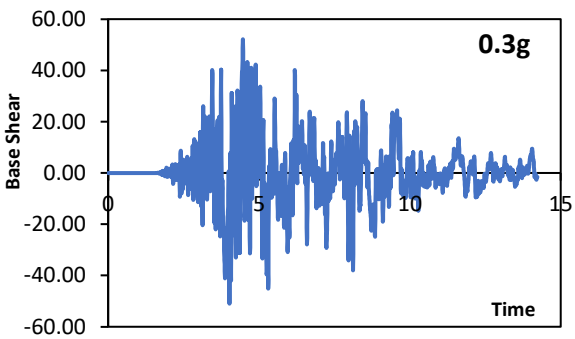
0.3g
Base Shear
Time
60.00
40.00
20.00
0.00
-20.00
-40.00
-60.00
0
5
10
15

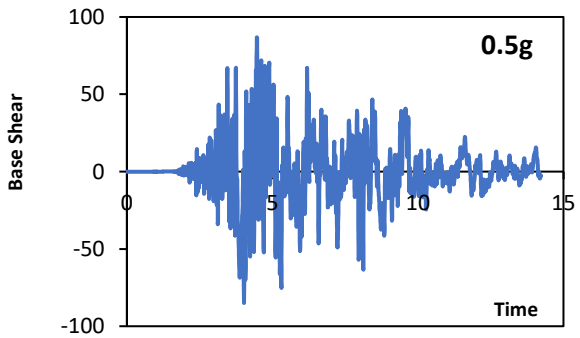
0.5g
Base Shear
Time
100
50
0
-50
-100
0
5
10
15

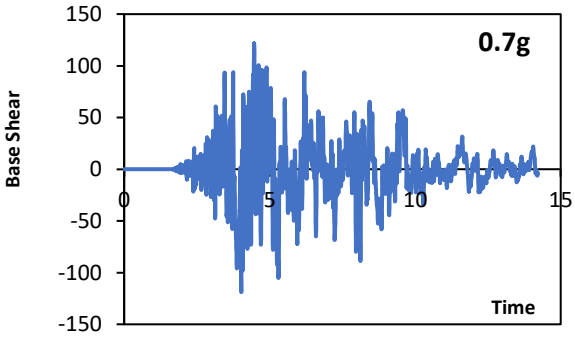
0.7g
Base Shear
Time
150
100
50
0
-50
-100
-150
0
5
10
15

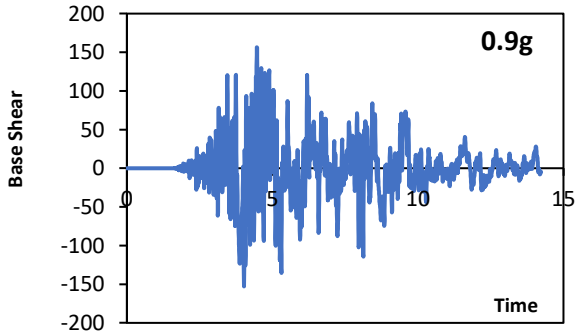
0.9g
Base Shear
Time
200
150
100
50
0
-50
-100
-150
-200
0
5
10
15

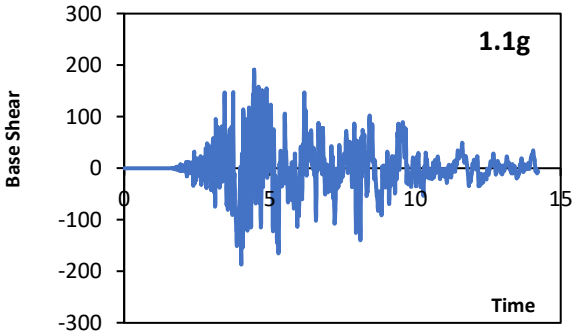
1.1g
Base Shear
Time
300
200
100
0
-100
-200
-300
0
5
10
15

L-Aquilla-FF

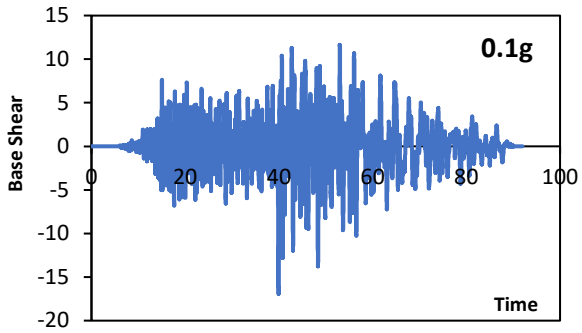

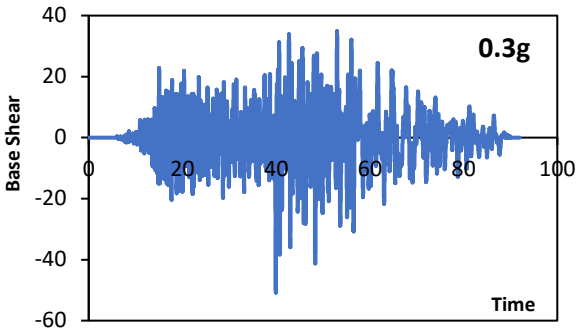

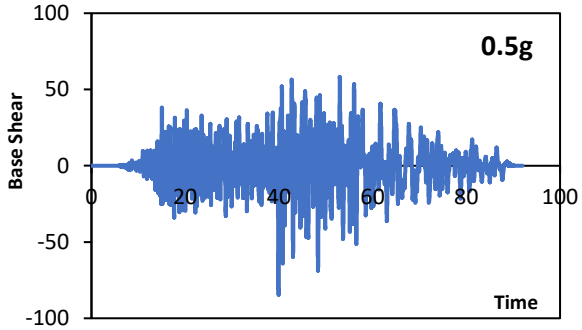

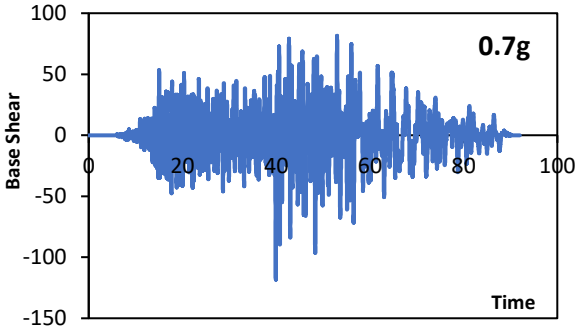

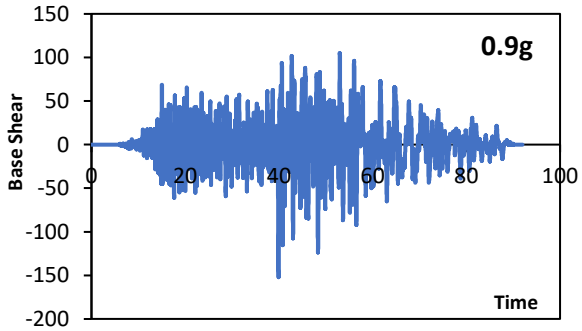

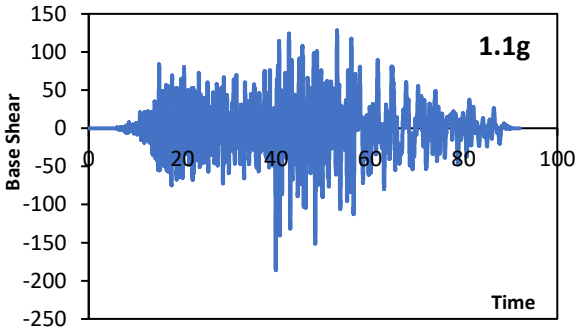

Loma Prieta-NF

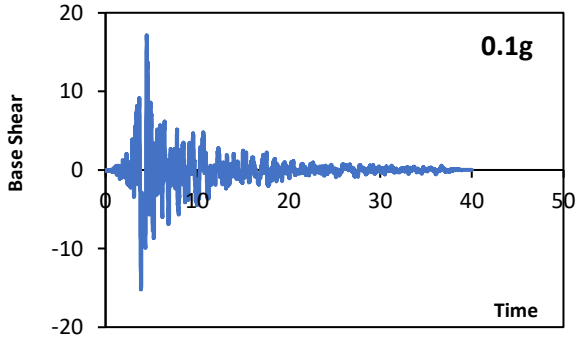

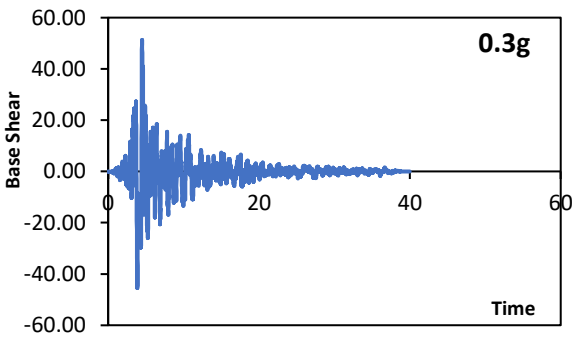

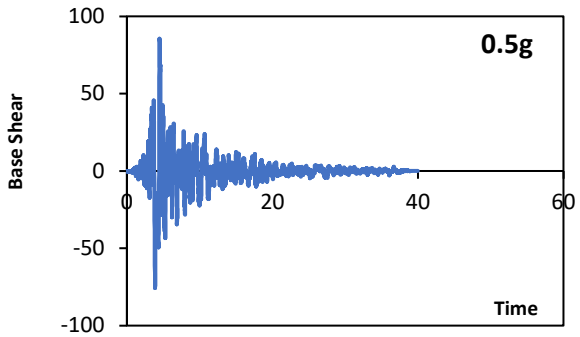

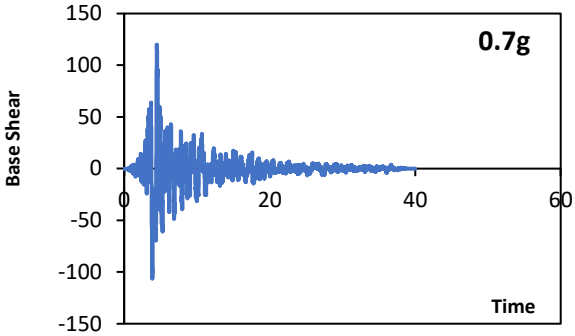

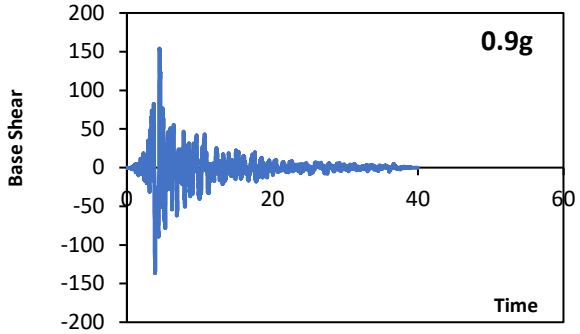

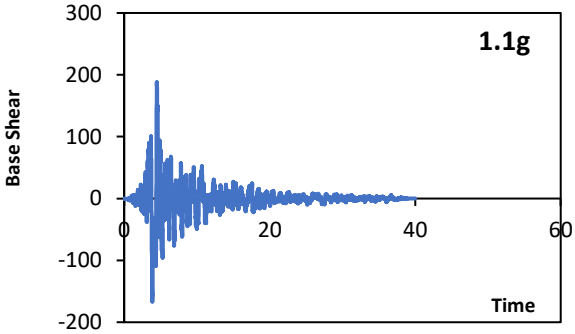

Loma Prieta-FF

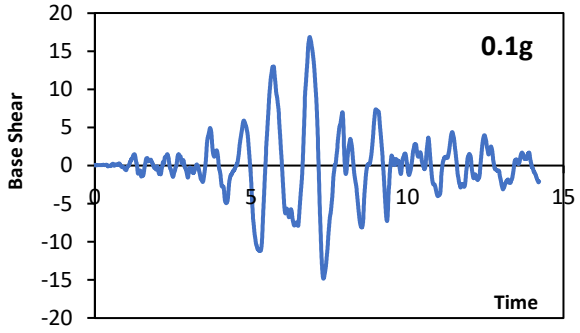

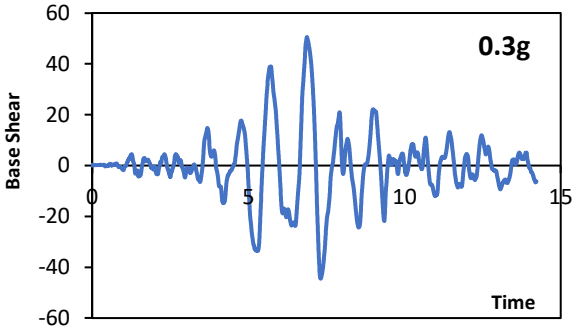

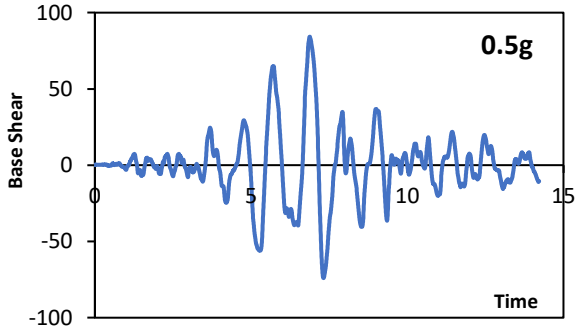

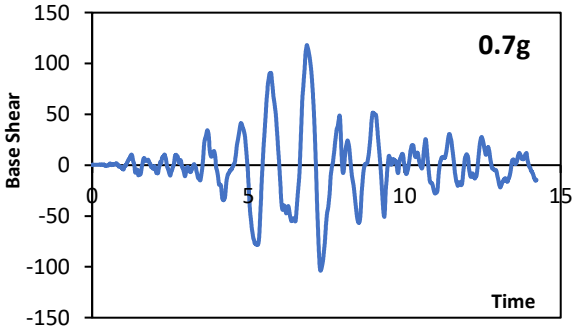

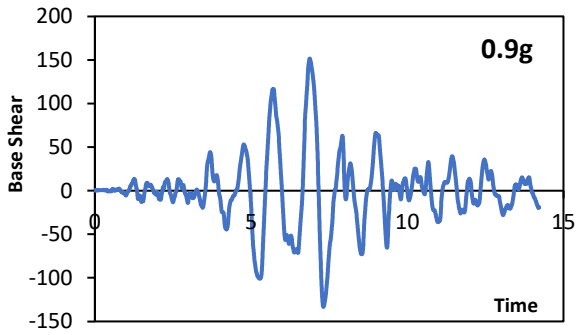

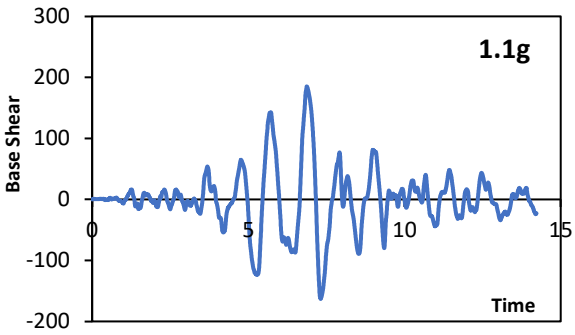

Montenegro-NF

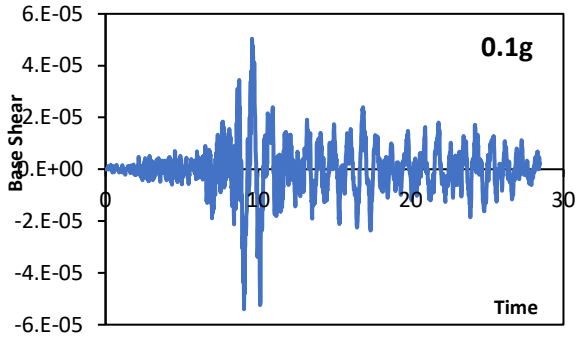

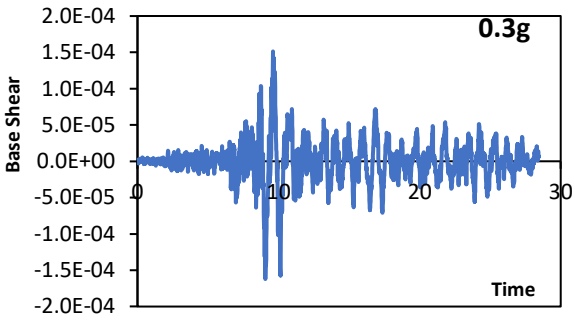

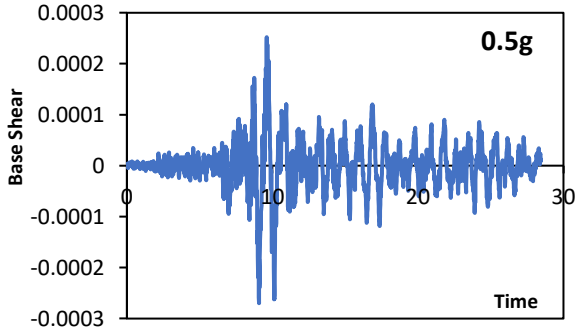

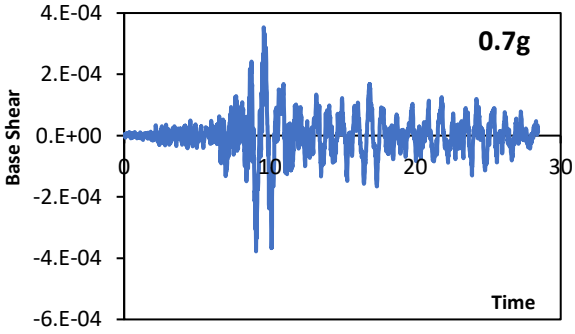

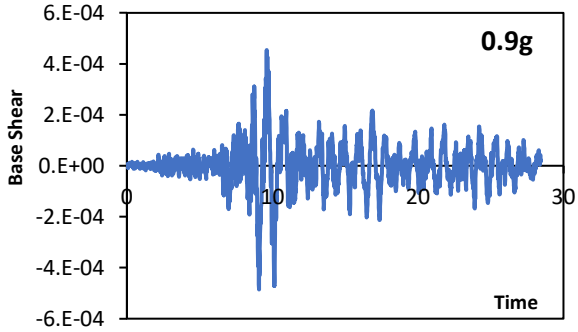

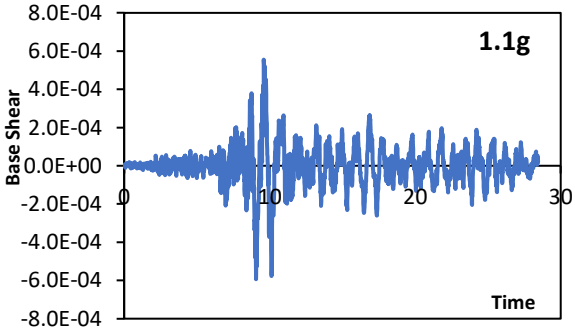

Montenegro-FF

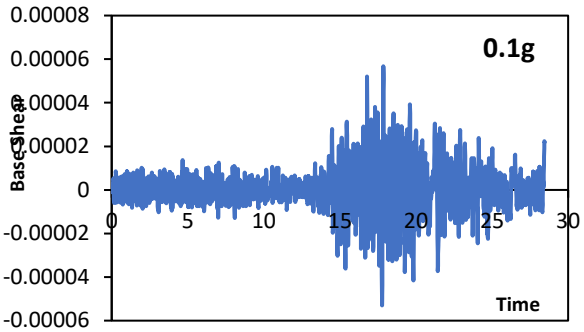

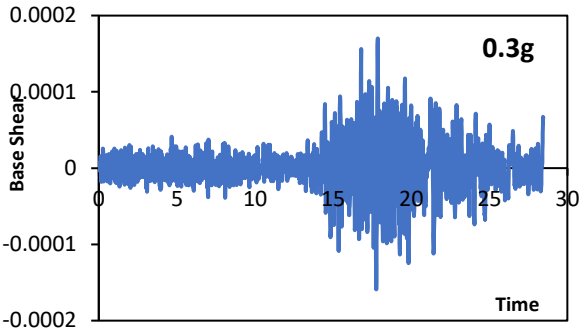

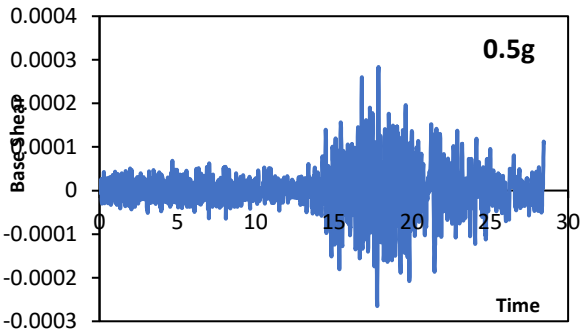

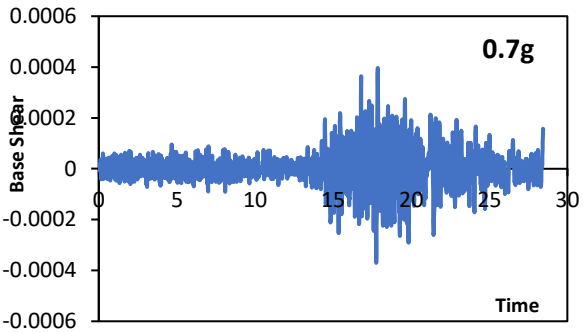

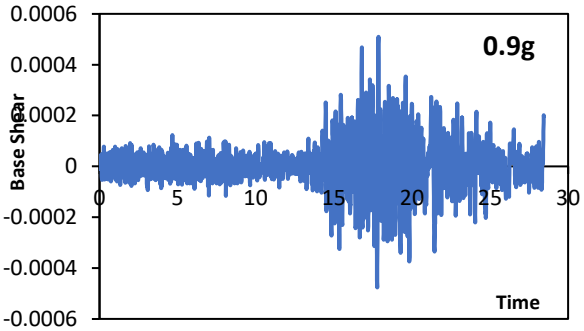

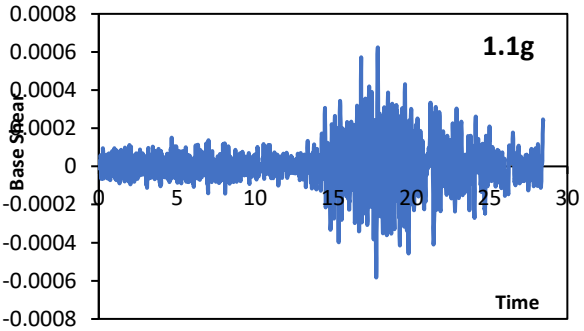

Niigata-FF

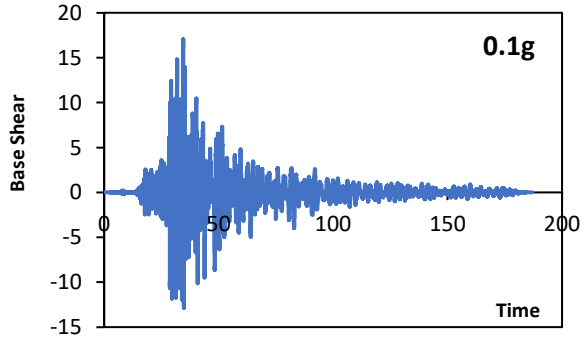

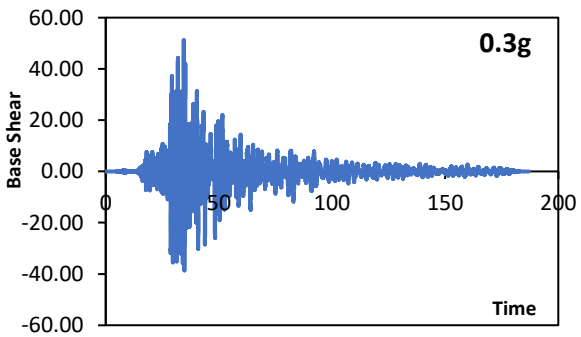

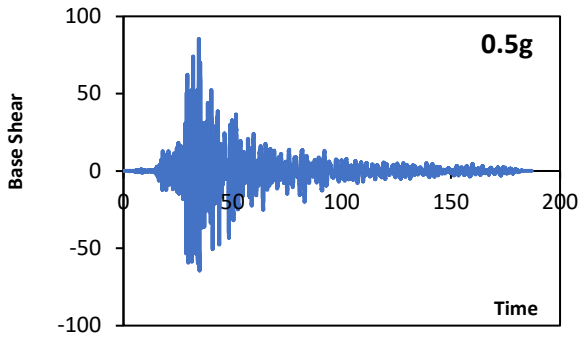

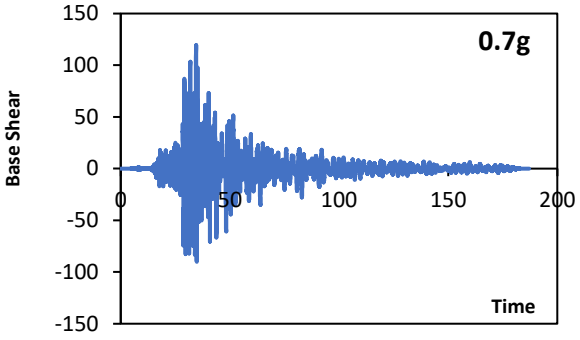

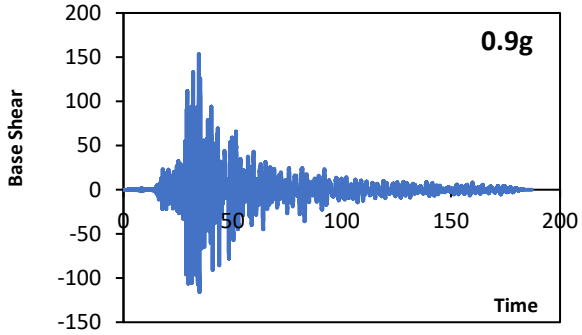

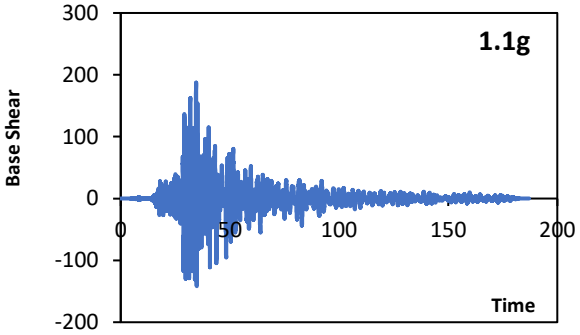

Northridge-NF

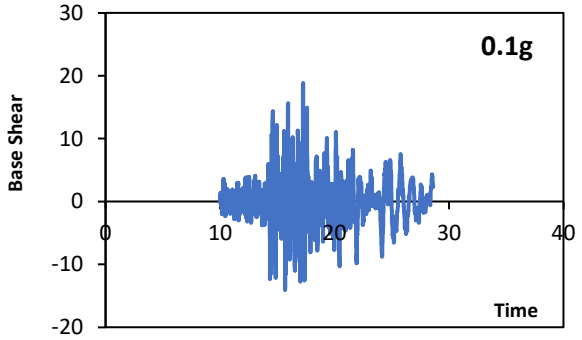

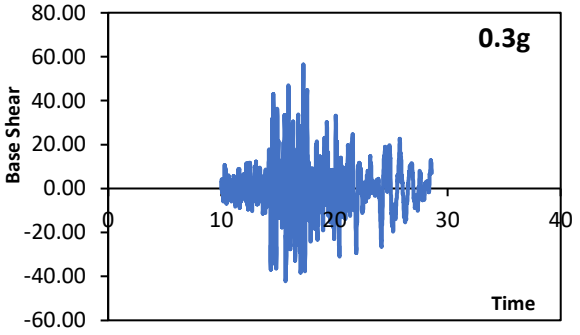

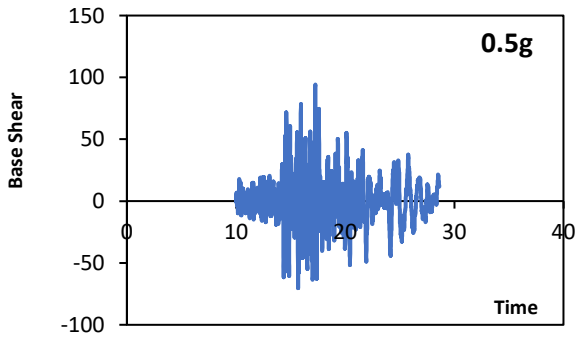

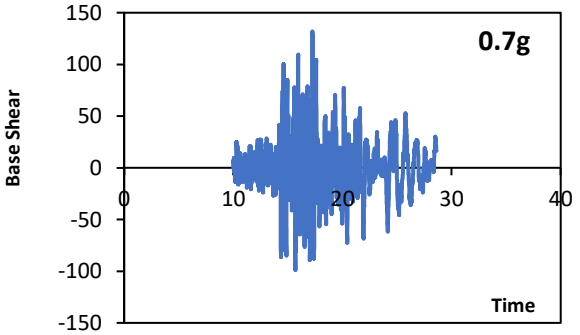

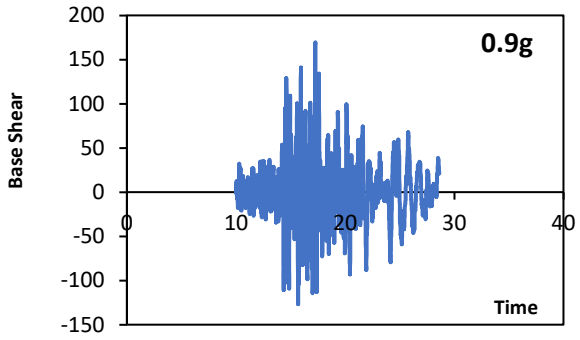

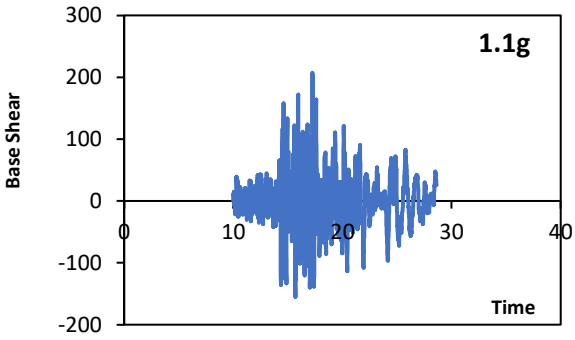

Northridge-FF

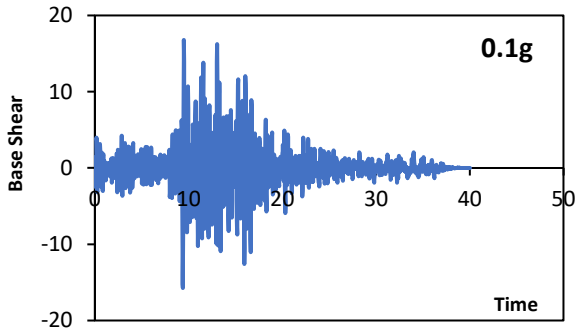

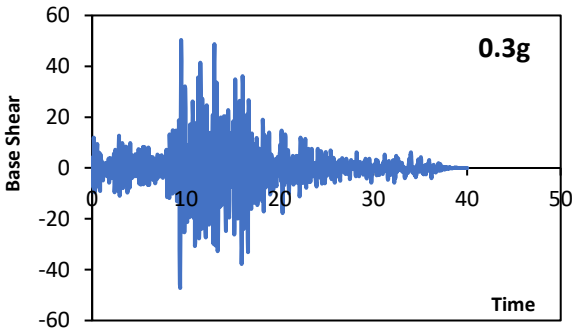

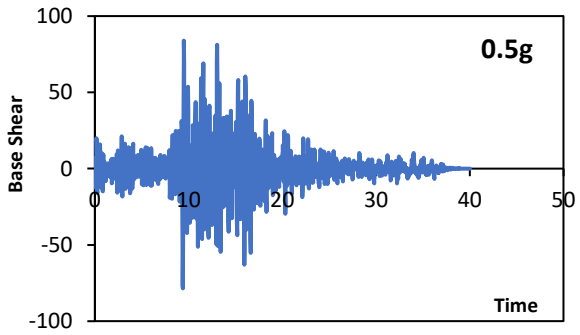

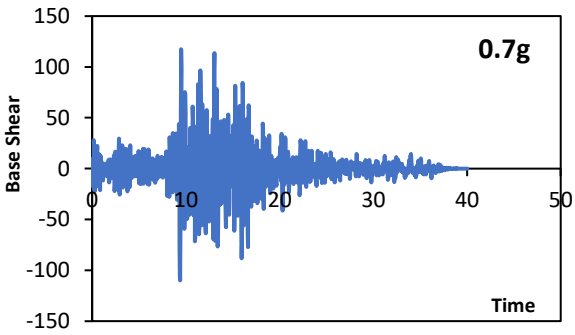

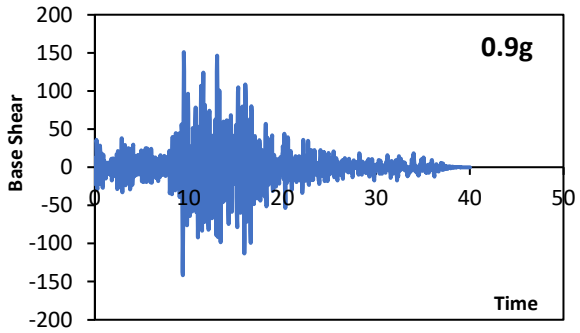

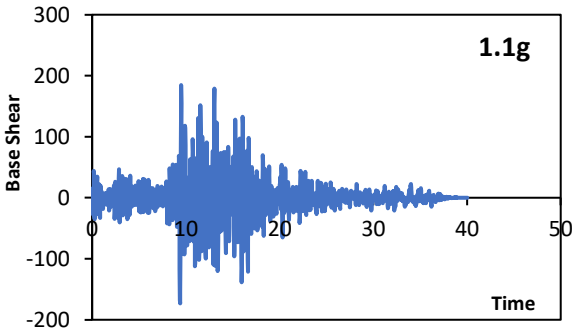

Parkfield-NF

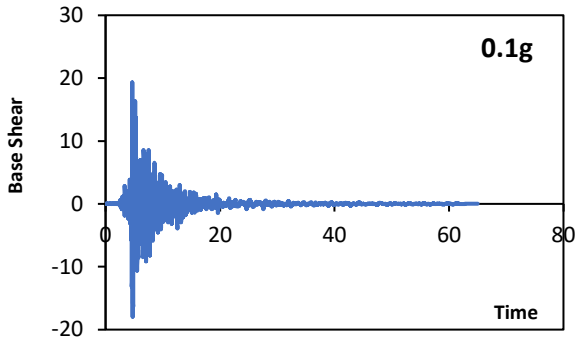

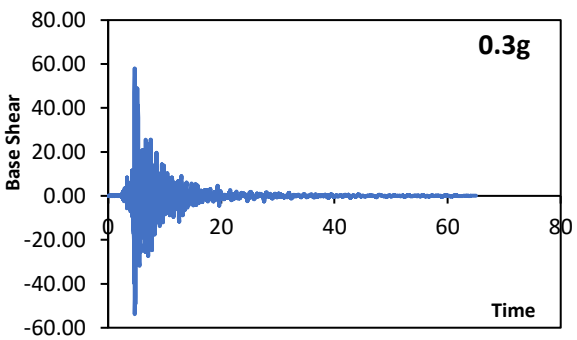

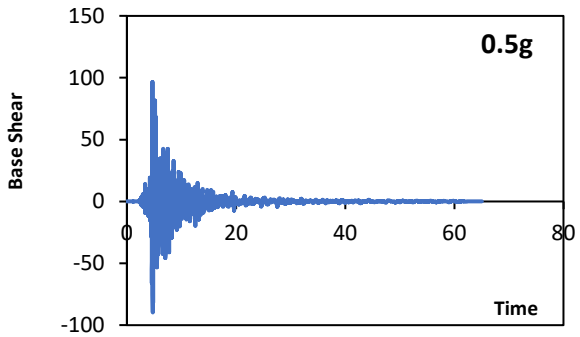

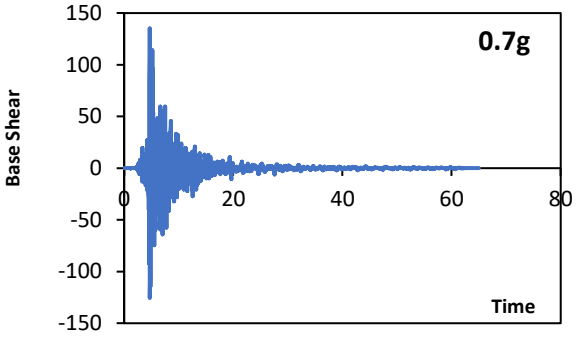

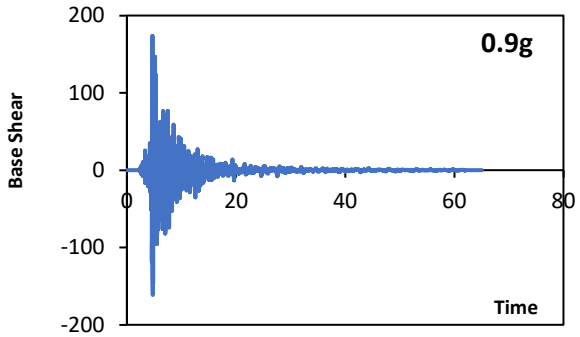

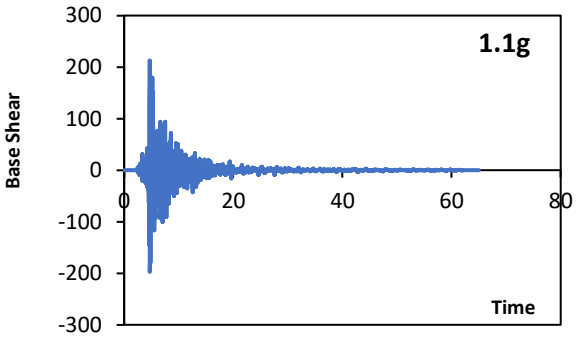

Parkfield-FF

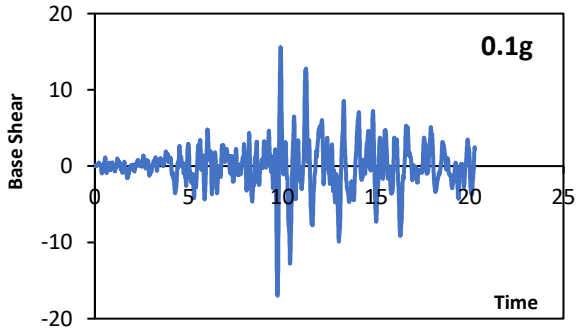

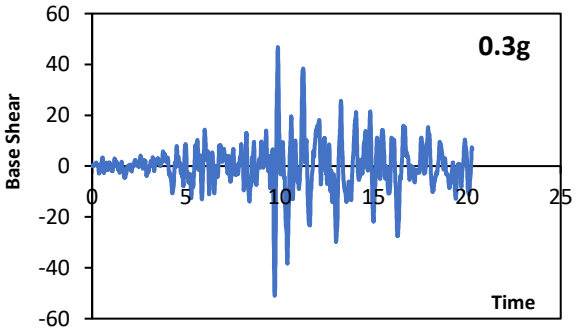

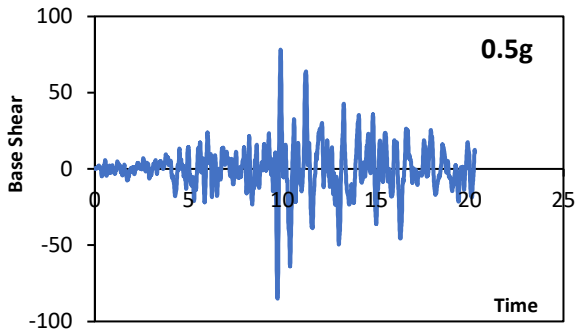

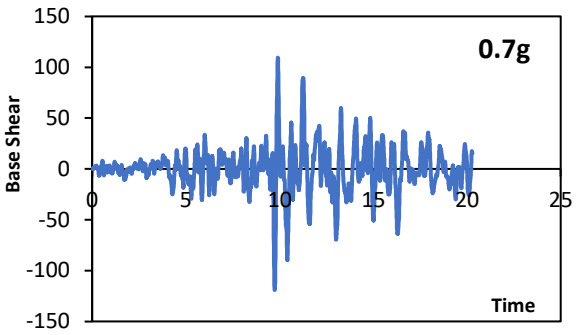

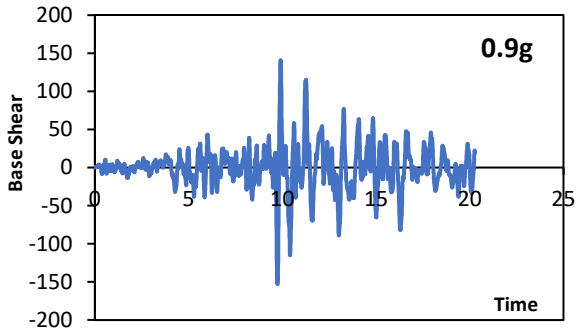

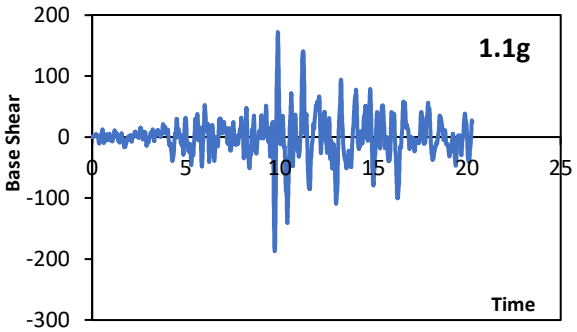

San Fernado-NF

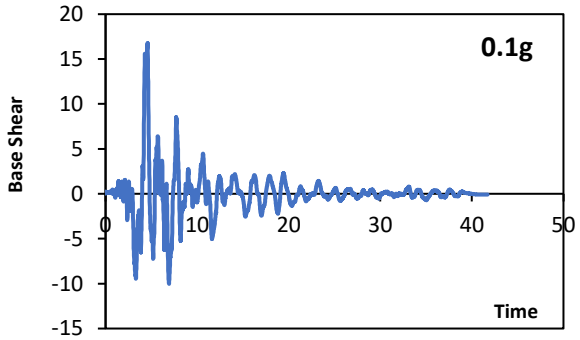

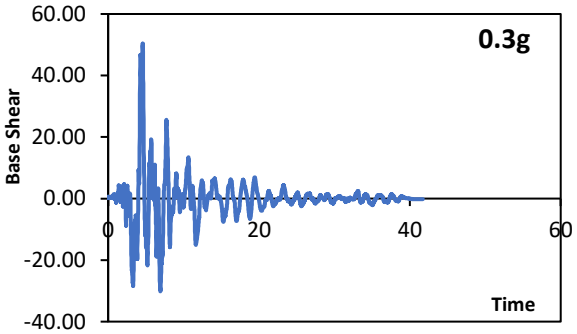

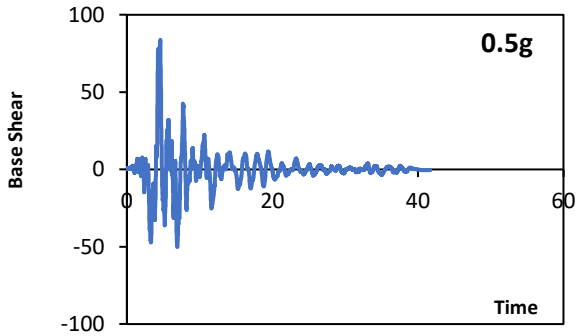

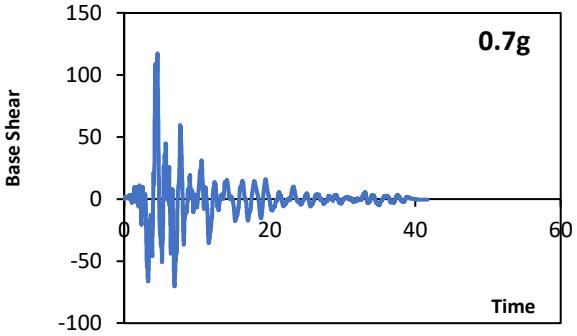

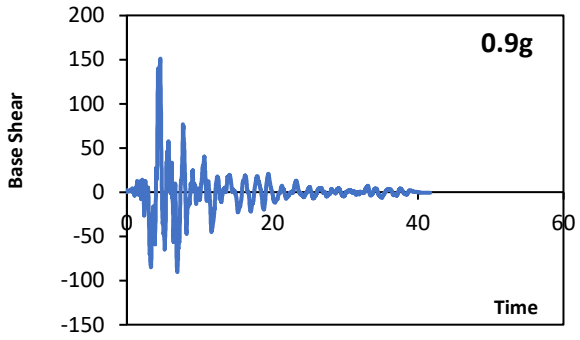

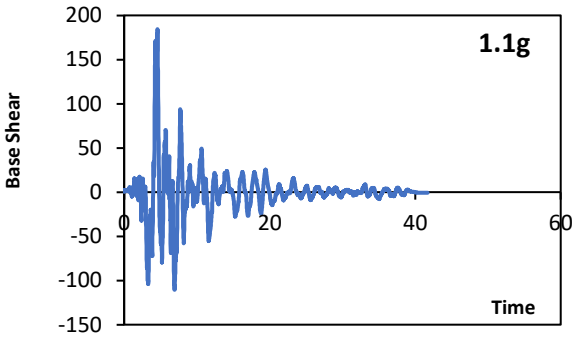

San Fernado-FF

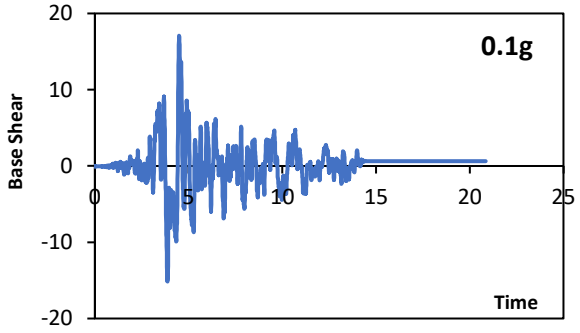

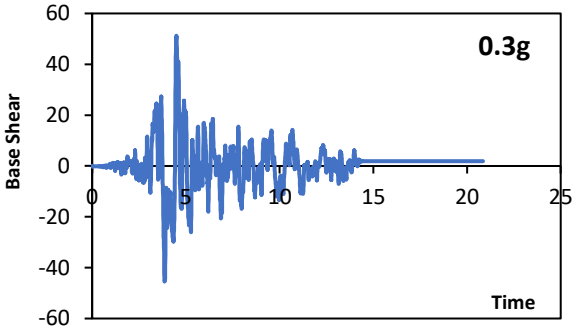

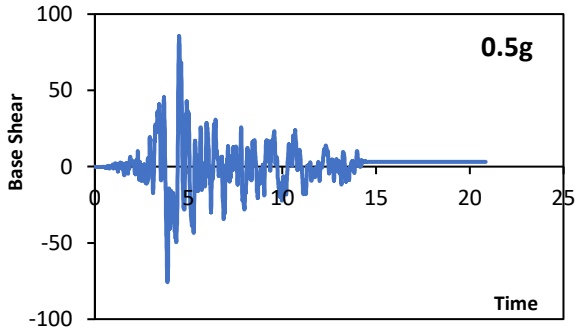

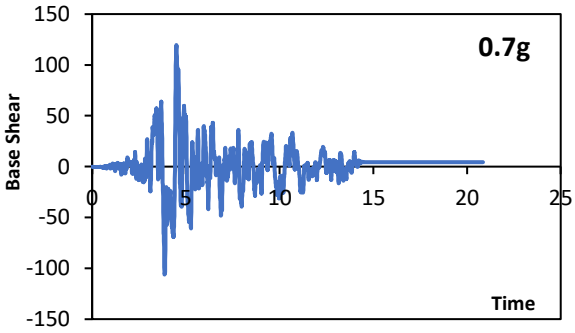

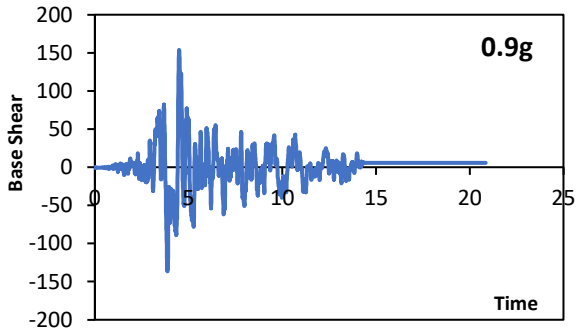

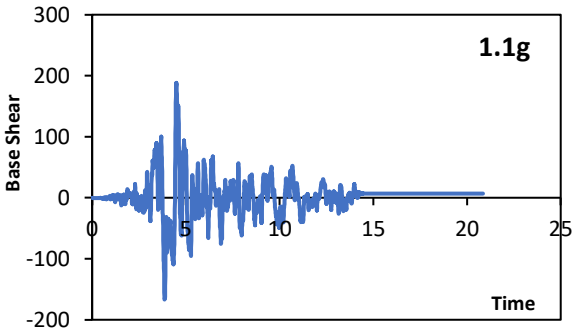

San Salvador-NF

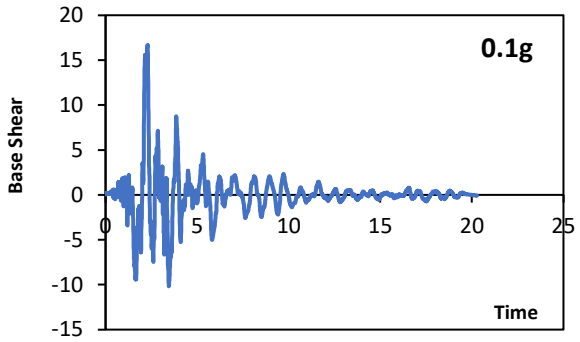

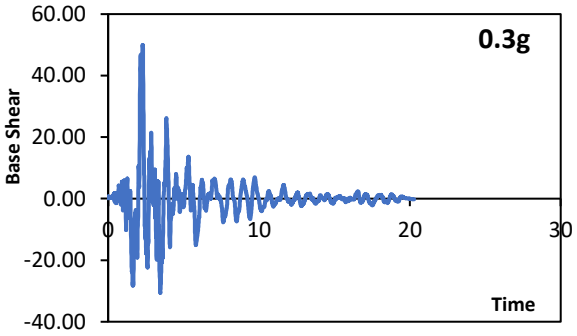

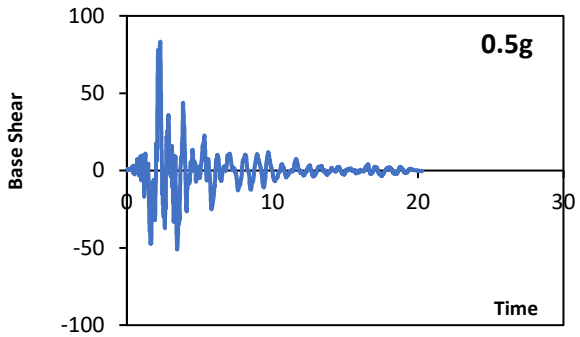

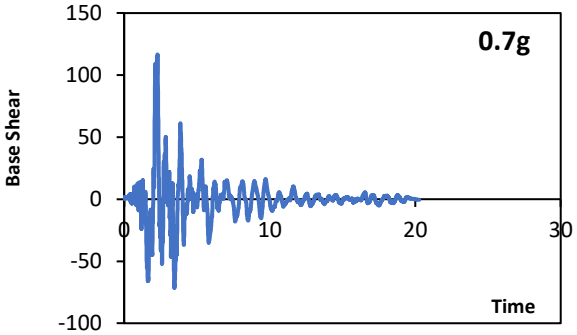

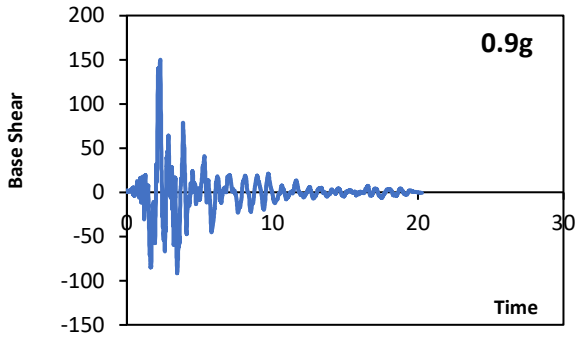

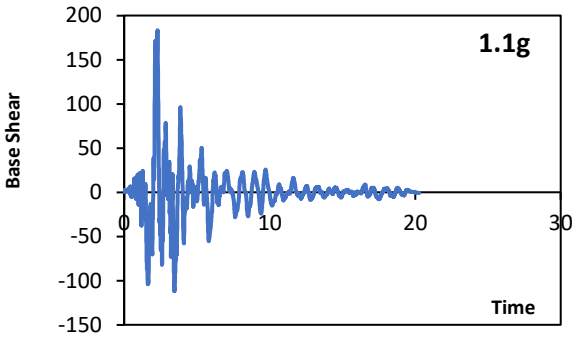

Superstition Hills-NF

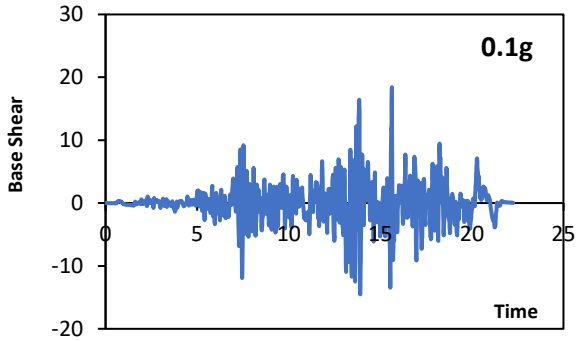

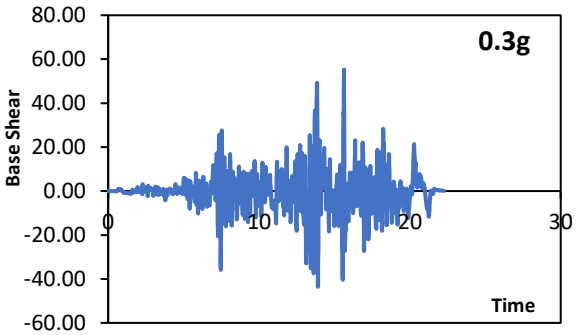

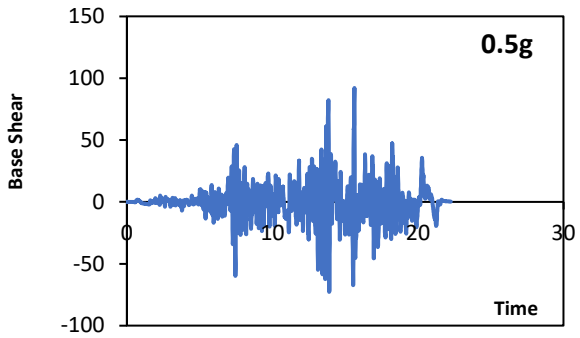

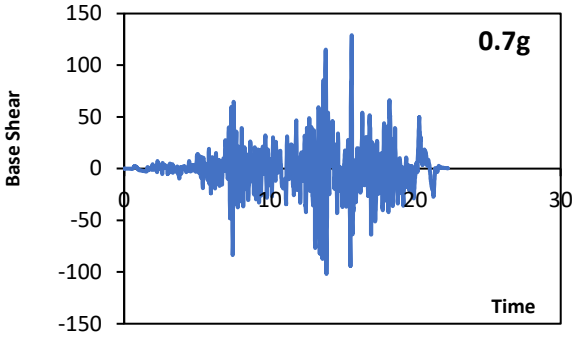

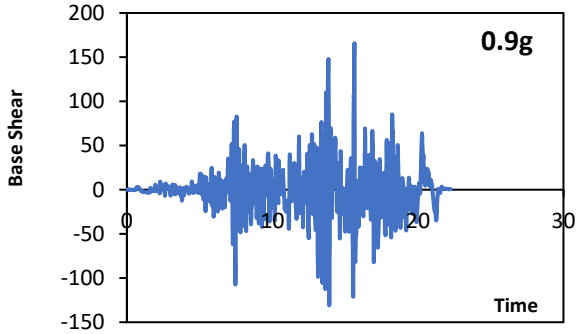

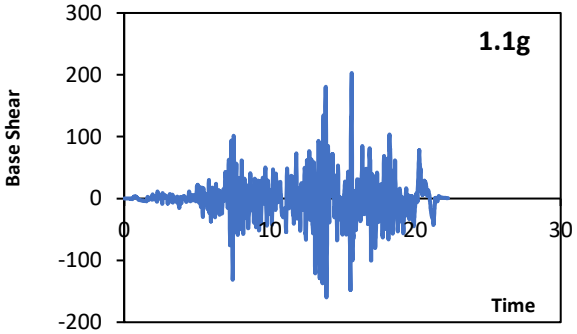

Superstition Hills-FF

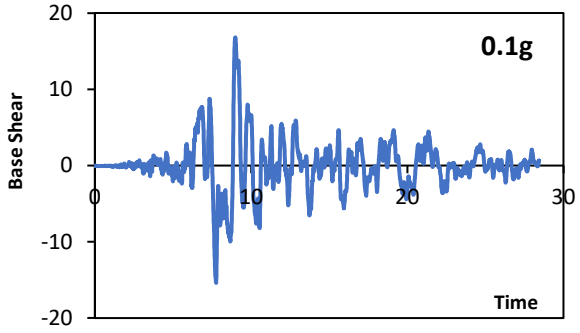

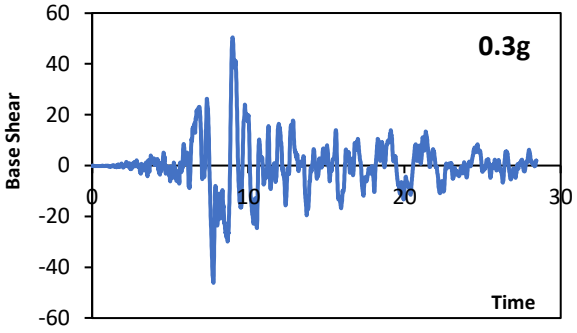

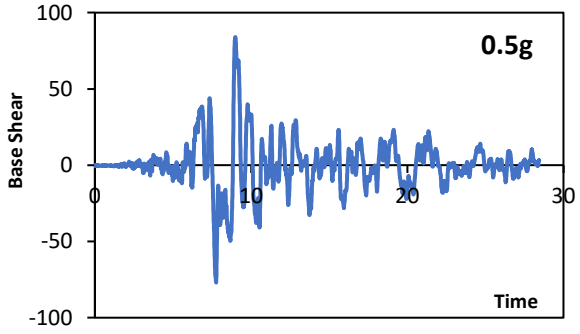

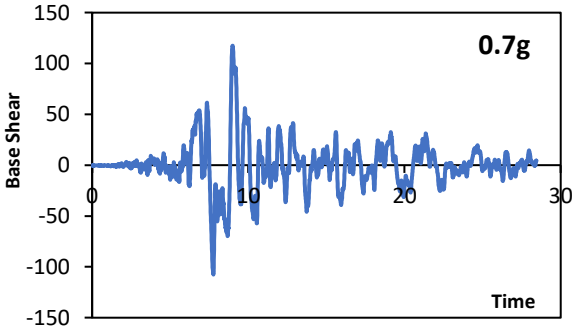

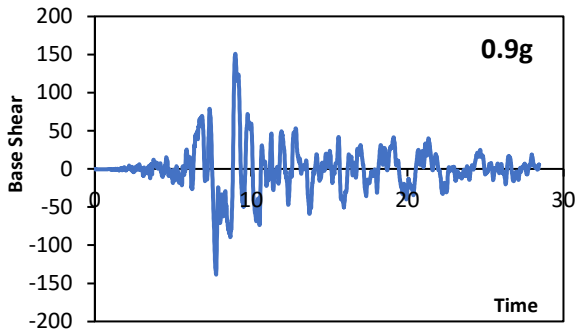
0.9g
Base Shear
Time
200
150
100
50
0
-50
-100
-150
-200
0
10
20
30

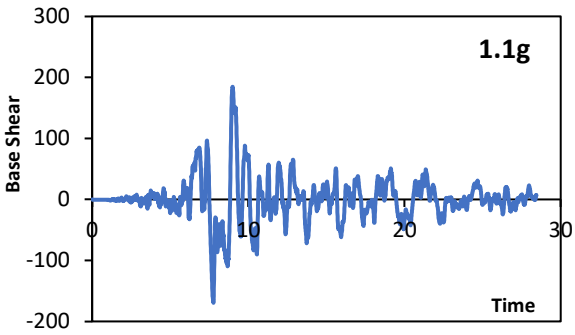
1.1g
Base Shear
Time
300
200
100
0
-100
-200
0
10
20
30

Tottori-NF

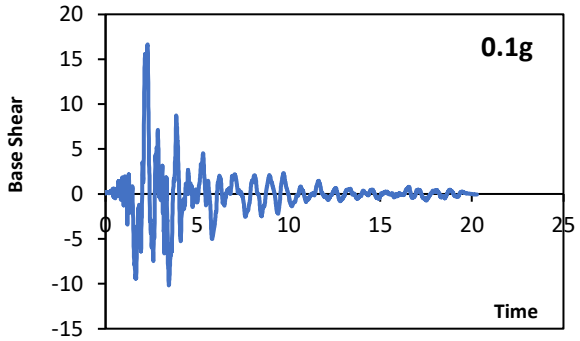
0.1g
Base Shear
Time
20
15
10
5
0
-5
-10
-15
0
5
10
15
20
25

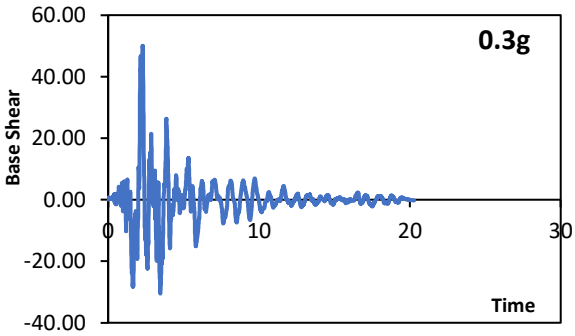
0.3g
Base Shear
Time
60.00
40.00
20.00
0.00
-20.00
-40.00
0
10
20
30

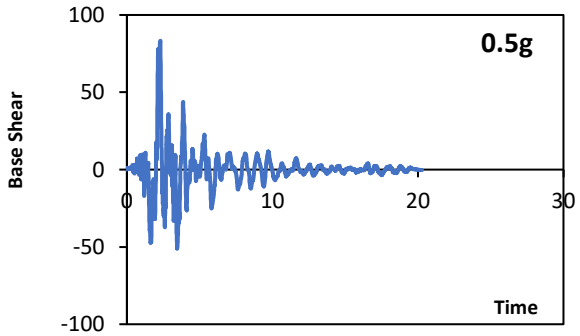
0.5g
Base Shear
Time
100
50
0
-50
-100
0
10
20
30

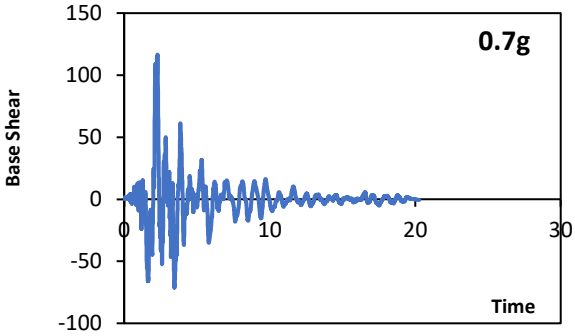
0.7g
Base Shear
Time
150
100
50
0
-50
-100
0
10
20
30

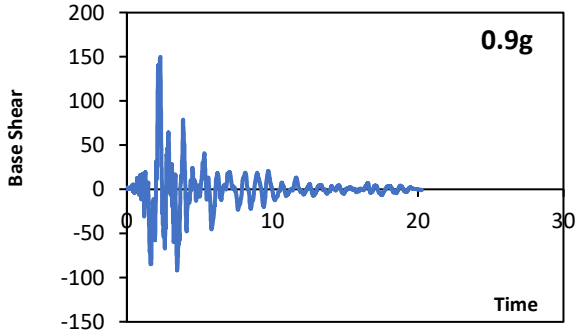
0.9g
Base Shear
Time
200
150
100
50
0
-50
-100
-150
0
10
20
30

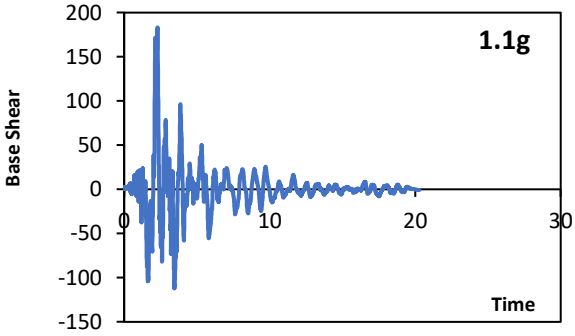
1.1g
Base Shear
Time
200
150
100
50
0
-50
-100
-150
0
10
20
30

Tottori-FF

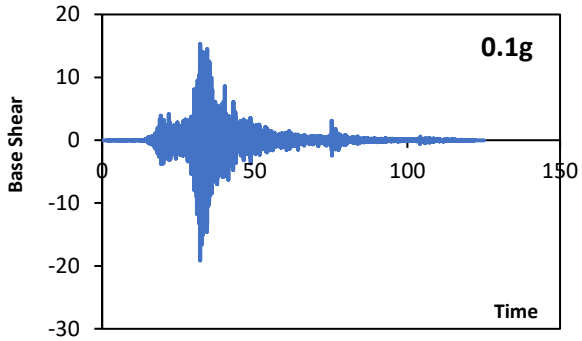

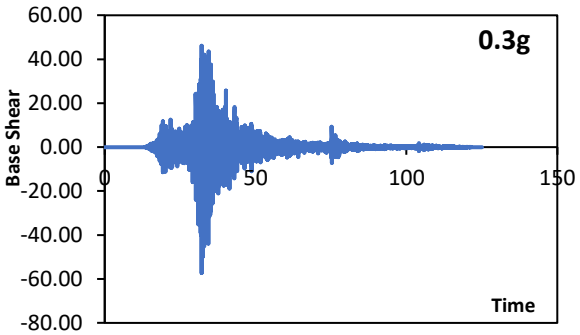

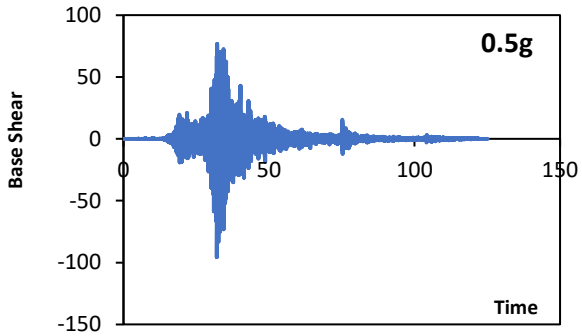

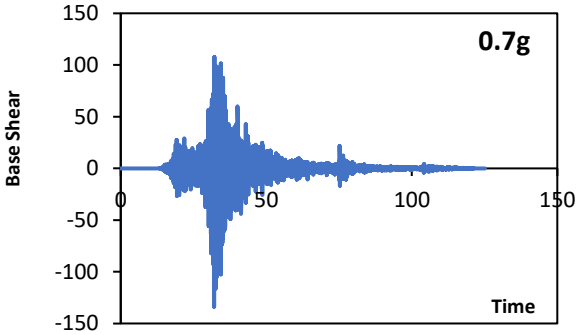

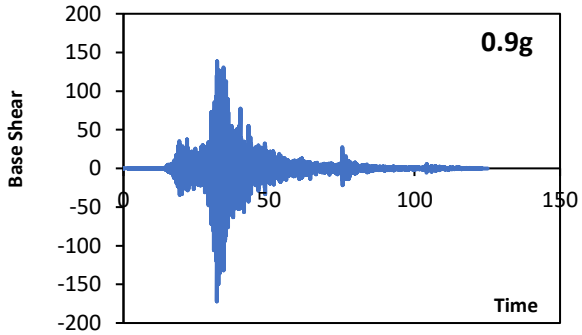

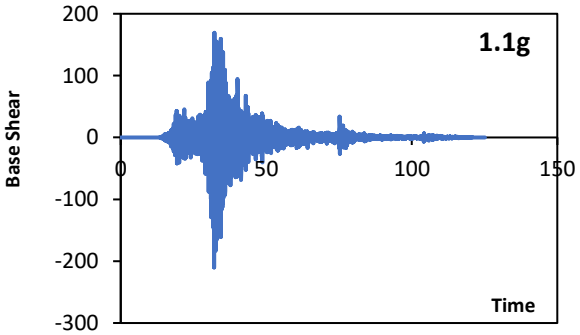

Westmorland-NF

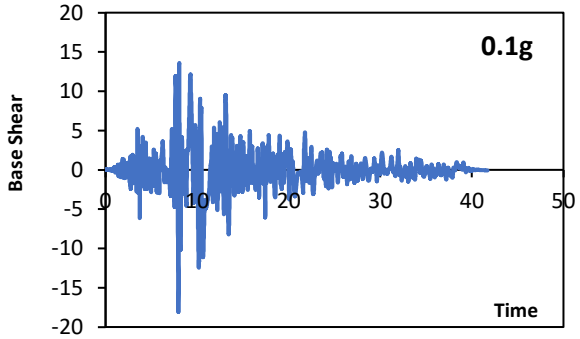

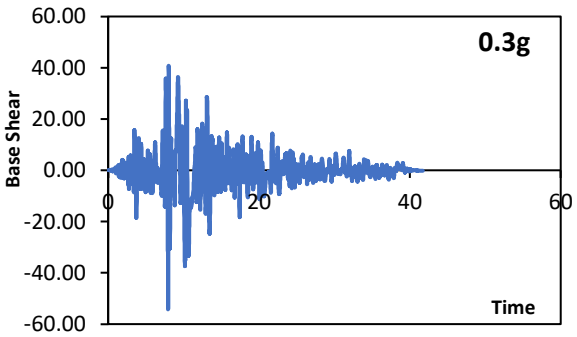

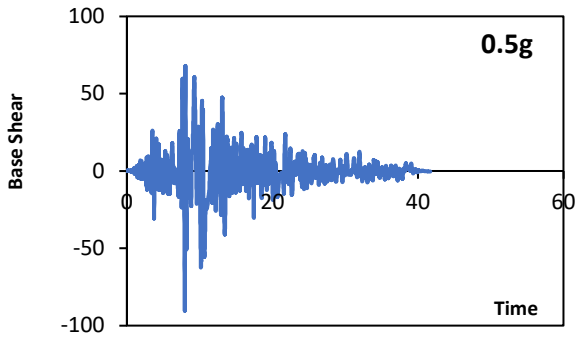

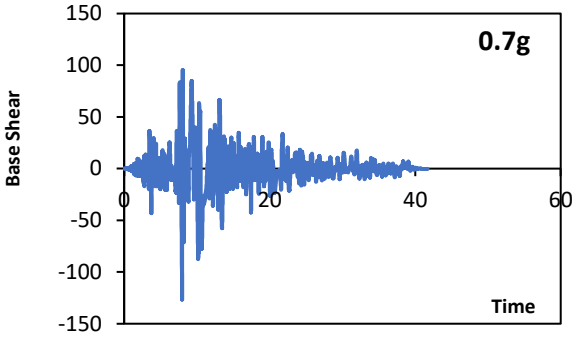

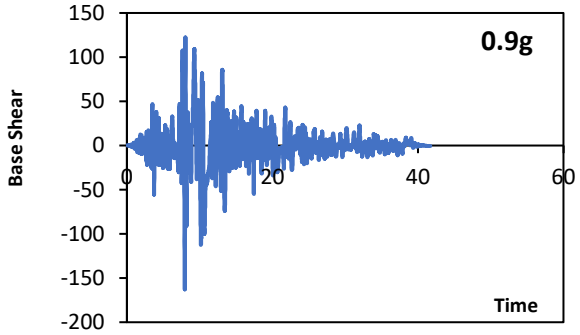

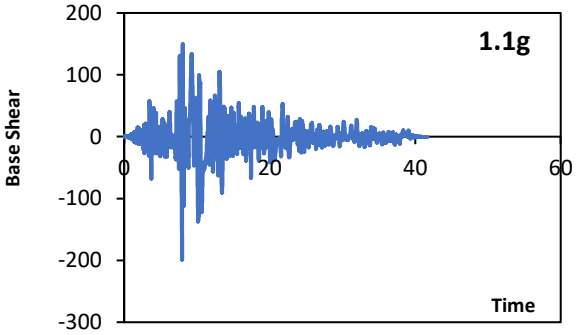

Westmorland-FF

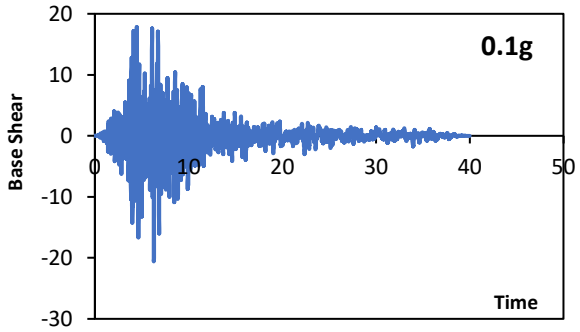

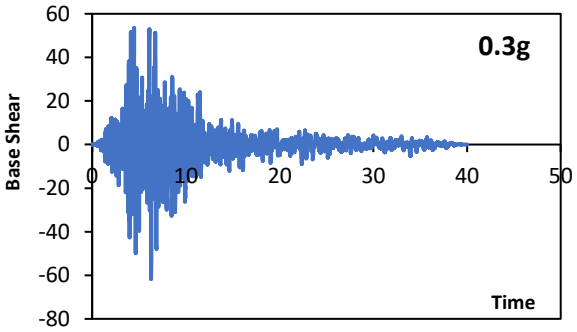

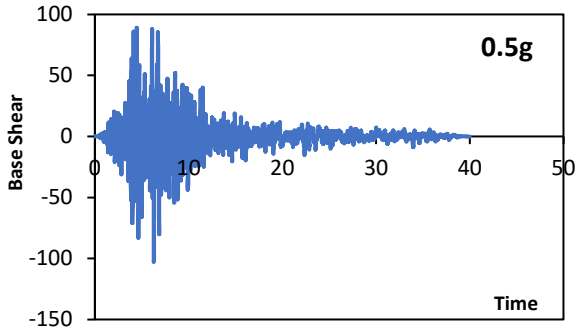

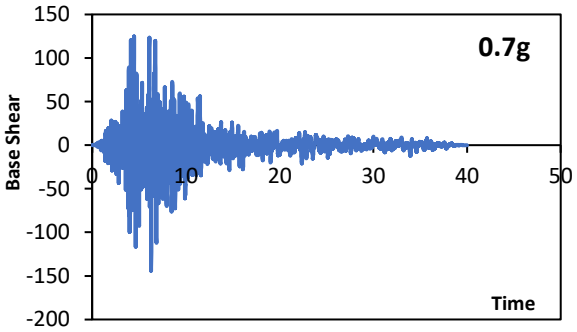

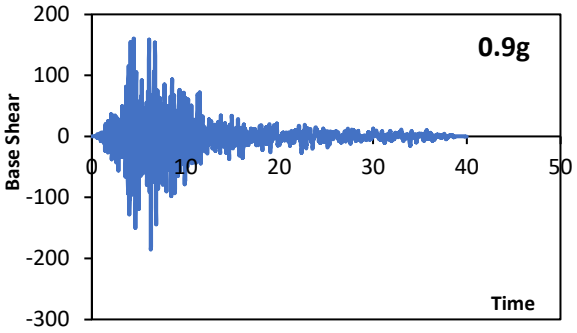
0.9g
Base Shear
Time
200
100
0
-100
-200
-300
0
10
20
30
40
50

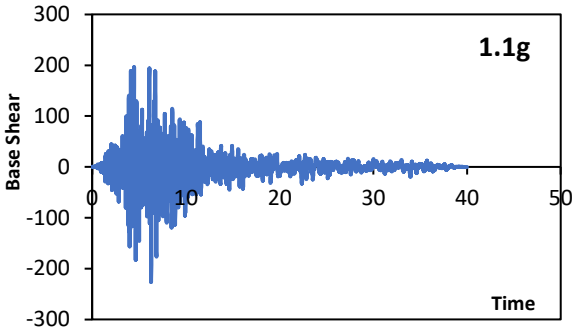
1.1g
Base Shear
Time
300
200
100
0
-100
-200
-300
0
10
20
30
40
50

Document Information

Analyzed document	YASHSWI_Thesis 802124025.pdf (D172447881)
Submitted	7/29/2023 4:26:00 PM
Submitted by	Trishna Choudhury
Submitter email	trishna.choudhury@thapar.edu
Similarity	3%
Analysis address	trishna.choudhury.thapar@analysis.urkund.com

Sources included in the report

SA **Thapar Institute Of Engineering And Technology / 802124018-THESIS FILE 4.pdf** 3
Document 802124018-THESIS FILE 4.pdf (D172445425)
Submitted by: abdanie@thapar.edu
Receiver: abdanie.thapar@analysis.urkund.com

SA **PID-129 AR Manish Sharma.docx** 1
Document PID-129 AR Manish Sharma.docx (D144646321)

SA **181160720010_Nidhi.pdf** 1
Document 181160720010_Nidhi.pdf (D74750362)

SA **Kowsi thesis.pdf** 1
Document Kowsi thesis.pdf (D143033934)

SA **adi.pdf** 2
Document adi.pdf (D33985012)

SA **vijay sahu RETROFITTINGThesis.docx** 1
Document vijay sahu RETROFITTINGThesis.docx (D74346903)

SA **adil thesis pdf.pdf** 1
Document adil thesis pdf.pdf (D162086952)

SA **Hadikhan Tehrani.docx** 1
Document Hadikhan Tehrani.docx (D7305626)

Entire Document

Effects of Near-field and Far-field ground motions on Non- linear response of RC Buildings